Bond between Textile Reinforced Mortar (TRM) and Concrete Substrate

A Thesis submitted for the degree of

Doctor of Philosophy in Civil and structural Engineering

at The University of Nottingham

by

Saad Mahmood Raoof

(4206714)

July 2017

Centre for Structural Engineering and Informatics

Department of Civil Engineering

Faculty of Engineering

ABSTRACT

There is a growing interest for strengthening and upgrading existing concrete structures both in seismic and non-seismic regions due to their continuous deterioration as a result of aging, degradation induced environment conditions, inadequate maintenance, and the need to meet the modern codes (i.e. Eurocodes). Almost a decade ago, an innovative cement-based composite material, the so-called textile-reinforced mortar (TRM), was introduced in the field of structural retrofitting. TRM comprises high-strength fibres in form of textiles embedded into inorganic matrices such as cement-based mortars. TRM offers well-established advantages such as: fire resistance, low cost, air permeability, and ability to apply on wet surfaces and at ambient of low temperatures.

It is well known that the effectiveness of any external strengthening system in increasing the flexural capacity of concrete members depends primarily on the bond between the strengthening material and member's substrate. This PhD Thesis provides a comprehensive experimental study on the bond behaviour between TRM and concrete substrate and also provides a fundamental understanding of the flexural behaviour of RC beams strengthened with TRM.

Firstly, the tensile properties of the textile reinforcement were determined through carrying out tensile tests on bare textiles, and TRM coupons. Secondly, the bond behaviour between TRM and concrete substrates both at ambient and, for the first time, at high temperature was extensively investigated. A total of 148 specimens (80 specimens tested at ambient temperature and 68 specimens tested at high temperatures) were, fabricated, and tested under double-lap shear. Parameters investigated at ambient temperature comprised: (a) the bond length; (b) the number of layers; (c) the concrete surface preparation; (d) the concrete compressive strength; (e) the textile surface condition; and (f) the anchorage through wrapping with TRM jackets. Whereas, the parameters examined at high temperatures included: (a) the strengthening systems (TRM versus FRP); (b) the level of temperature at which the specimens were exposed; (c) the number of FRP/TRM layers; and (d) the loading conditions. The results of ambient temperature tests indicated that the bond at the TRM-concrete interface is sensitive to parameters such as: the number of layers, the

textile surface condition, and the anchorage through wrapping with TRM. On the other hand, the results of high temperature tests showed that TRM exhibited excellent bond performance with concrete (up to 400 ^{0}C) contrary to FRP which practically lost its bond with concrete at temperatures above the glass trainset temperature (T_g).

The flexural strengthening of RC beams with TRM at ambient and for the first time at high temperature was also examined carrying out 32 half-scale beams. The examined parameters were: (a) the strengthening system (TRM versus FRP); (b) the number of layers; (c) the textile surface condition; (d) the textile fibre material; (e) the end-anchorage system of the external reinforcement; and (f) the textile geometry. The results of ambient temperature tests showed that TRM was effective in increasing the flexural capacity of RC beams but its effectiveness was sensitive to the number of layers. Furthermore, a simple formula used for predicting the mean FRP debonding stress was modified for predicting the TRM debonding stress based on the experiment data available. The results of high temperature tests showed that TRM maintained an average effectiveness of 55%, of its effectiveness at ambient temperature, contrary to FRP which has totally lost its effectiveness when subjected to high temperature. Finally, a stress reduction factor of TRM flexural effectiveness (compared to its ambient effectiveness) when subjected to high temperature was also proposed.

Acknowledgment

I feel the words are few to express my upmost gratitude and thanks to my supervisor, Dr. Dionysios Bournas. I have been so lucky working under his supervision. His engineering experience, advices, critical thinking, and unlimited support, was of great importance in guiding me to the right direction and completing my PhD. I would like also to thank Dr. Savvas Triantafyllou for his support and assistance in the last year of my PhD study.

I would like to thank the Higher Committee for Education Development in Iraq (HCED) for giving me this chance to complete my PhD study.

I also deeply thank Dr. Lampros Koutas for his valuable assistance during my PhD study. His scientific knowledge and experience, lab skills, positive thinking, and personal characters helped me in completion my PhD.

My deep gratitude also goes to my colleagues and my best friend Zoi. Her endless help and support was so important for me to overcome the challenges of the experimental works in the lab. Her generous advices, the way she delivers information and scientific ideas made a big difference.

I would like also to acknowledge: the lab manager Tom Buss (the manager of Wolfson Laboratory) and his team: Jason Greaves, Graham Malkinson and Max Mason; the lab manager Mike Langford (the manager of L2 laboratory), the chief technician in L2 laboratory Nigel Rook, the technicians Sam Cook, Bal Loyla and Gary Davies; and the senior technical manager Phil Bennett for their assistance to achieve the experimental work.

I would like also to thank my great friends: Mustapha Al-Behadili, Wisam Alani, Muayad Hasan, Wathiq Al-Hachami, Hayder Mohammed, Kamal Al-Hamdani, and Ramzi Al-Agele for their support during my PhD study.

Special thanks should go to Zahraa Alzalzala; her support during writing up my Thesis is highly appreciated.

I am deeply grateful to my parents, brothers, and sisters. Their warm feelings, positive energy inspired and helped me to finish my PhD study.

Finally, special heartfelt thanks should go to my sweetheart wife Iqbal, my lovely daughters Rusul, Rafel and Reem and my hero son Talal for being close to me all the time. Their sincere feelings, love, patient, encouragement dissipate the stress of the day and motivated me to achieve my goals.

Table of Contents

List of Tables

List of Figures

List of abbreviations

PBO	Polyparaphenylene Benzobis Oxazole
FRP	Fibre Reinforced Polymers
TRM	Textile Reinforced Mortar
LVDT	Linear Variable Differential Transducer
RC	Reinforced Concrete
$\boldsymbol{T_g}$	Glass Transient Temperature

List of Notations

A_f	Area of fibre
A_{rov}	Area of a roving
$A_{s,min}$	Minimum area of steel reinforcement
A_{s1}	Area of steel in tension zone
A_{s2}	Area of steel in compression zone
A_{sw}	Area of shear reinforcement
C_c	Compression force provided by concrete
C_{c2}	compression force provided by steel reinforcement in compression zone
$E_{f,FRP}$	Modules of elasticity of FRP composite
$E_{f,TRM}$	Modules of elasticity of TRM composite
$E_{f,tex.}$	Modules of elasticity of bare textile
E_s	Modules of elasticity of steel
L_b	Bond length
L_a	Anchorage length of the strengthening materials
L_{resd}	Residual anchorage length
$M_{Rd,bal}$	Design balanced moment
$M_{u,exp}$	Ultimate moment capacity obtained experimentally
N_{Ed}	Tension force provided by ultimate moment
N_{Rsd}	Tension force provided by tension steel reinforcement
P_{av}	Average value of ultimate load

P_{cr}	Cracking load
P_{max}	Ultimate load obtained from bond test
$P_{max}^{A.T.}$	Ultimate load obtained from bond test at ambient temperature
$P_{max}^{H.T.}$	Ultimate load obtained from bond test at high temperature
P_u	Ultimate load
P_y	Yielding load
T_f	Tensile force provided by TRM/FRP
T_{s1}	Tensile force provided by the steel in tension
$V_{R,max}$	Ultimate design shear force
b_f	Width of fibres
f_b	Bond strength at the concrete-matrix interface
f_{ck}	Compressive strength of concrete
f_{cm}	Mean concrete compressive strength
f_{ctm}	Mean tensile strength of concrete
f_{fbm}	Mean debonding stress in TRM/FRP reinforcement
f_{fu}	Ultimate tensile stress in the textile reinforcement
f_y	Yield stress in the steel rebar
k_b	Shape factor of strengthened beam
k_{bal}	Normalized balanced moment
k_c	Intermediate crack factor of strengthened beam
k_m	Matrix factor of strengthened beam
t_f	Nominal thickness of fibres
β_ℓ	Length factor of strengthened beam
δ_G	Coefficient of centroid of concrete stress block
δ_{cr}	Displacement corresponding to the cracking load
δ_{max}	Displacement corresponding to ultimate load in the bond test
δ_u	Displacement at ultimate load
δ_y	Displacement corresponding to the yielding load
ε_c	Compressive strain in concrete
ε_{fu}	Ultimate tensile strain in fibres
ε_{s1}	Strain in steel reinforcement at tension zone
ε_{s2}	Strain in steel reinforcement at compression zone

ρ_f	Textile reinforcement ratio
ρ_s	Steel reinforcement ratio
$\sigma_{eff,bond}$	Effective stress in the textile reinforcement obtained from bond test
$\sigma_{eff,exp}$	Effective stress in textile reinforcement obtained experimentally
D	Diameter of steel rebar
h	Total height of beam's cross section
z	lever arm
S	Spacing between shear links
b	Width of beam's cross section
d	Effective depth of beam
n	Number of strengthening layers
x	Depth of neutral axis
θ	Angle between the shear crack and the axis of the beam
φ	Coefficient of area of concrete stress block

Chapter 1

INTRODUCTION

1.1 Background

The need for retrofitting existing concrete infrastructure is progressively becoming more important due to their continuous deterioration as a result of ageing, environmental conditions induced degradation, lack of maintenance or need to meet the current design requirements (i.e. Eurocodes). Replacing the deficient concrete structures in the near future with new one seems not a viable option as it would be prohibitively expensive. For this reason, a shift from new construction towards renovation and modernization has been witnessed in the European construction sector. In specific, between 2004 and 2013, about 50% of the total construction output (i.e. €305bn) being turnover on renovation and rehabilitation of existing structures (Tetta et al., 2015).

Over the last three decades, the use of fibre-reinforced polymer (FRP) for retrofitting concrete and masonry structures, has gain popularity over other conventional strengthening systems (such as steel/RC jacketing). This is due to the favourable properties offered by FRP such as: resistance to corrosion, high strength to weight ratio, ease and speed of application and minimal change in the geometry. However, some drawbacks have been observed with the use of FRP, which are mainly associated to the use of epoxy resins. These drawbacks including: high cost, unsafe for manual workers, low permeability to water vapour, and poor behaviour at high temperatures (Triantafillou and Papanicolaou, 2006).

Almost a decade ago, an innovative cement-based composite material, the so-called textile-reinforced mortar (TRM), was introduced in the field of structural retrofitting (Bournas et al., 2007) as an alternative solution to FRP, addressing some of FRP’s drawbacks. Since that time, TRM progressively attracts the interest of the structural engineering community. TRM is a composite comprising fibre rovings made of carbon, basalt or glass in form of textiles embedded into inorganic materials such as cement-based mortars. TRM is relatively low-cost materials (mortars are generally lower cost compared to epoxy resins), compatible with concrete or masonry substrates, friendly materials for manual workers, can be applied at low temperatures or on wet surfaces, and resistant at high temperatures (Tetta and Bournas, 2016). In the last few years, a significant number of studies have been directed towards investigating the effectiveness of TRM as a mean of external strengthening. The results have indicated that TRM is a promising alternative to FRP in retrofitting structures.

It is well known that the effectiveness of any externally bonded strengthening system in increasing the load-carrying capacity of concrete members depends primarily on the bond between that strengthening material and the member’s substrate. Therefore, the study of the bond behaviour between TRM materials and concrete is of crucial importance, because it helps understanding the complex mechanisms of transferring stresses from the textile reinforcement to the surrounding matrix and eventually to the concrete substrate. It is also a fundamental step towards the development of design models to be used in real strengthening applications.

1.2 Research Aim and Objectives

The aim of this PhD study is to provide comprehensive understanding on the bond behaviour between TRM and concrete substrates both at ambient and high temperatures. The current study also aims to evaluate the effectiveness of TRM in flexural strengthening of RC beams at ambient and high temperature. To achieve these aims, the following objectives were set:

1. To study experimentally the bond behaviour between TRM and concrete substrates at ambient temperature.
2. To examine experimentally, the bond between TRM and concrete substrates at high temperatures, and also to compare the bond performance of TRM versus FRP and concrete substrates at high temperatures.
3. To study experimentally the effectiveness of TRM in flexural strengthening of half-scale RC beams and to assess whether the existing FRP formulas can be used for predicting the stress developed in the TRM reinforcement.
4. To evaluate experimentally the effectiveness of TRM in flexural strengthening of half-scale RC beams subjected to high temperature.

1.3 Thesis Outline

This Thesis comprises eight chapters including the current introductory chapter. Chapter 2 describes TRM as a composite material, and the use of TRM for strengthening and seismic retrofitting of concrete and masonry members. In particular, a detailed presentation is made on the following: the relevant studies on the bond between TRM and concrete substrate, the flexural strengthening of RC beams with TRM, and the performance of TRM at high temperatures. Case studies of real application of TRM worldwide, and the contribution of this study to the current knowledge is also included in this chapter. Chapter 3 describes the materials used for strengthening, namely: the binding materials (cement mortar and epoxy resin); and the textiles used as external reinforcement. The experimental work performed to determine the tensile properties of the textiles reinforcement and; TRM composite are also presented in this chapter. Chapter 4 reports the experimental programme conducted to investigate the bond between TRM and concrete at ambient temperature (*paper published in Composite Part B: Engineering Journal*), whereas Chapter 5 includes the experimental work carried out to investigate the bond performance of TRM versus FRP and concrete at high temperatures (*paper published in Composite Part B: Engineering Journal*). Chapter 6 presents the experiment study carried out to investigate the flexural behaviour of RC beams strengthening with TRM at ambient temperature. In specific, the effectiveness of TRM versus FRP in flexural strengthening of RC beams (*paper published in the Journal of construction and building materials*) is described in the first section, whereas the second section of this chapter reports the experimental programme carried out to evaluate the effect of textile geometry on the performance of TRM in flexural strengthening of RC beams. Chapter 7 includes the experimental programme conducted to assess the effectiveness of TRM versus FRP in flexural strengthening of RC beams subjected to high temperature (*paper submitted to construction and building materials journal*). Finally, the main findings of this PhD study and the proposed direction for future research is presented in Chapter 8.

Chapter 2

LITERATURE REVIEW

ABSTRACT

In this chapter, TRM as a composite material is briefly described. The use of TRM for strengthening and seismic retrofitting of concrete and masonry members is also covered. A detailed presentation of the available experimental studies on the following topics is included:(a) the bond behaviour between TRM and concrete substrate, (b) the flexural strengthened of RC beams with TRM, and (c) the performance of TRM at high temperature.

Selected case studies of actual application of TRM to existing concrete and masonry structures are briefly reported. Finally, the contribution of the current study to the available knowledge on: (a) the bond between TRM and concrete at ambient and high temperatures, and; (b) the flexural strengthening of RC beams with TRM at ambient and high temperatures is summarised at the end of this chapter.

2.1 Introduction

Over the last decades, the issue of upgrading and rehabilitation of existing reinforced concrete (RC) infrastructure has become of great importance due to their continues deterioration. Fibre-reinforced polymers (FRP) has gain popularity as a means of external strengthening, however some drawbacks (see Section 1.1) which are mainly associated to the epoxy resins have limited the use of FRP.

To overcome these drawbacks, researchers have suggested to replace the organic materials (epoxy resins) with inorganic materials (such as modified cement mortar). However, due to granularity of cement mortars, the impregnation (wetting) of continues fibre sheets was difficult to achieve, hence, the bond has become an issue. To overcome that issue, it was suggested replacing the continuous fibre sheets by an open mesh configuration in the form of textiles, thus the bond condition between fibres and mortar could be improved. This new cement-based composite material is known as textile-reinforced mortar (TRM) (Bournas et al., 2007). TRM is a composite comprising high-strength fibres made of carbon, basalt or glass in form of textiles embedded into inorganic materials such as cement-based mortars. TRM is also identified in the literature with the following acronyms: Textile Reinforced Concrete (TRC) (Brameshuber, 2006b); and Fibre Reinforced Cementitious Matrix (FRCM) (Carloni et al., 2016).

The textiles used as a reinforcement typically consist of long woven, unwoven, or knitted rovings fabricated at least in two directions (typically orthogonal). Figure 2.1a-d shows photos of some types of textiles which were fabricated from different fibres' materials and geometries. As shown in this Figure, the quantity, materials, and spacing between rovings in both orthogonal directions can be controlled independently which resulted in textiles with different geometries and materials in the two orthogonal directions.

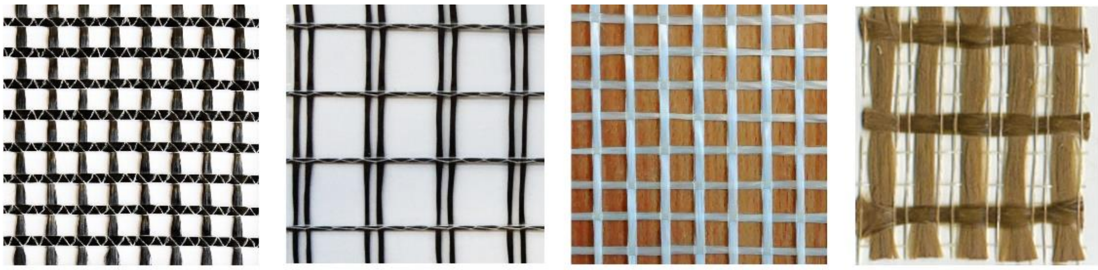

(a) (b) (c) (d)

Figure 2.1. Textile fibre reinforcements: (a) carbon-fibre textile; (b) basalt-fibre textile; (c) glass -fibre textile; and (d) PBO-fibre textile.

In the last decade, significant research effort has been put to take advantage of the use of textile cement-based composite materials for construction of new structural elements (Brameshuber, 2006a) or as a means of external strengthening of existing structures (Triantafillou and Papanicolaou, 2005). In the next sections, the experimental studies on the use of TRM as a means of external strengthening of concrete and masonry members are reported.

2.2 Using TRM for Strengthening and Seismic Retrofitting of RC and Masonry Members

This section presents the relevant experimental studies on the use of TRM as a means of external strengthening of concrete and masonry members subjected to static or cyclic loading. Indicative studies for each case of strengthening application are described in detail.

2.2.1 Confinement of RC columns with TRM

To begin with, Triantafillou et al. (2006); Bournas et al. (2007); Peled (2007); Ortlepp et al. (2010) studied the effectiveness of TRM as a means of confining reinforcement of concrete cylinders and short columns. In specific, Triantafillou et al. (2006) examined the effectiveness of TRM versus FRP in increasing the strength and deformation capacity of concrete cylinders (150 x 300mm) and short columns taking into account the number of layers as a parameter. It was mainly concluded that application of TRM substantially enhanced the strength and the deformation capacity. This enhancement was found to be sensitive to the number of layers. In terms of TRM versus FRP effectiveness, the results of short column tests indicated that TRM is 20 and 50% less effective than FRP in enhancing the strength and the deformability, respectively. Furthermore, Bournas et al. (2007) investigated the effectiveness of TRM versus FRP as a means of confining reinforcement of RC short columns. The experimental programme included testing of 15 RC short columns (with dimensions of 200x 200mm cross section and 380 mm high) subjected to concentric compression loading. They concluded that TRM is 10% less effective than FRP in improving the strength and deformation capacity of the tested columns.

TRM has also been investigated as a means of confining reinforcement of RC columns subjected to seismic loading (Bournas et al., 2007; Bournas et al., 2009; Bournas and Triantafillou, 2010; 2011; Bournas and Triantafillou, 2013; Ombres and Verre, 2015). In the study of Bournas et al. (2007), the effectiveness of TRM versus FRP as a means of seismic retrofitting of RC columns was evaluated. Three RC columns of 1.6 m length, and square cross section of 250 x 250 mm were strengthened and tested under cyclic uniaxial flexure. The results indicated that TRM jacket is as effective as the equivalent FRP jacket in enhancing the deformation capacity and energy dissipation. Moreover, Bournas et al. (2009) performed cyclic uniaxial flexural tests on 10 RC cantilever columns to assess the effectiveness of TRM versus FRP in enhancing the deformation capacity and energy dissipation. The effect of the internal reinforcement configuration, namely continuous or lap-spliced bar (short or long) was also assessed. The authors concluded that the effectiveness of TRM in improving the deformation capacity and energy dissipation depends on the configuration of the internal reinforcement; for continuous reinforcing columns, TRM jacket was 50% higher, equal and slightly less effective than the equivalent FRP jacket when the internal reinforcement was continuous, long lap- splice length, and short lap- splice length, respectively.

2.2.2 Strengthening of RC slabs with TRM

TRM was also assessed as a measure of enhancing the flexural capacity of one-way (Jesse et al., 2008; Schladitz et al., 2012; Loreto et al., 2013) and two-way RC slabs (Papanicolaou et al., 2009; Koutas and Bournas, 2016). In all of these studies TRM was found to be a promising strengthening system in increasing the load-carrying capacity of retrofitted slabs. In specific, Papanicolaou et al. (2009); Koutas and Bournas (2016) examined the effectiveness of TRM in increasing the strength and deformation capacity of two-way RC slabs. Different parameters were investigated, namely: the textile materials (carbon and glass fibres textile), and the number of TRM layers (Papanicolaou et al., 2009; Koutas and Bournas, 2016), the strengthening configurations (fully or partially covering of the tension face of the slab with TRM), and the presence of cracks in the slab (Koutas and Bournas, 2016). It was mainly concluded that application of TRM considerably enhanced the load-carrying capacity of the slabs. This enhancement was also found to be sensitive to the number of layers, but it was comparable to the textiles having approximately the same axial stiffness (Papanicolaou et al., 2009; Koutas and Bournas, 2016). It was also observed that the presence of cracks (pre-cracked slab) reduced slightly the effectiveness of TRM in increasing the load-carrying capacity compared to the un-cracked slab, and finally, the flexural capacity of fully covered face slab was higher than that of partially covered face slab (Koutas and Bournas, 2016).

2.2.3 Shear strengthening of RC beams with TRM

Triantafillou and Papanicolaou (2006) investigated the effectiveness of TRM as a means of shear strengthening of RC beams. Parameters examined were: the strengthening configuration (typical wrapping versus spirally applied), the number of strengthening layers (1 or 2), and the type of strengthening system (TRM versus FRP). For one layer strengthened beams, it was found that TRM jacket is 45% less effective than the equivalent FRP jacket but still effective in increasing the shear capacity of strengthened beam (providing 40 kN) compared to the control. Moreover, both 2 layers TRM and FRP jackets provided substantial gain to the shear capacity (more than 60 kN compared to the control) of strengthened beams, however, the effectiveness of TRM versus FRP and also the strengthening configuration (typical wrapping versus spirally applied) were not evaluated due to the failure of that beams in flexure.

2.2.4 Seismic retrofitting of masonry-infilled RC frames with TRM

Koutas et al. (2014) studied the potential of using TRM as a means of seismic retrofitting of nearly full scale three-story masonry infilled RC frame subjected to cyclic loading. The results of experimental test indicated that application of TRM enhanced the global response of the frame in terms of lateral strength (56% increase) and deformation capacity (52% increase) at the top of the frame compared to the unretrofitted frame.

2.2.5 Strengthening of masonry members with TRM

TRM was also used as a means of external strengthening of masonry walls for enhancing their in-plane (Papanicolaou et al., 2007; Papanicolaou et al., 2011) and out-of-plane (Papanicolaou et al., 2008; Harajli et al., 2010; Papanicolaou et al., 2011; Babaeidarabad et al., 2013) loading capacity. In particular, Papanicolaou et al. (2007) performed experimental work to examine the effectiveness of TRM in enhancing the in-plane behaviour (i.e. load carrying capacity and deformability) of masonry walls subjected to in-plane cyclic loading. Parameter investigated were: the strengthening systems (TRM versus FRP), the number of layers, and the level of applied compressive stress. The authors concluded that: (a) TRM system is 65-70% as effective as FRP system in increasing the strength of the masonry wall, but more effective (15-30%) in increasing the deformation capacity; and (b) in both TRM and FRP strengthening systems, increasing the number of strengthening layers resulted in considerable enhancement in the strength but reduction in the deformation capacity.

Furthermore, Papanicolaou et al. (2008) compared the effectiveness of TRM versus FRP in enhancing the out-of-plane flexural behaviour (in terms of strength and deformability) of masonry walls subjected to cyclic loading. It was mainly concluded that the effectiveness of TRM was controlled by the failure mode. In specific, if the failure was within the masonry wall, TRM system is much effective than FRP in increasing the strength and deformation capacity, but if the failure was in the strengthening materials (i.e. due to textile rupture), TRM was slightly less effective than the equivalent FRP. Harajli et al. (2010) assessed the out-of-plane flexural behaviour of masonry walls strengthened with TRM and subjected to static and cyclic loading. The results of static tests demonstrated the effectiveness of TRM in enhancing the out-of-plane load carrying capacity and deformation capacity.

Furthermore, the result of the cyclic loading showed that the TRM strengthened walls exhibited significant improvement in the strength, deformation, stiffness, and energy dissipation.

Finally, TRM was also used as a confining reinforcement of masonry columns. In particular, Ombres (2015b) measured the effectiveness of one and two layers of TRM as a means of confining reinforcement of masonry columns subjected to eccentrical loading (the eccentricity e/H varied between 0 to 0.2). It was found that the enhancement of the load carrying capacity of strengthened specimens was depending on the value of eccentricity. In specific, the ultimate load of strengthened column subjected to axial compression load was increased by 78% compared to the unretrofitted specimen, whereas, the corresponding ultimate load increase varied between 20 to 42.9% for those columns strengthened with one and two layers and subjected to eccentric load, respectively. Contrary to the failure mode of unretrofitted specimen which was sudden and brittle, the TRM retrofitted specimens failed gradually due to rupture of the textile fibres.

2.3 Bond between TRM and Concrete

As mentioned previously, the effectiveness of any external strengthening systems in transferring stresses substantially depends on the bond between the strengthening material and concrete substrate. The stresses transfer between TRM and concrete is a complex phenomenon depending on several factors including: (a) the bond between a single fibre and the matrix (Peled et al., 1998; Banholzer, 2004; Banholzer et al., 2006; Hartig et al., 2008; Zastrau et al., 2008; D'Ambrisi et al., 2013), (b) the degree of penetration of cement matrix into single roving (Peled et al., 1998; Banholzer, 2004; Hegger et al., 2004; Xu et al., 2004; Banholzer et al., 2006; Hartig et al., 2008; Zastrau et al., 2008; D'Ambrisi et al., 2013); (c) the nature of the bond between the external fibres and the internal fibres in a single roving (Hartig et al., 2008); (d) the bond between the new matrix and the old concrete substrate (Ortlepp et al., 2004; D'Ambrisi and Focacci, 2011). All the aforementioned factors are depending on: (a) the fibre surface condition (dry or coated) (Hegger et al., 2006; Peled et al., 2008; Aljewifi et al., 2010), (b) the geometry of: single fibre/ roving (Bentur et al., 1997; Peled et al., 1998; Peled et al., 1999), or textile (Bentur et al., 1997; Peled et al., 1997; Peled and Bentur, 1998; Peled and Bentur, 2000; Soranakom and Mobasher, 2009), (c) the composition of the matrix and the degree of grain fineness, and (d) the quality of concrete surface preparation (D'Ambrisi et al., 2013). Therefore, it is of crucial importance to study the bond behaviour between TRM and concrete in order to understand the factors affecting stresses transferring from the textile reinforcement to the matrix and eventually to the concrete substrate. In the next two sections, the test setups adopted, the analytical and experimental studies conducted to investigate the bond of TRM-to-concrete are described in detail.

2.3.1 Test setups for investigation the bond of TRM-to-concrete

Past studies on the bond of FRP-to-concrete have mainly adopted two distinct test setups namely, single-lap shear and double lap shear test setups (Yao et al., 2005). In the single-lap shear test (see Figure 2.2a), the FRP strip was externally bonded to a concrete block, and then a classical pull out test was performed on the FRP strip while the concrete block was fixed. In the double-lap shear test on the other hand (see Figure 2.2b), FRP strips are externally bonded on two opposite sides of two concrete prisms which are connected only by the FRP strips, and then a tensile force is applied up to failure.

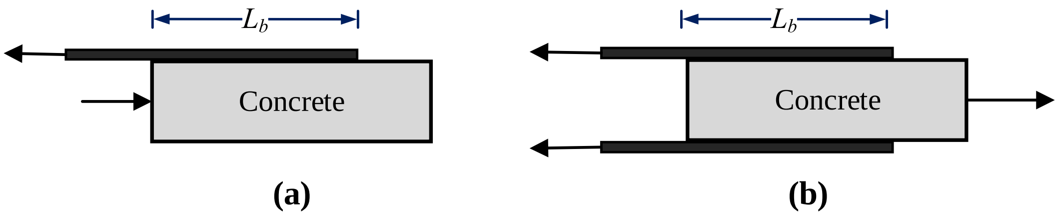

Figure 2.2. Bond test setups: (a) single-lap shear test; and (b) double-lap shear test (Yao et al., 2005).

Sneed et al. (2015) compared the results obtained from single-lap and double-lap shear tests conducted on one layer of PBO-TRM. It was mainly found that: (a) both, the single and double-lap setups can be used to investigate the bond between TRM and concrete, (b) the ultimate load measured form the double-lap shear test was slightly less than the load measured from the single-lap shear test of the identical specimen, (c) the results obtained from the double-lap shear tests is less scattered compared to those obtained from single-lap shear tests, and finally, (e) the shape of load response (up to the ultimate load) and the observed failure mode obtained from both tests were identical.

Undoubtedly, the stresses transferred from concrete to the composite materials in real strengthened RC beams is best simulated by bending tests of full-scale beams. However, such tests are expensive and time consuming. Therefore, the single and double-lap bond tests which is simple, economic, fast, and offer less bond strength compared to the bending test were adopted in the previous research to perform parametric study. Among these two test setups, the double-lap shear test is preferable due to its simplicity (Yao et al., 2005); symmetry and better control of normal stresses (Serbescu et al., 2013); and less scattered of the measured ultimate loads (Sneed et al., 2015).

Thus, the double-lap shear test setup which is a modification of the set-up proposed by Serbescu et al. (2013) was adopted in the current study to investigate the bond of TRM-to-concrete. The selection of this test setup was also deemed necessary for testing more than one TRM layers, as with such a set up the stresses are transferred from the concrete to the composite material indirectly, simulating realistically real-word applications. In contrast, in single-lap tests the load is applied directly to the composite material, which means that shear stresses between layers cannot be developed in case of more than one TRM layer.

2.3.2 Bond between TRM and concrete; analytical and experimental studies

The bond between TRM and concrete has been analytically analysed in order to suggest a model for predicting important parameters which can be used for design. In specific, Ortlepp et al. (2006); and D'Ambrisi et al. (2012) analysed the bond between PBO-TRM and concrete using local bond-slip relations. The models were calibrated using the results of the experimental work conducted by the authors. The proposed models allowed for the evaluation of several parameters which are important in the design of the strengthening. These parameters include, the ultimate bond strength and the effective bond length. However, these models are valid only for the tested types of mortar and fibres.

In the next paragraphs, the experimental studies that focused on the bond between TRM and concrete substrate are described in detail. A summary of the main findings of these studies is also presented at the end of this section.

The first experimental study on the bond between TRM and concrete was that of D'Ambrisi et al. (2013). In that study, double-lap shear tests were carried out on twelve specimens strengthened with PBO-TRM. The test specimen comprised two concrete prisms (with cross section of 100 x 100 mm and length of 250 mm for each prism) which were connected only by PBO-TRM. The parameters investigated were: the bond length (50, 100, 150, 200, and 250 mm), and the number of layers (1, and 2 layers). The following conclusions were drawn: (a) by increasing either the bond length or number of layers, the ultimate load was also increased, (b) the dominant failure mode regardless the number of layers or the bond length was slippage of the fibres through the mortar; and (c) an effective bond length which varied between 250-300 mm was suggested.

D'Antino et al. (2014) and Sneed et al. (2014) conducted single-lap shear tests to investigate the bond behaviour of one layer of PBO-TRM-to concrete. The test specimen had a cross section of 125 mm x 125 mm, whereas the specimen's length was either 375 or 515 mm depending on the tested bond length. The investigated parameters were: the bond length (100, 150, 250, 330, and 450 mm), and the bond width (34, 60, 43, and 80). It was mainly observed that: (a) the failure mode was slippage of the fibres through the mortar, (b) the bond width had no effect on the tensile stress in the textile reinforcement, and (c) the effective bond length was approximately 260 mm. Furthermore, D'Antino et al. (2014) performed twenty single-lap shear bond tests to investigated the effect of textile materials on the load response and failure mode. The textile reinforcement used were carbon, glass and steel fibres textiles. The results showed that the ultimate load was sensitive to the textile fibres materials. In specific, the carbon and steel textile strengthened specimens had the highest load followed by the glass fibres textile strengthened specimens. The failure mode was also sensitive to the textile materials. In particular, it was slippage of the fibres through the mortar for the carbon fibres textile strengthened specimens, whereas, it was debonding of the composite at the concrete-matrix interface for the steel textile retrofitted one and rupture of the textile fibres for the glass textile reinforced specimens.

Tran et al. (2014) performed twelve single-lap shear tests on PBO-TRM bonded to concrete prisms. Key investigated parameters were: the bond length (250, 300, 350, and 400 mm) and the concrete compressive strength (31, 39 and 41 MPa). The outcomes of this study were: (a) the effective bond length was approximately 250 mm, (b) the failure mode was debonding at the textile-matrix interface, and (c) the concrete compressive strength had very limited effect on the ultimate load, in particular, the high concrete strength specimen failed at slightly higher load.

Awani et al. (2015) conducted Twenty-seven double-lap shear tests to examine bond between carbon-TRM and concrete. The binding materials (cement mortar and epoxy resin), and the bond length (75, 100, and 150 mm) were the main highlighted parameters. The authors observed that: (a) the failure mode of TRM strengthened specimens was slippage of the fibres through the mortar, whereas the corresponding failure mode of the FRP strengthened specimens was rupture of the fibres, (b) the stress-strain curves of the TRM specimens showed bi-linear behaviour due to presence of cracks in the mortar, whereas, the corresponding stress-strain curves of the FRP specimens was linear up to failure, and (c) the measured ultimate load for TRM specimens was 28% lower than the corresponding ultimate load recorded for the equivalent FRP strengthened specimens.

D'Antino et al. (2015) assessed the effect of concrete surface preparation (untreated and treated with sandblasting), and the concrete compressive strength (33.5, and 26.9 MPa) on the bond of PBO-TRM-to-concrete. Twenty-one specimens with different bond length (330, and 450 mm), and bond width (60, and 80 mm) were tested under single-lap shear. It was observed that the failure mode was partially affected by the concrete surface condition; specifically, four out of eighteen specimens had untreated concrete surface failed due to debonding of the whole or part of the composite from concrete substrate due to the poor bond at that interface, whereas, the failure of the remaining fourteen specimens was identical (slippage of the fibres through the mortar) to the corresponding specimens that had the same bond length but with a treated concrete surface. It was also found that the concrete compressive strength had no effect on the measured ultimate load.

Finally, Ombres (2015a) analysed the effect of the bond length (150, 200, and 250 mm) and the number of layers (1 and 2 layers) on the bond behaviour (between TRM and concrete) in terms of ultimate load and failure mode. Twelve specimens were fabricated, strengthened with PBO-TRM and test under single-lap shear test. The author concluded that: (a) by increasing either the number of layers or the bond length, the failure load increased in non-proportional way, (b) the influence of the number of layers on the ultimate load was more pronounced than the bond length, and (c) the failure mode was sensitive to the number of layers; in specific, it was slippage of the fibres through the mortar for the one layer strengthened specimens, whereas, it was debonding of TRM at the concrete-mortar interface without including parts of concrete cover for the two layers retrofitted specimens.

To sum up, the main investigated parameters of the aforementioned studies were: the number of layers (1 and 2), the bond length (50-450 mm), the textile materials mainly PBO, and rarely carbon and glass fibres textiles, the concrete compressive strength, and the concrete surface preparation (treated and untreated with sandblasting). The main findings were: (a) the effective bond length varied between 200-300 mm, (b) the common failure mode was slippage of the fibres within the mortar except form (Ombres, 2015a) who concluded that increasing the number of layers from

1 to 2 alters the failure mode from slippage to debonding at the mortar-concrete interface without including parts of concrete cover, (c) the concrete compressive strength (Tran et al., 2014; D'Antino et al., 2015) and the concrete surface preparation (D'Antino et al., 2015) had very limited effect on the bond capacity. However, the conclusion in (c) was based on very limited number of specimens in which the failure was within the composite due to slippage, hence the concrete compressive strength and the concrete surface condition were not involved in that failure. Finally, it is noted that data is missing on: the influence of the number of layers beyond two, the textile surface condition (i.e. dry versus coated), and the concrete compressive strength if the failure was within the concrete cover on both the load response and failure mode.

2.4 Flexural Strengthening of RC Beams with TRM

The flexural capacity of RC beams is one of the most critical requirement when assessing the serviceability of beams in real structures. Due to corrosion of internal reinforcement, deterioration of concrete strength induced aging or environmental conditions, or the need to increase in the applied load, the external strengthening is becoming progressively needed. In the next paragraphs, the available experimental studies on the flexural strengthening of RC beams with TRM are described in detail. A summary of the main finding is also presented at the end of this section.

The first study on the flexural strengthening of RC beams with TRM was carried out by Triantafillou and Papanicolaou (2005). In this study, the effectiveness of TRM versus FRP in increasing the flexural capacity of RC beams was compared. A high strength carbon fibres textile was used as a reinforcement for the strengthened beams. It was found that TRM system is 30% less effective than FRP system in increasing the flexural capacity of RC beams. Moreover, the failure mode of the FRP strengthened beam was due to rupture of the fibres, whereas, the corresponding failure mode of the counterpart TRM-strengthened beam was due to interlaminar debonding.

D'Ambrisi and Focacci (2011) studied the flexural behaviour of Twenty-five RC beams strengthened with TRM. Key investigated parameters were: the number of TRM layers (1, 2, and 4), the textile fibres materials (carbon, and PBO) and the type of matrices (two commercial cement mortars). It was concluded that: (a) increasing the number of layers resulted in enhancement in the flexural capacity of the strengthened beams, (b) the performance of TRM in increasing the flexural capacity was strongly affected by the cement matrix design, (c) different textile materials resulted in different flexural capacity increases, and, (d) different failure modes were observed including: slippage of the fibres through the mortar, debonding of TRM due to fracture the surface at the concrete-mortar interface, and debonding at textile-mortar interface.

In Ombres (2011), the effectiveness of PBO-TRM in increasing the flexural capacity of RC beams was evaluated whereas, in Ombres (2012) the debonding behaviour of PBO-TRM strengthened beams was analysed. Parameters examined were: the number layers (1, 2, and 3) Ombres (2011; 2012), the ratio of internal reinforcement (Ombres, 2011), and the bond length of TRM (applied to the entire length of beams, and only at the constant moment zone) (Ombres, 2012). It was observed that: (a) application of TRM resulted in flexural capacity increases varying between 10-44 % depending on the ratio of internal reinforcement (Ombres, 2011), and the number of layers (Ombres, 2011; 2012), (b) the failure mode of strengthened beams was sensitive to the number of layers and the provided bond length. In particular, it was slippage of the fibres through the mortar for the 1 layer strengthened beam, whereas it was debonding at the concrete-matrix interface for the two and three layers retrofitted beams (Ombres, 2011). Finally, providing TRM along the entire length of the beams resulted in gradual failure, whereas, a sudden and catastrophic failure was observed when providing inadequate bond length (Ombres, 2012).

Elsanadedy et al. (2013) examined the effectiveness of basalt-TRM in increasing the flexural capacity of RC beams. The type of mortar (polymer modified cement versus cementitious mortar), the number of layers (5 and 10 layers), and the strengthening systems (TRM versus FRP) were parameters under investigation. The results showed that the polymer modified cement mortar exhibited higher performance in enhancing the flexural capacity than the cementitious one. Particularly, the specimen that received the former failed due to textile rupture, whereas the counterpart specimen that received the latter failed due to end debonding. When applying ten layers of basalt textile, the flexural capacity was increased by 90%. Finally, TRM was less effective than FRP in enhancing the flexural capacity, but more effective in increasing the deformation capacity.

Yin et al. (2013) studied the effect of the number of TRM's layers (1, 2, and 3) and the textile surface condition on the flexural performance of RC beams. The textile used was hybrid comprising carbon fibre rovings in the direction of loading and glass fibre rovings in the transversal direction. Prior to strengthening, the textile surface was treated by: impregnation with epoxy, impregnation with epoxy and adhering fine and coarse sand on the textile surface. The results showed that increasing the number of layers from 1 to 3, resulted in flexural capacity enhancement varied from 10% to 45%. Adhering the sand to the textile had a very limited effect on the textile effectiveness in increasing the flexural capacity of the beams.

Babaeidarabad et al. (2014) studies the effectiveness of BPO-TRM in increasing the flexural capacity of RC beams. The number of layers (1 and 4 layers) and the concrete compressive strength (29.1 MPa and 42.9 MPa) were the main examined parameters. The results showed that the flexural capacity increase was sensitive to the number of layers and the concrete compressive strength. In particular, the flexural capacity increase of the low concrete strength retrofitted beams varied between 32 and 92%, whereas, the corresponding increase of the high concrete strength retrofitted beams varied between 13 and 73 % for 1 and 4 layers, respectively.

Finally, Ebead et al. (2016) investigated the influence of: (a) the internal reinforcement ratio (ρ_s= 0.72% *and* ρ_s= 1.27%), (b) the type of textile materials (carbon and PBO fibres textile), and (c) the number of layers (1, 2, and 3) on the effectiveness of TRM in enhancing the flexural capacity of RC beams. The results showed that different textile materials and number of layers resulted in different flexural capacity increases. Particularly, the gain in the flexural capacity of carbon-TRM strengthened beams varied between 14 and 77%, whereas the corresponding enhancement in PBO-TRM strengthened beams varied between 8 and 27%. Furthermore, two failure modes were observed depending on the number of layers: the beam strengthened with 1 and 2 layers failed due slippage of the fibres through the mortar, whereas the beams strengthened with 3 layers of carbon-TRM failed due to delamination of TRM from concrete substrate without including concrete cover.

To sum up, the investigated parameters in these studies were: the textile-fibre materials, the number of layers, the strengthening configuration, the concrete compressive strength, the type of textile-fibre materials, and the strengthening system (i.e. TRM versus FRP). The main conclusions were: (a) application of TRM to RC beams considerably enhanced their flexural capacity; (b) increasing the number of layers enhanced the flexural capacity and altered the failure mode (Ombres, 2011; Ebead et al., 2016). Regarding the effectiveness of TRM versus FRP, Triantafillou and

Papanicolaou (2005) reported on the basis of two specimens, that TRM was 30% less effective than FRP. Whereas, Elsanadedy et al. (2013) found that TRM was slightly less effective than FRP in increasing the flexural capacity but more effective in enhancing the deformation capacity. This conclusion was made based on two tested specimens, one with five layers of TRM in form of U-shaped jacket made of basalt-fibre textile and another retrofitted with one layer of basalt FRP. Based on the above studies, it is clear that more research is needed to cover the subject of the effectiveness of TRM versus FRP in flexural strengthening of RC beams.

2.5 Performance of TRM at High Temperatures

As mentioned previously, some drawbacks have been observed with the use of FRP system mainly the poor performance at high temperature, as under loading, epoxy resins normally lose their tensile capacity. Therefore, unless protective (thermal insulation) systems are provided (Kodur et al., 2006), the bond strength between the FRP and concrete substrate significantly deteriorates at temperatures above the glass transition temperature (T_g). A review on the behaviour RC members strengthened with FRPs and subjected to fire or high temperature was recently conducted by Firmo et al. (2015b).

TRM could outperform FRP systems at high temperatures or fire due to the breathability, non-combustibility, and non-flammability offered by mineral-based cement mortars used as binding materials. In general, research on the performance of TRM systems at high temperature or under fire scenario and comparison with FRP systems is extremely limited. This is attributed to the inherent experimental difficulties applying simultaneously loading and high temperature, even for medium or small-scale specimens. For this reason, the past studies have mainly focused on determination of the residual strength of TRM coupons after being exposed to high temperatures and cooled down to the ambient temperature. In the next paragraphs, the relevant literature on the behaviour of TRM at high temperatures is summarised.

Colombo et al. (2011); de Andrade Silva et al. (2014); Rambo et al. (2015) performed uniaxial tensile tests on TRM coupons made of one layer of glass fibres textile (Colombo et al., 2011), one layer of carbon fibres textile (de Andrade Silva et al., 2014), and 1, 3, and 5 layers of basalt fibres textile (Rambo et al., 2015). The test procedure included the following steps: (a) exposure to elevated temperatures of 20, 200, 400, and 600 ^{0}C (Colombo et al., 2011); 20, 100, 150, 200, 400, and 600 ^{0}C (de Andrade Silva et al., 2014); and 20, 75, 150, 200, 300, 400, 600, and 1000 ^{0}C (Rambo et al., 2015); (b) keeping the specimens at those temperatures for: 2 hrs (Colombo et al., 2011), 3 hrs (de Andrade Silva et al., 2014), and 1 hr (Rambo et al., 2015) (stabilizing phase); (c) cooling down to the ambient temperature; and (d) applying a uniaxial tensile load up to failure. The main conclusion of these studies was that TRM coupons maintained their ambient tensile strength at high temperatures up to 200 ^{0}C (Colombo et al., 2011; de Andrade Silva et al., 2014), and 150 ^{0}C (Rambo et al., 2015). However, above these temperatures, the residual tensile strength was gradually decreased with the increase of temperature due to the deterioration of tensile strength of the textile fibres themselves.

Ombres (2015a), examined the bond between TRM and concrete at elevated temperatures. Parameters investigated were the number of PBO-TRM layers (1, and 2 layers), and the exposed temperature (50, and 100 ^{0}C). The specimens were firstly exposed to predefined temperatures (50 and 100 ^{0}C) for 8 hrs, cooled down to the ambient temperature, and then subjected to single-lap shear test. It was found that the bond between TRM and concrete was significantly affected from the elevated temperatures. Particularly, the ultimate load was dropped (compared to the ambient load) by 0%, and 36% for one layer; and 28%, and 38% for two layers strengthened specimens when subjected to 50, 100 ^{0}C, respectively.

Regarding the performance of TRM versus FRP at high temperatures, the only studies reported in the literature on the effectiveness of TRM versus FRP at high temperature were that of Tetta and Bournas (2016) and Bisby et al. (2013). In Tetta and Bournas (2016), the effectiveness of TRM versus FRP in shear strengthening of half-scale rectangular beams and full-scale T-beams at high temperatures was compared. The investigated parameters were: the temperature at which the specimens were exposed (20 ^{0}C, 100 ^{0}C, 150 ^{0}C and 250 ^{0}C), the number of strengthening layers (2 and 3), and the strengthening configuration. The results indicated that TRM jackets had far better performance in increasing the shear capacity of strengthened beams at high temperature than FRP jackets which totally lost effectiveness when subjected to temperature above T_g. Finally, in Bisby et al. (2013), FRP and TRM flexurally retrofitted beams were subjected to a sustained load and then exposed to increasing high temperature up to failure. In those specimens, the end anchorage zones were kept cold assuming that the debonding at this zone due to high temperature is prevented by a mechanical means. It was concluded that both strengthening systems (TRM and FRP) can have the same performance at high temperature if the anchorage zones of the beams were kept cold. However, in that study, the effect of high temperature on the debonding mechanism was not addressed because the bond condition was not realistically simulated due the cold anchorage zones. Hence, the effectiveness of the strengthening materials in increasing the flexural capacity of beams subjected to high temperature was not adequately evaluated.

2.6 Real Applications of TRM: Selected Case Studies

In the last decade, TRM has been successfully used worldwide for strengthening and seismic retrofitting of concrete and masonry structures. Selected case studies of real applications of TRM in the construction field can be found in Bournas (2016). In the next paragraphs, examples of those case studies are summarised.

The first case of real application of TRM as a mean of external strengthening was that of the San Siro stadium (Italy 2003). A TRM composite made of high strength carbon fibres textile was used for retrofitting of RC beams in order to increase their flexural and shear capacities (Figure 2.3).

(a) (b)

Figure 2.3. (a) Application of U-shaped TRM jacket; and (b) application of the external layer of cement mortar.

Other examples of real applications of TRM for retrofitting of concrete structures can be summarised as follows:

- Flexural strengthening of RC slabs, and shear reinforcement of unreinforced masonry walls of school building in Karystos, Greece (2007) using carbon-TRM.
- Confinement of RC bridges piers in Novosibirsk, Russia (2007) using PBO-TRM.

- Retrofitting of the cooling towers of The Niederaussem Power Station in Germany (2012) using PBO-TRM.

As mentioned previously, TRM has also been used for retrofitting of masonry structures, examples of these structures as follows:

- Strengthening and seismic retrofitting of the historical San Roque Church located in Spain (2008) which experienced an earthquake that induced an out of plane separation of the exterior walls.
- Retrofitting of masonry chimney with a total height of 38m and diameter ranging from 3.6 m at the bottom to 1.7 m at the top. This chimney located in Gerardmer, France, represents symbol of industrial heritage. Carbon TRM was selected for strengthening where it was applied in the vertical and transversal directions of the chimney.
- Strengthening of the main dome of the Molla Celebi Mosque in Turkey (2013) using four layers of basalt TRM.

2.7 Contribution of this Study

TRM is a new strengthening material and more experimental studies are required to better understand its behaviour. Based on the literature survey, the following points can be highlighted:

1. It is obvious from the literature survey described in Section 2.3 that the bond between TRM and concrete has not covered adequately yet. In particular, the main focus of the previous studies was on PBO textile fibres with the maximum number of layer being equal to two. The common conclusion was that the failure occurred within the composite materials due to slippage of the fibres through the mortar. Contrary to the failure mode observed in FRP which is often debonding from

concrete substrate. Thus, Chapter 4 of this PhD Thesis examines systematically a great variety of parameters the majority of them were not investigated previously including: (a) the number of TRM layers from 1 to 4, which is beyond the current limit of two, (b) the bond length (50-450 mm), (c) the concrete surface preparation, (d) the concrete compressive strength, (e) the coating of the textile, which has not been investigated before in comparison with uncoated textiles, and (f) the anchorage of tested bond length through wrapping with TRM jackets (see Chapter 4), which is again a parameter investigated for the first time.

2. Research on the bond between TRM and concrete at high temperatures is very scarce. The only available study (see Section 2.5) is that of Ombres (2015a) which was built on a very limited set of high temperatures (only 50 and 100 ^{0}C) where the specimens were cooled down, thus the bond behaviour was not evaluated realistically. For that reason, Chapter 5 of this PhD Thesis examines experimentally for the first time the bond between TRM and concrete at high temperatures in realistic way by applying simultaneously high temperatures and loading, and also compares for the first time the bond between TRM versus FRP and concrete at high temperatures. Parameters investigated were: (a) the strengthening systems (TRM versus FRP); (b) the number of layers (3 and 4 layers) which is beyond the current limit of 2 layers; (c) the level of high temperatures (up to 500 ^{0}C) which is beyond the current limit of 100 ^{0}C; and (d) the loading condition which is again a parameter investigated for the first time.
3. More research is needed to cover the subject of the effectiveness of TRM in flexural strengthening of RC beams and comparison with the corresponding effectiveness of FRP. This PhD study (in Chapter 6) provides a fundamental understanding on the flexural behaviour of RC beams strengthened with TRM by

testing 22 half-scale RC rectangular beams and investigating wide range of parameters comprising: (a) the strengthening system (TRM versus FRP); (b) the number of layers; (c) the textile surface condition (dry versus coated) which was not studied before; (d) the textiles material; (e) the end-anchorage system of the external reinforcement; and (f) the textile geometry which is a parameter not studied before .

4. The only available study in the literature on the effectiveness of TRM versus FRP in flexural capacity of RC beams at high temperature is that of Bisby et al. (2013). However, in that study, the effectiveness of TRM versus FRP was not evaluated adequately due the cold anchorage zones as described in Section 2.5. Chapter 7 of this PhD Thesis investigates for the first time the effectiveness of TRM versus FRP in flexural strengthening of RC beams subjected simultaneously to high temperature and loading, without protecting the TRM and FRP anchorage zones from high temperature. The following parameters were examined for the first time: (a) the strengthening materials (TRM versus FRP); (b) the number of strengthening layers (1, 3, and 7); (c) the textiles material (carbon, glass and coated basalt); (d) the textile surface condition (dry versus coated) of carbon-fibre textiles and (e) the end-anchorage of the main FRP/TRM reinforcement.

Chapter 3

MECHANICAL CHARACTERISATION OF MATERIALS USED FOR STRENGTHENING

ABSTRACT

This chapter describes the materials used for strengthening, namely: the binding materials (cement mortar and epoxy resin used as bonding agents for specimens that received TRM and FRP, respectively), and the textiles used as external reinforcement. It is also report the experimental work carried out to determine the mechanical properties of the textile reinforcements used for strengthening. Firstly, the tensile properties of bare textiles, namely, the ultimate tensile stress, the ultimate tensile strain and the modulus of elasticity were obtained by conducting uniaxial tensile tests on coupons made of one layer. Secondly, the tensile properties of TRM coupons made of one and two layers were also determined through uniaxial tensile tests. Finally, the tensile properties of FRP were also obtained through tensile tests performed on FRP coupons made of one layer. A summary of the findings is presented at the end of this chapter.

3.1 Cement Mortar

The matrix used for specimens retrofitted with TRM was an inorganic modified cement mortar comprising cement and polymers. The ratio of cement to polymers is 8:1 by weight, whereas, the water cement ratio was 0.23:1, resulting in a mix with a very good workability and plastic consistency. The flexural and compressive strength of the mortar were experimentally obtained on the day of testing. The test was conducted according to BS EN 1015-11 (1999) on three standard mortar prisms with dimensions of 40x40 mm cross section and 160 mm length.

It is generally recommended that the cement matrix should meet the following requirements: no shrinkage; high level of workability so as to allow for using a trowel during application; high viscosity in order to facilitating the application of mortar on overhead surfaces; and slowly rate of losing workability which allows for application the mortar layer while the previous one is still in a fresh state (Triantafillou, 2011).

3.2 Epoxy Resin

For those specimens strengthened with FRP system, a commercial epoxy resin (Sikadur® 330) was used as a binding material. This epoxy consisted of two epoxy parts, the mixing ratio of these two parts was 4:1 by weight. According to the product datasheet, the tensile strength, modulus of elasticity, and the glass transition temperature (T_g) of this adhesive was 30 MPa, 3.8 GPa, and 68 ^{0}C, respectively.

3.3 Textile Fibre Materials

Seven different types of textile fibre materials were used in this study as means of external reinforcement. Three of them were fabricated with fibre rovings (made of the same fibres materials) distributed equally in two orthogonal directions, namely: dry carbon_ fibre textiles (C), coated basalt_ fibre textile (BCo), and dry glass_ fibre textile (G) (Figure 3.1). Details of the textiles, such as mesh size, weight, density, equivalent thickness, tensile strength and modulus of elasticity (according to the manufacturer datasheets) of each textile material, are also given in Figure 3.1. It is noted that the textile fibres thickness (t_f) in each direction was calculated based on the equivalent smeared distribution (the ratio of areal weight to density) of fibres.

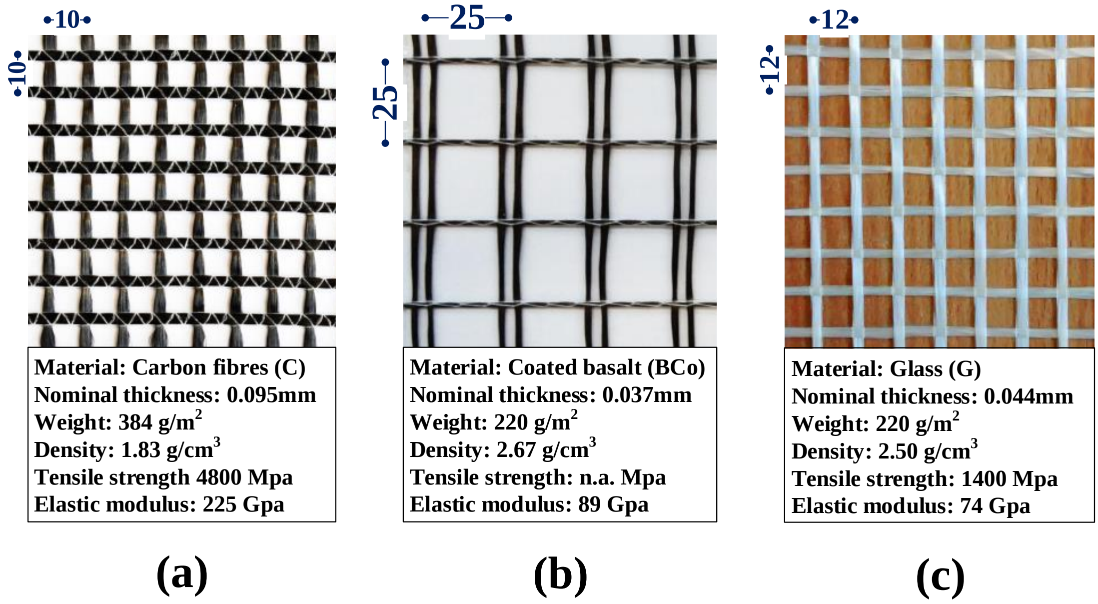

Figure 3.1. Textile made of equal fibre rovings distributed equally in two orthogonal directions: (a) carbon fibres textile (C); (b) coated basalt fibres textile (BCo); and (c) dry glass fibres textile (G), (dimensions in mm).

The dry carbon fibres textile was coated using low viscosity two-part epoxy resin in order to investigate the effect of textile surface condition (dry versus coated carbon fibre textile) on the performance of the textile. The acronym used for the coated carbon fibres textile is CCo. The procedure for application of coating included, impregnation the textile with low viscosity epoxy resin using a plastic roll and leaving the textile for two days (prior to use) at the ambient temperature for curing. According to the manufacturer data sheets, the tensile strength and the modulus of elasticity of the adhesive used for coating were equal to 72.4 MPa and 3.18 GPa, respectively.

The remaining four types of textiles were hybrid and fabricated (by a UK company) using two different types of fibre materials in the two-orthogonal directions. The longitudinal direction (direction of loading) comprising carbon fibre rovings, whereas, the transversal direction consisting of glass fibre rovings (Figure 3.2a-d). All four types of the hybrid textiles had the same quantity of carbon fibres in the direction of loading compared to the dry carbon fibre textile (i.e. C). The only difference was the spacings between rovings; in specific, two hybrid textiles had the same area/distance (i.e. 10 mm) of the carbon rovings in the loading direction compared to the dry carbon textile (C), whereas, the remaining two had double spacing (i.e. 20 mm)/area of the carbon rovings in the loading direction compared to the dry carbon fibres textile. The transversal rovings on the other hand, comprising glass fibres with two different spacing between rovings, namely, 20 and 40 mm which resulted in textile geometries with the following acronyms and details:

- F10x20: Hybrid textile had 10 mm spacing between the longitudinal carbon rovings and 20 mm spacing between the transversal glass rovings (Figure 3.2a).
- F10x40: Hybrid textile had 10 mm spacing between the longitudinal carbon rovings and 40 mm spacing between the transversal glass rovings (Figure 3.2b).
- F20x20: Hybrid textile had 20 mm spacing between the longitudinal carbon rovings and 20 mm spacing between the transversal glass rovings (Figure 3.2c).
- F40x40: Hybrid textile had 20 mm spacing between the longitudinal carbon rovings and 40 mm spacing between the transversal glass rovings (Figure 3.2d).

The weight, density, nominal thickness, and modulus of elasticity of the carbon fibres in the loading direction for all four types of the hybrid textiles were the same and equal to 174 g/m^2, 1.83 g/m^3, 0.095 mm, and 225 GPa, respectively (according to the manufacturer datasheets).

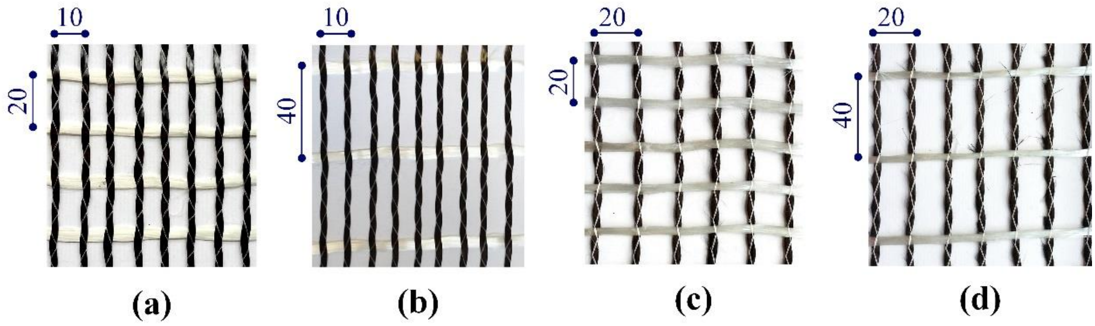

Figure 3.2. Geometry of hybrid textiles used in this study: (a) F10x20; (b) F10x40; (c) F20x20; (d) F20x40, (dimensions in mm).

3.4 Tensile Tests on Bare Textiles

Uniaxial tensile tests were conducted on coupons comprised one layer of bare textile in order to determine their tensile properties in the direction of loading. Three identical coupons with dimensions of 380 mm clear length and 50 mm width were tested for each type of textile materials. The test was carried out using a universal testing machine of 50-kN capacity (Figure 3.3a). The specimens were gripped to the testing machine using two aluminium plates (with dimensions of 60 mm long and 50 mm width) that were glued to their ends using a low viscosity epoxy resin. An extensometer was mounted at the centre of the coupons over a gage length of 160 mm to measure the tensile strain (Figure 3.3a). The load was applied monotonically under displacement control at a rate of 2 mm/min up to failure. All textiles coupons failed due to rupture of the fibres at the central region of the coupon within the gauge length of the extensometer, examples of failed specimens are provided in Figure 3.3b.

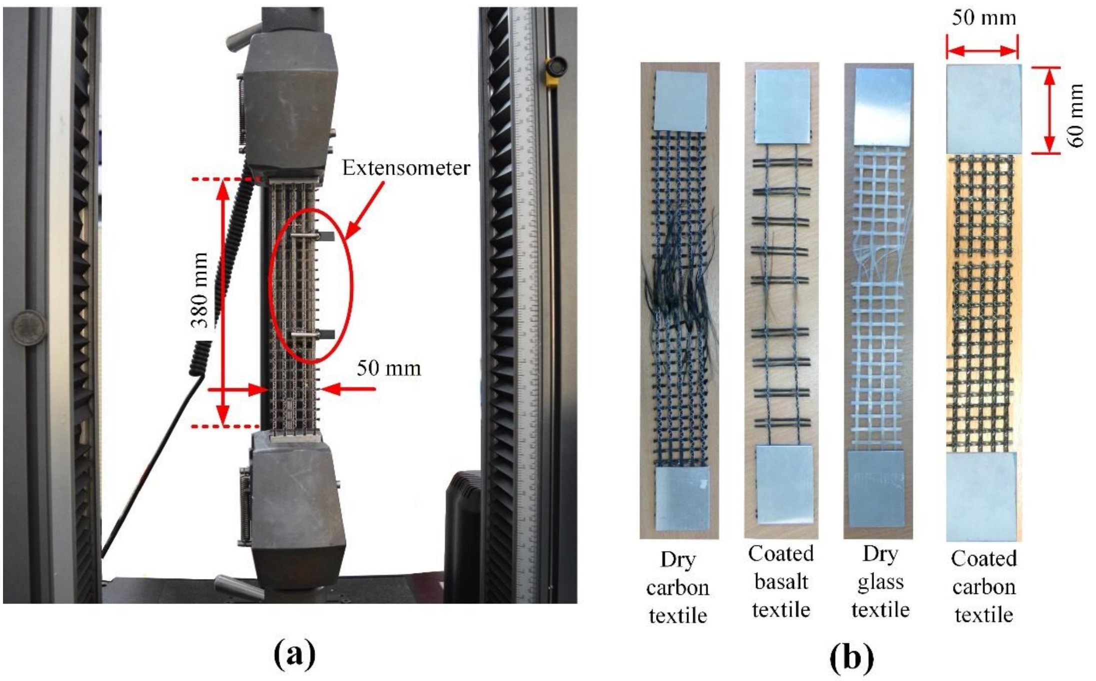

Figure 3.3. (a) test setup; and (b) failure mode of the textile fibre coupons (rupture of the textile fibres).

The results of the tensile tests are presented in Figure 3.4a and b in form of stress-strain curves. Figure 3.4a shows the stress-strain curves of the dry carbon, coated carbon, coated basalt and dry glass fibres textiles, whereas, Figure 3.4b depicts the corresponding stress-strain curves of all four types of the hybrid textiles. As shown in both Figures, the behaviour of the stress-strain curves for all textiles is linear up to failure.

Table 3.1 summarises the tensile properties of the textile fibres namely: the ultimate tensile stress (f_{fu}), the ultimate tensile strain (ε_{fu}) and the modulus of elasticity ($E_{f,tex}$). It is noted that the ultimate tensile stress was calculated by dividing the maximum measured load to the cross-sectional area of the textile fibres (b_f*t_f), where b_f is the textile width (50 mm) and t_f is the nominal thickness of the textiles in the direction of loading (see Figure 3.1). The modulus of elasticity ($E_{f,tex.}$) was calculated by dividing the ultimate tensile stress (f_{fu}) to the corresponding ultimate tensile strain (ε_{fu}) because the behaviour of the textile is linear up to failure (see Figure 3.4a and b).

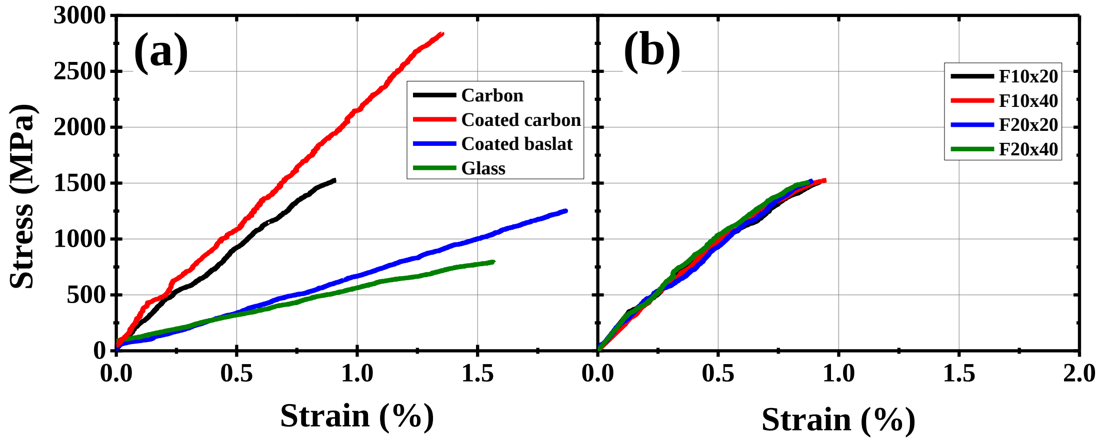

Figure 3.4. Stress-strain curves: (a) dry and coated carbon, coated basalt and glass fibre textiles, and (b) all four types of the hybrid textiles.

Table 3.1. Tensile properties of the bare textile reinforcment coupons.

Textile name	f_{fu} (GPa)	ε_{fu} (%)	$E_{f,tex.}$ (GPa)
C	1527 (7)*	0.911 (0.03) *	167.6 (4.8) *
CCo	2842 (19) *	1.361 (0.04) *	208.8 (5.6) *
BCo	1162 (47) *	1.867 (0.02) *	64.1 (3.2) *
G	760 (20) *	1.636 (0.05) *	47.3 (1.75) *
F10x20	1513 (13) *	0.927 (0.04) *	163.2 (8.9) *
F10x40	1527 (19) *	0.948 (0.03) *	166.1 (11.3) *
F20x20	1522 (14) *	0.893 (0.05) *	170.4 (7.6) *
F20x40	1508 (24) *	0.874 (0.06) *	172.5 (11.1) *

*Standard deviation in parenthesis

3.5 Tensile Tests on TRM Coupons

Uniaxial tensile tests were conducted on TRM coupons comprising one and two textile layers, in order to evaluate the tensile properties of the composite materials. Three identical specimens (TRM coupons) made of one and two layers for each type of textile material (described in Section 3.43.3) were fabricated and tested. The geometry of the coupons is shown in Figure 3.5a, whereas the test setup is depicted in Figure 3.5b. The TRM coupons had a dumbbell shaped which was a modification of the setups adopted by Brameshuber (2006a); Orlowsky and Raupach (2008). The coupon was gripped to the tensile machine using special steel fixtures (see Figure 3.5b) that were used to fit the curved parts of the coupons and also used to apply the tension load. Each coupon was instrumented with two LVDTs (one on each side) which were mounted at the centre of the coupon to measure the tensile strain of the composite material in a gauge length of 240 mm. The load was applied monotonically under displacement control at a rate of 2 mm/min using a 200-kN capacity universal testing machine up to failure.

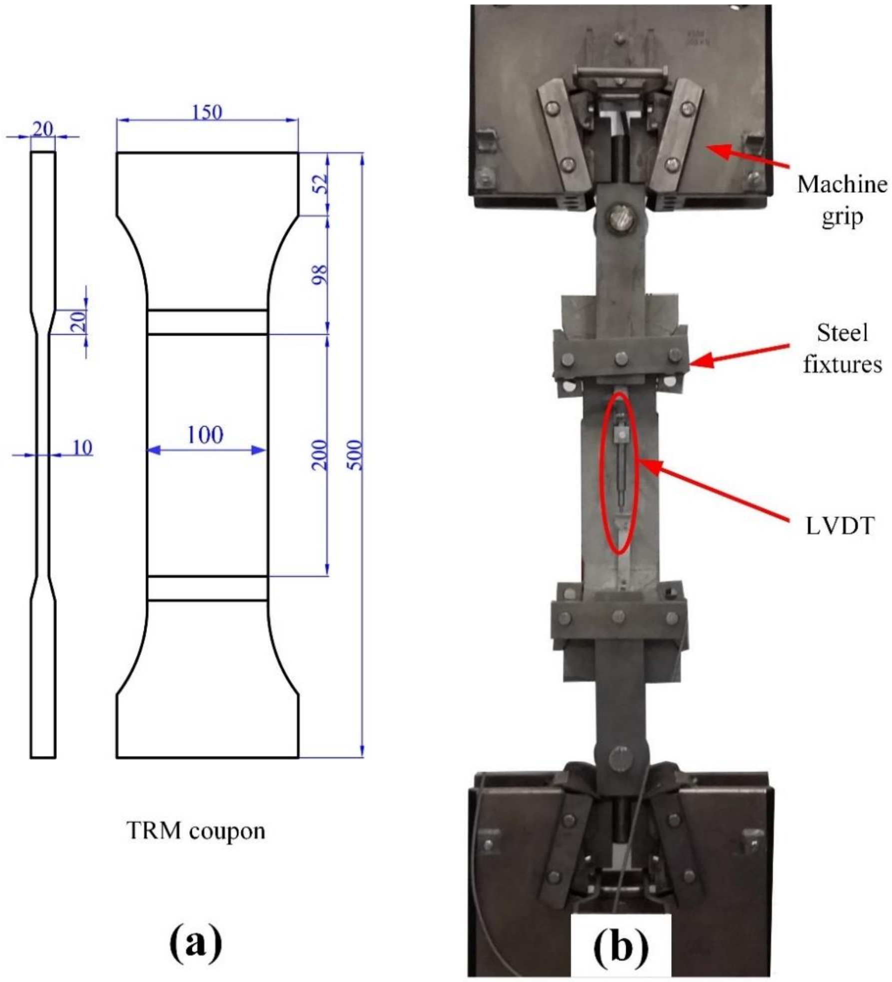

Figure 3.5. (a) Geometry of TRM coupons, and (b) test setup for tensile test of TRM coupons.

All coupons failed due to rupture of the fibres at the central region of the gauge length (see Figure 3.6). During the test and after initiating of the first crack, as the load increase more cracks were appeared and developed until the failure occurred. It is noted that the crack pattern of the two layers' TRM coupons was denser than that of one layer, hence better stress distribution was achieved when the number of layers increased.

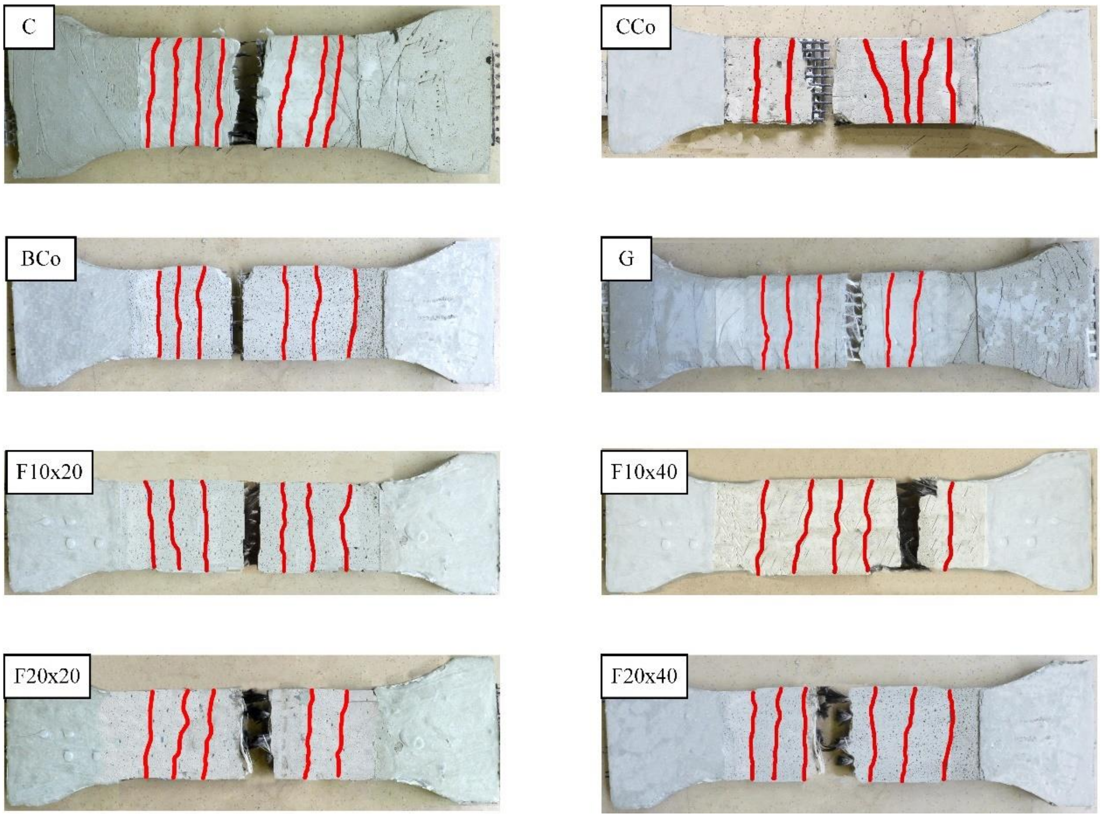

Figure 3.6. Failure of TRM coupons.

The results of the tensile tests were presented in form of stress-strain curves. Figure 3.7 shows a typical stress-strain curve of a TRM coupon made from one layer of dry carbon textile. As shown in this Figure, the stress-strain curve of the TRM coupon is characterised by two distinct stages: (1) linear elastic behaviour until the first crack occurred in the mortar, and (2) non-linear stage (cracking stage) with progressively decreasing slope (due to mortar cracking) up to failure due to fibres rupture.

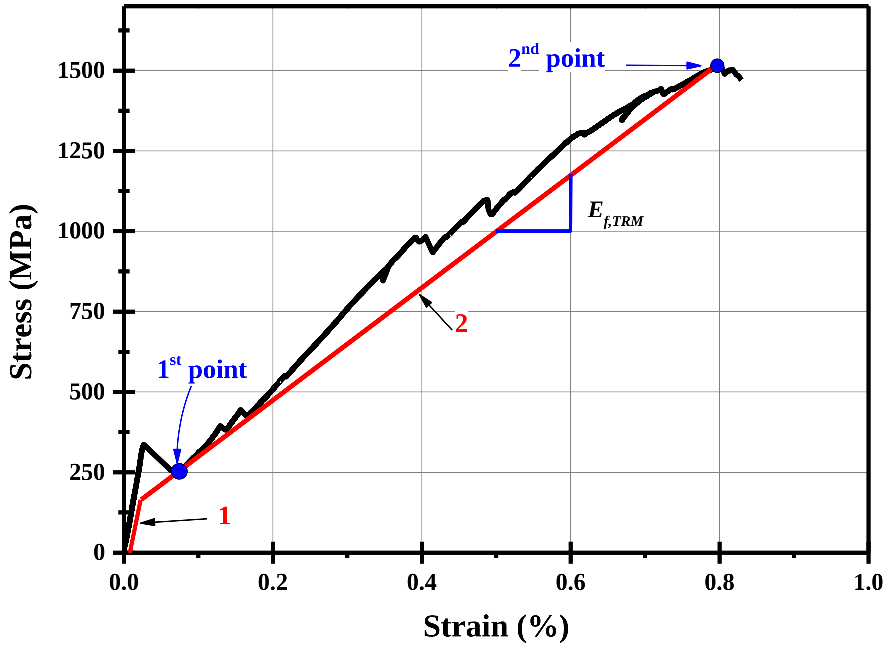

Figure 3.7. Typical stress-strain curve of TRM coupon made of one layer of dry carbon fibres textile.

Figure 3.8 depicts the stress-strain curves of all tested coupons fabricated using textile mesh with equal quantity of fibres in two orthogonal directions (i.e. C, CCo, BCo, and G), whereas, Figure 3.9 presents the corresponding results of TRM coupons fabricated using the four types of the hybrid textiles. Each shaded region shown in both Figures envelops the three stress-strain curves of each type of TRM coupons.

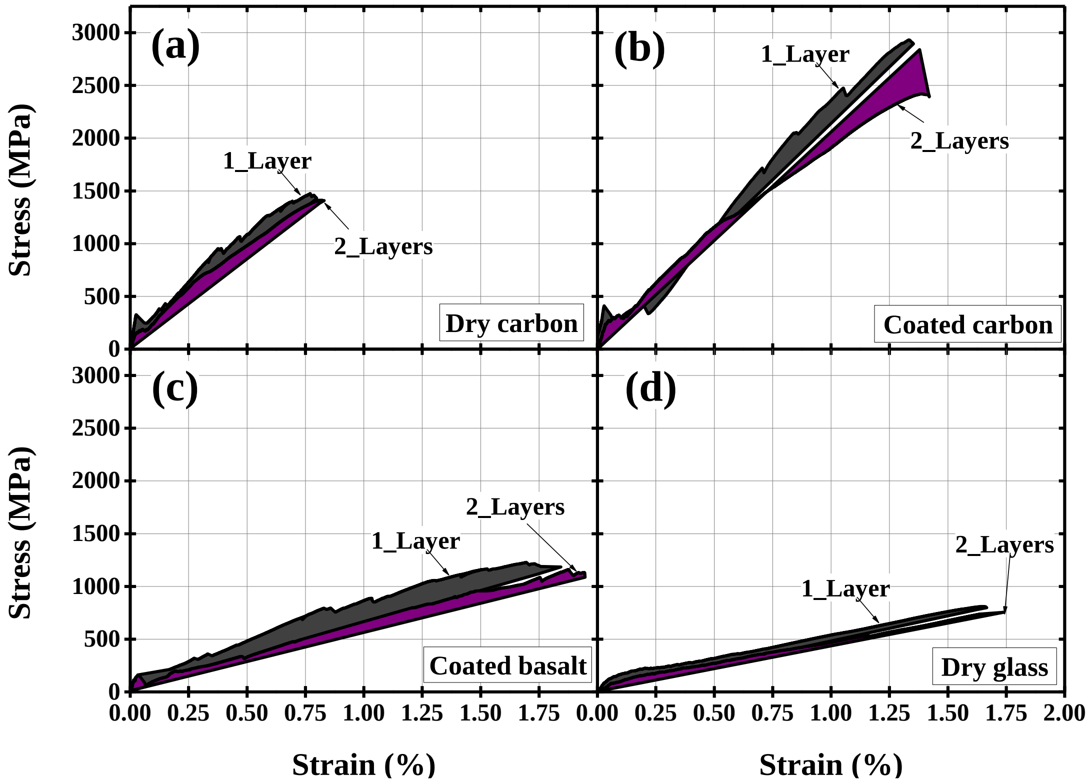

Figure 3.8. Stress-strain envelope areas of: (a) dry carbon fibres textile, (b) coated carbon fibres textile, (c) coated basalt fibres textile, and (d) dry glass fibres textile.

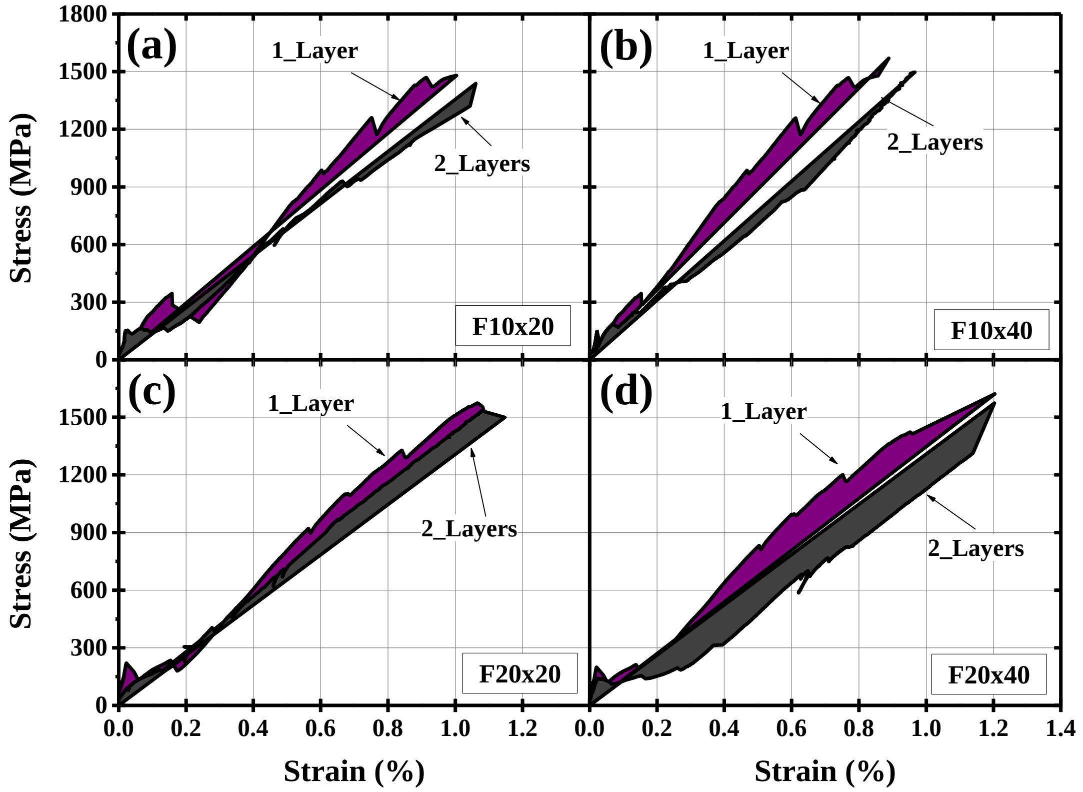

Figure 3.9. Stress versus strain envelope areas of: (a) F10x20, (b) F10x40, (c) F20x20, and (d) F20x40.

Table 3.2 reports the mean values of ultimate stress (f_{fu}), ultimate strain (ε_{fu}), and modulus of elasticity ($E_{f,TRM}$). The ultimate stress (f_{fu}) was calculated by dividing the ultimate load to the cross-sectional area of the TRM coupon in the direction of loading. The cross-sectional area of the coupon was calculated by multiplying the width of the coupon (the same width of the textile) by the nominal thickness of the fibre reported in Figure 3.1. The modulus of elasticity of the TRM coupons ($E_{f,TRM}$) was calculated as the secant modulus of elasticity of the stress-strain curve during the 2nd stage of response (modulus of elasticity of the cracked section), which is the slope of the line connecting the first point corresponding to the beginning of the non-linear stage (cracking stage) and the point corresponding to the maximum tensile strength (Figure 3.7).

Table 3.2. Summary of results of the tensile tests of TRM coupons.

Textile- fibres materials	No. of layers	No. of bundles	Ultimate tensile strength (f_{fu})(MPa)	Ultimate tensile strain (ε_{fu}) (%)	Modulus of elasticity ($E_{f,TRM}$) (GPa)
Dry carbon textile (C)	1	10	1518 (7.4)*	0.793 (0.03)*	166.8 (4.7)*
	2		1386 (85)	0.820 (0.07)*	162.4 (16)*
Coated carbon Textile (CCo)	1	10	2843 (25)*	1.39 (0.03)*	200.5 (3.9)*
	2		2624 (127)	1.386 (0.11)*	183.1 (8)*
Coated basalt Textile (BCo)	1	5	1190 (20)*	1.825 (0.02)*	63.7 (1.7)*
	2		1163 (43)*	1.876 (0.07)*	61.3 (4)*
Glass Textile (G)	1	8	794 (9)*	1.66 (0.03)*	41.1 (2 .9)*
	2		778 (5)*	1.732 (0.08)*	40.7 (1.4)*
F10x20	1	10	1452 (26)*	0.994 (0.11)*	165.6 (9)*
	2		1409 (43)*	1.04 (0.13)*	155.7 (13)*
F10x40	1	10	1512 (47)*	0.888 (0.08)*	169.1 (7)*
	2		1485 (11)*	0.956 (0.10)*	153.1 (11)*
F20x20	1	5	1553 (39)*	0.988 (0.07)*	161.1 (7)*
	2		1513 (28)*	1.04 (0.10)*	159.6 (8)*
F20x40	1	5	1612 (55)*	1.06 (0.13)*	159.3 (13)*
	2		1534 (43)*	1.12 (0.09)*	154.4 (12)*

*Standard deviation in parenthesis

Figure 3.10 illustrates the effect of the number of layers on the tensile properties of the composite materials. In general, increasing the number of TRM layers reduced marginally the tensile stress (f_{fu}), the modulus of elasticity ($E_{f,TRM}$), and increased slightly the ultimate tensile strain (ε_{fu}) due to better activation of the textile reinforcement in the direction of loading.

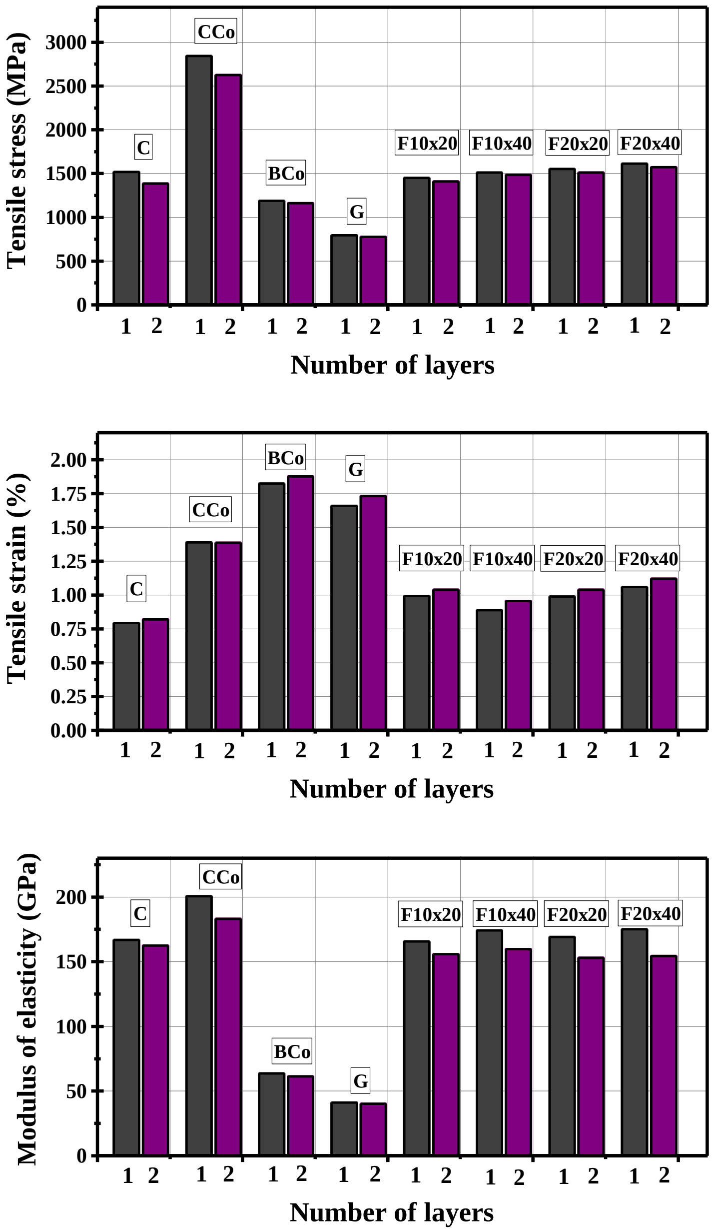

Figure 3.10. Effect of the number of layers on: (a) the ultimate tensile strength (f_{fu}), (b) ultimate tensile strain (ε_{fu}), and (c) modulus of elasticity ($E_{f,TRM}$).

3.6 Tensile Tests on FRP Coupons

The FRP composite used as external strengthening of RC beams comprised three different types of textile materials namely: the dry carbon, the coated basalt and the dry glass fibre textiles in combination with epoxy resin described in Section 3.2. As in the case of TRM system, uniaxial tensile tests were carried out on FRP coupons consisted of one layer of textile reinforcement in order to determine their tensile properties in the direction of loading. The FRP coupons had a rectangular shape and were designed according to the requirements of ACI 440.3R-04 (2008). Three identical coupons were tested for each type of textile material. The geometry of the coupons is shown in Figure 3.11a, whereas, the test setup is depicted in Figure 3.11b. The coupon was gripped to the tensile machine using two aluminium plates (see Figure 3.11a) which were glued to the ends of each coupon. Two LVDTs were fixed at the centre of the coupon (one on each side) to measure the tensile strain of the composite material in a gauge length of 300 mm. The load was applied monotonically under loading control at a rate of 5 kN/min (440) using a universal testing machine with a capacity of 200-kN. All coupons failed at the central region of the coupons within the gauge length due to rupture of the fibres (Figure 3.11c). The results of tensile tests are presented in Figure 3.12a-c in form of stress-strain curves. As shown this Figure, the behaviour of all curves is linear up to failure.

Table 3.3 reports the mean values of ultimate stress (f_{fu}), ultimate strain (ε_{fu}), and modulus of elasticity ($E_{f,FRP}$). The tensile strength of FRP coupons was calculated in the same way described for the TRM coupon, whereas the elastic modulus of FRP coupons was calculated directly from the stress-strain curves by dividing the ultimate stress (f_{fu}) to the corresponding ultimate strain (ε_{fu}) because the behaviour of the stress-strain curves almost linear up to failure.

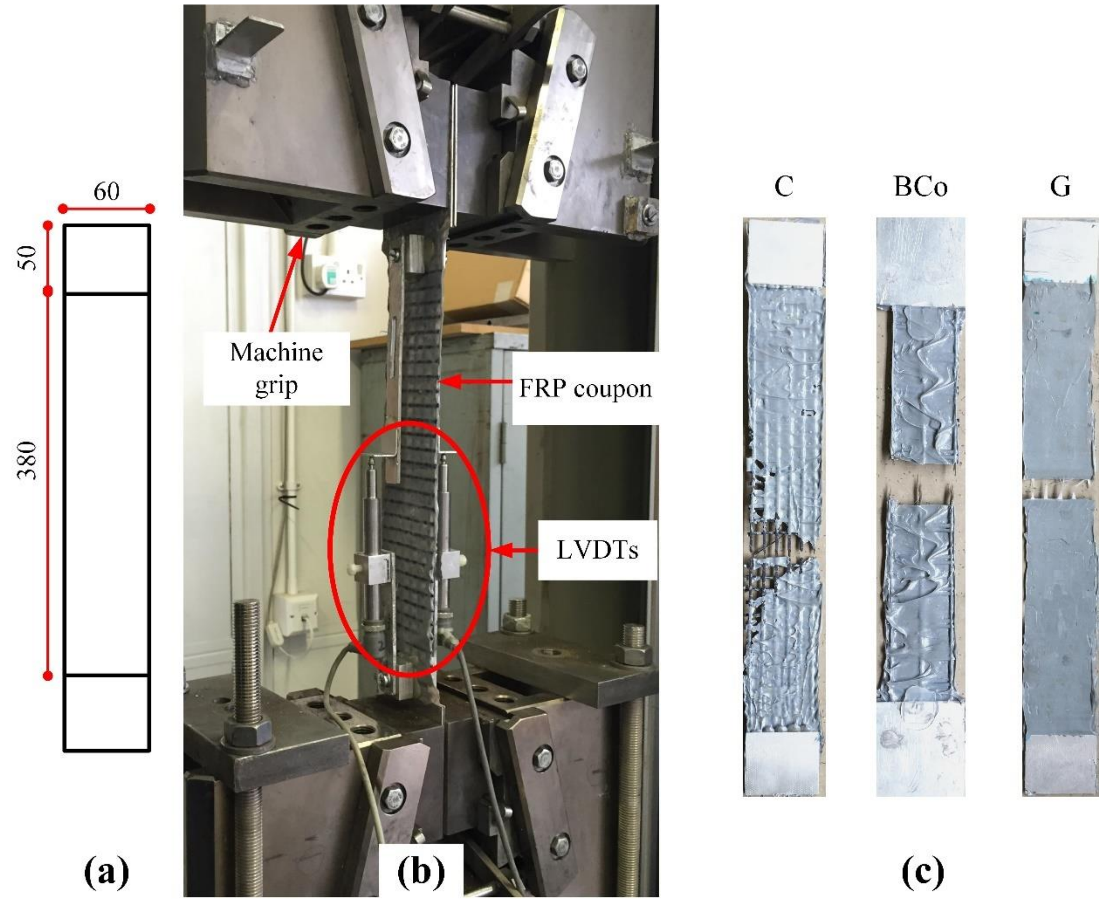

Figure 3.11: (a) geometry of FRP coupons; (b) test setup; and (c) failure mode of FRP coupon.

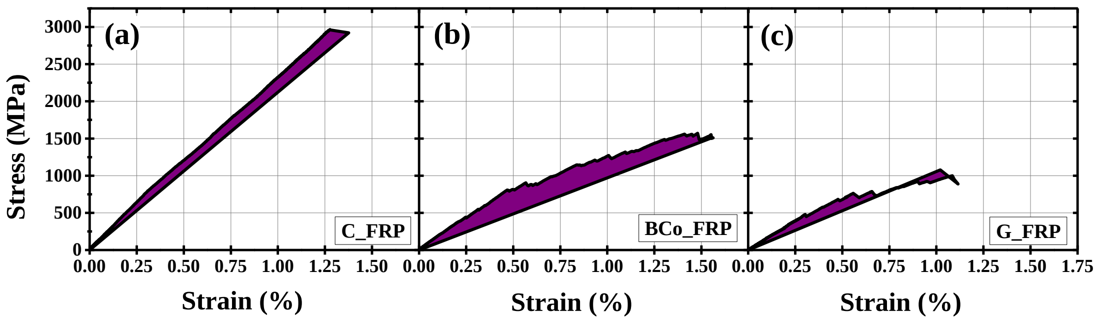

Figure 3.12. Stress-strain envelope areas of FRP coupons made of; (a) dry carbon fibre textile, (b) coated basalt fibres textile, and (c) dry glass fibres textile.

Table 3.3. Summary of results of FRP coupons.

Textile-fibres materials	No. of bundles	f_{fu} (MPa)	ε_{fu} (%)	$E_{f,FRP}$ (GPa)
Dry carbon	6	2936 (31.5)*	1.33 (0.03)*	219 (4)*
Coated basalt	3	1501 (15)*	1.508 (0.02)*	99.5 (2.6)*
Dry glass	5	1019 (31)*	1.02 (0.05)*	93.3 (8) *

*Standard deviation in parenthesis

3.7 Comparison between the Behaviour of TRM and FRP Coupons

Figure 3.13 compares the stress-strain curves of FRP and TRM coupons made of one layer of the dry carbon fibre textile (C). As shown in this Figure, the behaviour of the stress-strain curve of FRP coupon is linear up to failure, whereas the corresponding behaviour of the equivalent TRM coupon comprises two stages (as discussed in Section 3.5) due to mortar cracking.

Furthermore, the tensile properties (i.e. $f_{fu}, \varepsilon_{fu}, E_f$) of the FRP coupons were higher than that of the corresponding TRM coupons although the same textile material was used. This is mainly attributed to the effect of binding materials; using epoxy resin as a binding material ensures full impregnation of the fibres and hence better activation of the fibre in carrying tensile forces was achieved, whereas, in the case of TRM composite, only the outer filaments in a single roving were impregnated with mortar resulted in activation of the outer filaments while the inner filaments experience slippage.

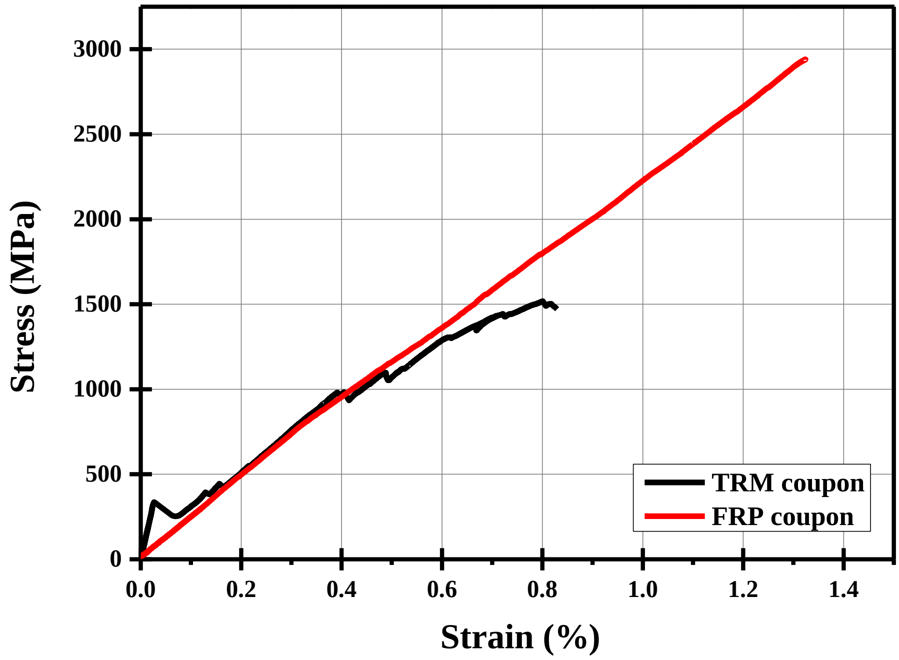

Figure 3.13. Comparison between the stress-strain curves of FRP versus TRM coupons.

3.8 Summary

The main conclusions drawn from this chapter are summarized below:

- In general, the tensile properties obtained from testing one layer of bare textiles coupons were approximately identical to that measured from the equivalent TRM coupons. Hence, for design purposes, it is suggested that both tests can be used to determine the tensile properties of TRM as a composite material.
- Increase the number of TRM layers from one to two, reduced slightly the ultimate tensile strength (average of 4%), and increased marginally the ultimate tensile strain (average of 4%).
- All hybrid textiles showed approximately identical tensile behaviour in both tests, the bare textile and the TRM composite. Moreover, their tensile properties (i.e. ultimate tensile stress, ultimate tensile strength and modulus of elasticity) were approximately the same to that of the dry carbon fibre textile (C). Such behaviour

indicated that the effect of the fibre's materials (carbon or glass) and the distance between the rovings in the transversal direction was not significant.

- The type of binding materials (cement mortar or epoxy resin) significantly affects the tensile properties of the resulted composite materials. FRP coupons showed considerably higher tensile properties than that of the corresponding equivalent TRM coupon made of the same textile fibres materials. This is mainly attributed to the degree of impregnation of the fibres with the binding material, that completed in the case of FRP composites, whereas in TRM composites only the outer filaments of a roving are impregnated as the mortar particles are bigger than resin and cannot penetrate into the inner filaments. This resulted in fracture of portion of the outer fibres, while the core ones experience a degree of slippage.

Chapter 4

BOND BETWEEN TRM AND CONCRETE: DOUBLE-LAP SHEAR TEST AT AMBIENT TEMPERATURE

ABSTRACT

This chapter presents an experimental study on the bond behaviour between TRM and concrete substrates. The parameters examined include: (a) the bond length (from 50 mm to 450 mm); (b) the number of TRM layers (from 1 to 4); (c) the concrete surface preparation (grinding versus sandblasting); (d) the concrete compressive strength (15 or 30 MPa); (e) the textile coating; and (f) the anchorage through wrapping with TRM jackets. A total of 80 specimens were fabricated and tested under double-lap shear test. It is mainly concluded that: (a) after a certain bond length (between 200 mm and 300 mm for any number of layers) the bond strength marginally increases; (b) by increasing the number of layers, the bond capacity increases in a non-proportional way, whereas the failure mode is altered; (c) concrete sandblasting is equivalent to grinding in terms of bond capacity and failure mode; (d) concrete compressive strength has a marginal effect on the bond capacity; (e) the use of coated textiles alters the failure mode and significantly increases the bond strength; and (f) anchorage of TRM through wrapping with TRM jackets substantially increases the ultimate load capacity.

** The content of this work has been published as a journal paper: "Bond between textile-reinforced mortar (TRM) and concrete substrates: Experimental investigation", Composites Part B: Engineering. 2016, 1;98:350-361; DOI:10.1016/j.compositesb.2016.05.041.*

4.1 Experimental Programme

4.1.1 Test Specimens and experimental parameters

The main objective of this chapter is to investigate the bond between TRM and concrete substrate considering different parameters. A total of 80 specimens were fabricated, strengthened and subjected to double-lap shear test. The details of the specimens are provided in Figure 4.1a-f. Each specimen comprised two RC prisms with cross sectional area of 100x100mm, and length of 265, or 515 depending on the tested bond length.

The procedure for specimen's preparation was as follows: an acrylic plate with dimensions of 100x100 mm cross sectional was fixed at the middle of a steel mould (Figure 4.1a) in order to isolate the two prisms during casting stage. The acrylic plate was provided with two acrylic rods with 10 mm diameter fixed at the position shown in Figure 4.1b so as to create holes into concrete mass of each prism. Each prism was reinforced with a steel cage with the details shown in Figure 4.1c to prevent the failure of prisms due to concrete splitting during the test. A 16-mm bar was fitted at the centre of each prism to allow for the application of the load during the test (Figure 4.1d). After 24-hour of casting, the specimen (two prisms) was removed from the mould, the acrylic plate was removed from the central zone, and the two prisms were reconnected to each other's using a 10 mm diameter acrylic rods that were inserted into the premade holes (see Figure 4.1d). The purpose of these two acrylic rods was to ensure fully alignment between the two prisms and reduce the error in the measurements during the test resulted from possible bending of specimen due to misalignment between the two prisms. Finally, full details of the design of the test specimen and a 3D overview is shown in Figure 4.1e and f, respectively.

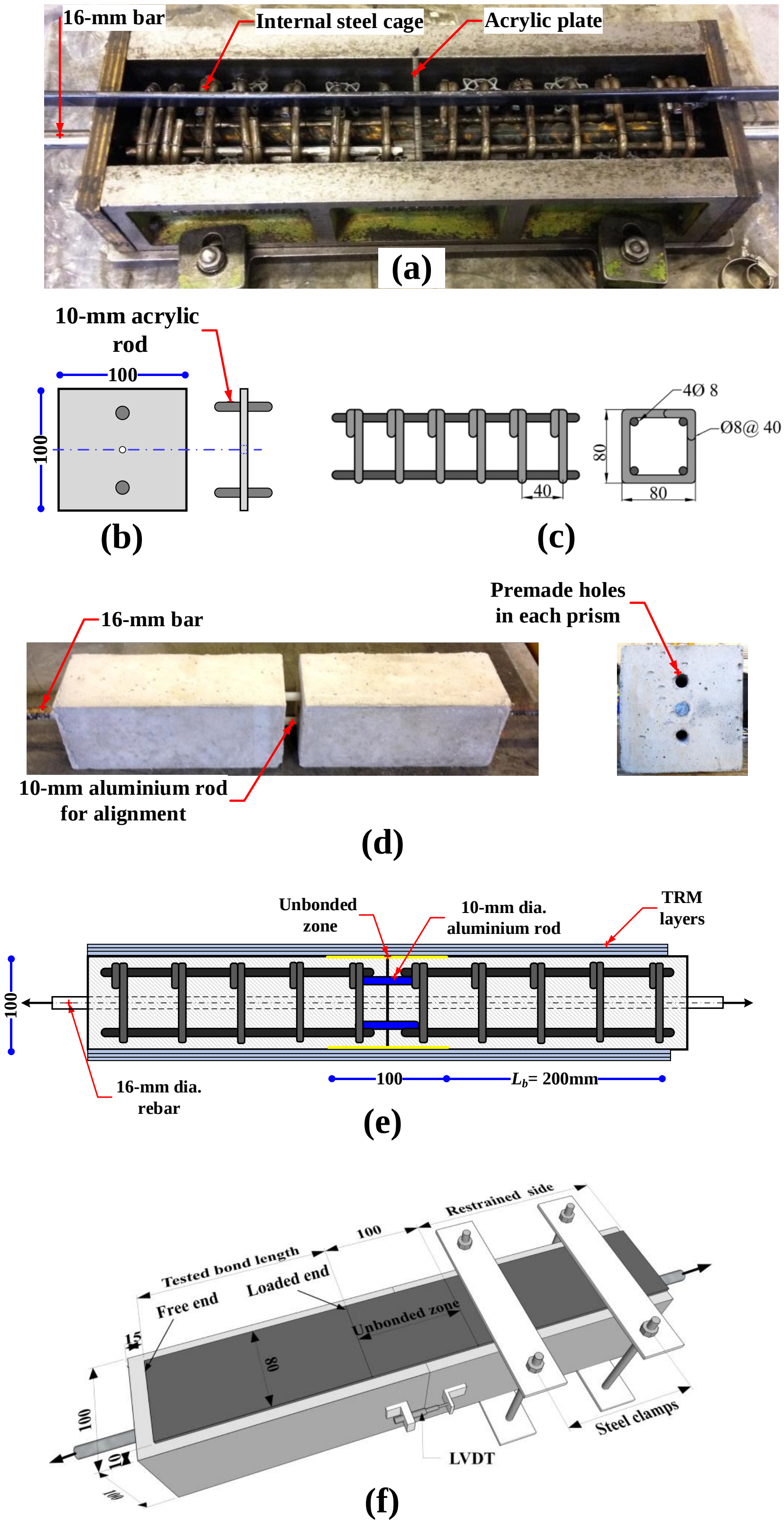

Figure 4.1. Specimen details: (a) specimen preparation; (b) details of acrylic plate; (c) details of internal reinforcement; (d) details of alignment of the prisms; (e) overall design details of the test specimen; and (f) 3D over view (Dimensions in mm).

The key investigated parameters were: (a) the bond length, (b) the number of TRM layers, (c) the concrete surface preparation, (d) the concrete compressive strength, (e) the coating of the textile, and (f) the anchorage through wrapping with TRM jackets.

The 80 specimens comprised 40 twin specimens as follows: 22 twin specimens (44 specimens in total) were used to examine parameters (a) and (b) with the bond length varying from 50 to 450 mm and the number of layers from one to four. Six twin specimens were tested to investigate parameter (c), namely the effect of the concrete surface preparation (grinding or sandblasting), whereas other six twin specimens were examined to evaluate the effect of the concrete compressive strength (15 or 30 MPa) on the load response and failure mode [parameter (d)]. Four twin specimens were tested to examine the influence of textile coating on the ultimate load and failure mode [parameter (e)], and two twin specimens were used to investigate the effect of anchorage through wrapping with TRM jackets [parameter (f)]. The notation of specimens addressing parameters (a) and (b) was LX_N, where X is the bond length and N is the number of TRM layers. For the other specimens, the notation used was LX_N_Y, with Y denoting the investigated parameter: S for concrete surface preparation; Ls for low concrete compressive strength; CCo for coated textile and W for TRM wrapping. Details of the different strengthening configurations and number of tested specimens for each parameter are listed in Table 4.1.

Table 4.1. Specimens details, concrete compressive strength, and mortar properties on the day of testing.

Specimen notation	Specimen's name	Bond length (mm)	No. of layers	Additional remarks	Concrete Compressive (MPa)	Mortar (MPa)	
						Flexural strength	Compressive strength
LX_N	L50_1	50	1	-	31.2	9.17	38.8
	L50_2		2				
	L50_3		3				
	L50_4		4				
	L100_1	100	1	-	30.4	8.24	33.8
	L100_2		2				
	L100_3		3				
	L100_4		4				
	L150_1	150	1	-	31.2	9.23	39.7
	L150_2		2				
	L150_3		3				
	L150_4		4				
	L200_1	200	1	-	32.8	8.54	35.9
	L200_2		2				
	L200_3		3				
	L200_4		4				
	L250_1	250	1	-	32.5	8.95	37.6
	L250_2		2				
	L250_3		3				
	L250_4		4				
	L450_1	450	1	-	29.5	9.4	40.1
	L450_2		2				
LX_N_S	L100_3_S	100, 150, 200	3	S= Surface preparation	29.3	8.68	36.8
	L100_4_S		4				
	L150_3_S		3				
	L150_4_S		4				
	L200_3_S		3				
	L200_4_S		4				
LX_N_Ls	L100_3_Ls	100, 150, 200	3	Ls= Low concrete strength	14.7	8.98	35.2
	L100_4_Ls		4				
	L150_3_Ls		3				
	L150_4_Ls		4				
	L200_3_Ls		3				
	L200_4_Ls		4				
LX_N_CCo	L150_1_CCo	150, 200	1	CCo= Coated textile	30.4	8.35	32.7
	L150_2_CCo		2				
	L200_1_CCo		1				
	L200_2_CCo		2				
LX_N_W	L100_3_W	100	3	W= Anchorage wrapping with TRM		8.35	32.7
	L100_4_W		4				

4.1.2 Materials and strengthening procedure

The RC prisms were cast in different groups and dates. For all tested specimens, the targeted concrete compressive strength was 30 MPa except for group LN_X_Ls (twelve specimens) where the targeted compressive strength was lower and equal to 15 MPa. The compressive strength of all specimens was measured on the day of the testing (average value of three 150x150x150 mm cubes) and is given in Table 4.1.

The textile reinforcement used for strengthening was the dry carbon fibres textile (C) described in Section 3.3. The binding material comprising the inorganic cement mortar described in Section 3.1. The compressive and flexural strength of the mortar (average value from 3 prisms) were experimentally obtained on the day of testing using prisms with dimensions of 40x40x160 mm according to BS EN 1015-11 (1999) and are reported in Table 4.1.

Prior to strengthening, the concrete surface was prepared by removing a thin layer of concrete (using of a grinder) and creating a grid of groves (with a depth of approximately 3 mm_Figure 4.2a). This procedure was performed for all specimens, except for those of group LX_N_S, where the concrete surface was sandblasted (Figure 4.2b). After cleaning and dampening the concrete surface, the first layer of mortar with approximately 2 mm thickness was placed on the concrete surface using a metallic trowel (Figure 4.3a). Then the first textile layer was applied and pressed slightly into the mortar, which protruded through the perforations between the fibre rovings as shown in Figure 4.3b. This procedure was repeated until the required number of TRM layers was applied. Finally, an external layer of mortar with approximately 3 mm thickness was applied and levelled by trowel (Figure 4.3c). Of crucial importance in this method was the application of each mortar layer while the previous one was still in a fresh state.

The specimens in group LX_N_CCo were retrofitted using the coated carbon textile (CCo) described in Section 3.3. For the specimens that received wrapping, namely the main TRM reinforcement was anchored through TRM jackets wrapped around the concrete prism (group LX_N_W), additional surface preparation was made prior to strengthening including rounding of the prism corners to a radius of 10 mm. After applying the required number of main TRM layers, the prism side under investigation was wrapped with two TRM layers following the strengthening procedure described previously. The width of the textile used for wrapping was 100 mm which was equal to the bond length of the main TRM reinforcement (Figure 4.3d). It is worth mentioning that the bond width of TRM reinforcement for all tested specimens was the same and equal to 80 mm.

(a) (b)

Figure 4.2. Different concrete surface preparation: (a) grinding and creating a grid of groves; and (b) sandblasting.

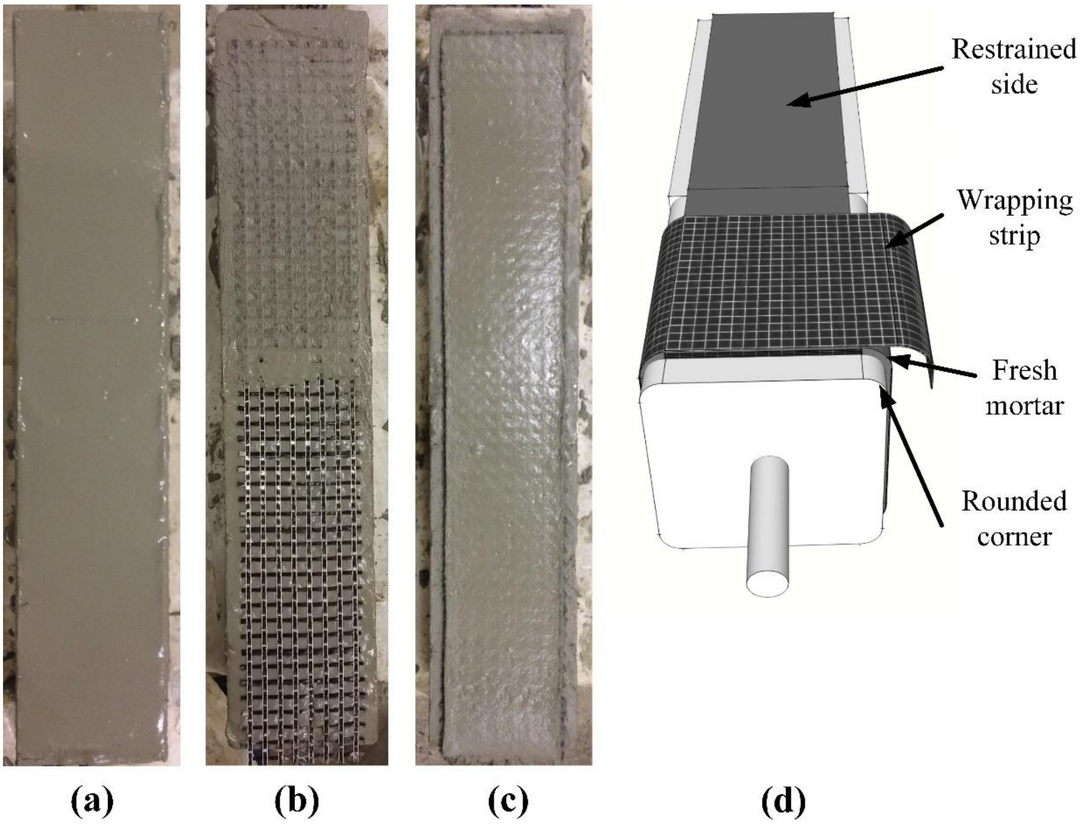

Figure 4.3. (a) Application of the first layer of mortar; (b) application of the first layer of textile layer into the mortar; (c) application of the final layer of mortar; and (d) wrapping with TRM jacket at the side of specimen under examination for specimens in group LN_X_W.

4.1.3 Experimental setup and procedure

All specimens were tested after a curing period of six weeks (same curing conditions were applied to all specimens). As mentioned previously (see Section 2.3.1) the double-lap shear test was adopted in the current study. The experimental setup included two steel clamps which were fixed at one side (restrained side) of the specimen to ensure that failure would occur in the monitored side (Figure 4.4). The TRM composite was left un-bonded at a 100 mm-long central zone (50 mm at each prism) of the specimen (Figure 4.1f) to prevent concrete-edge failure which could have adverse effects. This was achieved by wrapping the central zone (prior to strengthening) with a plastic tape in order to isolate the strengthening materials from the concrete prisms at this zone and prevent any possible attachment with the concrete surface. All tests were carried out using a universal testing machine of 250-kN capacity. The specimens were gripped to the tensile machine using the 16 mm steel bars fitted at the centre of each prism during casting (these bars were terminated at the interface between the two prisms). The load was applied monotonically under displacement control with rate of 0.2 mm/min. Two LVDTs were mounted to the unstrengthened sides of the specimens to measure the relative displacement between the two prisms (Figure 4.4).

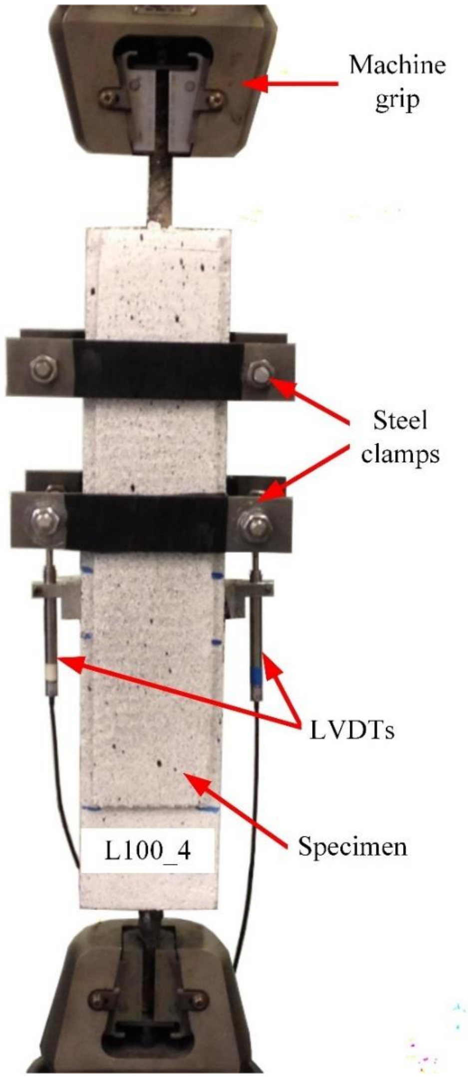

Figure 4.4. Details of the test set-up.

4.2 Experimental Results

Figure 4.5 shows the free body diagram of the tested side of the specimen. By assuming perfect symmetry (up to peak load) between the two TRM strip in the tested side, each side will carry half of the measured ultimate load ($P_{u.}$), whereas, the relative displacement between the two concrete prisms measured at ultimate load is the average of the two LVDTs' readings (i.e. $\delta_{max} = (\delta 1+\delta 2)/2)$.

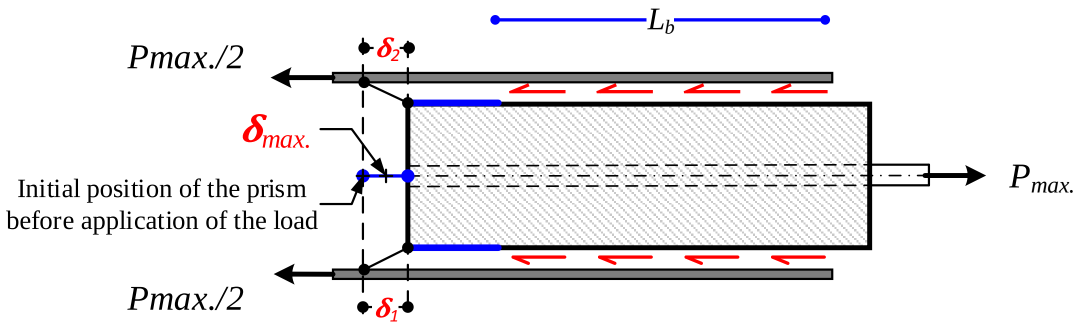

Figure 4.5. Schematic diagram for the free body diagram of the tested side of the specimen.

Key results of all tested specimens are presented in Table 4.2 which includes:

1. the maximum load (P_u) carried out by the TRM strips for both twin specimens S_1 and S_2.
2. the displacement (average of two LVDTs readings) which corresponds to the maximum load ($\boldsymbol{\delta}_{max}$).
3. the average ultimate load (P_{av}) of the two twin specimens.
4. the average displacement (δ_{av}) of the two twin specimens.
5. the average bond strength developed at the concrete-matrix interface (f_b).
6. the average tensile stress in the textile reinforcement (σ_{eff}).
7. the failure mode.

The average bond strength (f_b) and the average tensile stress in the textile reinforcement (σ_{eff}) were calculated from Eq. 4.1 and Eq. 4.2, respectively:

$$f_b = \frac{(P_{av}/2)}{L_b\ b_f} \quad 4.1)$$

$$\sigma_{eff} = \frac{(P_{av}/2)}{n * t_f * b_f} \quad 4.2)$$

where $P_{av.}$ is the average ultimate load, L_b is the bond length, b_f is the bond width (b_f=80 mm), n is the number of TRM layers, t_f is the nominal thickness of the textile in the loading direction (t_f=0.095mm).

Eq. 4.2 was used to calculate the effective stress of the fibres excluding the contribution of the mortar. This is typical in the case of TRM systems, and is valid for the ultimate capacity, since the matrix has already been cracked. At this load level, all the tension force is carried by the textile reinforcement.

Starting from the specimens LX_N that were strengthened with one up to four TRM layers at bond lengths of 50, 100, 150, 200 and 250 mm, the maximum load recorded (average from twin specimens) was (see also Table 4.2): (a) 7.7, 11.6, 12.2, 13.9, and 16.1, kN, respectively, for the specimens with one TRM layer, (b) 18.4, 23.5, 25.3, 28.1, and 29.4kN, respectively, for the specimens with two TRM layers, (c) 22.6, 31.2, 35.1, 36.0, and 38.03 kN, respectively, for the specimens with three TRM layers, and (d) 27.9, 35.0, 37.9, 41.5, and 41.8 kN, respectively, for the specimens with four TRM layers. The bond length of 450 mm was investigated only for one and two TRM layers, with the corresponding maximum load equal to 17.4 and 31.6 kN, respectively.

Table 4.2. Summary of test results.

Specimen	(1) Maximum load, $P_{max.}$ (kN)		(2) Displacement at maximum load δ_{max} (mm)		(3) Average maximum load, $P_{av.}$ (kN)	(4) Average displacement at maximum load δ_{av} (mm)	(5) Average bond strength (f_b) (MPa)	(6) Tensile stress (σ_{eff}) (MPa)	(7) Failure mode**
	S1*	S2*	S1*	S2*					
L50_1	7.15	8.29	0.2s5	0.23	7.7	0.24	-	507	S
L50_2	19.12	17.76	0.79	0.70	18.4	0.75	-	605	
L50_3	23.95	21.16	0.72	0.66	22.6	0.69	2.83	496	D
L50_4	26.46	29.31	0.46	0.62	27.9	0.54	3.49	459	
L100_1	12.28	10.96	0.53	0.50	11.6	0.52	-	763	S
L100_2	22.82	24.14	1.01	1.00	23.5	1.01	-	773	
L100_3	29.62	32.82	0.85	1.04	31.2	0.95	1.95	684	D
L100_4	32.77	37.27	0.83	0.92	35.0	0.88	2.19	576	
L150_1	11.74	12.58	1.32	1.21	12.2	1.27	-	803	S
L150_2	25.25	25.34	1.10	1.11	25.3	1.11	-	832	
L150_3	34.49	35.62	1.05	1.07	35.1	1.06	1.46	770	D
L150_4	38.55	37.2	1.4	1.51	37.9	1.46	1.58	623	
L200_1	13.51	14.25	1.23	1.24	13.9	1.24	-	915	S
L200_2	27.65	28.59	1.35	0.81	28.1	1.08	-	924	
L200_3	37.44	34.55	1.56	1.9	36.0	1.73	1.13	790	D
L200_4	41.26	41.74	1.31	1.57	41.5	1.44	1.30	683	
L250_1	14.92	17.32	2.29	2.55	16.1	2.42	-	1059	S
L250_2	30.25	28.63	1.2	1.6	29.4	1.40	-	967	
L250_3	38.55	37.51	1.56	1.55	38.03	1.56	0.95	834	D
L250_4	42.79	40.89	1.22	1.35	41.8	1.29	1.05	688	

L450-1	17.54	17.2	2.51	2.15	17.4	2.33	-	1145	S
L450-2	32.8	30.4	3.51	3.62	31.6	3.57	-	1040	
L100_3_S	30.64	31.77	1.27	1.46	31.2	1.37	1.95	684	D
L150_3_S	34.99	32.74	0.99	1.05	33.9	1.02	1.41	743	
L200_3_S	40.18	40.57	1.85	1.19	40.4	1.52	1.26	886	
L100_4_S	35.63	36.58	1.24	0.75	36.1	1.00	2.26	594	
L150_4_S	37.64	36.74	1.19	0.80	37.2	1.00	1.55	612	
L200_4_S	41.45	42.35	1.35	1.19	41.9	1.27	1.31	689	
L100_3_Ls	29.9	29.84	1.04	1.12	29.9	1.08	1.87	656	D
L150_3_Ls	30.67	30.79	1.36	1.29	30.7	1.33	1.28	673	
L200_3_Ls	33.68	36.17	1.81	1.99	34.9	1.90	1.09	765	
L100_4_Ls	32.67	31.76	0.92	0.85	32.2	0.89	2.01	530	
L150_4_Ls	34.7	35.54	1.13	1.45	35.1	1.29	1.46	577	
L200_4_Ls	36.81	38.63	1.48	1.39	37.7	1.44	1.18	620	
L150_1_CCo	22.7	21.08	1.45	1.64	21.9	1.55	-	1441	ID
L200_1_CCo	23.21	24.6	1.44	1.54	23.9	1.49	-	1572	
L150_2_CCo	29.1	29.89	0.8	0.89	29.5	0.85	-	970	
L200_2_CCo	32.94	30.77	0.95	1.05	31.9	1.00	-	1049	
L100_3_W	38.43	41.47	1.21	1.29	40.0	1.25	-	877	S
L100_4_W	49.19	52.31	1.17	1.25	50.75	1.21	-	835	

* Specimen number.

** S: Slippage and partial rupture of textile fibres through the mortar; D: Debonding of TRM from the concrete substrate including part of the concrete cover; ID: Debonding due to fracture the surface at the textile-mortar interface (interlaminar shearing).

Figure 4.6 shows the load-displacement curves (average of the two LVDTs readings) recorded for specimens LX_N. For better illustration, only one of the twin specimen's response curve is included. Moreover, they have been grouped according to the number of TRM layers applied. It is noted that the trend of the curves of twin specimens was similar in all the cases (see "S_1" and "S_2" columns in Table 4.2). A common characteristic of all curves is their behaviour up to the maximum load. In specific, a first ascending linear branch with high axial stiffness is followed by a second ascending non-linear branch with progressively decreasing stiffness due to mortar cracking.

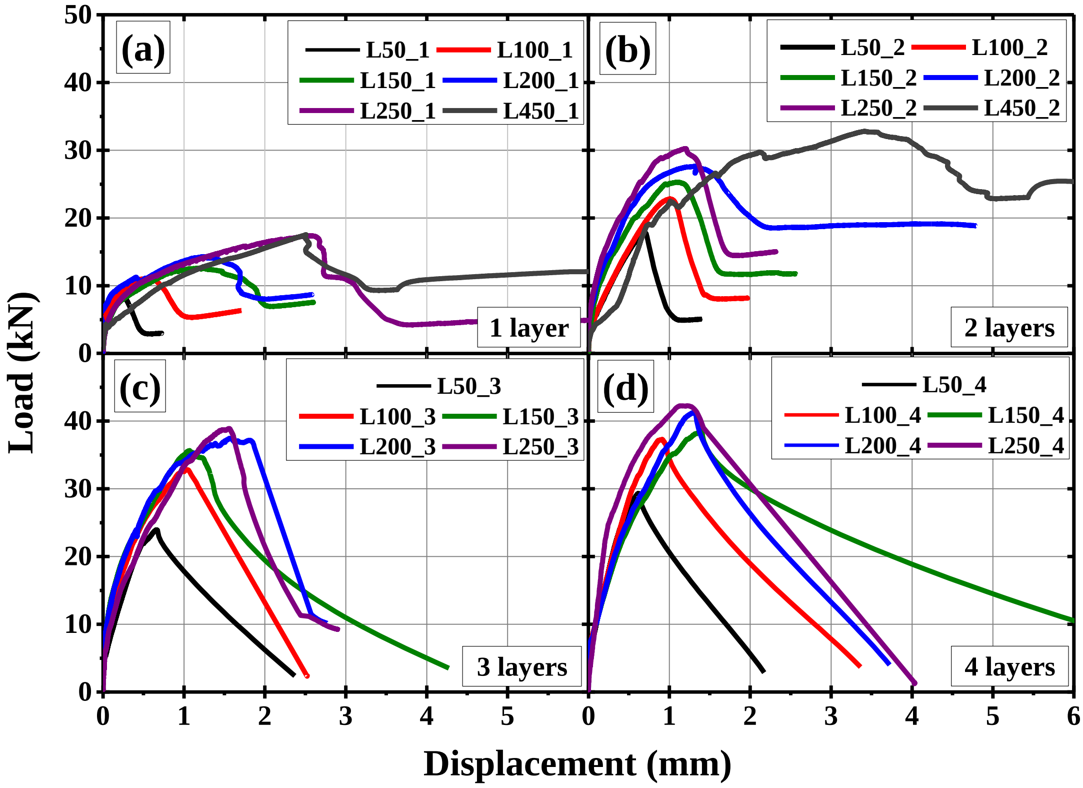

Figure 4.6. Load-displacement curves of LX_N group specimens.

The post-peak behaviour was different depending on the failure mode which in turn was different depending on the amount of TRM reinforcement. For one and two TRM layers, the post-peak behaviour was generally characterized by a progressive load-drop to a residual strength (Figure 4.6a and b). In contrast, when three and four

TRM layers were applied the load-drop was sudden without any residual strength provided (Figure 4.6c and d).

The failure modes observed in LX_N specimens can be classified in two types: (a) slippage of the fibres within the mortar; examples of this failure mode are shown in Figure 4.7, and (b) debonding of TRM from the concrete substrate with peeling off parts of the concrete cover (Figure 4.8). The first failure mode occurred in all specimens strengthened with one or two TRM layers, whereas the second occurred in all specimens with three or four layers.

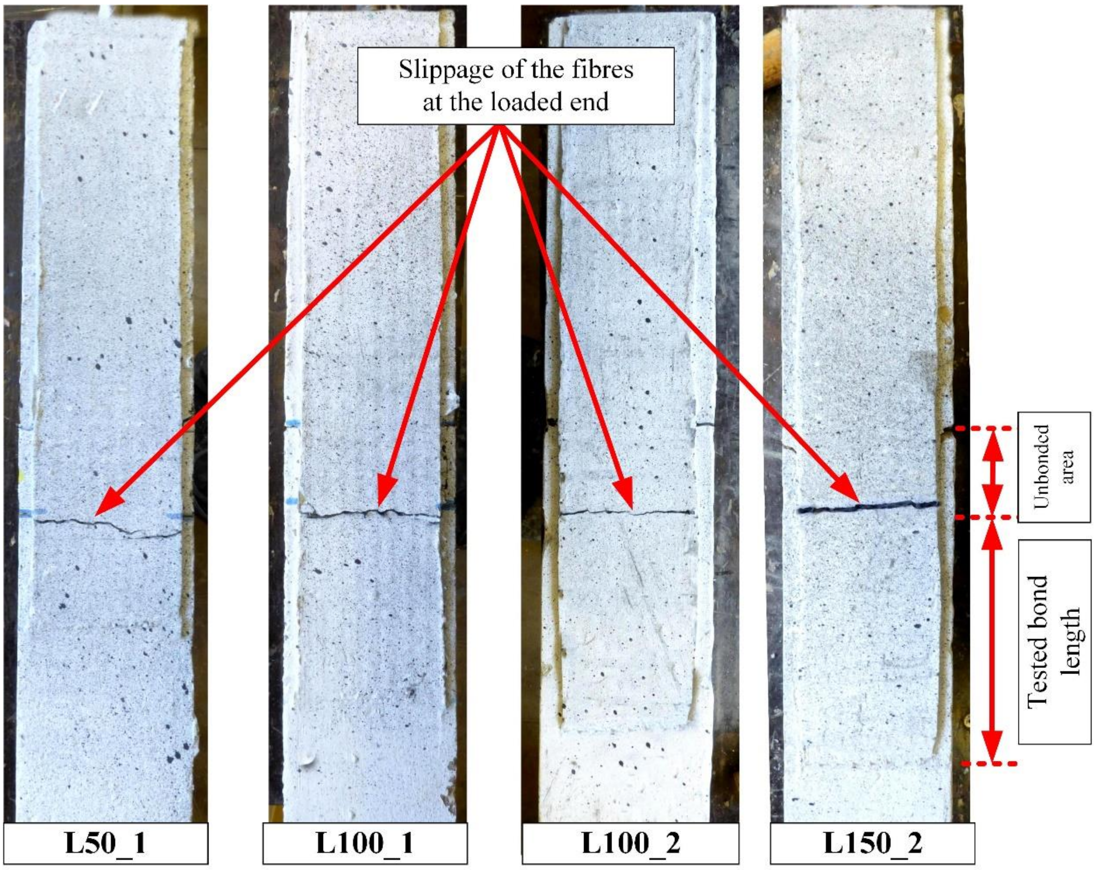

Figure 4.7. Failure mode of specimens strengthened with one and two layers of TRM and different bond length.

For the specimens strengthened with one or two TRM layers, the failure mechanism was controlled by slippage and partial rupture of the longitudinal fibres through the mortar at the loaded end, where a single crack was developed (at an early loading stage) and further opened at the end of the test (Figure 4.7). After failure, a residual strength was recorded which was attributed both to the contribution of friction between the inner filaments themselves and the outer filaments with the surrounding matrix.

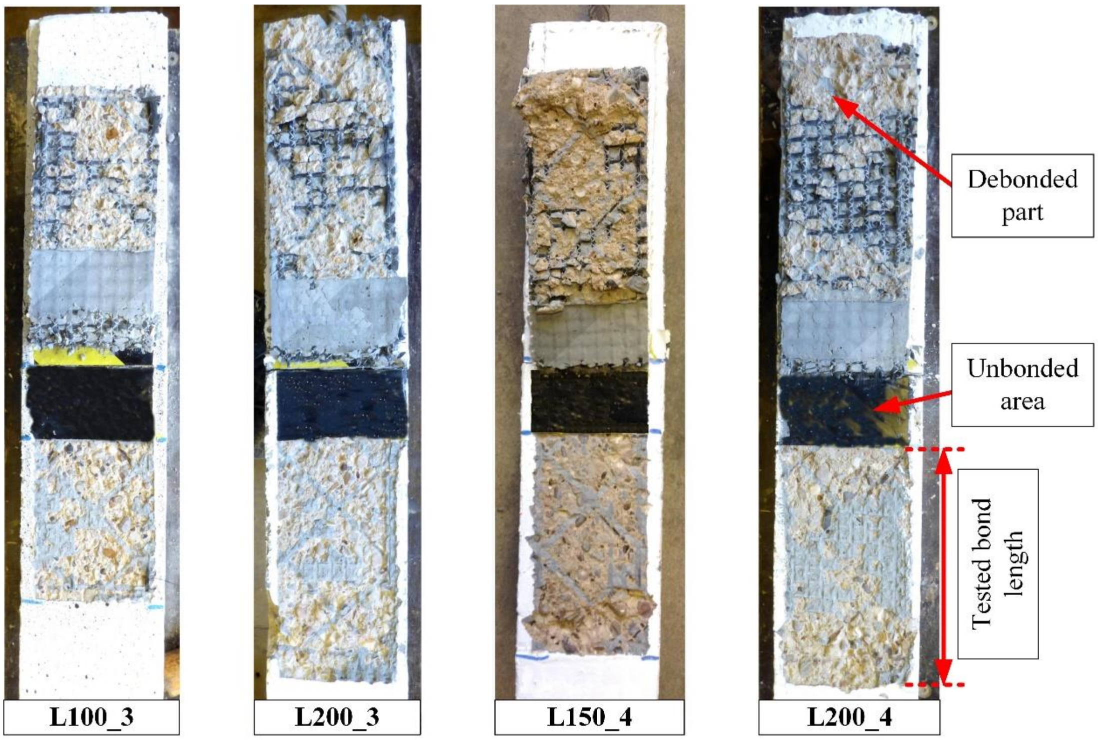

Figure 4.8. Failure mode of specimens strengthened with three and four layers of TRM and different bond length.

When TRM debonding from the concrete substrate occurred, it was accompanied by removal of a thin concrete cover layer (Figure 4.8). Failure was initiated by the formation of a longitudinal crack at the loaded end; this crack was continuously propagating towards the free end as the load was increasing. At peak load, propagation of the crack up to free end caused full detachment (debonding) of the TRM composite from the concrete surface and the load dropped to zero. A noticeable difference between the specimens failed due to fibres slippage and those specimens failed due to TRM debonding is that in the latter case several transversal cracks developed on the TRM face as shown in Figure 4.9. Hence, a better distribution of stresses along the bond length was achieved in these cases due to better activation of the textile reinforcement when the number of layers increased.

After debonding occurred, a rotation of the specimen with respect to the longitudinal axes was observed (Figure 4.9). This is because the failure was control by one of the two monitored sides of the concrete prism. However, this rotation had no effect on the bond behaviour because it happened after reaching the ultimate load.

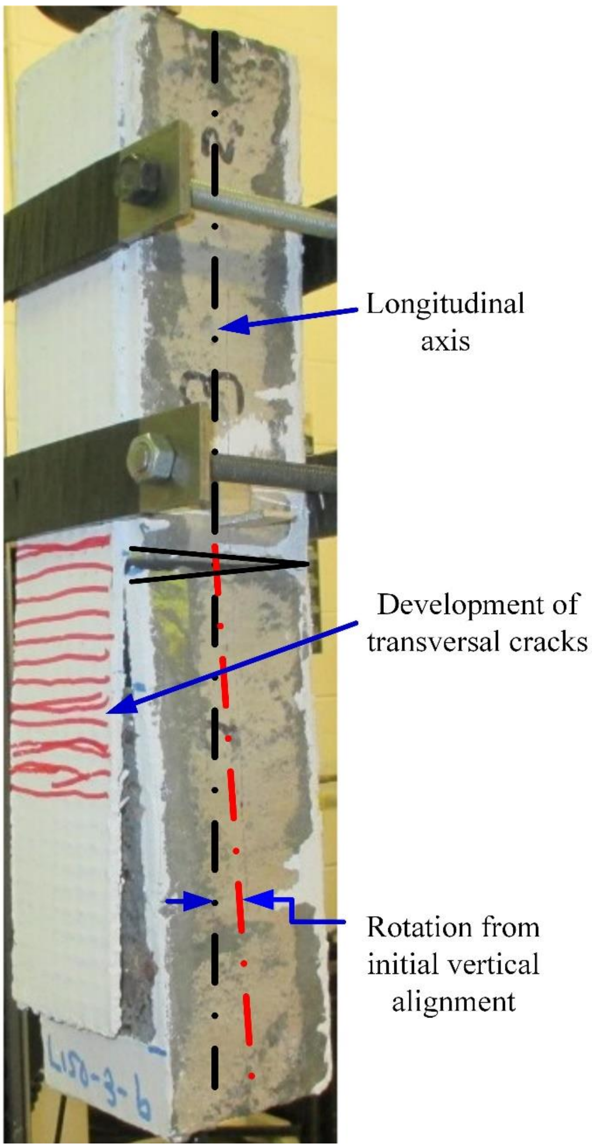

Figure 4.9. Development of transversal cracks and the rotation of the specimen with respect to the initial alignment after ultimate load.

Specimens LX_N_S, with different concrete surface preparation (sandblasting instead of grinding), attained maximum loads of 31.2, 33.9 and 40.4 kN for three layers, and 36.1, 37.2 and 41.9 kN for four layers, for bond lengths equal 100, 150 and 200 mm, respectively. As illustrated in Figure 4.10a, the global behaviour of these specimens (in terms of force-displacement curves) is nearly identical to their counterparts equivalent specimens from the LX_N group (with grooves surface preparation), indicating that the concrete surface preparation did not affect the bond behaviour. Also, the failure mode remained unchanged, comprising TRM debonded from the concrete substrate at the concrete-mortar interface with a thin layer of the concrete cover being peeled-off (Figure 4.11a).

As shown in Table 4.2, specimens with low concrete strength (LX_N_Ls) reached an ultimate load of 29.9, 30.7 and 34.9 kN for three layers, and 32.2, 35.1 and 37.7 kN for four layers, for bond lengths of 100, 150 and 200 mm, respectively. As also illustrated in Figure 4.10b, the global behaviour of this group of specimens in terms of force-displacement curves was very similar to their counterparts with higher concrete strength (i.e. group LX_N). The failure mode was also identical to their counterpart equivalent specimens including debonding of TRM from the concrete substrate accompanied with removal of concrete particles which remained attached to the debonded TRM strip (Figure 4.11b). It is observed that the quantity of concrete cover being peeled off was thicker than that of the corresponding specimens, and this is due to the weaker concrete surface resulted from lower concrete strength.

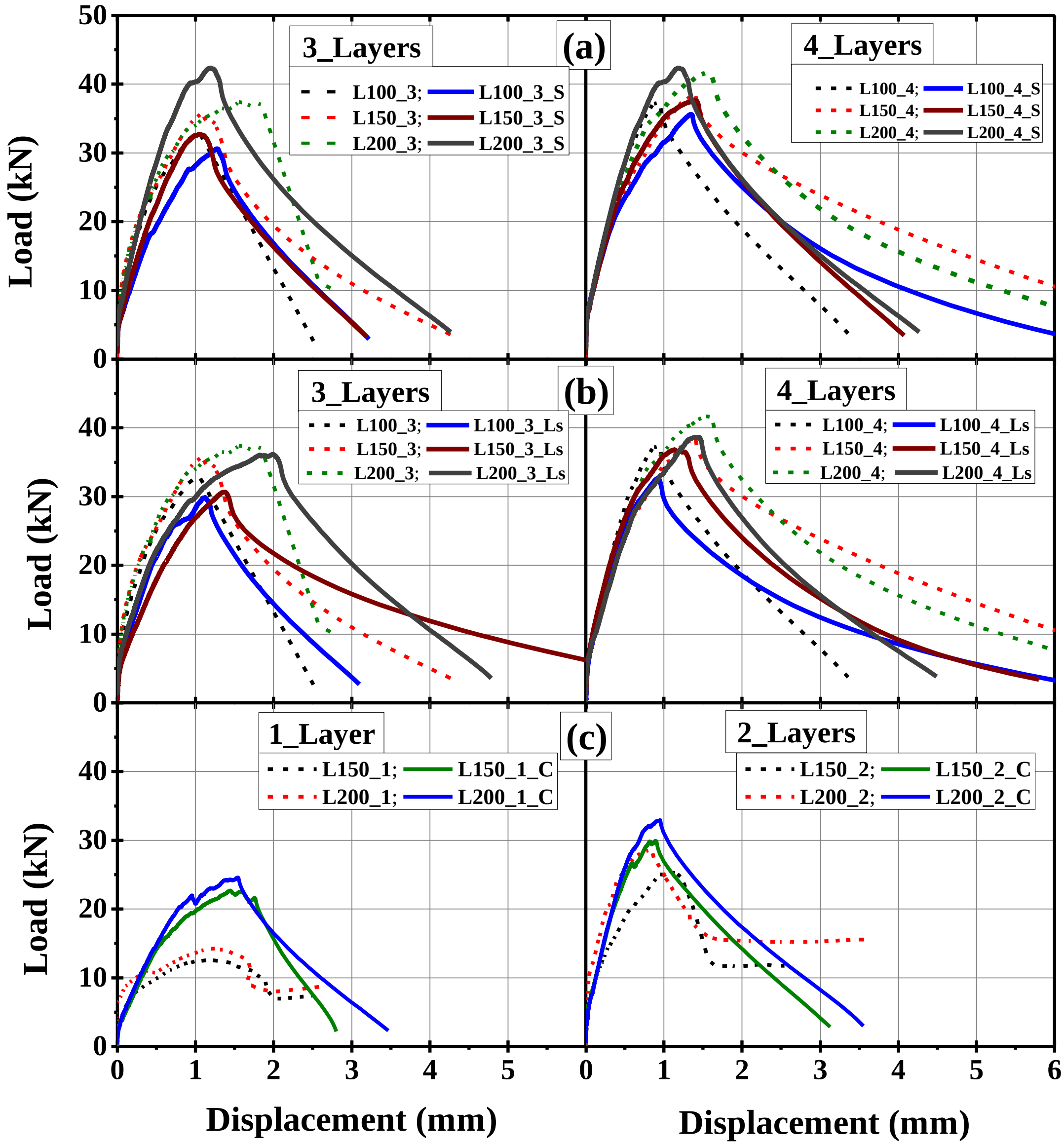

Figure 4.10. Load-displacement curves for specimens having as a parameter; (a) the concrete surface preparation, (b) the concrete compressive strength and (c) the textile coating.

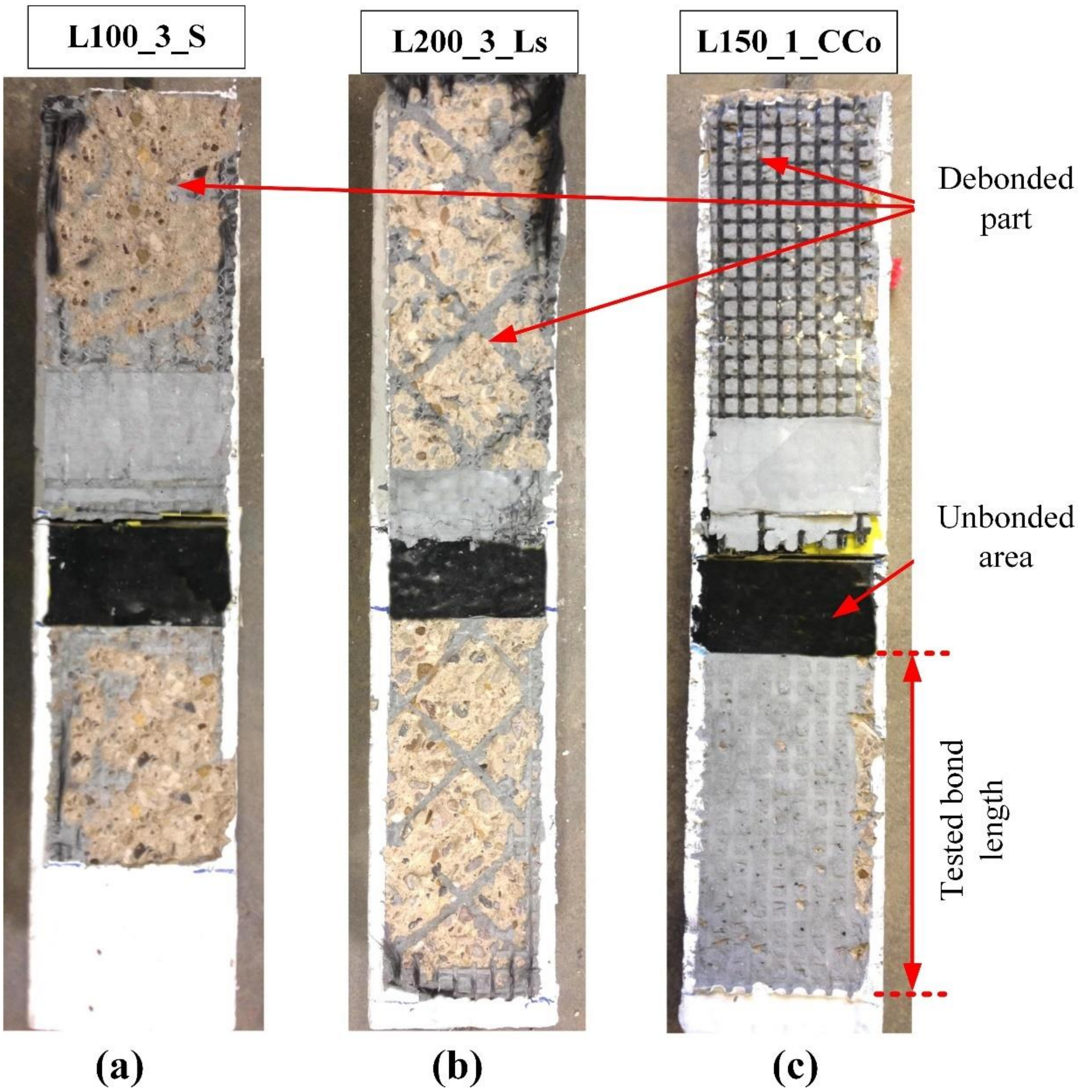

Figure 4.11. Typical failure mode of specimens with: (a) sandblasted concrete surface, (b) low concrete compressive strength, and (c) coated textiles.

The load-displacement curves of the specimens retrofitted with coated textiles (LX_N_CCo) are presented in Figure 4.10c. The ultimate load measured for one TRM layer was 21.9 kN and 23.9 kN for 150 and 200 mm bond length, respectively, which is substantially higher with respect to their counterpart's specimens strengthened using dry carbon textile. The corresponding ultimate load of the two TRM layers was 29.5 and 31.9 kN for 150 and 200 mm bond length, respectively. As shown in Figure 4.10c the post-peak behaviour of LX_N_CCo specimens was different from their counterparts from group LX_N, owing to the different failure mode observed. In particular, all specimens with coated textiles failed due to debonding of TRM due to fracture the surface at the textile-mortar interface (Figure 4.11c). This failure mode was different from their counterpart's specimens which experience slippage of the textile fibres through the mortar (Figure 4.7). Coating the textile with epoxy significantly enhance the bond between the inner and the outer filaments in a single roving. As a result, failure due to slippage of the fibre through the mortar was prevented, and damage was shifted to the textile-mortar interface, which seems the weakest among all interfaces. This type of failure mode can also be described as inter-laminar shearing. A denser crack pattern was observed in all specimens with the coated textiles, indicating a better activation of the textile fibres in tension.

Finally, the load-displacement curves for specimens LX_N_W, which were wrapped with two TRM layers in order to provide better anchorage, are shown in Figure 4.12a. Specimens L100_3_W and L100_4_W, reached an ultimate load of 40 and 50.8 kN for three and four layers, respectively (for 100 mm bond length). In terms of ultimate load response, they performed better than their counterparts (see Table 4.2) due to delay the premature debonding, whereas a change on the failure mode was also observed. Wrapping of the prism did not allow for debonding of the TRM strips and damage was localized in the loaded-end, where a single transversal crack appeared Figure 4.12b. Ultimately, the textile fibres slipped through the mortar resulting in a residual capacity as shown in Figure 4.12a.

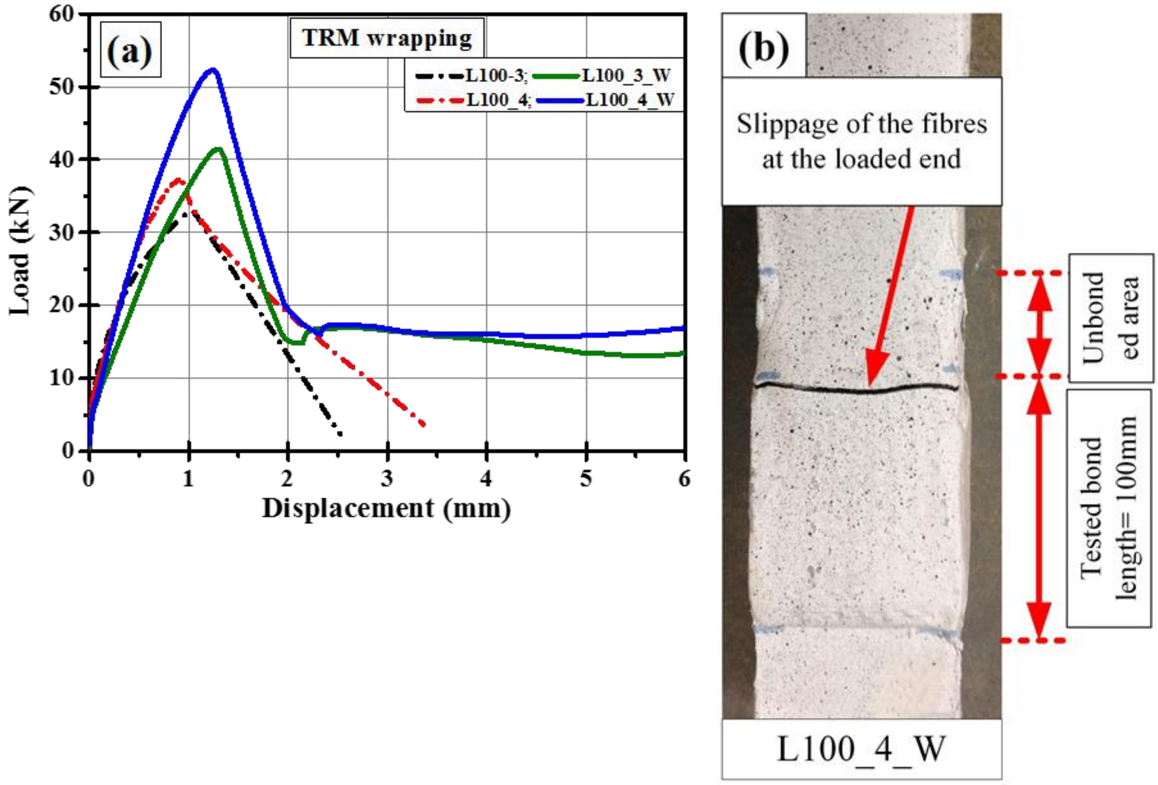

Figure 4.12. (a) Comparison of the load-displacement curves of specimens with anchorage through wrapping with counterpart specimens without anchorage; and (b) typical failure of specimens with anchorage through wrapping with TRM jackets.

4.3 Discussion

In terms of the various parameters investigated in this experimental programme, an examination of the results in terms of ultimate loads and failure modes revealed the following information.

4.3.1 Influence of the bond length and the number of layers

The effect of the bond length and the number of layers on the load-carrying capacity is depicted in Figure 4.13. The curves in Figure 4.13 clearly demonstrate that by increasing either the bond length or the number of layers, the bond capacity increases in a non-proportional way. Similar to the bond behaviour of FRP strips (Yao et al., 2005), after a certain bond length the anchorage force tends to reach a constant value which is considered as the maximum anchorage force. This length is called “effective bond length" (L_{eff}) and according to the curves provided in Figure 4.13 is in the range of 200 and 300 mm for the number of layers (one to four) investigated.

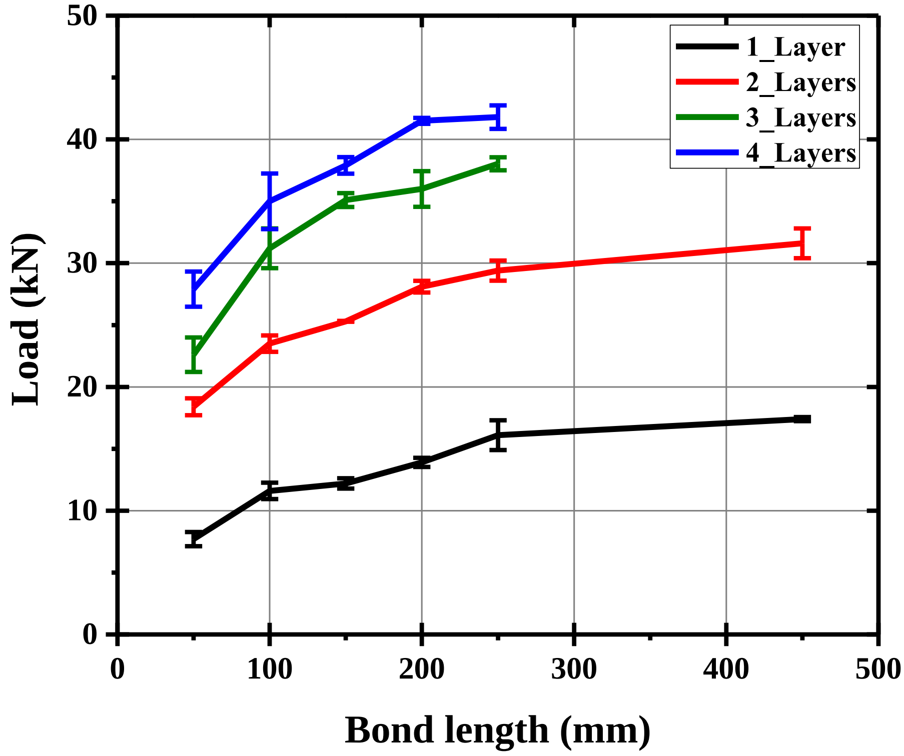

Figure 4.13. Variation of ultimate load with both, the bond length and number of layers.

The suggested value of effective bond length is in agreement with the conclusions of previous studies (D'Ambrisi et al., 2013; Sneed et al., 2014; Tran et al., 2014). Even in cases with one and two TRM layers, where there is significant friction between the inner and outer filaments when slippage occurs, by providing a large bond length (450 mm) the load capacity was marginally increased.

For the same bond length, increasing the number of layers resulted in an increase in the load-carrying capacity. This effect was more pronounced for the transition from one to two layers, whereas for more layers it was gradually becoming less significant. Almost the same trend was followed for all examined bond lengths between 50 and 250 mm. The most important effect of increasing the number of layers though, is related to the change in the failure mode. In particular, as explained in Section 4.2, specimens of LX_N group strengthened with one or two layers failed due to slippage of the textile fibres through the mortar (see Figure 4.7), whereas specimens with three or four layers failed due to TRM debonding from the concrete substrate with peeling off of a part of the concrete cover (Figure 4.8).

The above finding adds new information to the existing knowledge, because in all previous studies on bond between TRM and concrete (where the maximum number of layers examined was two), failure occurred either at the interface between fibres and mortar or at the interface between concrete and mortar without involving the concrete cover. It is noted that failure of TRM involving peeling off of the concrete cover has also been reported in the study of Tetta et al. (2015), where RC beams were retrofitted in shear with TRM U-jackets. This type of failure is very common in case of FRP bonded to concrete (Yao et al., 2005), indicating that TRM can behave similar to FRP by increasing the number of strengthening layers.

The bond length had also an effect on the residual bond strength of the specimens failed due to slippage of the fibres, which is related to the friction developed between the inner and the outer filaments of each individual fibre roving. Table 4.3 shows the percentage of residual load compared to the maximum load recorded for specimens one and two TRM layers. It is generally concluded that the larger the bond length, the higher the slipping surfaces become, so the residual strength do.

Table 4.3. Percentage of the residual load due to friction with respect to maximum recorded load for specimens strengthend with one and two layers of TRM.

Name	**Percentage of residual load (%)**	
	S_1*	**S_2***
L50_1	36.4	36.2
L50_2	33.5	28.5
L100_1	46.9	57.8
L100_2	33.3	34.0
L150_1	60.7	60.1
L150_2	46.6	43.4
L200_1	57.0	61.1
L200_2	56.8	65.8
L250_1	42.2	61.2
L250_2	52.2	52.4
L450-1	71.3	70.3
L450-2	75.0	81.6

* Specimen number

The bond length had also effect on the bond strength (f_b_calculated from Eq. 4.2) at the concrete-matrix interface. It is noted that the bond strength was calculated only for those specimens failed due to debonding of TRM from concrete substrate (see Table 4.2). As shown in Figure 4.14, as the bond length increase, the bond strength at the concrete-mortar interface decrease (approximately in proportional way). This is typical behaviour because increasing the bond length led to increase the area of interface that resist the applied load. Furthermore, it is noted that the effect of the number of layers on the bond strength at the concrete- matrix interface was very limited attributed to the identical observed failure mode (debonding).

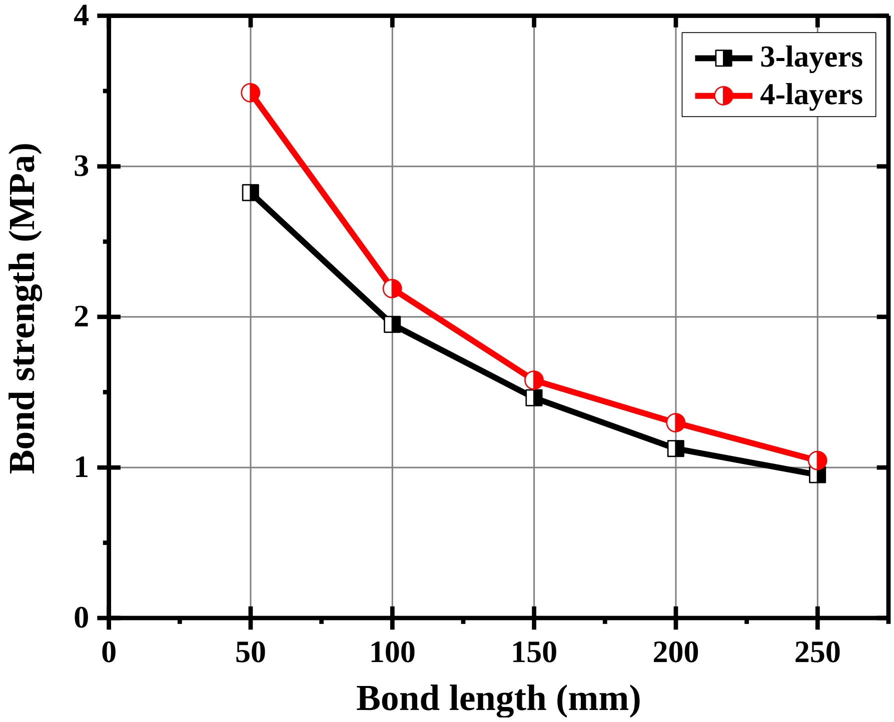

Figure 4.14. Variation of bond strength developed at the concrete-mortar interface with both, the bond length and number of layers.

Finally, Figure 4.15 shows the variation of the tensile stress in the textile fibres reinforcement (calculated from Eq. 4.2) with the bond length for different number of TRM layers. It is generally observed that by increasing the number of layers, the normal stress decreases, which is consistent with the behaviour of FRP bonded plates to concrete (Yao et al., 2005).

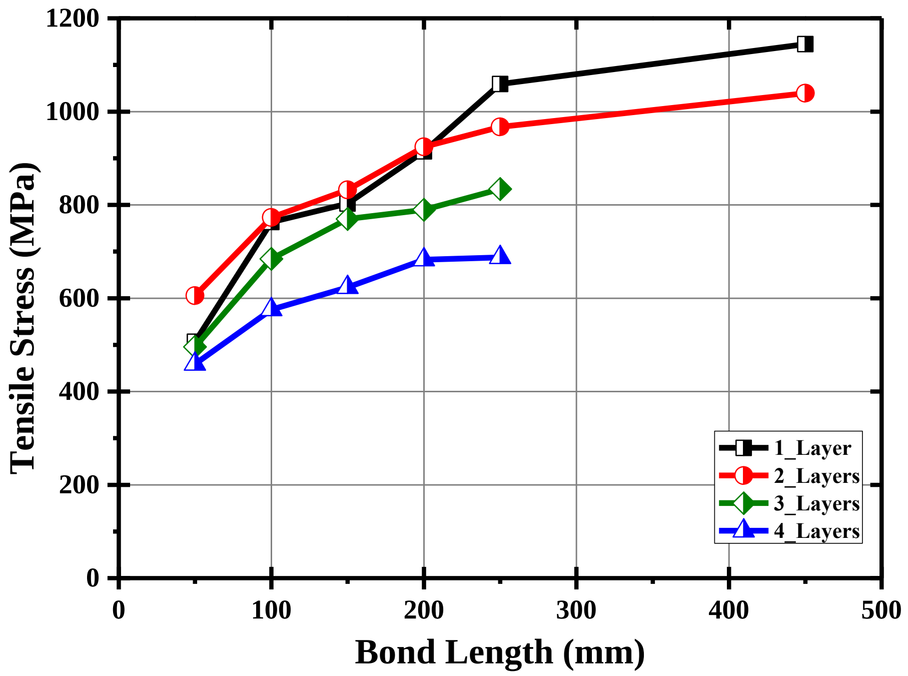

Figure 4.15. Variation of tensile stress in the textile reinforcement with the number of layers and bond length.

4.3.2 Influence of surface preparation

Figure 4.16a and b show a comparison between the ultimate loads of specimens having the same bond length but different concrete surface preparation, for three (Figure 4.16a) and four (Figure 4.16b) TRM layers. In the majority of the cases, grinding the concrete surface and creating of a grid of grooves is as effective as sandblasting in transferring shear stresses from TRM to concrete. Moreover, the shape of the force-displacement curves in Figure 4.10a is the same for both surface preparation methods. Hence, it can be concluded that both ways of surface preparation are suitable, something that needs further investigation for other textile geometries and other types of mortar. The current finding is in agreement with the study of D’Antino et al. (2015) where no differences were observed between specimens with untreated and sandblasted concrete surfaces, strengthened with one PBO-fibres TRM layer.

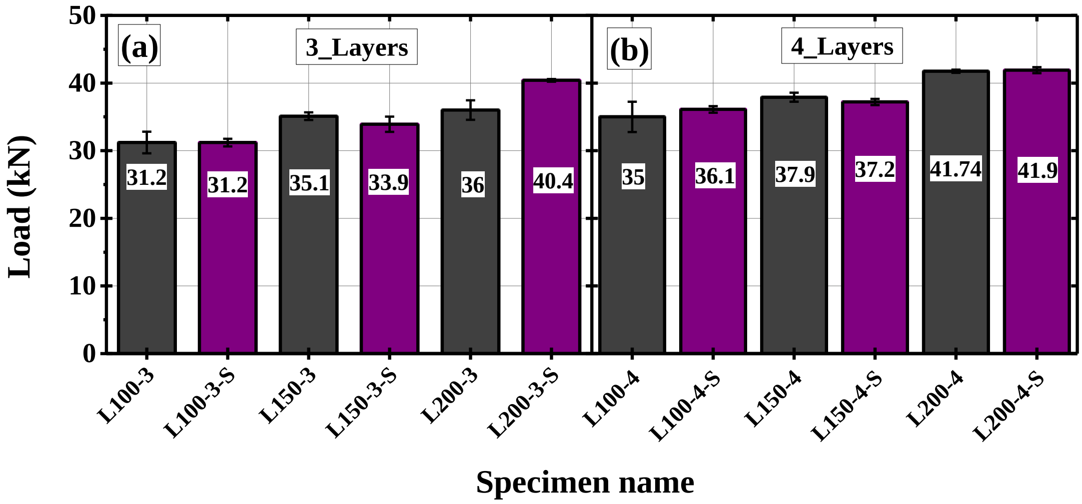

Figure 4.16. Influence of surface preparation on the ultimate load of specimens strengthened with: (a) three TRM layers; and (b) four TRM layers.

4.3.3 Influence of concrete compressive strength

The concrete compressive strength was selected to be investigated only for three and four TRM layers. This is because of the failure mechanism observed in LX_N specimens. In particular, TRM debonding from the concrete substrate involving part of the concrete cover (a failure mechanism which is associated to the concrete strength) occurred only in the case of three and four TRM layers. When one or two TRM layers were used, the failure was attributed to the concentration of the damage in one single crack. For this reason, it is believed by the authors that the concrete strength would not influence the results of specimens with one and two TRM layers.

A comparison of the ultimate loads between the LX_N_Ls specimens (lower compressive strength – approximately 15 MPa) and the LX_N specimens (higher compressive strength – approximately 30 MPa) is made in Figure 4.17a and b. In all cases, the use of a lower compressive strength concrete had an adverse impact on the load-carrying capacity of the specimens. For specimens with lower concrete strength, the reduction in the ultimate bond capacity was 4.1%, 12.5% and 3.1% for three TRM layers and 8%, 7.4% and 9.2% four TRM layers, and for bond lengths equal to 100, 150, and 200 mm, respectively. As expected, the lower (by 50%) compressive strength resulted in a decrease in the ultimate load which on average was equal to approximately 7.5%. This reduction, though, cannot be considered as significant as it may be in the range of the statistical error. It is noted that the insignificant effect of the concrete strength on the load capacity has also been reported by D'Antino et al. (2015). However, in their study the concrete was not directly involved in the failure mode which was at the interface between the matrix and the fibres.

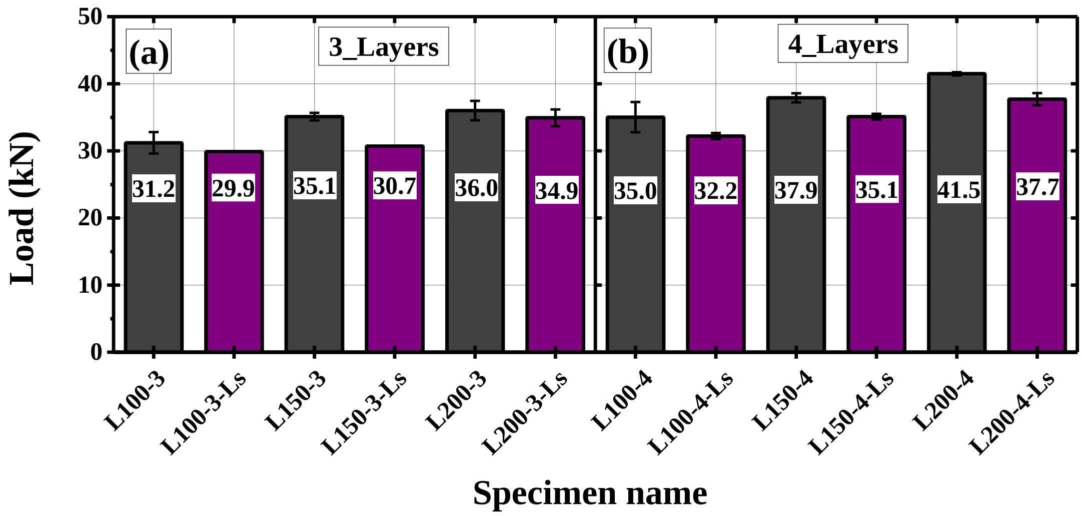

Figure 4.17. Effect of concrete compressive strength on the ultimate load of specimens strengthened with: (a) three TRM layers; and (b) four TRM layers.

4.3.4 Influence of coating

Coating the textile fabric with epoxy resin was investigated only for specimens with one and two TRM layers, in order to prevent the premature failure due to slippage of the fibres through the mortar that observed in these specimens with uncoated textiles. According to the results, the effect of coating was twofold: (a) change in the failure mode, and (b) significant increase of the load-carrying capacity. The failure mode changed from slippage of the fibres through the surrounding matrix to debonding of

TRM at the textile-mortar interface (interlaminar shearing). Comparison of the ultimate loads of specimens with one and two layers of coated textiles and of spciemens with uncoated textiles is shown in Figure 4.18a and b, respectively, for different bond lengths. The ultimate load was increased by 79.5% and 71.9% for specimens with one layer and 16.6% and 13.5% for specimens with two layers, for bond lengths equal to 150 and 200 mm, respectively.

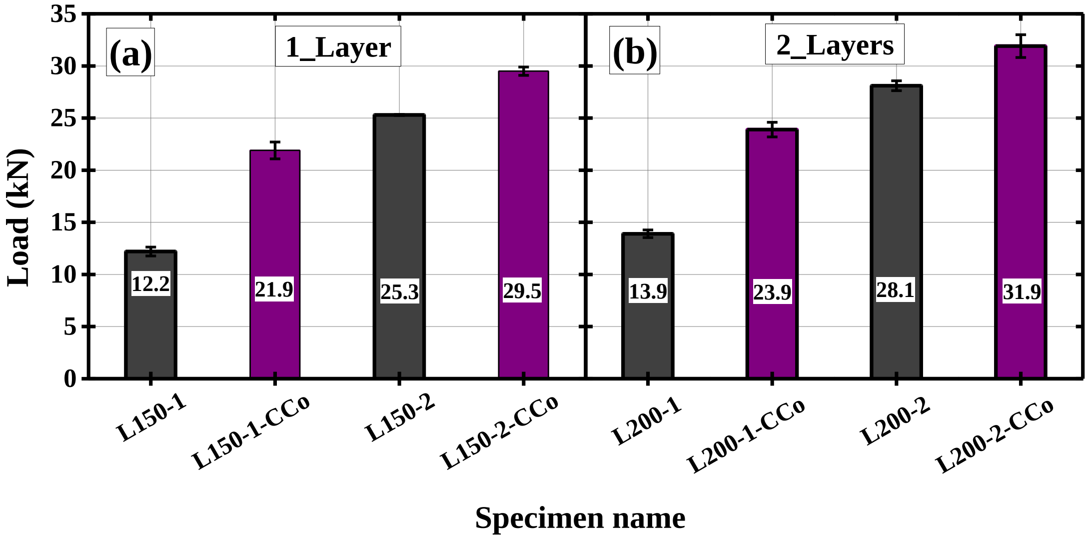

Figure 4.18. Effect of textile surface condition on the ultimate load of specimens strengthened with: (a) one TRM layer; and (b) two TRM layers.

Coating the textile with epoxy resin made the textile more stable and easy-to-apply, while at the same time it increases its rigidity. When a good level of impregnation of the fibres with resin is achieved, the inner filaments of the rovings are better bound to the outer filaments. As a result, the mechanism of transferring stresses from the fibres to the matrix is improved providing better mechanical interlock conditions. Ultimately, the textile fibres are better utilized in carrying tensile forces and the load capacity increases. A more uniform distribution of stresses is also achieved (something that is indicated by the formation of several transversal cracks) and the failure mode changes from local slippage of the fibres to global debonding of the TRM strips with the failure surface though being within the TRM thickness (textile-mortar interface).

4.3.5 Influence of anchorage through wrapping

The influence of anchorage through confinement (full wrapping) was investigated for a short bond length (100 mm) and for 3 and 4 TRM layers. The idea behind that was to improve the bond conditions when a short bond length (less than the effective bond length) is provided, by preventing early TRM debonding. As shown in Figure 4.19, the load capacity was increased by 28% and 45% when three and four TRM layers, respectively were anchored through wrapping with TRM jackets. Note that the bond length was equal to 100 mm whereas two TRM layers were used for wrapping. As expected, the failure mode changed from TRM debonding to partial rupture and slippage of the fibres across a single crack developed at the loaded end (Figure 4.12b).

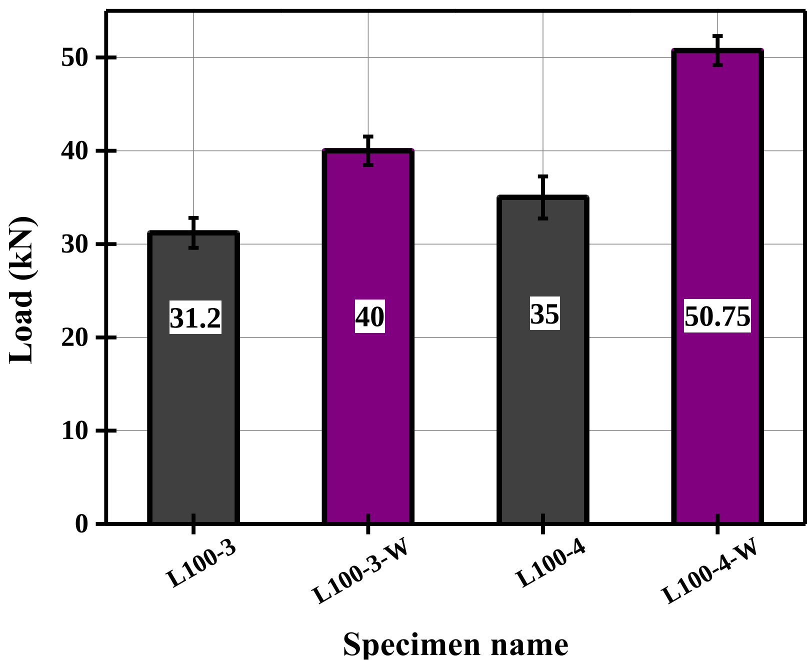

Figure 4.19. Effect of anchorage through wrapping with TRM jackets on the ultimate load of specimens strengthened with one and two TRM layers and bond length of 100mm.

A conclusion that must be highlighted is that the anchored TRM strips with a short bond length (100 mm) not only reached, but exceeded the load capacity of non-anchored strips with much higher bond length. Particularly, by comparing specimen L100_3_W with specimens L200_3 and L250_3, an increase of the maximum load of 11.1% and 5.2%, respectively, is observed. Similarly, by comparing specimen L100_4_W with specimens L200_4 and L250_4, the increase in the maximum load reaches 22.3% and 21.4%, respectively. Therefore, wrapping with TRM jackets is recommended to improve the bond conditions when the available length for anchorage of TRM reinforcement is limited.

4.4 Summary

This Chapter builds on the results of a comprehensive experimental programme for the investigation of the bond between TRM and concrete. Eighty specimens were fabricated and tested under double-lap shear. This poly-parametric study included the investigation of: (a) the TRM bond length, (b) the number of TRM layers, (c) the concrete surface preparation, (d) the concrete compressive strength, (e) the coating of the textile, and (f) the anchorage through wrapping. The main conclusions drawn are summarized below:

- By increasing the bond length, the bond capacity increases in a non-proportional way for all the number of TRM layers examined (1 to 4). After a certain bond length, the so-called effective bond length, the increase in the bond capacity was not significant. This length is ranging between 200 to 300 mm for the examined number of layers and for the materials used in this study.
- By increasing the number of TRM layers for the same bond length, the bond capacity increases in a non-proportional way. The increase was more pronounced

for the transition from one to two layers due to the change in the failure mode, whereas for more layers it was gradually becoming less significant.

- The number of layers has a significant effect on the failure mode. For one and two TRM layers the failure was due to slippage of the textile fibres through the mortar at a single crack close to the loaded end. For three and four TRM layers the failure was attributed to debonding at the mortar/concrete interface including detachment of a thin concrete layer, similarly to EB FRP systems.
- Different concrete surface preparation methods (grinding and formation of a grid of grooves versus sandblasting) did not influence the bond characteristic between TRM and concrete, suggesting that both methods are suitable.
- The use lower concrete compressive strength marginally affected the bond strength of the TRM to concrete. A 50% reduction in concrete's compressive strength resulted in an average decrease of the ultimate bond capacity of 7.5%, without affecting the failure mode.
- Coating the textile with an epoxy adhesive has a twofold effect: (a) change in the failure mode from slippage through the mortar to TRM debonding at textile-mortar interface, and (b) increase the ultimate load by 75% and 15% (comapred to their counterpart speicmens strengthened wiht dry textile) for specimens retrofitted with one and two layers, respectively.
- The anchorage of TRM strips through wrapping with TRM jackets results in substantial increase of the bond strength (up to 28% and 45% for 3 and 4 TRM layers, respectively), by preventing the premature debonding from the concrete substrate.

Chapter 5

BOND BETWEEN TRM AND CONCRETE: DOUBLE-LAP SHEAR TEST AT HIGH TEMPERATURES

ABSTRACT

This chapter examines for the first time the bond performance between TRM and concrete interfaces at high temperatures and, also compares for the first time the bond of both FRP and TRM systems to concrete at ambient and high temperatures. The key investigated parameters include: (a) the strengthening systems (TRM or FRP), (b) the level of high temperature to which the specimens are exposed (20, 50, 75, 100, and 150 ^{0}C) for FRP-reinforced specimens, and (20, 50, 75, 100, 150, 200, 300, 400, and 500 ^{0}C) for TRM-strengthened specimens, (c) the number of FRP/TRM layers (3 and 4), and (d) the loading conditions (steady state and transient conditions). A total of 68 specimens (56 specimens tested in steady state condition, and 12 specimens tested in transient condition) were constructed, strengthened and tested under double-lap direct shear. The result showed that overall TRM exhibited excellent performance at high temperature. In steady state tests, TRM specimens maintained an average of 85% of their ambient bond strength up to 400 ^{0}C, whereas the corresponding value for FRP specimens was only 17% at 150 ^{0}C. In transient test condition, TRM also outperformed over FRP in terms of both the time they sustained the applied load and the temperature reached before failure.

** The content of this work has been accepted as a journal paper: ‘‘Bond between TRM versus FRP composites and concrete at high temperatures’’, Composites Part B: Engineering; DOI: 10.1016/j.compositesb.2017.05.064.*

5.1 Test Specimens, Investigated Parameters, Materials and Strengthening Procedure

The main aim of this chapter is to investigate the bond behaviour of TRM-to-concrete at high temperatures, and also to compare the bond of TRM versus FRP with concrete at different high temperatures and loading conditions. In total 68 specimens (34 twin specimens) were constructed, strengthened and tested under double-lap shear test. The specimen's setup is described in detail in Section 4.1.1 supported with Figure 4.1a-f. Each specimen comprised two RC prisms with dimensions of 100x100mm cross section and 265 mm length. The two prisms were connected only by FRP/TRM layers which were bonded on two opposite sides of the prisms.

The parameters examined were: (a) the matrix used to impregnate the fibres, namely resin or mortar, resulting in two strengthening systems (TRM or FRP), (b) the temperature to which the specimens were exposed (50, 75, 100, 150 ^{0}C) for FRP and (50, 75, 100, 150, 200, 300, 400 and 500 ^{0}C) for TRM retrofitted specimens (c) the number of layers (3 and 4), and (d) the loading condition, namely steady state test and transient test conditions. In the steady state test, 56 (28 twin) specimens were heated up to a predefined temperature (see Table 5.1), kept at this temperature for 60 min., and then loaded monotonically up to failure. In the transient test, 12 (6 twin) specimens were first loaded (at ambient temperature) up to a load fraction equal to 25%, 50%, and 75% of the bond strength of the corresponding specimens tested at ambient temperature and then the specimens were heated up to failure.

The notation used for the specimens is BN_T, where B represents the type of binding material (R for epoxy resin and M for cement mortar), N refers to the number of FRP/TRM layers, whereas T denotes the exposed temperature for steady state tests, and the loading fraction of specimens tested at ambient for transient test condition. For example, M4_400 refers to a specimen strengthened with 4 TRM layers and tested monotonically (in steady state condition) at 400 ^{0}C; whereas, M4_75% denotes to a 4 layers TRM specimen, subjected to a load fraction of 75% of the bond strength measured at ambient temperature, and then exposed to high temperature up to failure. Details for each parameter of all specimens are also presented in Table 5.1.

The bond length (L_b) of FRP/TRM reinforcement was the same and equal to 200 mm for all tested specimens. This length was selected on the basis of the results of bond test of TRM to concrete presented in Chapter 4:Chapter 4, where it was found that the effective bond length (for 3-4 strengthening carbon layers) was approximately equal to 200 mm (see Section 4.3.1). For FRP system, preliminary tests were conducted to determine the effective bond length and found that this length is approximately 150 mm (see Figure 5.1).

The specimens were cast in different groups using the same mix design. The concrete compressive strength was obtained on the day of the testing. Table 5.1 reports the value of the concrete compressive strength (average of three 150 mm cubes).

Table 5.1. Specimens details, concrete compressive strength, and mortar properties on the day of testing.

Specimen	Temp. (^{0}C)	No. of layers	Concrete compressive strength (MPa)*	Mortar	
				Flexural strength (MPa)*	Compressive strength (MPa)*
M3_20[1]	Ambient	3	32.8	9.9 (0.3)	39.9 (2.1)
M3_50	50	3	33.7 (1.8)	3.93 (0.07)	20.8(2.2)
M3_75	75	3		3.49 (0.35)	19.1(1.9)
M3_100	100	3		2.35 (0.12)	14.5(1.6)
M3_150	150	3		2.2 (0.18)	14.1(0.9)
M3_200	200	3		2.3 (0.19)	15.2 (1.2)
M3_300	300	3		3.31 (0.05)	19.8(0.8)
M3_400	400	3		3.73 (0.08)	21.9(2.7)
M3_500	500	3		1.31 (018)	12.7(0.6)
M4_20[1]	Ambient	4	32.8	10.6 (1)	40.9 (2.5)
M4_50	50	4	31.4 (2.3)	3.93 (0.07)	20.8(2.2)
M4_75	75	4		3.49 (0.35)	19.1(1.9)
M4_100	100	4		2.35 (0.12)	14.5(1.6)
M4_150	150	4		2.2 (0.18)	14.1(0.9)
M4_200	200	4		2.3 (0.19)	15.2 (1.2)
M4_300	300	4		3.31 (0.05)	19.8(0.8)
M4_400	400	4		3.73 (0.08)	21.9(2.7)
M4_500	500	4		1.31 (018)	12.7(0.6)
R3_20	Ambient	3	32.8 (1.6)	-	-
R3_50	50	3		-	-
R3_75	75	3		-	-
R3_100	100	3		-	-
R3_150	150	3		-	-
R4_20	Ambient	4	29.7 (2.1)	-	-
R4_50	50	4		-	-
R4_75	75	4		-	-
R4_100	100	4		-	-
R4_150	150	4		-	-

[1] presented in Table 4.2.
*Standard deviation in parenthesis

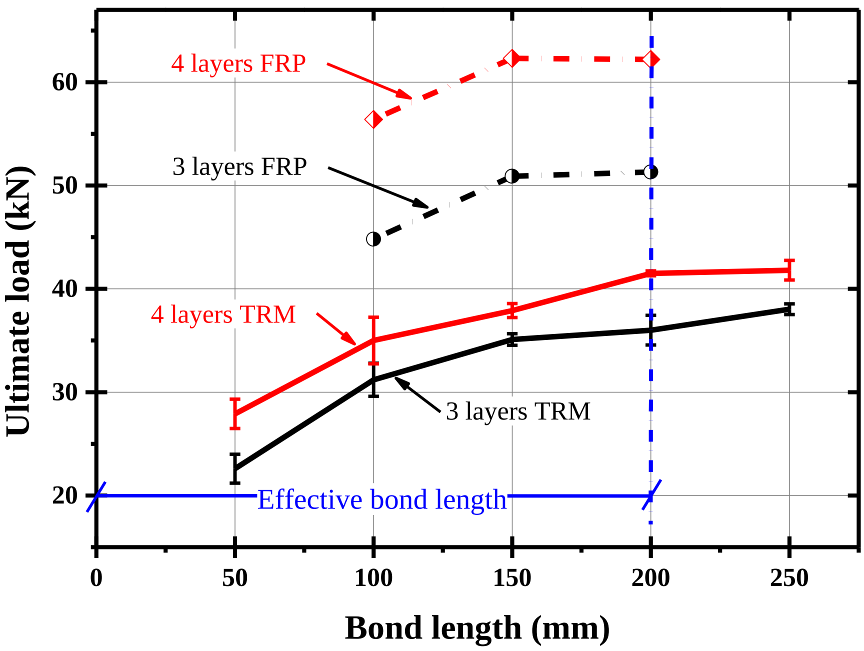

Figure 5.1. Variation of ultimate load with the number of layers and the bond length for both FRP and TRM strengthening systems.

The textile used as an external reinforcement was the dry carbon fibres textile (C) described in Section 3.3. The cement mortar described in Section 3.1was used as a binding material for the specimens strengthened with TRM. The compressive and flexural strength of the cement mortar both at ambient and high temperatures were experimentally obtained on the day of testing. Three mortar prisms with dimensions of 40x40x160 mm were used to determine the compressive and flexural strength. The prisms were fixed in the furnace as shown in Figure 5.2, heated up to the desired temperature, kept for 60 min. at this temperature, and then tested according to the BS EN 1015-11 (1999). Table 5.1 reports the results of compressive and flexural strength of the mortar prisms (average value from 3 prisms). For the specimens retrofitted with FRP, the epoxy resin described in Section 3.13.2 was used as a binding material.

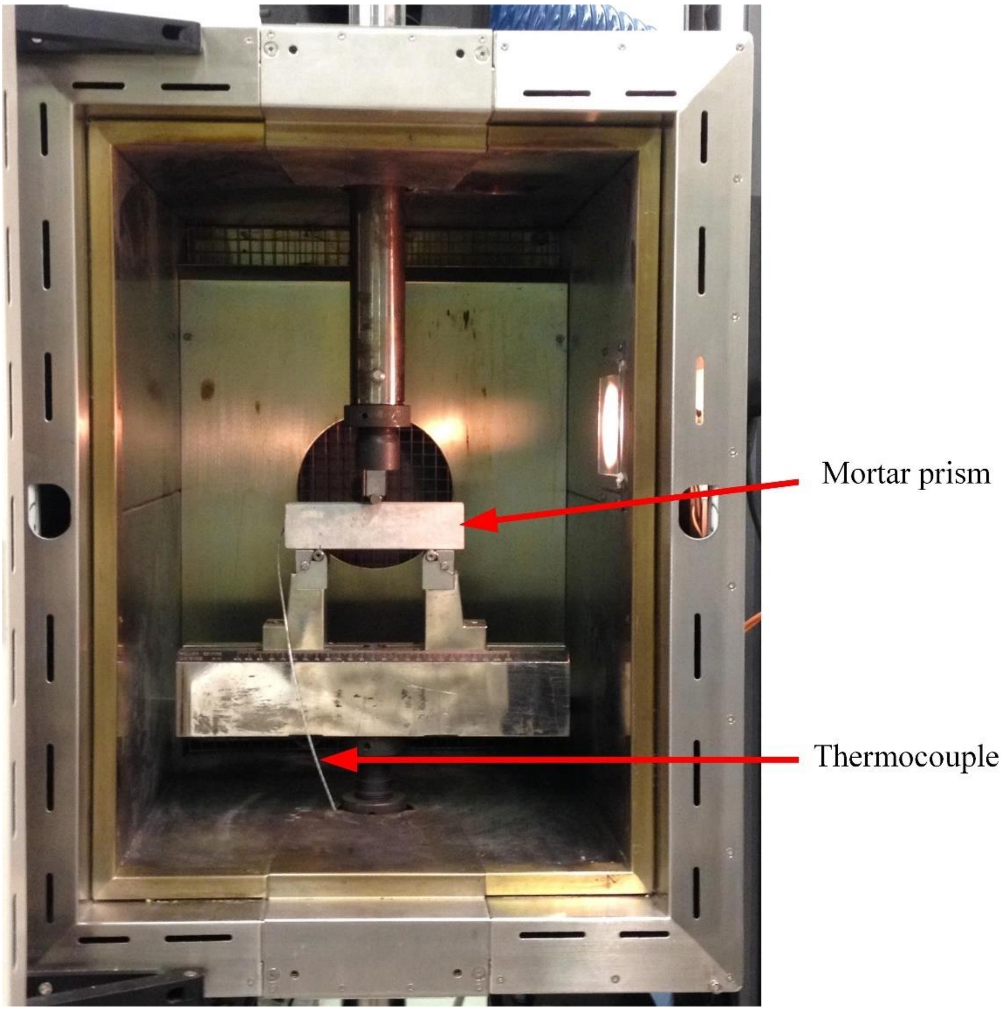

Figure 5.2. Test setup for the mortar prisms tested at high temperature.

The strengtheneing procedure for TRM speicmens was presented in Section 4.1.2 and including the following steps: (a) preparation the concrete surface (Figure 5.3a); (b) application of the first layer of mortar followed by the first layer of textile (Figure 5.3b). For specimens that received FRP, the concrete surface was prepared by removing a thin layer of concrete cover followed by roughening the surface (Figure 5.3c), then the first layer of the textile fibres was applied on a thin layer of epoxy resin and impregnated using a plastic roll (Figure 5.3d). For both strengthening systems, the above procedure was repeated until the required number of layers (3 or 4 layers) was applied.

Note that, before application of strengthening materials, a 100 mm-long central zone was wrapped with a foil tape (Figure 5.3a and c) in order to isolate the strengthening materials from the concrete prisms at this zone and prevent any possible attachment with the concrete surface. This was performed in order to prevent concrete-edge failure as described in Chapter 4 (Section 4.1.3). Note also that the bond width of FRP/TRM reinforcement was the same for all tested specimens and was equal to 80 mm.

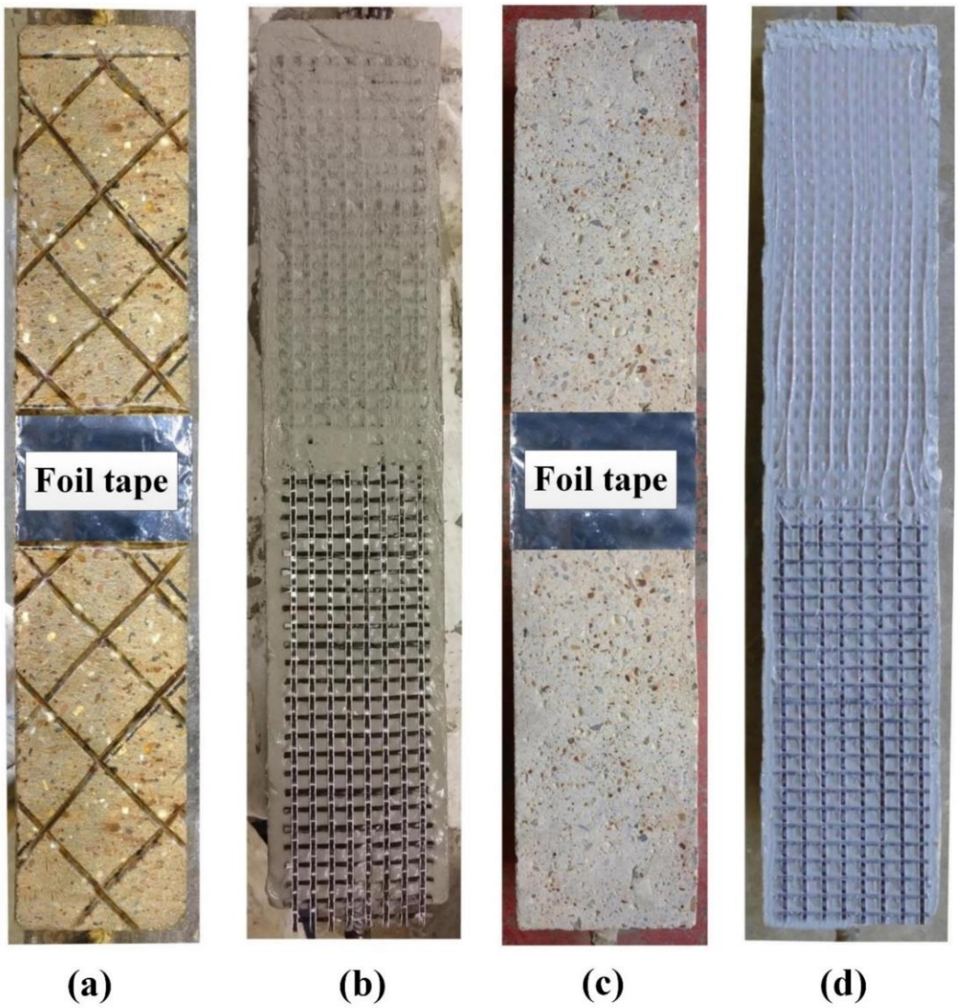

Figure 5.3. Strengthening procedure: (a) surface preparation for TRM specimens; (b) application of the first layer of mortar and first layer of textile; (c) surface preparation for FRP specimens; and (d) application of the first layer of textile for FRP specimens.

5.2 Test Setup, Instrumentations and Procedure

The specimens were positioned inside a furnace with inner chamber dimensions of 600 mm x 400 mm x 400 mm and maximum temperature of 600 ^{0}C. The furnace was installed into a universal testing machine of 250-kN capacity, as shown in Figure 5.4a.

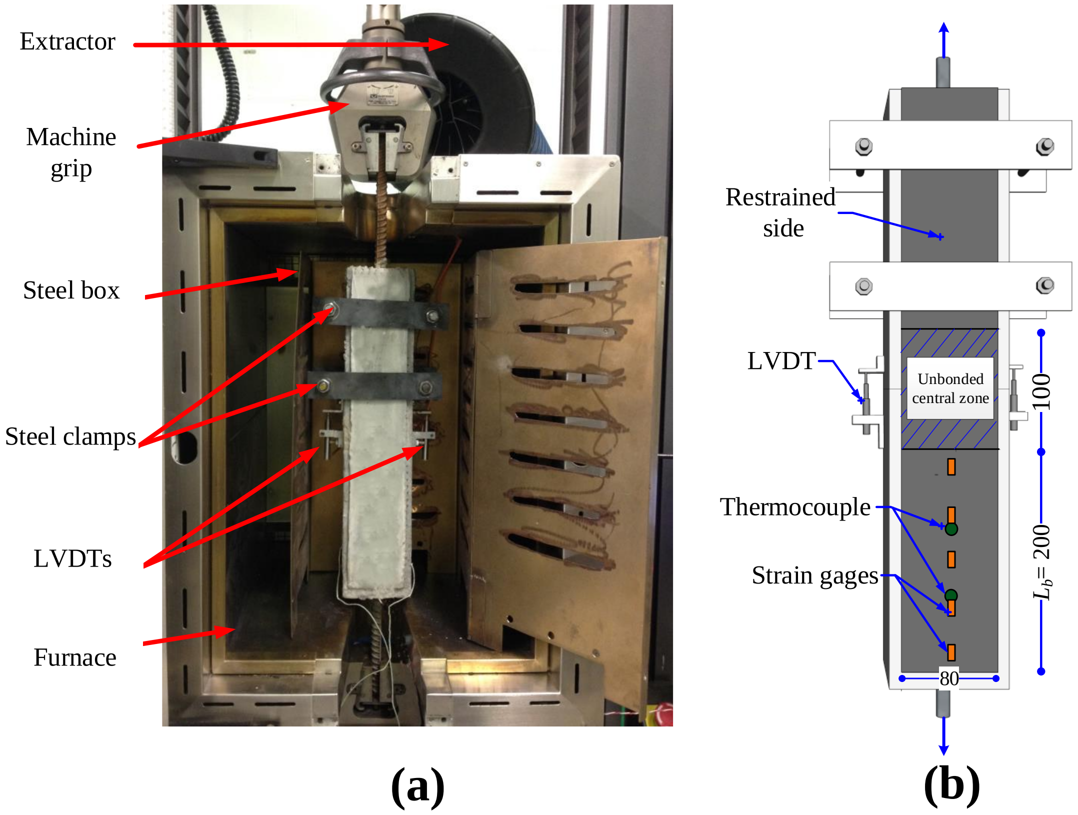

Figure 5.4. (a) Details of the test setup; and (b) details of test specimen.

The instrumentations used for specimens tested in steady state condition included: (i) Two high temperature LVDTs, fixed to the specimens' un-strengthened sides to measure the relative displacement between the two prisms (Figure 5.4a and b); (ii) two thermocouples type-K with diameter of 1.2 mm, fixed at the matrix-concrete interface and located at the positions shown in Figure 5.4b to monitor the temperature at this interface; (iii) Five high temperature strain gages mounted to the surface of TRM an located at the positions shown in Figure 5.4b to measure the strain along the bond length. Two steel clamps were fixed to the non-instrumented side of the specimens (Figure 5.4a and b) so as to prevent the failure in the un-instrumented side and ensure that the failure would occur in the instrumented side. Finally, the specimen was encased in a steel box to protect the furnace in case of explosion (Figure 5.4a).

For specimens tested in steady state condition the following steps were adopted: (a) positioning of the specimens inside the furnace and fixing only to the upper grip of the testing machine (Figure 5.4a); (b) heating up to the predefined target temperature described in Table 5.1, with an average heating rate of 5.25 ^{0}C/min, and keeping the target temperature constant for 60 min. (Figure 5.5); (c) fixing to the lower grip of the testing machine; and (d) monotonic loading up to failure, under displacement control at a rate of 0.2 mm/min.

For specimens tested in transient condition, the following procedure was carried out: (a) positioning in the furnace (at ambient temperature) and fixing to the machine grips; (b) loading up to the targeted load fraction of 25%, 50%, and 75% of the average ultimate load recorded for the specimens tested at ambient temperature; (c) heating the specimens with the same heating rate (5.25 ^{0}C/min) up to failure. For all tested specimens, an extractor was used to remove the smoke if was released as a result of heating the specimens up.

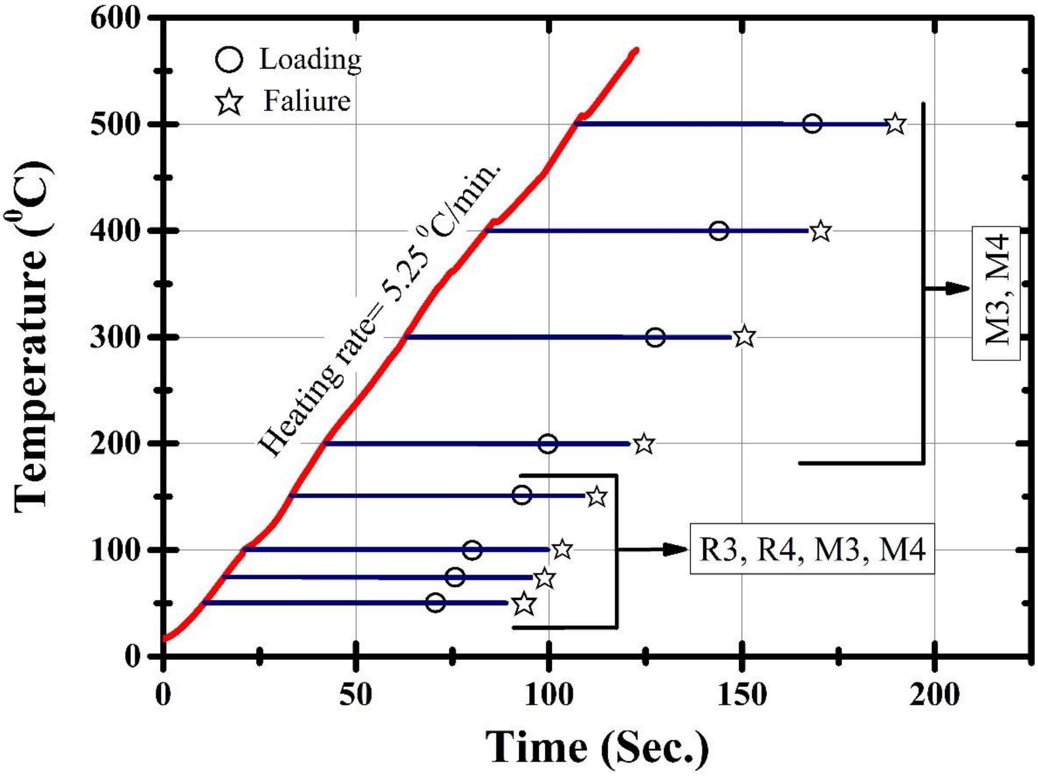

Figure 5.5. Scheme of time-temperature curve.

5.3 Experimental Results

As already mentioned in Section 4.2 supported with Figure 4.5, by assuming a perfect symmetry (up to peak load) between the two TRM strip in the tested side, each side will carry half of the measured ultimate load ($P_{u.}$), whereas, the relative displacement between the two concrete prisms measured at ultimate load will be the average of the two LVDTs' readings; (i.e. $\delta_{max}= (\delta 1+\delta 2)/2$_see Figure 4.5).

The main experiment results of all specimens tested in both loading conditions are presented in Table 5.2 and Table 5.3. Table 5.2, reports the results of the steady state test including: (1) the ultimate load (P_u) recorded for twin specimens S_1 and S_2; (2) the relative displacement (δ_{max}) recorded at the ultimate load (P_u); (3) the value of average load (P_{av}) of the twin specimens; (4) the average displacement (δ_{av}) of the twin specimens; (5) the ratio of high to ambient temperature bond strength, expressed as $P_u^{H.T}/P_u^{A.T}$ to quantify the effect of high temperatures on the bond strength; (6) the average bond strength (f_b) developed at the concrete-adhesive interface, calculated from Eq. 4.1; (7) the average effective tensile stress (σ_{eff}) in the textile reinforcement, calculated from 4.2; and (8) the observed failure mode.

Table 5.3 lists the results of the transient condition tests comprising: (1) the constant load (25%, 50% or 75% of the ambient temperature bond strength) in which specimens were subjected; (2) the time required to reach failure for both twin specimens S_1 and S_2; (3) the corresponding average time to failure for the twin specimens; (4) the temperature reached at the concrete-matrix interface at failure for twin specimens; (5) the corresponding average temperature; and (6) the observed failure mode.

It is worth mentioning that the measurements of the strain gages at high temperatures were not reliable and therefore are not presented here.

Table 5.2. Summary of test results.

Specimen	(1) P_u (kN)		(2) δ_{max} (mm)		(3) $P_{av.}$ (kN)	(4) δ_{av} (mm)	(5) $P_u^{H.T}/P_u^{A.T}$	(6) f_b (MPa)	(7) σ_{eff} (MPa)	(8) Failure mode**
	S_1*	S_2*	S_1*	S_2*						
R3_20	52.2	50.4	0.52	0.69	51.3	0.61	-	1.60	1125	D
R3_50	30.9	29	0.6	0.78	30.0	0.69	0.58	0.94	657	
R3_75	18.2	17.5	0.44	0.57	17.9	0.51	0.35	0.56	391	A
R3_100	15.8	13.5	0.53	0.68	14.7	0.61	0.28	0.46	3121	
R3_150	9.4	8.7	0.23	0.37	9.1	0.30	0.18	0.28	198	
R4_20	63.2	61.1	0.77	1.1	62.2	0.94	-	1.94	1022	D
R4_50	42.4	38.8	0.76	0.88	40.6	0.82	0.65	1.27	668	
R4_75	24.3	20.8	0.53	0.42	22.6	0.48	0.36	0.70	371	A
R4_100	16.7	14.8	0.5	0.67	15.8	0.59	0.25	0.49	259	
R4_150	10.4	9.1	0.37	0.51	9.8	0.44	0.16	0.30	160	
M3_20[1]	37.4	34.6	1.57	1.9	36.0	1.74	-	1.13	789	D
M3_50	29.0	29.6	0.75	0.99	29.3	0.87	0.81	0.92	643	D
M3_75	28.9	24	1.29	1.1	26.5	1.20	0.73	0.83	580	
M3_100	29.8	29.0	1.3	1.04	29.4	1.17	0.82	0.92	645	
M3_150	29.1	32.7	1.1	1.33	30.9	1.22	0.86	0.97	678	
M3_200	27.2	25.1	1.35	1.56	26.2	1.46	0.73	0.82	573	
M3_300	33.8	38	1.79	1.46	35.9	1.63	1.00	1.12	787	
M3_400	33.2	37.6	1.84	1.55	35.4	1.70	0.98	1.11	776	
M3_500	16.6	19.2	0.7	0.78	17.9	0.74	0.50	0.56	393	
M4_20[1]	41.7	41.3	1.57	1.31	41.5	1.44	-	1.30	683	D
M4_50	36.7	31.3	1.14	1.39	34.0	1.27	0.82	1.06	559	D
M4_75	32.3	36.4	1.02	0.85	34.4	0.94	0.83	1.07	565	
M4_100	36.2	36.2	1.28	1.25	36.2	1.27	0.87	1.13	595	
M4_150	36.9	36.1	1.17	1.26	36.5	1.22	0.88	1.14	600	
M4_200	38.5	35.2	1.44	1.05	36.9	1.25	0.89	1.15	606	
M4_300	36.5	41.2	1.46	1.18	38.9	1.32	0.94	1.21	639	

M4_400	37.6	40.7	1.72	1.43	39.2	1.58	0.94	1.22	644	
M4_500	21.8	24.3	0.75	0.87	23.1	0.81	0.56	0.72	379	

* Specimen number.
** D: Debonding of FRP/TRM from the concrete substrate including part of the concrete cover; A: Adhesive failure at the concrete-resin interface.
1 Specimens included in Table 4.2.

Table 5.3. Results of transient condition test.

Specimen	**(1) Load (kN)**	**(2) Time (min.)**		**(3) Average time (min.)**	**(4) Temperature (^{0}C)**		**(5) Average temperature (^{0}C)**	**(6) Failure mode****
		S_1*	S_2*		S_1*	S_2*		
R4_25%	15.5	19.9	18	19.0	100.8	91.8	96.3	A
R4_50%	31.1	16.3	17.7	17.0	66.4	74.9	70.7	D
R4_75%	46.6	11.9	12.7	12.3	47.5	50.2	48.9	D
M4_25%	10.4	65.6	58.3	62.0	329.8	309.2	319.5	D
M4_50%	20.8	62.3	55.2	58.8	319.6	301.1	310.4	D
M4_75%	31.1	18	21	19.5	72.4	82.2	77.3	D

* Specimen number
** A: Adhesive failure at the concrete-resin interface (see Figure 5.13a); D: Debonding of FRP/TRM from the concrete substrate with peeling off part of the concrete cover (see Figure 5.13b and c for FRP specimens and Figure 5.13d-f for TRM specimens).

5.3.1 Temperature profile

Figure 5.6 presents a typical temperature-time curve obtained from the two thermocouples affixed at the concrete- matrix interface, for a specimen tested in steady state condition and heated up to 400 ^{0}C. Since the readings (in all tests) were identical, the average (of the two thermocouples) temperature was used. Figure 5.7 displays the actual temperature-time curves for all FRP and TRM-strengthened specimens tested in steady state condition. It can be observed that: (a) the heating rate is identical between all specimens and (b) all specimens were exposed to predefined temperature for one hour before application of the load, and then tested under displacement control up to failure. Any further exposure time (more than one hour) was related to the time required to test the specimens up to failure. Note that the consistency in the heating procedure for all tested specimens is important to reduce errors, obtain reliable, and comparable results

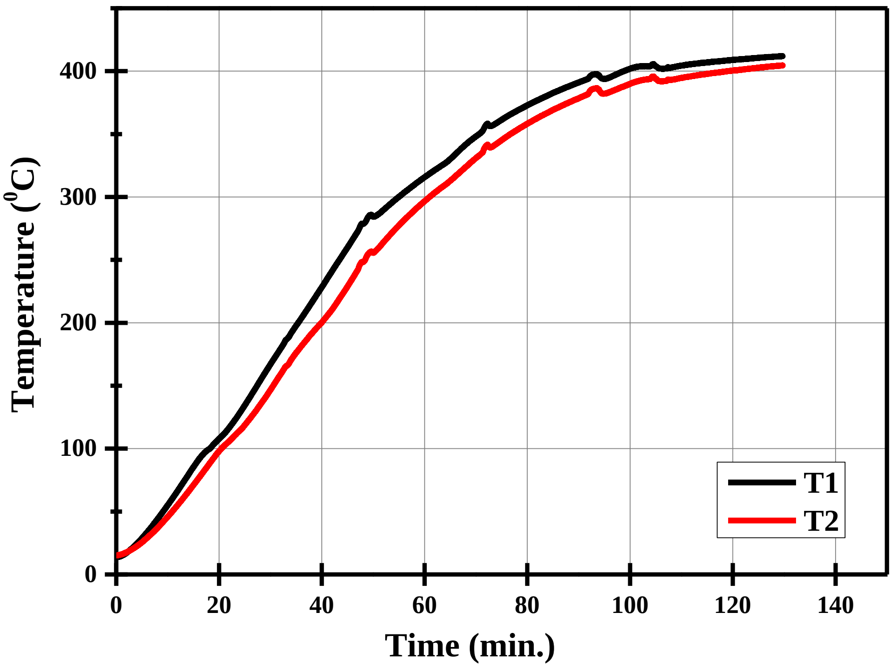

Figure 5.6. Time-temperature curve obtained from the two thermocouples for a specimen tested in steady state and heated up to 400 ^{0}C.

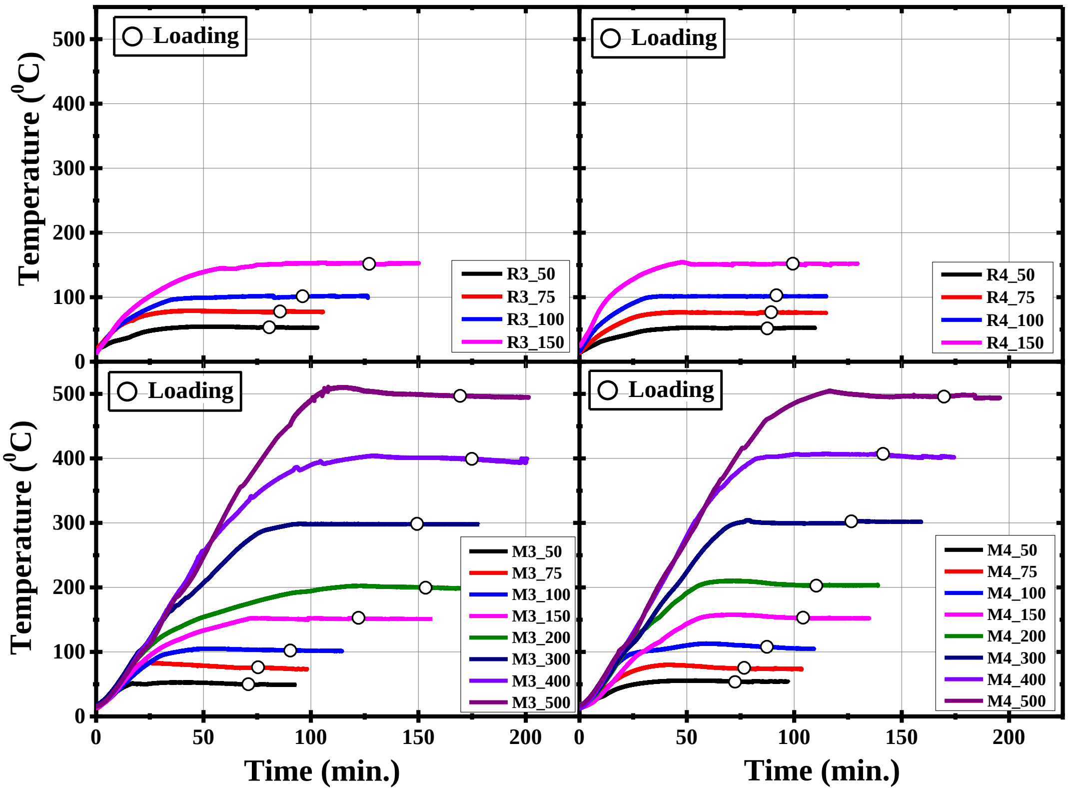

Figure 5.7. Actual time-temperature curve of all FRP and TRM specimens tested in steady state condition.

5.3.2 Load-displacement curves

Figure 5.8 presents the load-displacement curves of all FRP/TRM strengthened specimens tested in steady-state condition. For better clarity, only one of the twin specimen's curves is presented in this Figure. Moreover, they were grouped on the basis of the strengthening materials used and number of layers.

Starting from FRP-retrofitted specimens (Figure 5.8a and c), the load versus displacement curves were characterised by a linear ascending branch with progressive decreasing in the stiffness (due to softening of the resin at the concrete-resin interface) up to failure. On the other hand, the TRM-strengthened specimens' curves were characterized by two ascending branches; the first ascending branch was linear with high axial stiffness up to mortar cracking, followed by a nonlinear one with progressively decreasing stiffness up to failure (Figure 5.8b and d).

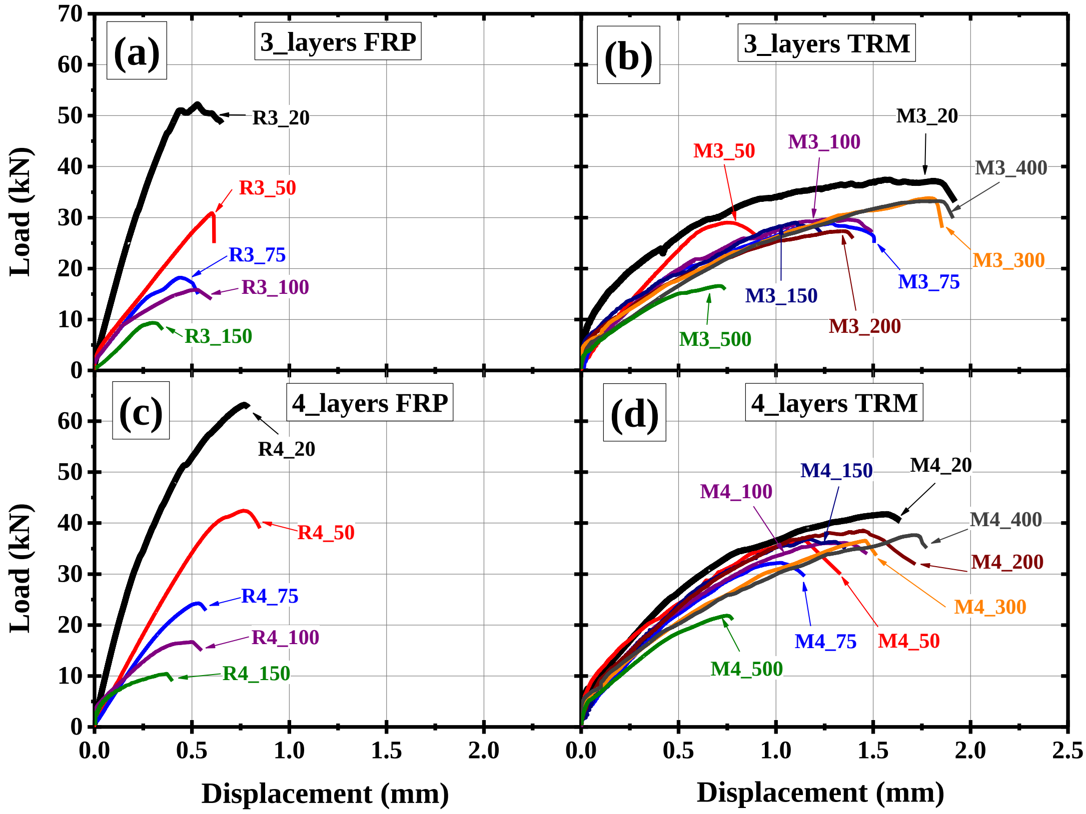

Figure 5.8. Load-displacement curves of the specimens strengthened with different materials and number of layers: (a) three layers FRP specimen; (b) three layers TRM specimens; (c) four layers FRP specimens; and (d) four layers TRM specimens.

Figure 5.9a and b, depicts the increase of the crosshead displacement and the average temperature at the concrete-adhesive interface with time, for specimens strengthened with 4 FRP and TRM layers, respectively, and tested in transient condition. The initial part of the curves shows the stage of loading to reach the predefined load fractions (25%, 50%, or 75% of the ambient load); whereas the second part represents the increase of the cross-head displacement due to the heating of the specimens up to failure. It is noted that the behaviour of the second part of all curves shown in Figure 5.9 (for both strengthening systems) was almost linear up to failure.

This is due the progressive decreasing in the stiffness of adhesive resulted from increasing the temperature at the concrete-adhesive interface.

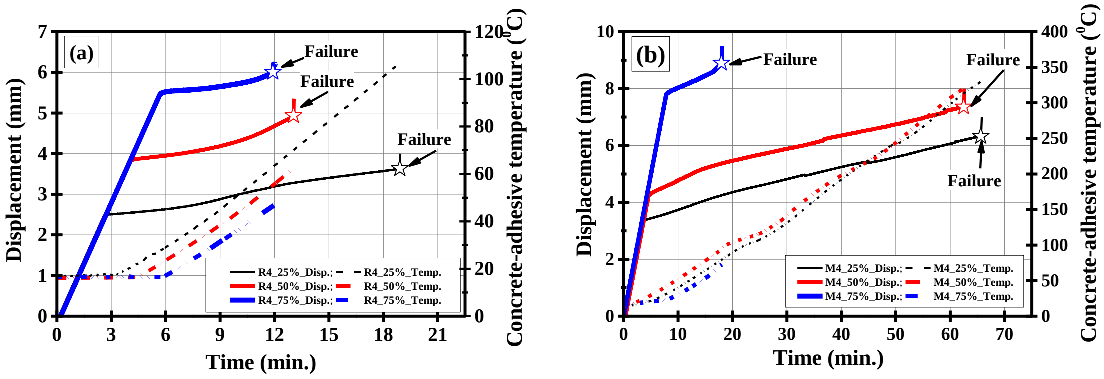

Figure 5.9. Cross-head displacement increase and average temperature at the bonded interface versus time of specimens tested in transient condition and strengthened with (a) 4-layers FRP and (b) 4-layers TRM.

5.4 Loading Condition

5.4.1 Steady state test: ultimate load and failure mode

For the FRP retrofitted specimens, the ultimate load recorded (average of two specimens) was: (a) 51.3, 30.0, 17.9, 14.7, and 9.1 kN, and (b) 62.2, 40.6, 22.6, 15.8, and 9.8 kN, for the specimens strengthened with 3 and 4 layers, and exposed to temperatures of 20, 50, 75, 100, and 150 ^{0}C, respectively. For the TRM-retrofitted specimens the ultimate load attained was : (a) 36.0, 29.3, 26.5, 29.4, 30.9, 26.2, 35.9, 35.4, and 17.9 kN; and (b) 41.5, 34.0, 34.4, 36.2, 36.5, 36.9, 38.9, 39.2, and 23.1 kN (average of two specimens) for specimens reinforced with 3 and 4 layers of TRM and testes at ambient, 50, 75, 100, 150, 200, 300, 400, and 500 ^{0}C, respectively (see Table 5.2).

Two types of failure modes were observed for FRP-strengthened specimens: (a) deboning of FRP from the concrete substrate including parts of the concrete cover being peeled off (Figure 5.10a-d), and (b) adhesive failures at the concrete-resin interface (Figure 5.10e-j).

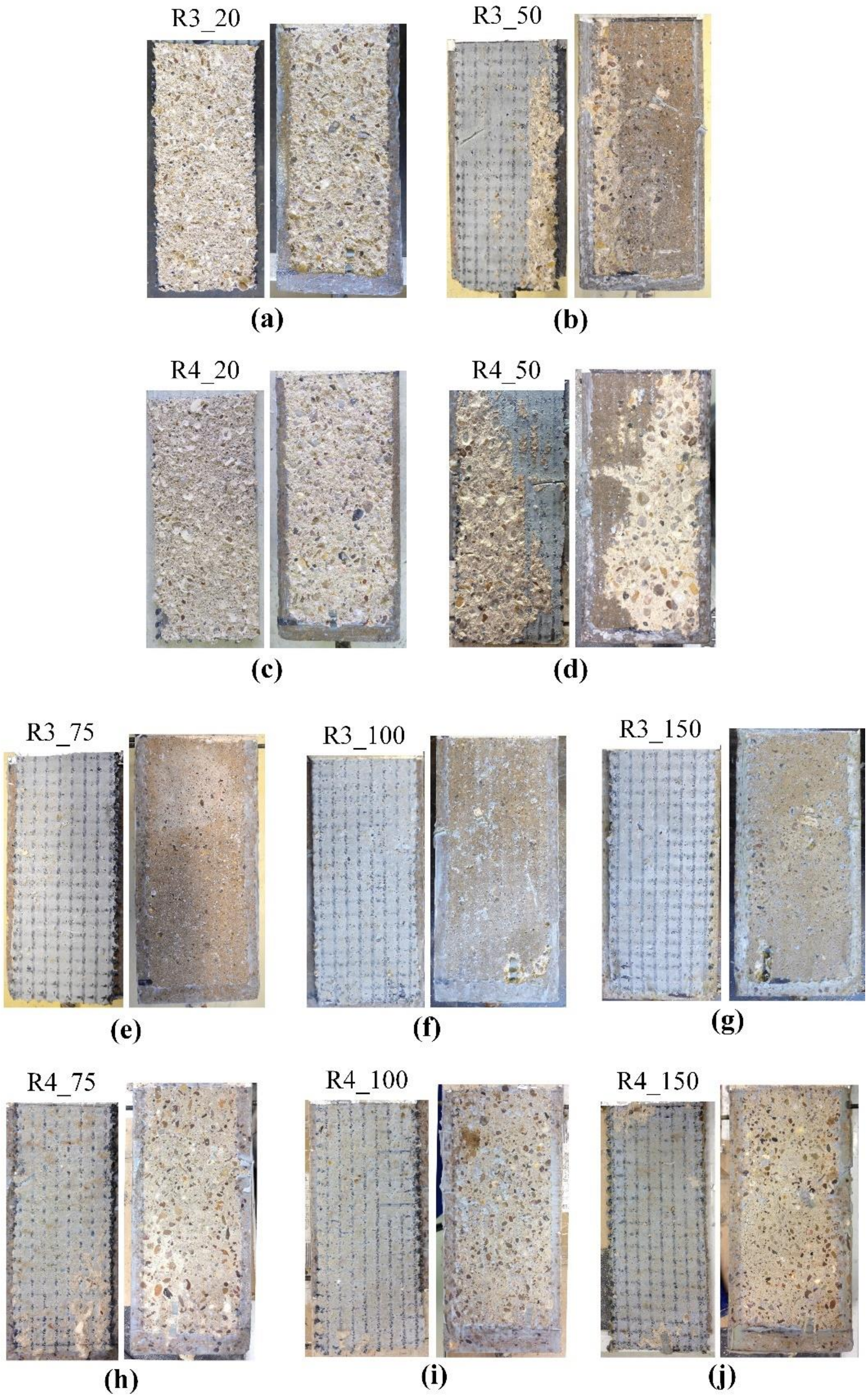

Figure 5.10. Failure mode of specimens strengthened with three and four layers of FRP tested in steady state condition at different elevated temperature varied from 20 to 150 ^{0}C.

The first failure mode occurred in all FRP-strengthened specimens tested at 20 ^{0}C and 50 ^{0}C, whereas, when the temperature increased to 75, 100 and 150 ^{0}C, adhesive failure at the concrete-resin interface occurred for all specimens, due to the poor bond behaviour of epoxy resin at temperature above the T_g. On the contrary, for all TRM-retrofitted specimens, regardless the number of layers, the only observed failure mode was debonding of TRM from the concrete substrate accompanied with parts of concrete cover (Figure 5.11a-i, and Figure 5.12a-i).

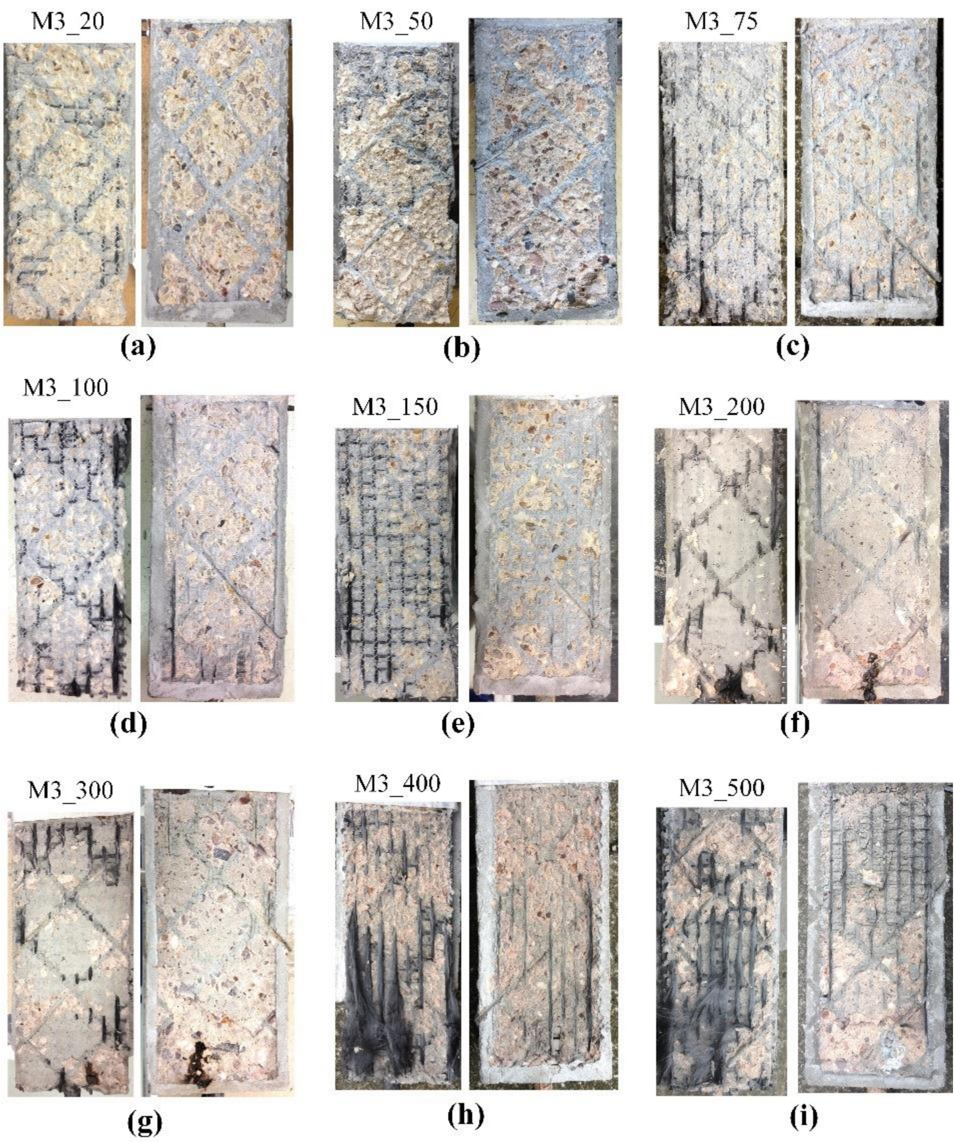

Figure 5.11. Failure mode of specimens strengthened with three layers of TRM tested in steady state condition at different elevated temperature varied from 20 to 500 ^{0}C.

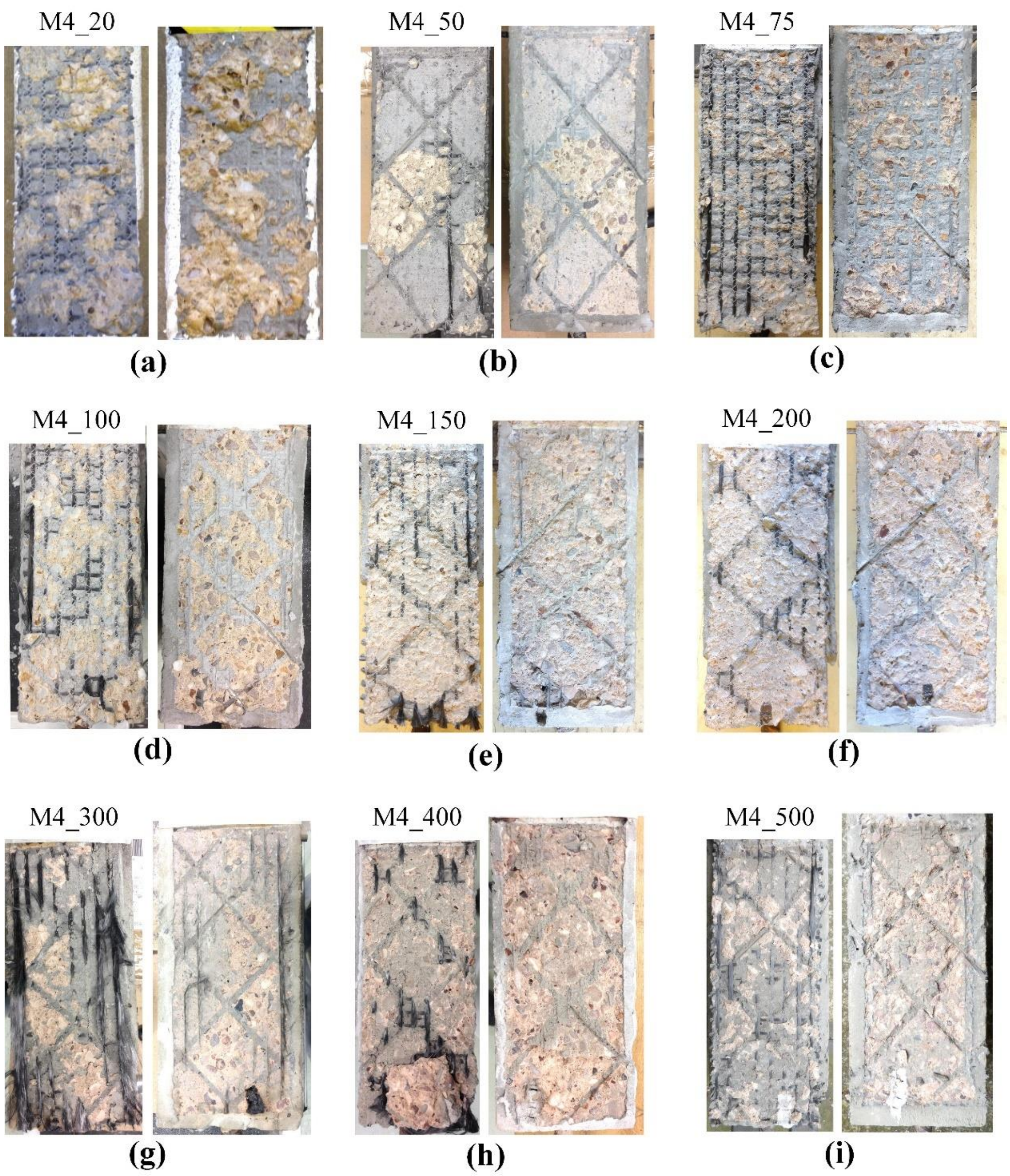

Figure 5.12. Failure mode of specimens strengthened with four layers of TRM tested in steady state condition at different elevated temperature varied from 20 to 500 ^{0}C.

5.4.2 Transient test: time, temperature at failure, and failure mode

As reported in Table 5.3, the average time and temperature at failure for FRP-reinforced specimens were: 19.0 min, 17.0 min, and 12.3 min and 96.3 ^{0}C, 70.7 ^{0}C, and 48.9 ^{0}C, respectively, for specimens loaded up to 25%, 50%, and 75% of their ambient bond strength. The corresponding values of TRM-retrofitted specimens

(M4_25%, M4_50%, and M4_75%) were significantly higher namely, 62.0 min, 58.8 min, and 19.5 min and 319.5 ^{0}C, 310.4 ^{0}C, and 77.3 ^{0}C.

Adhesive failure at the concrete-resin interface (Figure 5.13a) was observed for FRP-strengthened specimens subjected to the low load fraction (R4_25%), whereas debonding of FRP from the concrete substrate with including parts of concrete cover (Figure 5.13b and c) was noted for the moderate and high load fractions (R4_50%, and R4_75%). These failure modes were essentially related to temperature developed at the interface at the onset of failure, namely debonding and adhesive failures for temperatures below and above the T_g, respectively.

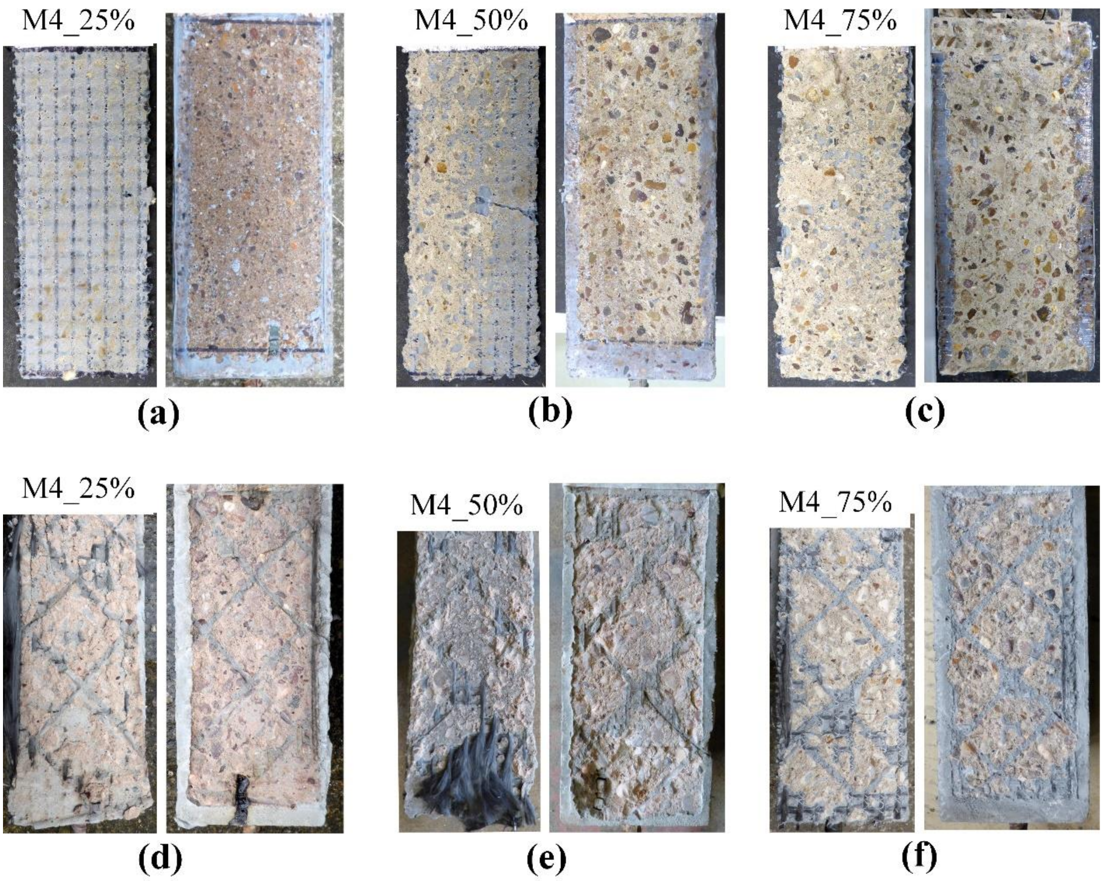

Figure 5.13. Failure mode of FRP and TRM specimens tested in transient condition.

For TRM strengthened specimens, premature adhesive failure modes were prevented due to the better resistance of mortar than resin at temperatures above T_g, with all specimens failing due to debonding including part of the concrete cover (Figure 5.13d-f).

5.5 Discussion

In terms of the various parameters investigated in this experimental programme, an examination of the results (Table 5.2 and Table 5.3) revealed the following information.

5.5.1 Matrix materials (TRM versus FRP)

The matrix material (epoxy resin or mortar) significantly affects the bond performance of FRP and TRM composites with concrete at ambient and especially at high temperatures. At 20 ^{0}C, although both FRP and TRM-strengthening specimens failed due to debonding including part of concrete cover, the bond performance of FRP-strengthened specimens was considerably better than TRM ones. In particular, the bond strength of 3 and 4 layers FRP specimens was 1.4, and 1.5 times higher than that of counterpart TRM specimens respectively, (see Table 5.2). This is attributed to the excellent bond between FRP composite and concrete substrate which is confirmed by the amount of concrete being peeled off (see Figure 5.10a and c for FRP specimens and Figure 5.11a and Figure 5.12a for three and four TRM specimens, respectively). However, at high temperatures, the TRM system exhibited excellent bond performance with concrete, which was superior to that of FRP systems. In particular, in steady-state tests, the TRM specimens retained an average of 85% of their ambient bond strength up to 400 ^{0}C. On the contrary, the FRP systems maintained approximately 17% of their ambient bond strength at 150 ^{0}C due to the premature adhesive bond failure at the concrete-resin interface. In the next sections a comparison between the effectiveness of FRP versus TRM materials at high temperatures is made in terms of the exposed temperature, the number of layers, and the loading condition.

5.5.2 Temperature

Figure 5.14a shows the variation of the ultimate load with both the temperature and the number of layers for all FRP and TRM specimens tested in steady-state condition. The bond of the FRP strengthening system to the concrete substrate was dramatically reduced with the temperature increase. In specific, the average bond strength was decreased by 42, 65, 71, and 82%; when the temperature increased from 20 to 50, 75, 100, and 150 ^{0}C, respectively, for specimens strengthen with 3 FRP layers. The corresponding decreases in the case of 4 layers were almost identical, namely 35, 64, 75 and 84%, respectively. Similar observations were made by Firmo et al. (2015a), where the reductions in the bond strength were 68 and 77% when the measured temperature at the concrete-adhesive interface of FRP-strengthened specimens was 90 and 120 ^{0}C, respectively. Also, the current results, are in agreement with those of Tetta and Bournas (2016), where the contribution of FRP U-jackets in resisting shear forces in RC strengthened beams decreased by 60 and 88% (compared to the strengthened beam tested at 20 ^{0}C) when the beams heated up to 100 and 150 ^{0}C, respectively, due an identical adhesive bond failure mode at the concrete-resin interface.

For TRM specimens, regardless the number of layers, the curves in Figure 5.14a clearly demonstrate that the effectiveness of TRM in transferring the load is not significantly affected by increasing the temperature up to 400 ^{0}C. Compared to the bond strength at 20 ^{0}C, the average reduction in the bond strength was 19, 27, 18, 14, 27, 0, 2, and 50%; for the specimens subjected to temperatures of 50, 75, 100, 150, 200, 300, 400, and 500 ^{0}C, respectively, and strengthened with 3 TRM layers. The corresponding reductions for 4 TRM layers were equal to 18, 17, 13, 12, 11, 6, 6, and 44 %.

A fluctuation in the bond strength was noted at temperatures varied between 50 and 200 ^{0}C, and this could be attributed to the corresponding mechanical properties of the used cement mortar. As shown in Figure 5.14b, the flexural and compressive strength of the mortar considerably deteriorated, possibly due to water vapouring process which occurred at these ranges of temperatures. However, above 200 ^{0}C, an enhancement in the TRM bond strength was observed (Figure 5.14a) resulting in marginal bond reductions in comparison with the ambient strength, namely equal to 3 and 4% when the temperature attained 300 and 400 ^{0}C, respectively. The highest reduction in the bond strength was 48% for TRM specimens tested at 500 ^{0}C (Figure 5.14a) seems to be attributed to the reduced tensile and compressive strength of the mortar by 87% and 68% at that temperature (Figure 5.14b).

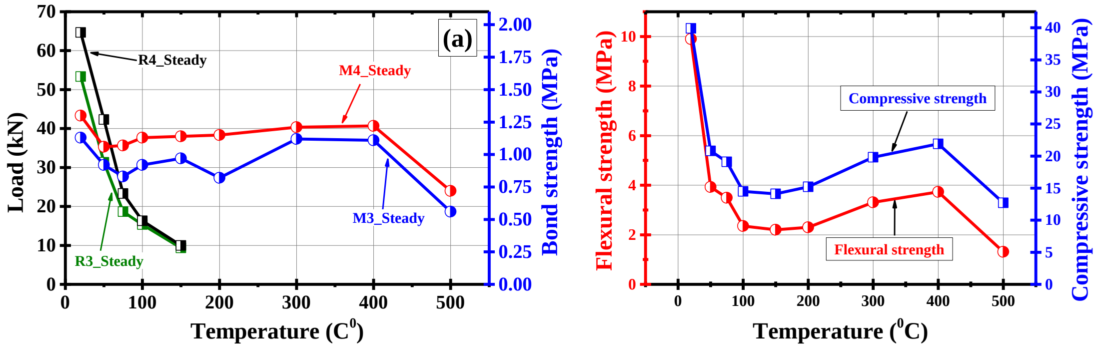

Figure 5.14: (a) Variation of ultimate load and bond strength with the temperature, the strengthening materials and the number of layers (steady state tests), and (b) variation of mortar flexural and compressive strength with the temperature.

The observation that the reduction of bond strength is associated with the mortar strength is better explained if someone compares the quantity of concrete being peeled off. All TRM-strengthened specimens tested at ambient and high temperature failed due to deboning, but the concrete cover detached at high temperature was thinner than the cover detached at ambient (see Figure 5.11c versus Figure 5.11a), indicating the effect of the tensile strength of the mortar on the bond strength even for failure at the concrete substrate.

Finally, an attempt was made to examine the bond performance of TRM at 600 ^{0}C; however, when the interface temperature reached 550 ^{0}C, the specimen failed due to spalling of the concrete cover in an explosive manner. It is worth noting though that the TRM was still bonded to the concrete substrate even after the specimen's failure as illustrated in Figure 5.15. Such a type of failure was also observed by Chowdhury et al. (2007) in FRP strengthened column tests under fire scenario.

Figure 5.15. Exploded specimen heated up to 550 ^{0}C.

5.5.3 Influence of the number of layers

As depicted in Figure 5.14a, when the number of layers increased from 3 to 4, the ultimate load increased by 1.21 and 1.15 for FRP and TRM specimens tested at ambient temperatures, respectively. However, at high temperatures, the influence of the number of layers on the bond strength was more pronounced for the TRM than FRP specimens. As shown in Figure 5.14a, for FRP specimens, the effect of number of layers on the bond strength was almost disappeared above the T_g, as it was controlled by the properties of the epoxy resin.

The influence of the number of TRM layers on the bond strength was not that clear, nevertheless, specimens retrofitted with 4 TRM layers showed an overall higher bond strength for all temperatures investigated. It is worth mentioning that Rambo et al. (2015)observed similar results in TRM coupon tensile test, in which the tensile behaviour at high temperature of TRM coupons made of 3 and 5 fabric layers was better than the tensile performance of a TRM coupon made of one layer. Furthermore, Tetta and Bournas (2016) concluded that by increasing from 2 to 3 TRM layers the bond of TRM to concrete at high temperatures increases considerably.

5.5.4 Loading conditions

Figure 5.16a, and b shows the influence of loading condition (steady and transient test condition) on the bond performance of both FRP and TRM specimens, respectively. It is noted that only four layers FRP and TRM specimens were tested in transient condition, because the results of the steady state tests showed that the number of layers has limited effect on the bond strength at high temperatures.

As it can be observed from Figure 5.16 for both FRP and TRM specimens tested in transient condition, when the load fraction level was increased, the time to reach failure was decreased and consequently the temperature did. Also, it is illustrated that the TRM outperformed their FRP counterparts for all load fractions. Particularly, the time required to reach failure of the TRM specimens was 3.3, 3.5 and 1.58 times higher for the low, moderate and high load fractions, respectively. Correspondingly, the attained temperature at failure was 3.3, 4,4 and 1.58 higher in the TRM-strengthened specimens.

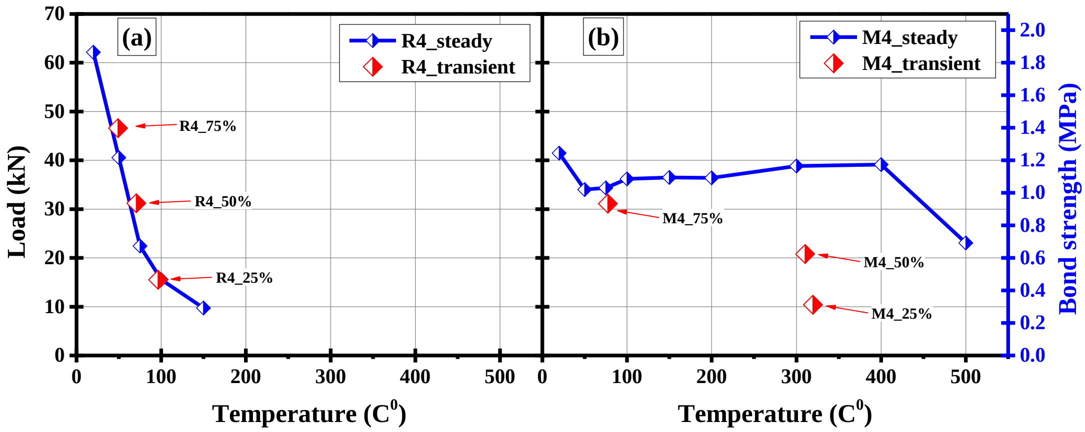

Figure 5.16. Influence of the loading condition as a function of temperature on the bond behaviour of: (a) FRP-specimens, and (b) TRM specimens.

Another interesting observation from Figure 5.16a is that the bond strength attained at different temperatures was nearly identical for both loading conditions for the FRP-strengthened specimens. This confirmed that the temperature at the concrete-resin interface controlled the bond behaviour rather than the loading condition, as also reported by Firmo et al. (2015a). This was not the case for the TRM system which was sensitive to the loading conditions. In fact, the TRM specimens had increased bond strengths at higher temperatures in the steady state in respect with the transient tests. As illustrated in Figure 5.16b, the measured bond strength of M4_300 which was subjected to 300 ^{0}C, was almost double and triple the predefined bond strengths of specimens M4_50% and M4_25%, respectively which failed at around 300 ^{0}C.

5.6 Summary

This chapter investigates for the first time the bond between TRM versus FRP and concrete substrates at high temperatures for the first time. The investigated parameters included the strengthening system (TRM versus FRP), the exposure temperature, the number of FRP/TRM layers, and the loading conditions. For this purpose, 68 specimens were constructed, strengthened, and tested under double-lap direct shear at ambient and high temperatures. The main findings of the current study are summarized below:

- The bond between TRM strengthening system and concrete substrate remains excellent at high temperatures up to 400 ^{0}C.
- In steady state test the reduction in bond strength of FRP-strengthened specimens was significantly higher than for the TRM-retrofitted specimens with the increase of the temperature. The average reduction in the bond strength of FRP-concrete interface was about 83% when the temperature reached 150 ^{0}C. Whereas the corresponding values in TRM-concrete interface was about 15% when the temperature attained 400 ^{0}C.
- Two types of failure modes were observed in the FRP strengthened specimens tested in steady state condition. At ambient and moderate temperature (50 ^{0}C), cohesive failure was observed with parts of the concrete cover remaining attached to the adhesive. Whereas, at elevated temperatures (i.e. 75, 100, and 150 ^{0}C), adhesive failure at the concrete-resin interface was occurred. On the other hand, for TRM specimens subjected to temperatures up to 500 ^{0}C, the failure was due to TRM debonding with parts of concrete cover peeling off.
- The bond strength at the FRP-concrete interface was nearly identical for the same temperature regardless of the loading condition (transient or steady state). On the contrary, the bond behaviour at the TRM-concrete substrate was sensitive to the loading condition, and resulted to considerably higher bond strengths (for nearly the same temperature) in the steady state in respect with the transient tests.

Chapter 6

FLEXURAL STRENGTHENING OF RC BEAMS WITH TRM

ABSTRACT

This chapter presents experimental work conducted on half-scale RC beams tested in under four-point bending. Firstly, the effectives of TRM versus FRP in increasing the flexural capacity of strengthened beams was examined. Secondly, the influence of textile geometry (mesh characteristics) on the performance of TRM in flexural strengthening of RC beams was investigated. Finally, a simple formula proposed by fib model code (2010) for FRP reinforcement was also used to predict the mean debonding stress developed in the TRM reinforcement.

** The content of the work in the first Section (i.e. Section 6.1) has been accepted as a journal paper: "Textile-Reinforced Mortar (TRM) versus Fibre-Reinforced Polymers (FRP) in Flexural Strengthening of RC Beams", Construction and Building Materials. DOI. 10.1016/j.conbuildmat.2017.05.023.*

6.1 TRM versus FRP in Flexural Strengthening of RC Beams

6.1.1 Experimental programme

6.1.1.1 Test Specimens and experimental parameters

The main objective of this section is to compare the effectiveness of TRM versus FRP in increasing the flexural capacity of RC beams. Thirteen half-scale beams of rectangular section with dimensions of 101 mm width and 202 mm depth were fabricated, strengthened and tested under 4-point bending (Figure 6.1a). The length of the beams was 1675 mm, whereas the clear flexural and shear span were 1500 mm and 580 mm, respectively (Figure 6.1a).

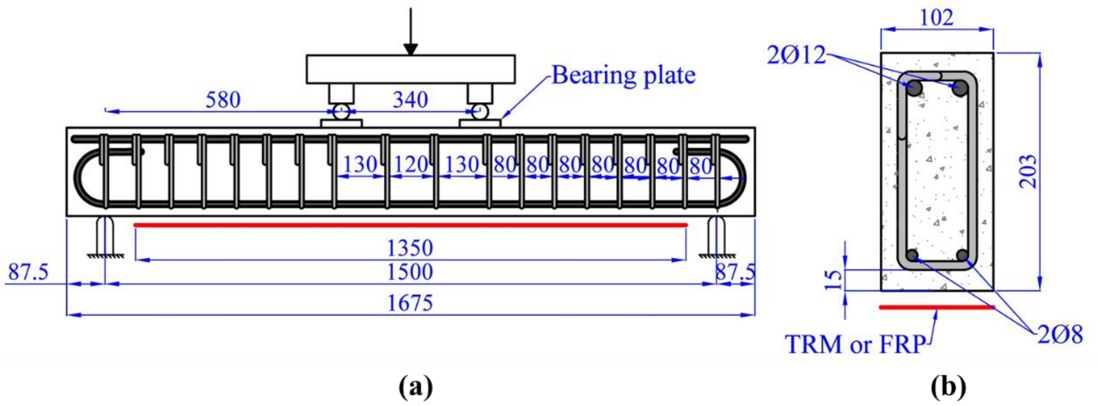

Figure 6.1. Details of internal reinforcement of test beams (dimensions in mm).

All beams were intentionally designed with a low amount of reinforcement ratio (ρ_s = 0.56%) in order to simulate flexural-deficient beams (the calculations of flexural and shear reinforcement of the control beam is provided in appendix A). The internal steel reinforcement comprised two 8 mm-diameter deformed bars in tension and two 12 mm deformed bars positioned in compression (Figure 6.1b). The shear reinforcement comprised 8 mm-diameter steel stirrups at a distance of 80 mm along the two shear spans of the beams, (expect for the constant moment zone), resulting-by design–to a shear resistance seven times higher than the shear force corresponding to the predicted flexural capacity of the unstrengthened beam. In all beams, the concrete cover was same and equal to 15 mm.

The investigated parameters were: (a) the reinforcement material (TRM versus FRP), (b) the number of TRM/FRP layers (one, three, five, and seven), (c) the textile-fibres material (carbon, glass and basalt), (d) the coating of the textile (coated carbon-fibre versus dry carbon-fibre textile), and (e) the end-anchorage of the externally bonded composite layers (U-jacketing). Table 6.1, with the support of Figure 6.2, provide a description of the tested specimens. The notation of the strengthened specimens is BN_F, where B represents the binding materials (R for epoxy resin, and M for cement mortar), N refers to the number of TRM or FRP layers and F denotes the type of textile fibres (C for dry carbon fibres, CCo for coated carbon fibres, BCo for coated basalt fibres and G for glass fibres). For the specimens retrofitted with U-jackets at their ends, an additional suffix (EA, standing for end-anchorage) is added to the notation. The description of the specimens follows:

- CON: unstrengthened beam which served as control specimen.
- R1_C and M1_C: beams strengthened with 1 dry carbon FRP and TRM layer, respectively.
- M1_ CCo: beam strengthened with 1 coated carbon TRM layer.
- R3_C and M3_C: beams strengthened with 3 dry carbon FRP and TRM layers, respectively.
- M5_C: beam strengthened with 5 dry carbon TRM layers.
- R7_BCo and M7_BCo: beams strengthened with 7 coated basalt FRP and TRM layers, respectively.
- R7_G and M7_G: beams strengthened with 7 dry glass FRP and TRM layers, respectively.

- R3_C_EA and M3_C_EA: 3 dry carbon FRP and TRM layers strengthened beam, anchored at their ends with two dry carbon FRP and TRM layers, respectively.

Table 6.1. Strengthening configuration and materials properties of test specimens.

Specimen	t_f (mm)	No. of layers	*Measured thickness of TRM (mm)*	*Ratio of axial stiffness **	ρ_f** (%)	Concrete Strength (MPa): Compressive strength+	Concrete Strength (MPa): Tensile splitting strength+
CON	-	-		-	-	19.9 (0.5)	2.1 (0.06)
TRM-retrofitted							
M1_C	0.095	1	3	1	0.0475	19.9 (0.5)	2.1 (0.06)
M1_CCo	0.095	1	5	1	0.0475	19.9 (0.5)	2.1 (0.06)
M3_C	0.095	3	6	3	0.1425	19.9 (0.5)	2.1 (0.06)
M5_C	0.095	5	10	5	0.2375	19.9 (0.5)	2.1 (0.06)
M7_BCo	0.0371	7	17	1.07	0.1299	19.9 (0.5)	2.1 (0.06)
M7_G	0.044	7	12	1.06	0.1540	19.9 (0.5)	2.1 (0.06)
M3_C_EA	0.095	3	7	3	0.1425	21.7 (0.3)	2.4 (0.05)
FRP-retrofitted							
R1_C	0.095	1		1	0.0475	21.7 (0.3)	2.4 (0.05)
R3_C	0.095	3		3	0.1425	21.7 (0.3)	2.4 (0.05)
R7_BCo	0.0371	7		1.07	0.1299	21.7 (0.3)	2.4 (0.05)
R7_G	0.044	7		1.06	0.1540	21.7 (0.3)	2.4 (0.05)
R3_C_EA	0.095	3		3	0.1425	21.7 (0.3)	2.4 (0.05)

* Axial stiffness of seven layers of coated basalt or dry glass fibres textiles divided by the axial stiffness of one layer of dry carbon fibres textile.

** Textile reinforcement ratio (as a percentage) which calculated as follows: $\rho_f = A_f / bh$, where b and h are the width and depth of the beam respectively.

+ Standard deviation in parenthesis.

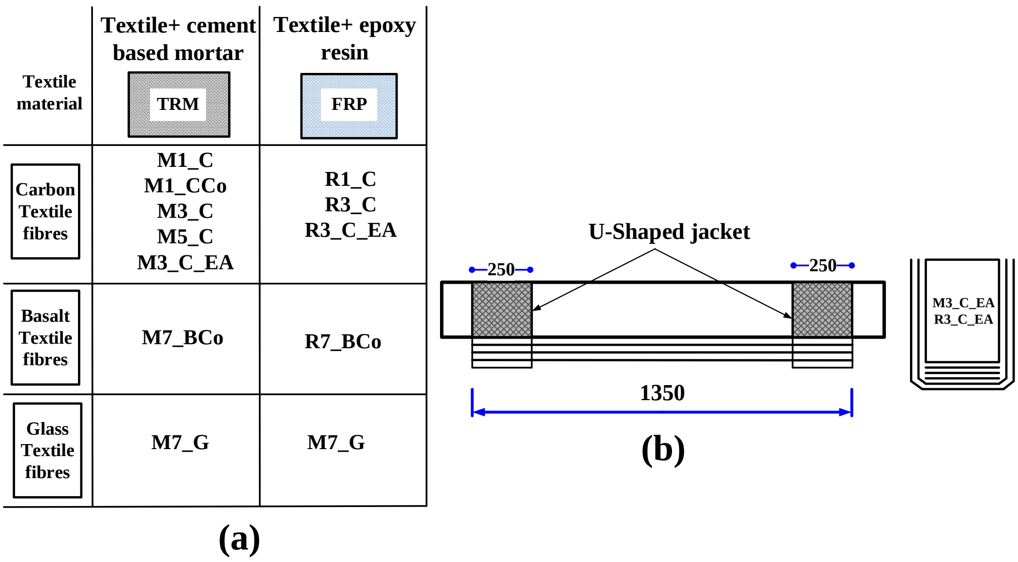

Figure 6.2. (a) Group of specimens; and (b) details of end anchorage system (dimensions in mm).

It is noted that seven layers of glass-fibre or basalt-fibre textile have approximately same axial stiffness of one dry carbon textile layer. The axial stiffness is expressed by the product $n \cdot t_f \cdot E_f$, where n is the number of textile layers, t_f is the nominal thickness and E_f is the elastic modulus of textile according to manufacturer data sheet (see Figure 3.1). Using this expression to calculate the axial stiffness of seven layers of coated basalt or glass yields approximately same value of axial stiffness of one layer of carbon fibres. Table 6.1 gives the normalized axial stiffness of the textile reinforcement used in all specimens (normalized to one layer of carbon-fibre textile).

6.1.1.2 Materials properties

The beams were cast in different groups using the same mix design of concrete. The compressive and splitting tensile strength of the concrete were determined on the day of testing. Three concrete cylinders (dimensions of 150 mm-diameter and 300 mm-height) were tested according to the BS EN 12390-3 and BS EN 12390-6 standards, respectively. The results are presented in Table 6.1.

The yield stress, ultimate strength, and ultimate strain of the 8 mm-diameter steel bars (which used for the tension and shear links reinforcement) was 569 MPa, 631 MPa and 7.85 %, respectively. The yield stress, ultimate strength, and ultimate strain of the 12 mm-diameter bars (compression reinforcement) were 561 MPa, 637 MPa and 12.8%, respectively. These values were obtained experimentally by testing three identical specimens of each type of bars. The stress-strain curves of the tested 8 and 12 mm steel bars are presented in Appendix A.

For both strengthening systems (FRP and TRM), three different textiles were used as external reinforcement, namely carbon-fibre textile (dry_C and coated_CCo), coated basalt fibre-textile (BCo), and dry glass-fibre textile (G). All textiles made of fibre rovings distributed equally in two orthogonal directions. Details of the textiles, such as weight, mesh size and equivalent thickness (calculated based on the equivalent smeared distribution of fibres), are illustrated Figure 3.1.

The binding material used for TRM strengthened beams was the cement mortar described in Section 3.1. The compressive and flexural strength of the mortar were obtained on the day of testing according to BS EN 1015-11 (1999) on three mortar prisms with 40x40 mm cross section and 160 mm length. The average flexural and compressive strength of the mortar were 39.2 MPa, and 9.8 MPa, respectively. For those beams that received FRP, the epoxy resin described in Section 3.2 was used as a binding material.

6.1.1.3 Strengthening procedure

The strengthening material (TRM or FRP) was externally bonded to the bottom of the beams over a length of 1350 mm (see Figure 6.1a). The strengthening procedure for both strengthening systems had the characteristics of a typical wet lay-up application and comprised the following steps:

- Prior to strengthening, the concrete surface was prepared as follows: for FRP strengthened beam, the surface was roughened using a grinding machine and the resulted concrete surface was cleaned from dust with compressed air (Figure 6.3a); For TRM-strengthened specimens, a 50-mm grid of grooves with a depth of approximately 3 mm was made using a grinding machine, as a means of improving the bond. Finally, the concrete surface was cleaned with compressed air (Figure 6.3b).
- The procedure for application of TRM materials included: (i) dampening the concrete surface with water (Figure 6.3b); (ii) application of a layer of mortar with approximately 2-3 mm-thickness (Figure 6.3c); (iii) application of the textile into

the mortar, and gently pressing with hand to ensure good impregnation with cement mortar (Figure 6.3d).

- The procedure for FRP-retrofitted specimens included: application of the textile over a thin layer of resin and then impregnated with resin using a plastic roll (Figure 6.3e).
- The above procedure for both strengthening systems was repeated in case of more than one textile layers were applied.
- For TRM-retrofitted beams, the final layer of textile was covered with a final layer of mortar with approximately 3 mm thickness and levelled (Figure 6.3f).

Similar surface preparation was used for the specimens that received U-shaped FRP or TRM end strips as an anchorage system (R3_C_EA and M3_C_EA), as shown in Figure 6.3g and h, respectively. The application of the two layered U-jackets commenced immediately after the application of the longitudinal external reinforcement.

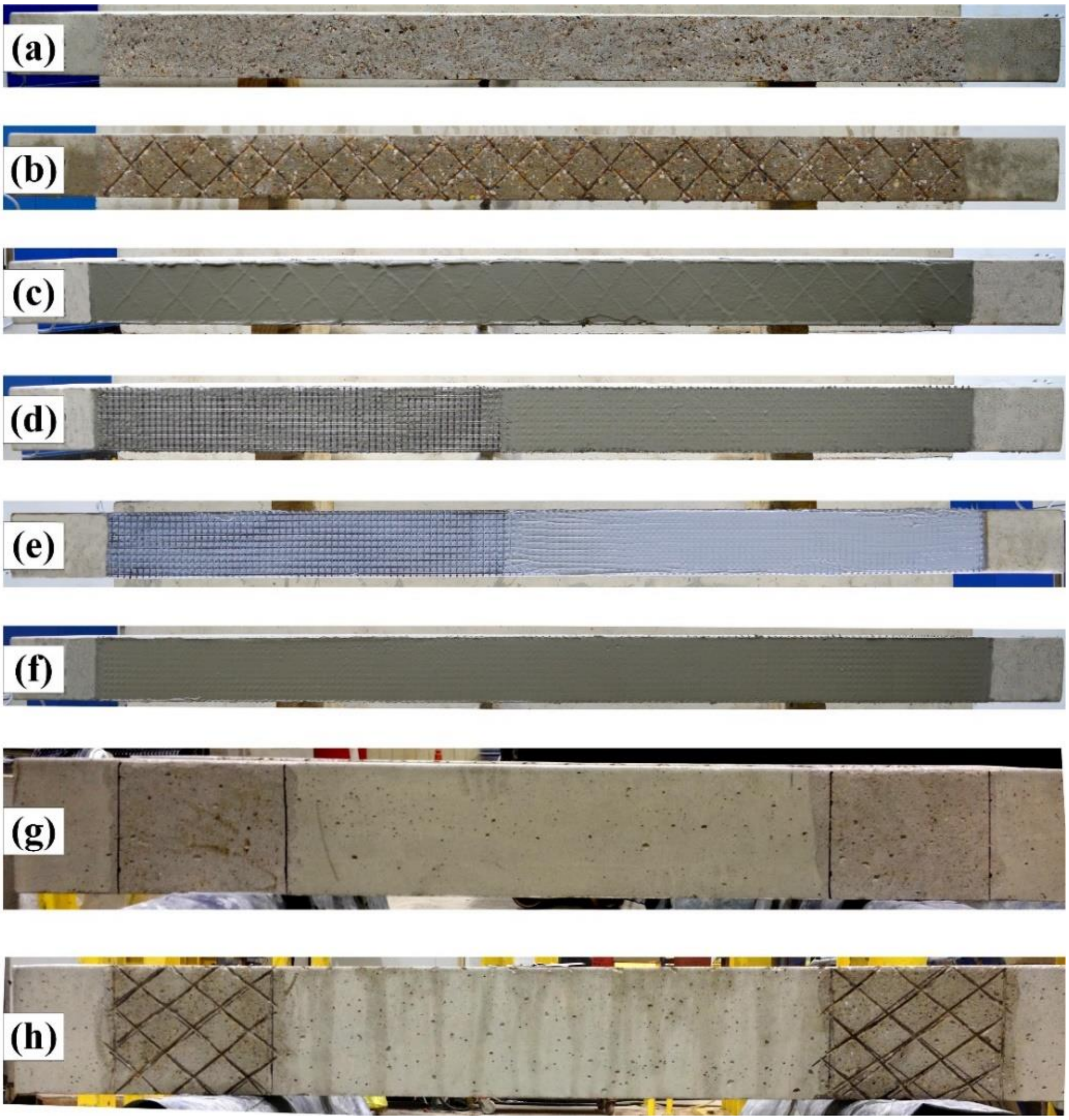

Figure 6.3. Strengthening procedure: (a) surface preparation of FRP-strengthened beams, (b) surface preparation of TRM-retrofitted beams, (c) application of first layer of mortar, (d) application of first layer of TRM, (e) application of the first layer of FRP, (f) application of final layer of mortar for TRM reinforced specimens, (g) surface preparation of FRP U-shaped jacket, and (h) surface preparation for TRM U-shaped jacket.

6.1.1.4 Experimental setup and procedure

All beams were tested as simply supported and were subjected to four-point bending. As shown in Figure 6.1b, the flexural span was 1500 mm, and the selected configuration resulted in a 340 mm-long constant moment zone and a 580 mm-long shear span. Calculations were made to ensure that a sufficient anchorage length of the FRP and TRM reinforcements was provided at the ends of beams. Details of these calculations are presented in Appendix A. The load was applied using a 100 kN-capacity servo-hydraulic actuator which was vertically fixed on a stiff reaction frame. A picture of the test setup is shown in Figure 6.4.

All specimens were loaded monotonically up to failure, under displacement control with a rate of 1 mm/min. In addition to the internal LVDT (linear variable differential transformer) of the actuator, two LVDTs were fixed at the mid-span of the beam (one on each side) to measure the mid-span deflection. Two bearing plates with square dimensions of 100 mm and 25 mm thickness were fixed under the points of load application in order to prevent the local failure of the specimen due to concrete crushing. During the test, the load and displacement data were recorded at a sampling rate of 4 Hz, using a fully-automated data acquisition system.

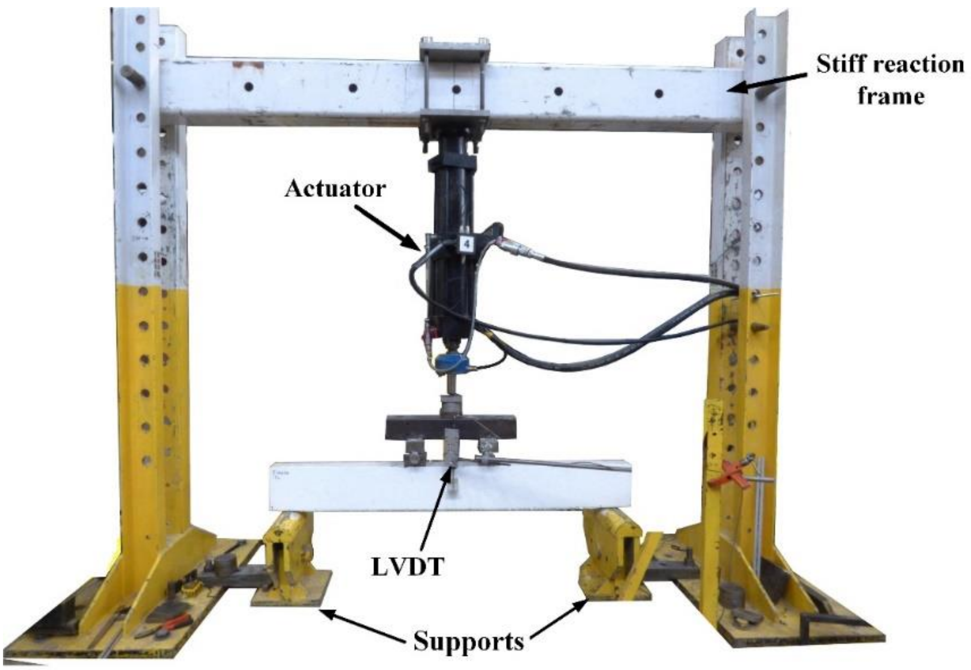

Figure 6.4. A picture of test setup (four-point bending).

6.1.2 Experimental results

The main results of all tested beams are presented in Table 6.2, including: (1) The cracking load (P_{cr}). (2) The yield load (P_y) (which is defined as the load corresponding to the steel yielding). (3) The ultimate recorded load (P_u). (4) The displacement corresponding to cracking load (δ_{cr}). (5) The displacement corresponding to the yielding load (δ_y) (average mid-span deflection from two LVDTs corresponding to P_y). (6) The displacement at ultimate load (δ_u) (average of mid-span deflection from two LVDTs at the ultimate load (P_u). (7) The flexural capacity increase due to application of strengthening. (8) The observed failure mode.

Table 6.2. Summary of test results.

Specimens name	Load (kN)			Deflection (mm)			(7) Capacity increase (%)	(8) Failure mode [a]
	(1) Cracking (P_{cr})	(2) Yield (P_y)	(3) Ultimate (P_u)	(4) Crack (δ_{cr})	(5) Yield (δ_y)	(6) Ultimate (δ_u)		
CON	9.8	30.1	34.6	1.06	6.1	30	-	CC
TRM-retrofitted								
M1_C	10	35.6	39.0	0.98	7.3	13.2	12.7	S
M1_CCo	11.6	37	41.3	0.95	6.8	13.6	19.4	ID
M3_C	12.8	43	55.3	1	7.6	14.7	59.8	D
M5_C	16	57.2	62.2	0.76	6.7	8.6	79.8	D
M7_BCo	10.5	38.5	46.9	0.77	7.1	18.4	35.5	FR
M7_G	9.8	40.2	43.2	0.77	7.7	10.3	24.9	FR
M3_C_EA	12	41.3	57.1	1	7	18.4	65.0	DS
FRP-retrofitted								
R1_C	11.8	38.1	43.9	1	6.8	16	26.9	D
R3_C	11.3	51.1	60.4	0.64	8.1	13.7	74.6	D
R7_BCo	13.4	43.7	54.2	1	7.1	24.9	56.6	FR
R7_G	10	41.5	48.2	1	7.9	18.4	39.3	FR
R3_C_EA	11.6	50.7	83.7	1	7.6	26	141.9	FR

[a] CC: Concrete crushing; S: slippage and partial rupture of the fibres through the mortar; ID: TRM debonding at the textile-mortar interface (inter-laminar shearing); D: TRM debonding from concrete substrate, FR: fibres rupture, DS: Debonding of TRM from concrete substrate, followed by slippage of the fibres at the region where the longitudinal TRM meets the TRM U-jacket.

6.1.2.1 Load-deflection curves

The idealized load-displacement curve for strengthened beams is presented in Figure 6.5. The curves of strengthened beams were characterised by three distinct stages (ascending branches with decreasing slope) up to the maximum load: (1) Stage I: un-cracked beam; (2) Stage II: development of cracking up to yielding of the steel reinforcement; and (3) Stage III: post-yielding response up to failure.

Figure 6.6a-d presents the actual load-deflection curves of all tested beams. Any difference between the curves of the retrofitted beams and the control one (Figure 6.6), is attributed to the contribution of strengthening materials to the flexural performance of the beams. The effect of strengthening was more pronounced during Stages II and III, where development of flexural cracks was in progress. In specific, during Stage II both steel and TRM reinforcement were activated in tension and contributed to the increase of the beam's flexural resistance. In Stage III, the contribution of the steel reinforcement remained almost constant (increased marginally due to steel hardening) due to steel yielding and the further activation of TRM/FRP in tension became the main mechanism contributing to the flexural resistance increase.

The post-peak behaviour of all retrofitted beams was almost identical; after failure, the load dropped to the levels of the un-retrofitted (CON) beam's flexural capacity, indicating that the effect of strengthening had totally been lost. After that point, the plastic behaviour of the beams resulted in the development of large deflections under constant residual load. The tests were terminated when a mid-span deflection of 40 mm was reached (specimen CON was tested up to 80 mm, when the longitudinal steel reinforcement was fractured).

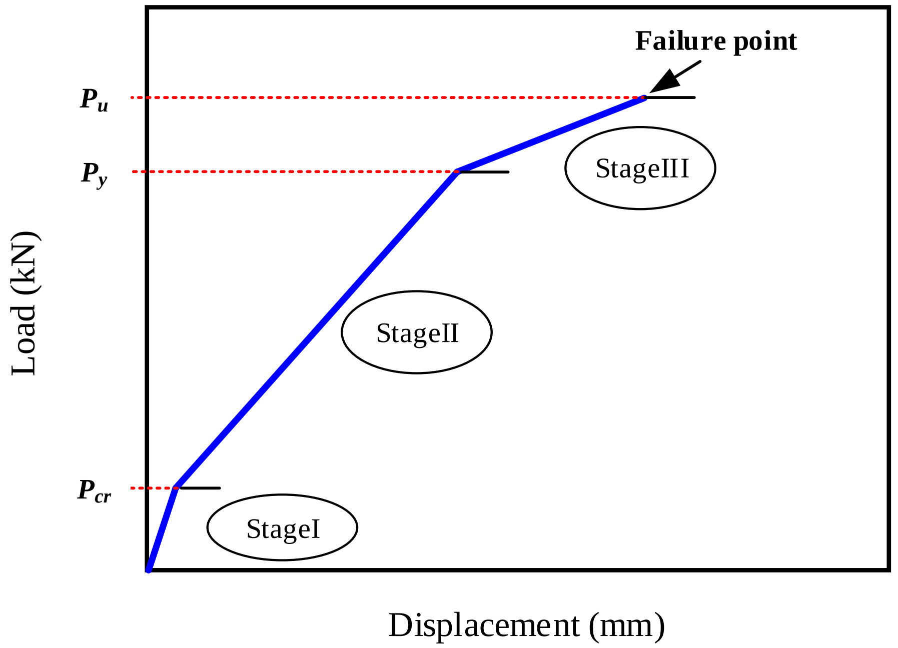

Figure 6.5. Idealized load-defelction curve for strengthened beams.

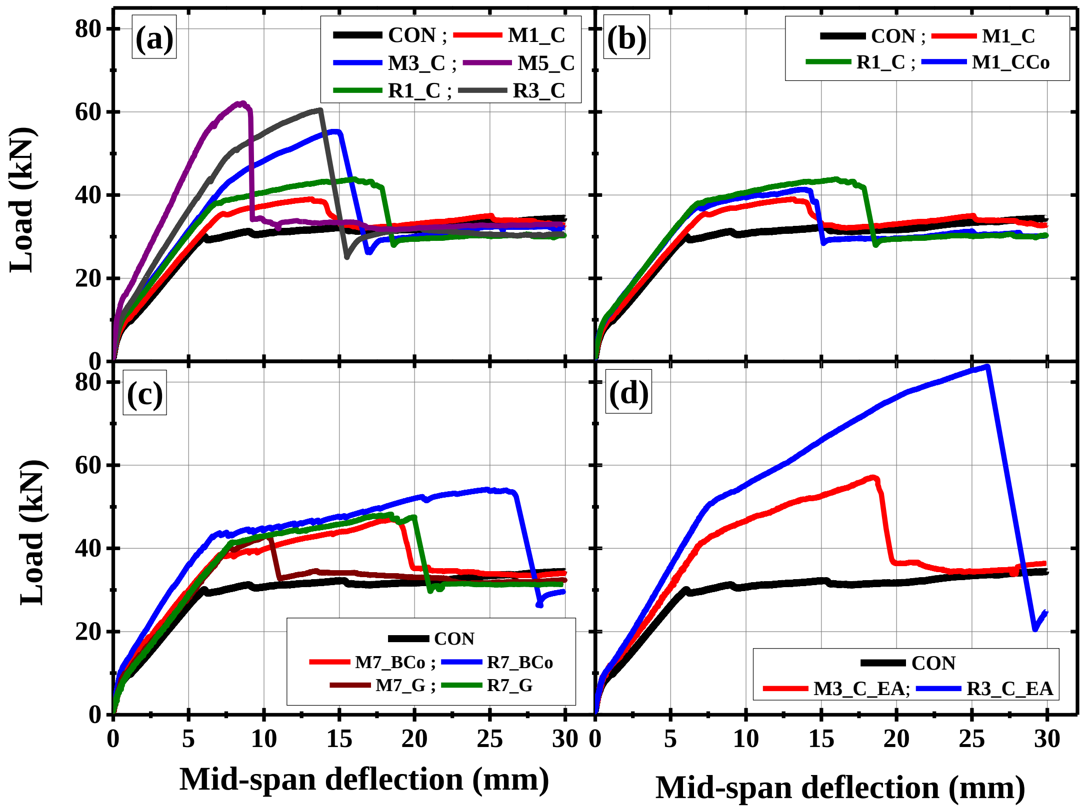

Figure 6.6. Load versus mid-span deflection curves of tested beams.

6.1.2.2 Ultimate loads and failure modes

The values of maximum loads and the observed failure modes of all tested beams are presented in Table 6.2, supported by Figure 6.7. The reference beam (CON) failed in flexure after the formation of large flexural cracks at the constant moment region. The failure was due to yielding of the tensile reinforcement followed by concrete crushing at the compression zone (Figure 6.7a). This type of failure mode is typical for under-reinforced beams. The yield and ultimate load was 30.1 kN and 34.6 kN, respectively, at corresponding mid-span deflection of 6.1 mm and 30.0 mm, respectively.

All FRP strengthened beams also failed in flexure at loads substantially higher than the control beam (Table 6.2). The ultimate load recorded for specimens R1_C, R3_C, R7_BCo, R7_G and R3_C_EA was 43.9, 60.4, 54.2, 48.2 and 83.7 kN, respectively. Thus, the contribution of various FRP strengthening systems in increasing the flexural capacity was 26.9%, 74.6%, 56.6%, 39.3% and 141.9%, respectively.

Two distinct failure modes were observed in the FRP-retrofitted beams. Specimens retrofitted with one and three layers of carbon-fibre reinforcement (R1_C and R3_C), failed due to debonding of the FRP composite from the concrete surface. Debonding was initiated from an intermediate shear crack (Figure 6.7b and c) which caused debonding of the FRP composite from the concrete and propagated from the mid-span towards the end of the beam. Eventually, the FRP strip completely debonded from the beam’s soffit with parts of concrete cover being attached. Details of the failure mode for those beams are also provided in Figure 6.7b and c). This kind of failure mode is brittle and quite common for FRP reinforced beams (Commitee, 2008). The beams strengthened with seven layers of coated basalt-fibre reinforcement (R7_BCo), seven layers of glass-fibre reinforcement (R7_G), and three layers of carbon-fibre reinforcement anchored at the beam's ends (R3_C_EA), failed due to fibres rupture at the constant moment region of the beam (Figure 6.7d-f, respectively).

Similar to the FRP-retrofitted beams, all specimens strengthened with TRM failed in flexure after displaying flexural strength considerably higher compared to the control specimen. The maximum load recorded for specimens M1_C, M1_CCo, M3_C, M5_C, M7_BCo, M7_G and M3_C_EA was 39.0, 41.3, 55.3, 62.2, 46.9, 43.2 and 57.1 kN, respectively, which yields 12.7%, 19.4%, 59.8%, 79.8%, 35.5%, 24.9% and 65.0% increase in the flexural capacity, respectively.

Five different failure modes were observed in the TRM-retrofitted beams depending on the number of TRM layers and the textile fibres material:

- Loss of composite action due to slippage of the fibres within the mortar accompanied by partial rupture of the fibres, at a single crack within the maximum moment region (Figure 6.7g). This type of failure mode was not brittle (see the post-peak curve in Figure 6.6a) and was observed in specimen M1_C which retrofitted with one layer of dry carbon-fibre textile. A progressive load-drop was recorded as a result of the fibres slippage through the cement matrix. This type of failure mode was consistent with that observed in TRM to concrete bond tests presented in Section 4.2, for the same number of TRM layers and the same textile fibre materials (i.e. dry carbon), it is also reported in Raoof et al. (2016).

- Debonding of TRM due to fracture the surface at the textile-mortar interface. This kind of failure mode was observed in specimen M1_CCo (strengthened with one layer of coated carbon fibre-textile). Debonding was initiated at the intermediate shear crack and propagated towards the end of the beam (Figure 6.7h). This kind of failure, which can also be described as interlaminar shearing, is attributed to the effect of coating. Coating the textile with epoxy leads to a strong bond between the inner and the outer filaments of each roving, which increases the rigidity of the textile in both directions and creates strong joints in the junctions between the longitudinal and transversal fibre rovings. As a result, failure due to slippage of the fibre through the mortar was prevented, and damage was shifted to the textile-mortar interface, which was the weakest among all interfaces. The same failure mode was also observed in the TRM to concrete bond tests for the same number of TRM layers and the same textile fibre materials (see Section 4.3.4). A detailed picture of the TRM failure surface is also given in Fig. 8h.

- Debonding of TRM from the concrete surface accompanied with part of the concrete cover. The debonding initiated from an intermediate shear crack (Figure 6.7i) and propagated from the constant moment zone towards one end of the TRM reinforcement. Eventually TRM debonded form the concrete surface with a part of concrete cover being peeled off (Figure 6.7i). This failure mode was observed in specimen M3_C and M5_C, and it was the same as in its counterpart FRP-retrofitted beam (R3_C). Again, the same failure mode was also observed in TRM to concrete bond tests for three layers of the same materials (see Section 4.3.1 and Raoof et al. (2016)).

- Fibres rupture in the region of maximum moment (Figure 6.7 j and k). This type of failure mode was noted in specimens M7_BCo and M7_G, strengthened with seven layers of coated basalt and glass-fibre textile, respectively.

- Debonding of TRM from the concrete substrate (part of the concrete cover was also included) at an intermediate shear crack (Figure 6.7l), followed by slippage of the fibres at a different region. This failure mode was observed in specimen M3_C_EA which was retrofitted with three layers of dry carbon-fibre textile and anchored with

TRM U-jackets at their ends to provide anchorage. It is noted that providing U-jacket at the ends of the beam prevented debonding of TRM, but slippage of fibres finally occurred at the region where the longitudinal TRM meets the TRM U-jacket (Figure 6.7l). The same failure mode was also observed in in TRM to concrete bond tests for the same number of TRM layers and the same textile fibre materials (see Section 4.3.5).

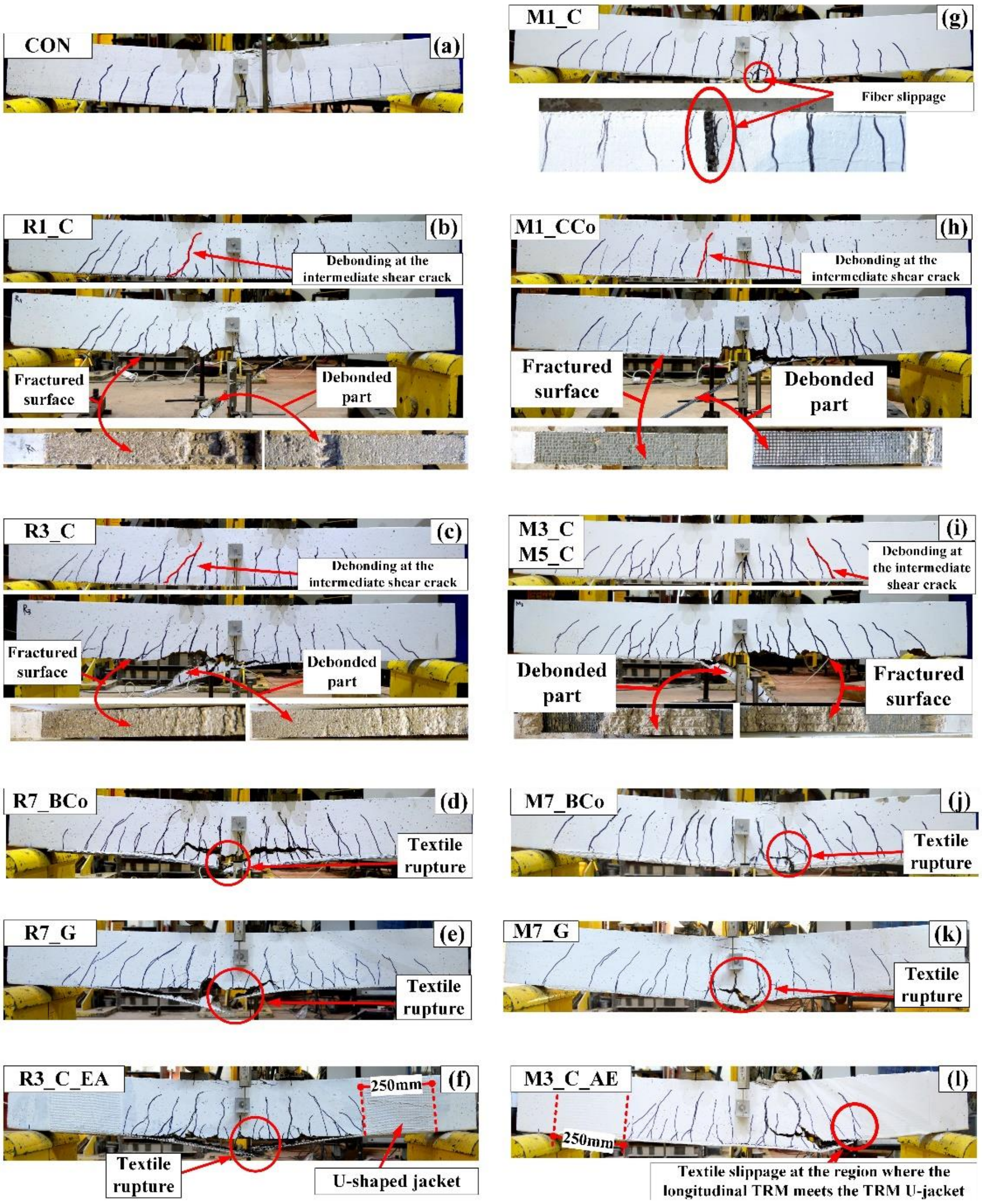

Figure 6.7. Failure mechanisms and details of failure modes of tested beams.

6.1.2.3 Bending stiffness and crack pattern

The bending stiffness of the tested beams at several stages (pre-cracking, cracking and post-yielding) is reported in Table 6.3. It was calculated form the load versus mid-span deflection curves as the tangent stiffness of the pre-cracking, cracking and post-yielding stages. As shown in Table 6.3, the application of strengthening (TRM or FRP) enhanced the cracking and post-yielding stiffness compared to the reference beam. It is noted that the increase in the cracking and post-yielding stiffness was sensitive to the investigated parameters such as the strengthening system (TRM or FRP), the number of TRM/FRP layers, the textile fibre material, and the strengthening configuration.

Table 6.3. Comparison of stiffness at pre-cracking, cracking and post-yielding stage.

Specimens	**Stiffness (kN/mm)**		
	Pre-cracking	**Cracking**	**Post-yielding**
CON	9.2	4.0	0.19
TRM-retrofitted			
M1_C	10.2	4.1 (1)*	0.58 (206)*
M1_CCo	12.2	4.3 (8)*	0.63 (236)*
M3_C	12.8	4.6 (14)*	1.73 (820)*
M5_C	13.1	6.9 (72)*	2.63 (1298)*
M7_BCo	12.7	4.4 (10)*	0.74 (295)*
M7_G	12.9	4.4 (9)*	1.15 (513)*
M3_C_EA	12.0	4.9 (21)*	1.39 (636)*
FRP-retrofitted			
R1_C	11.8	4.5 (13)*	0.63 (235)*
R3_C	13.7	5.3 (32)*	1.66 (782)*
R7_BCo	13.4	5.0 (23)*	0.59 (213)*
R7_G	10.0	4.6 (13)*	0.64 (239)*
R3_C_EA	11.6	5.9 (47)*	1.79 (853)*

*Percentage increase (%) in stiffness with respect to CON included in parentheses.

6.1.3 Discussion

All strengthened specimens responded as designed and failed by the loss of strengthening after yielding of the internal steel reinforcement. On the basis of the various parameters investigated in this experimental programme, an examination of the results (Table 6.2) in terms of strength, stiffness and failure modes, revealed the following information.

6.1.3.1 Number of strengthening layers

The effect of the number of layers on the beams flexural capacity was investigated for the case of dry carbon-fibre textiles, and is depicted in Figure 6.8a. For FRP-strengthened beams, tripling the amount of reinforcement (from one to three layers) resulted in almost proportional increase in the flexural capacity, namely 2.8 times. The corresponding enhancement in the TRM-strengthened beams was equal to 4.7 times (non-proportional increase). To further investigate the effect of increasing the number of TRM layers on the flexural capacity increase, a beam strengthened with five TRM layers was also tested. As shown in Figure 6.8a, applying five layers of TRM resulted in 6.3 times increase compared to one TRM layer. The non-proportional increase observed in the TRM strengthened (especially for the transition from one to more layers) is associated to the different failure modes observed, as described below.

The cracking and post-yielding stiffness were enhanced by increasing the number of layers for both strengthening systems in an identical manner (Figure 6.8b). In the FRP-strengthened beams, tripling the number of layers resulted in an increase of 1.2 and 2.7 times in the cracking and post-yielding stiffness, respectively. The corresponding enhancement in TRM-retrofitted beams was similar, namely 1.1 and 3 times, respectively. It seems that the increase in the post-yielding stiffness was almost directly proportional to the number of layers even for the case of M5_C (4.5 times compared with M1_C). This is attributed to the fact that the only mechanism contributing to the flexural capacity increase is the activation of the externally applied materials in tension.

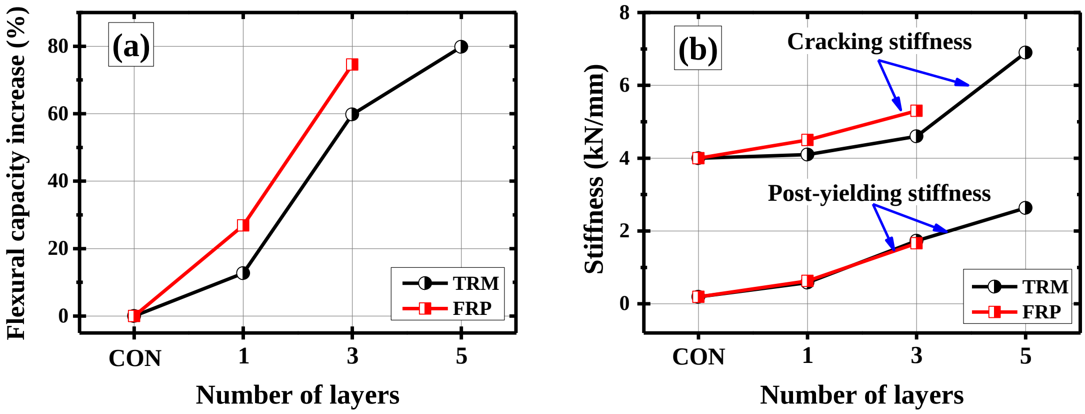

Figure 6.8. Effect of number of layers on: (a) the ultimate flexural capacity; and (b) the cracking stiffness, and post-yielding stiffness.

The failure mode of FRP strengthened specimens was not sensitive to the number of layers; it was always debonding of FRP from the concrete substrate including part of concrete cover (Figure 6.7b and c). However, in the case of TRM-retrofitted beams, the failure mode was sensitive to the number of layers. In particular, the failure mode altered when three or five layers of dry carbon-fibre textile were applied instead of one. With 3 or 5 layers, slippage of the fibres through the mortar was prevented and the failure, as in the case of FRP, was attributed to TRM debonding including part of concrete cover (Figure 6.7i). This behaviour is identical with the observations made by Tetta et al. (2015) in shear strengthening of RC beams with TRM when the number of layers increased from 1 to 2, also noted in double-lap shear TRM-to-concrete bond tests (see Section 4.3.1). Improved mechanical interlock between the increased number of textile layers and the surrounding mortar is believed to be the main reason for this behaviour.

6.1.3.2 Textile-fibres coating

Beam M1_C, strengthened with one TRM layer of dry (uncoated) carbon-fibre textile, failed prematurely due to local slippage of the fibres through the mortar, and since the coated textile exhibited good performance in the bond tests, it was decided to retrofit a beam using the same textile but with coated fibres (M1_CCo). As a result of that, the flexural capacity was further increased by 52% (compared to beam M1_C). Additionally, the failure mode was changed from slippage of the fibres through the mortar to debonding of TRM due to fracture at the textile-mortar interface (Figure 6.7h; interlaminar shear failure. Such a failure mode was also observed in bond tests when the same textile with the same coating was used (see Section 4.3.4 and also presented in Raoof et al. (2016)). As illustrated in Figure 6.9a-c, although the performance of the beam M1_C was poor compared to its counterpart FRP-strengthened specimen (R1_C), when coated textile was used, the behaviour of TRM became comparable to FRP. Coating the textile leads to improved bond between the inner and the outer filaments of each roving of the textile. Hence, the textile develops higher tensile stresses, and the matrix is called to transfer higher shear stresses, which leads to shear failure of the mortar (interlaminar shearing).

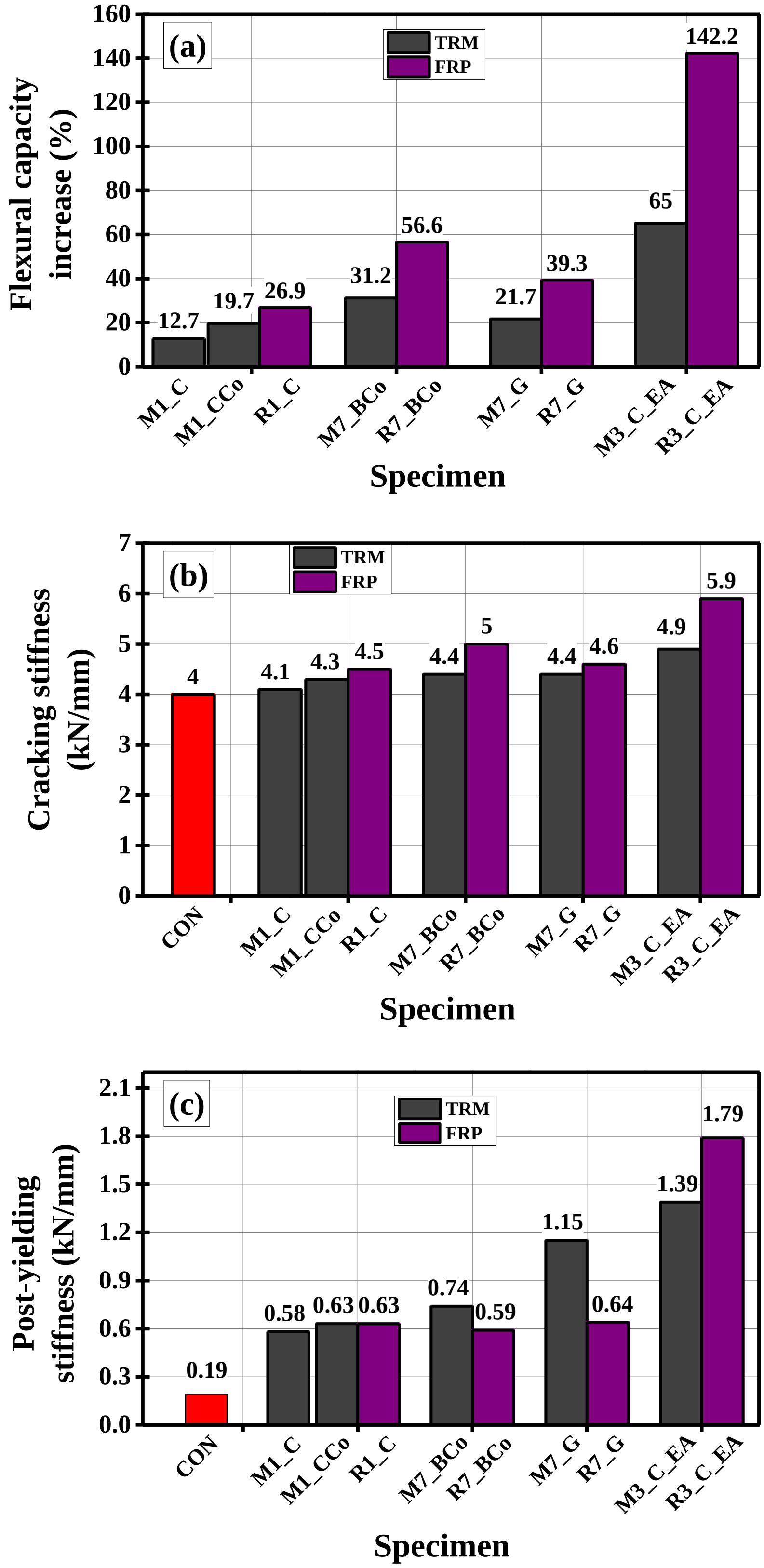

Figure 6.9. Comparison of TRM versus FRP strengthened beams in terms of: (a) flexural capacity increase; (b) cracking stiffness; and (d) post-yielding stiffness.

6.1.3.3 Textile-fibres material

According to the results (Figure 6.9a), in both TRM and FRP strengthening systems, the highest flexural capacity increase was achieved in the beams retrofitted by the coated basalt-fibre reinforcement. In TRM-strengthened beams, specimen M7_BCo recorded a 45% higher capacity increase compared to specimen M1_CCo with equivalent axial stiffness of the strengthening layers, and beam M7_G recorded a 49% higher capacity increase compared to beam M1_C. Note that the above comparisons were made on the basis of similar textile surface conditions (dry or coated textiles). Similarly, in FRP-retrofitted beams, the flexural capacity increase of beam R7_BCo was 52% and 30 % higher than that of beams R1_C and R7_G, respectively. This disparity in the flexural capacity increase between beams with external reinforcement of approximately the same axial stiffness, can be attributed to the influence of the numbers of layers (one layer of TRM reinforcement was less effective than multiple no. of layers as discussed in Section 6.1.3.1), and to the fact that the basalt-fibre textile was coated, which was beneficial at least in the case of the TRM strengthening system.

6.1.3.4 End-anchorage with U-jackets

An end-anchorage system comprising U-jackets at both ends of the beams was applied only for specimens strengthened with three layers of carbon TRM or FRP, as a means of preventing premature debonding from the concrete substrate. As illustrated in Figure 6.9a, in the case of beam R3_C_EA, the strengthening efficiency was substantially increased (by 90%) compared to the beam without end-anchorage (R3_C). However, this enhancement was limited in the case of the TRM strengthened beam (only 9%). The difference in the behaviour between specimens R3_C_EA and M3_C_EA is attributed to the difference in the failure mode observed. Beam R3_C_EA failed due to rupture of the textile fibres (Figure 6.7f) achieving full composite action. In contrary, in beam M3_C_EA even if TRM debonding was prevented, a full composite action was not achieved due to slippage of the textile fibres at the junction where the longitudinal TRM meets the U-jacket (Figure 6.7.l).

6.1.3.5 TRM versus FRP effectiveness factor

Table 6.4 reports the values of the TRM versus FRP effectiveness factor (*k*), which is defined as the ratio of the flexural capacity increase achieved by TRM to the increase achieved by the equivalent FRP. This factor varied between 0.46 and 0.80 for the different parameters examined in this study.

Increasing the number of dry carbon-fibre textile layers from one to three, resulted in enhancement of the effectiveness factor from 0.47 to 0.80, which was associated to the change in the failure mode of TRM retrofitted beams (from slippage of the fibres to debonding from the concrete substrate). Coating the carbon textile with epoxy resin in the case of 1 TRM layer increased the *k* factor from 0.47 to 0.73, as a result of prevention of fibres slippage.

The effectiveness factor for the specimens retrofitted with either coated basalt, or glass-fibre textiles was the same and equal to 0.63. In this case, although both FRP and TRM-retrofitted specimens failed due to rupture of textile fibres, the reduced effectiveness of TRMs can be attributed to the lower tensile strength of TRM composites compared to FRPs (as shown from the results of the coupons tensile tests_ see Table 3.2 and Table 3.3).

Finally, in terms of strengthening configuration, specimen M3_C_EA recorded an effectiveness factor of 0.46. This low value of k factor was due to the presence of slippage at the junction where the longitudinal TRM reinforcement meets the U-jacket (Figure 6.7l). This slippage considerably reduced the TRM effectiveness and prevented a full composite action.

Table 6.4. TRM versus FRP effectivness factor.

Specimen	TRM versus FRP effectiveness factor, k	Failure mode
M1_C	0.47	S
M1_CCo	0.72	ID
M3_C	0.80	D
M5_C	n.a.	D
M7_BCo	0.63	FR
M7_G	0.63	FR
M3_C_EA	0.46	D

6.1.4 Analytical calculations

To calculate the effective stress, σ_{eff}, of the TRM or FRP reinforcement, an inverse analysis method was used. The effective stress is defined here as the tensile stress of the composite material in the region of maximum moments at the instant of ultimate load. By using the experimental values of the flexural moment of resistance, $M_{u,exp}$ (Table 6.5), a standard cross section analysis was performed for each of the retrofitted beams. The procedure for the calculation of σ_{eff} in this method is built on the equilibrium of internal forces and strains compatibility described in Triantafillou (2006) (Figure 5.10a-d). Also, the following assumptions were adopted:

- There is perfect bond between the FRP/TRM strengthening layers and the concrete substrate.
- The ultimate compressive allowable strain of concrete (ε_c) is 0.0035.
- The strengthening material behaves linearly up to failure.

From equilibrium condition, the resultant of compression forces is equal to the resultant of the tension forces ($i.e. C = T$):

The compression and tension forces can be expressed as follow (see also Figure 6.10c):

$$C_c + C_{s2} = T_{s1} + T_f \qquad 6.1$$

where; C_c, C_{s2}, T_{s1}, and T_f is the compression force provided by concrete, the compression force provided by steel (in compression zone), the tensile force provided by steel (in tension zone), and the tensile force provided by FRP or TRM, respectively.

The above-mentioned terms (i.e. C_c, C_{s2}, T_{s1}, and T_f) are the product of the following expressions:

$$C_c = \varphi\, f_{ck}\, b\, x \qquad 6.2$$

$$C_{s2} = A_{s2}\, E_s\, \varepsilon_{s2} \qquad 6.3$$

$$T_{s1} = A_{s1}\, f_y \qquad 6.4$$

$$T_f = A_f\, E_f\, \varepsilon_f \qquad 6.5$$

where; φ is the coefficient of area of the stress block and can be calculated from the following expression:

$$\varphi = \left\{ \begin{array}{ll} 1000\, \varepsilon_c \left(0.5 - \frac{1000}{12} \varepsilon_c\right) & for\ \varepsilon_c \le 0.002 \\ 1 - \frac{1000}{12} \varepsilon_c & for\ 0.002 \le \varepsilon_c \le 0.0035 \end{array} \right\} \qquad 6.6$$

In any case, the value of φ should not exceed 0.8; otherwise $\varphi = 0.8$

δ_G is the coefficient of centroid of stress block, and can be calculated from the following expression:

$$\delta_G = \begin{cases} \frac{8-1000\varepsilon_c}{4(8-1000\varepsilon_c)} & for\ \varepsilon_c \leq 0.002 \\ \\ \frac{1000\varepsilon_c(3000\varepsilon_c-4)+2}{2000\ \varepsilon_c\ (3000\varepsilon_c-2)} & for\ 0.002\ \leq \varepsilon_c \leq 0.0035 \end{cases} \qquad 6.7$$

δ_G should not exceed 0.4; otherwise $\delta_G = 0.4$, f_{ck} is the concrete compressive strength (see Table 6.1), b is the beam's width= 100 mm, x is the depth of the neutral axis, A_{s2}, E_s, and ε_{s2} is the area, the modulus of elasticity (E_s= 200 GPa), and the strain of the steel in compression. A_{s1}, f_y is the area and yielding stress of the steel in tension. A_f, E_f, and ε_f is the area, the modulus of elasticity, and the tensile stain of the TRM or FRP.

From the strain compatibility (see Figure 6.10b), the strain in the compression steel (ε_{s2}) can be expressed in terms of the strain in the fibres (ε_f) as follows:

$$\varepsilon_{s2} = \varepsilon_f \frac{x-d_2}{h-x} \qquad 6.8$$

The theoretical ultimate moment can be calculated from Eq. 6.9 (by taking a moment about the centroid of the concrete block_ see Figure 6.10d):

$$M_{u,theor} = A_{s1}f_y(d-\delta_G x) + A_f E_f \varepsilon_f(h-\delta_G x) + A_{s2}E_s(\varepsilon_f \frac{x-d_2}{h-x})(\delta_G x - d_2) \qquad 6.9$$

Now to determine the effective strain (ε_{eff}) in the fibres, the value of x and ε_{eff} is assumed to meet the two following conditions:

$$C_c + C_{s2} \approx T_{s1} + T_f \text{ and } M_{u,theor.} \approx M_{u,exp.}$$

If this condition is achieved, then the effective stress in the textile reinforcement ($\sigma_{eff.}$) is calculated using Eq. 6.10 as follows:

$$\sigma_{eff.} = \varepsilon_f E_f \qquad 6.10$$

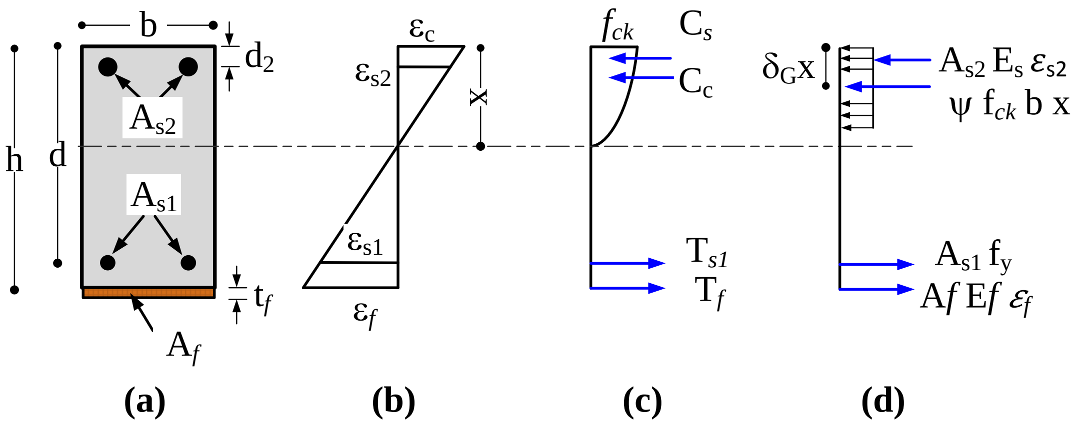

Figure 6.10. Analysis of cross section at ultimate stage; (a) beam's cross section, (b) strain diagram, (c) stress block diagram, and (d) equivalent stress block.

All the above procedure is summarized in the following flow chart:

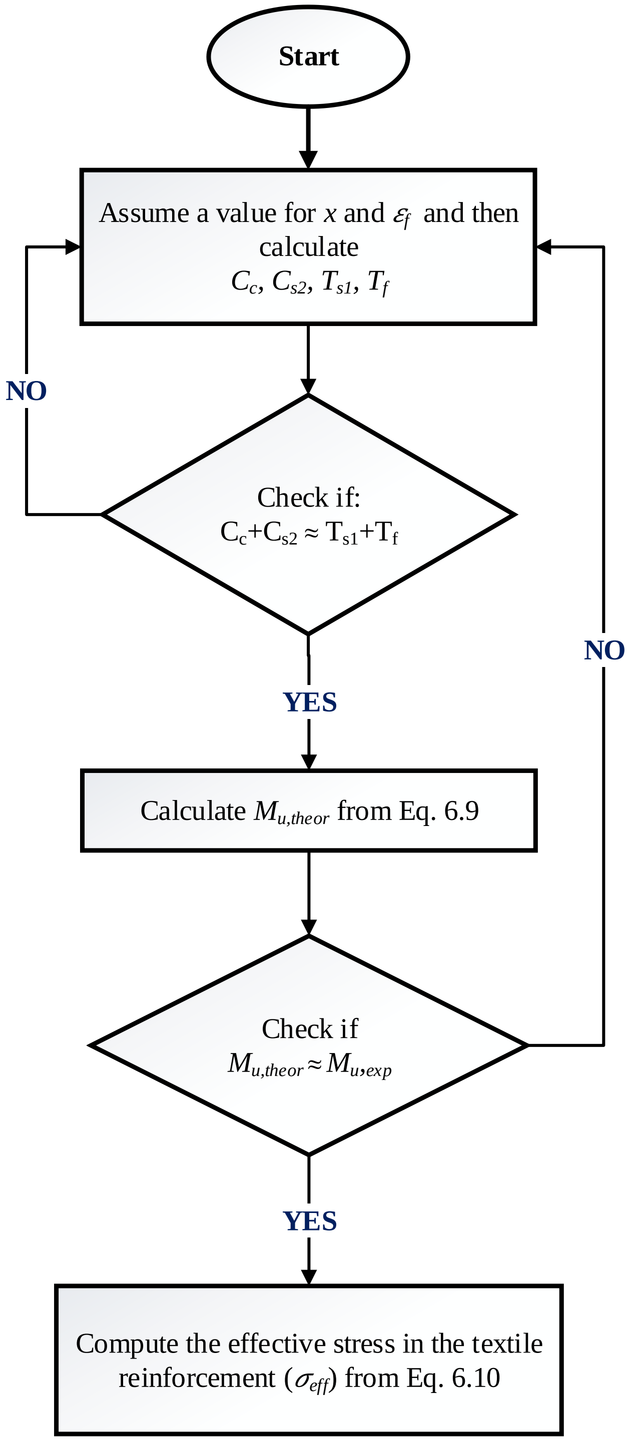

It is worth mentioning that the mechanical properties of the external reinforcement (E_f and f_{fu}) were taken from Table 3.2 (for TRM composite) and Table 3.3 (for FRP composite).

The experimental values of the effective stress, $\sigma_{eff,exp}$ resulted from the inverse analysis, are presented in Table 6.5. As shown in the same Table, the ratio of the effective stress ($\sigma_{eff,exp}$) to the ultimate stress obtained from coupon test (f_{fu}) was always less than one, except for the beam R3_C_EA (probably due to the effect of the end-anchorage system).

The theoretical values of the debonding stress of the composite material, $f_{fbm.theor}$ were calculated according to Eq. 6.11 [*fib model code (2010)*] equation for flexural strengthening with FRP) and are presented in Table 6.5 (without safety factors). Note that Eq. 6.11 can only be used for debonding failures occurring at the concrete substrate.

$$f_{fbm} = k_c k_m k_b \beta_\ell \sqrt{\frac{2E_f}{t_f} f_{cm}^{2/3}} \qquad 6.11$$

In the above equation, f_{fbm} is the mean debonding stress of the composite material; k_c is the intermediate crack factor and equal to 2; k_m is the matrix factor and equal to 0.25 for the case of epoxy bonded CFRP system (the same value was used here for the case of the carbon-TRM system); k_b is the shape factor (calculated from Eq. 6.12 below); β_ℓ is the length factor which can be taken equal to 1; E_f is the elastic modulus the composite material (obtained from coupon test); t_f is the equivalent thickness of the textile and f_{cm} is the concrete compressive strength.

$$k_b = \sqrt{\frac{2 - b_f/b}{1 + b_f/b}} \geq 1 \qquad 6.12$$

where; b_f is the width of the composite, and b is the width of the beam.

Eq.6.11 was used here to calculate both FRP and TRM debonding stresses in the cases of debonding failures. A comparison of the stresses calculated according to Eq. 6.11 with that stress developed in the FRP and TRM composite calculated based on cross section analysis using the ultimate moment obtained experimentally is presented Table 6.5. It was found that the debonding stress calculated by Eq.6.11 is in a good agreement with the experimental results of that beams reinforced with high FRP and TRM reinforcement ratio (M3_C, M5_C and R3_C) and failed due to debonding of FRP or TRM from the concrete substrate including part of the concrete cover.

Figure 6.11 shows the relationship between the effective stress obtained experimentally $\sigma_{eff,exp}$ and the product $\rho_f E_f$; together with the curve corresponding to Eq. 6.11. Where ρ_f is the textile fibres reinforcement ratio ($\rho_f = A_f / bh$), and E_f is the modulus of elasticity of the composite material obtained from coupon tests. It is clear from this figure that the effective stress developed in the textile fibres reinforcement is inversely proportional to the product $\rho_f E_f$ when the failure is associated to debonding of the externally bonded reinforcement, regardless the binding material (epoxy resin or mortar). This trend of the effective stress is consistent with the trend of the theoretical stress calculated by Eq. 6.11 and shown in Figure 6.11a and b.

Based on the above findings, in design of flexural retrofitting with TRM system, the effective stress can be the minimum value obtained from coupon tests (f_{fu}) and Eq. 6.11, applying the same safety factors as in FRP systems until more data become available and a semi-probabilistic approach can be applied to obtain TRM-specific safety factors. Nevertheless, this design approach is suggested to be used only when the failure mode is either TRM debonding at an intermediate crack or fibres rupture. According to the results of the present experimental study, this applies when more than 2 TRM layers are used for retrofitting.

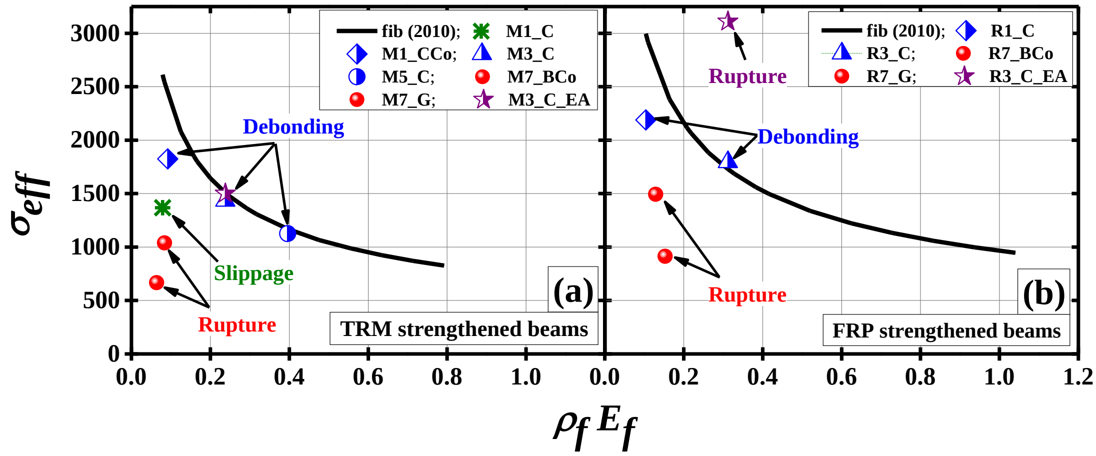

Figure 6.11. Experimentally obtained effective stress versus ρ_f E_f and comparison with the theoretical formula suggested by Fib-Model-Code. (; (a) TRM-strengthened beams; and (b) FRP- strengthened beams.

Table 6.5 also compares the effective stress in the TRM composite ($\sigma_{eff,exp}$) with the debonding stress obtained through direct shear-bond tests ($\sigma_{eff,bond}$) given in Table 4.2. The comparison is made on the basis of the same number of TRM layers used in both studies, with the same materials. The $\sigma_{eff,bond}$values used for the comparison was correspond to 200 mm bond length, which was found to be the effective bond length and was provided as an anchorage length for the strengthened beams. Although identical failure modes were noted in both flexural and bond tests (for identical specimens having the same textile fibre materials and number of TRM layers) the debonding stresses recorded at failure were lower in the bond tests, leading to lower utilisation of the textile fibres reinforcement.

Table 6.5. Experimental values of ultimate moment capacity and effective stress in TRM/FRP reinforcement.

Specimen	$M^{*}_{u,exp}$ kN.m	$\sigma^{**}_{eff,exp}$ MPa	FM^{*}	f^{+}_{fu} MPa	$\frac{\sigma_{eff,exp}}{f_{fu}}$	f^{++}_{fbm} MPa	$\frac{\sigma_{eff,exp}}{f_{fbm}}$	$\sigma^{a}_{eff,bond}$ MPa	FM^{b}	$\frac{\sigma_{eff,exp}}{\sigma_{eff,bond}}$
CON	10.03	-			-	-				
TRM-retrofitted										
M1_C	11.31	1368	S	1518	0.90	n.a.	n.a.	915	S	0.75
M1_CO	12.01	1825	ID	2843	0.64	n.a.	n.a.	1572	ID	0.55
M3_C	16.04	1434	D	1518	0.94	1466	0.98	790	D	0.55
M5_C	18.04	1126	D	1518	0.74	1136	0.99	n.a.	D	n.a.
M7_B	13.60	1019	FR	1190	0.86	n.a.	n.a.	1046[c]	FR[c]	0.88
M7_G	12.53	658	FR	794	0.83	n.a.	n.a.	709[c]	FR[c]	0.89
M3_C_EA	16.56	1501	D	1518	0.99	n.a.	n.a.	877	D	0.58
FRP-retrofitted										
R1_C	12.73	2190	D	2936	0.75	2995	0.73	n.a.	n.a.	n.a.
R3_C	17.52	1796	D	2936	0.61	1729	1.04	n.a.	n.a.	n.a.
R7_B	15.72	1493	FR	1501	0.99	n.a.	n.a.	n.a.	n.a.	n.a.
R7_G	13.98	914	FR	1019	0.90	n.a.	n.a.	n.a.	n.a.	n.a.
R3_C_EA	24.30	3110	FR	2936	1.06	n.a.	n.a.	n.a.	n.a.	n.a.

[*] Ultimate moment capacity obtained experimentally.
[**] Effective stress in TRM/FRP reinforcement calculated based on experimental results.
[***] Failure mode of strengthened beams.
[+] Ultimate stress in the textiles fibres obtained from coupon tests (see Table 3.2 and Table 3.3).
[++] Mean debonding stress in TRM/FRP reinforcement calculated according to Eq. 6.11.
[a] Average stress in TRM reinforcement obtained from bond test included in Table 4.2.
[b] Failure mode observed in bond test (see Section 4.3.1).
[c] Bond tests.

6.1.5 Summary

Section 6.1 investigates experimentally the effectiveness of TRM versus FRP composite in flexural strengthening of RC beams. Several parameters were examined namely: (a) the strengthening material (TRM and FRP); (b) the number of FRP/TRM layers; (c) the textile surface condition; (d) the textile-fibre materials and (e) the end anchorage system. The obtained results revealed the following Findings:

- The effectiveness of TRM system in increasing the loading carrying capacity of retrofitted beams was less than that of FRP. Nevertheless, TRM effectiveness was sensitive to the number of layers. It was found that the effectiveness factor increased from 0.47 to 0.80 when the number of TRM layers increased from 1 to 3.
- Coating the carbon fibres textile with epoxy adhesive significantly enhanced the performance of TRM materials. When one layer of coated carbon textile was used instead of one layer of dry carbon textile, the flexural capacity gain increased from 12.7 to 19.7% (about 55% enhancement).
- Different textile fibres materials (carbon, coated basalt, and glass) having approximately the same axial stiffness resulted in different flexural capacity increases. In both strengthening systems, seven coated basalt-fibre textile layers recorded the highest flexural capacity increase, followed by seven dry glass-fibre textile layers, and finally by one carbon-fibre textile layer. This variance in the performance was related to the effect of number of layers (in both FRP and TRM strengthening systems), but also to the textile surface condition (dry or coated textiles) in TRM strengthening system.
- Providing end-anchorage with U-jackets to FRP-retrofitted beams resulted in 90% enhancement in the flexural capacity compared to non-anchorage beam. However,

the corresponding enhancement in TRM-retrofitted beam was limited (9%) and was attributed to the presence of slippage of the textile at the U-jacket – longitudinal TRM sheets.

- Two types of failure mode were observed in the FRP-retrofitted beams, these failure modes were: debonding from concrete substrate (for specimens M1_C and M3_C), and fibres rupture at the constant moment zone (for specimens M7_BCo, M7_G and M3_C_EA). Whereas, in the TRM-retrofitted beams five different failure modes were observed, namely slippage of the rovings through the surrounding cement mortar (specimen M1_C), fracture the surface at the textile-matrix interface (interlaminar debonding-specimen M1_CCo), debonding of TRM from the concrete with peeling off parts concrete cover (specimen M3_C and M5_C), rupture of the textile fibres at the constant moment zone (M7_BCo and M7_G), and debonding of TRM from the concrete substrate followed by slippage of the fibres at a different region (specimen M3_C_EA). These failure modes were found to be sensitive to the number of TRM layers, the textile fibres materials (carbon, coated basalt or glass fibres), and the textile surface condition (dry or coated fibres).
- The failure modes observed in the TRM strengthened beams were identical to the failure modes noted in the bond tests (described in Chapter 4) for the same number of TRM layers and the same textile fibre materials.
- For both strengthening systems (TRM and FRP), the cracking and post-yielding stiffness of strengthened beams was substantially enhanced compared to the unstrengthened beam (up to 72% and 1298%, respectively).
- A formula proposed by *fib model code (2010)* was used to predict the debonding stress in FRP reinforced for those specimens failed due to debonding of FRP from concrete substrate. This formula was also used to predict the debonding stress of

TRM reinforcement for those specimens that have same failure mode (i.e. debonding). It was found that this formula is in a good agreement with the effective stress calculated based on the experimental results providing that TRM properties are obtained from coupon tests.

6.2 Influence of Textile Geometry on the Performance of TRM in Flexural Strengthening of RC Beams

6.2.1 Experimental programme

This section evaluates the effect of textile geometry on the flexural behaviour of RC beams strengthened with TRM. For this purpose, eleven beams were fabricated, strengthened and tested under four point-bending. The geometry, internal reinforcement of the test beams is identical to that beams presented in Section 6.1.1.1 (see Figure 6.1a-b). The investigated parameters were: (a) the number of TRM layers (1 and 3), (b) the geometry of textiles namely: the area of a single carbon roving in the direction of loading, and the material (carbon and glass) and spacing between rovings in the transversal direction. The textiles reinforcement used were the hybrid group F10x20, F10x40, F20x20, and F20x40 and the dry carbon fibres textile (C) described in Section 3.3. Figure 6.12 shows the textile characteristics namely: the mesh size, the area of carbon rovings in the loading direction, and the material and spacing between the transversal rovings. It is worth mentioning that the area of the carbon fibres in the loading direction is equal for all five types of textiles.

Two out of the eleven specimens have already been presented in Section 6.1. These specimens are M1_C, and M3_C which were strengthened with 1 and 3 layer of the dry carbon textile (C). The details of the remaining nine specimens were as follows: one specimen was left without strengthening and served as a control beam (CON), whereas, the remaining eight specimens were strengthened with 1 and 3 layers of the four hybrid textiles. The notation of the hybrid strengthened specimens is FX_N, where X denotes to the type of hybrid textile (F10x20, F10x40, F20x20, and F20x40-

see Figure 6.12), N refers to the number of TRM layers. Table 6.6, with the support of Figure 6.13, provides a description of the tested specimens.

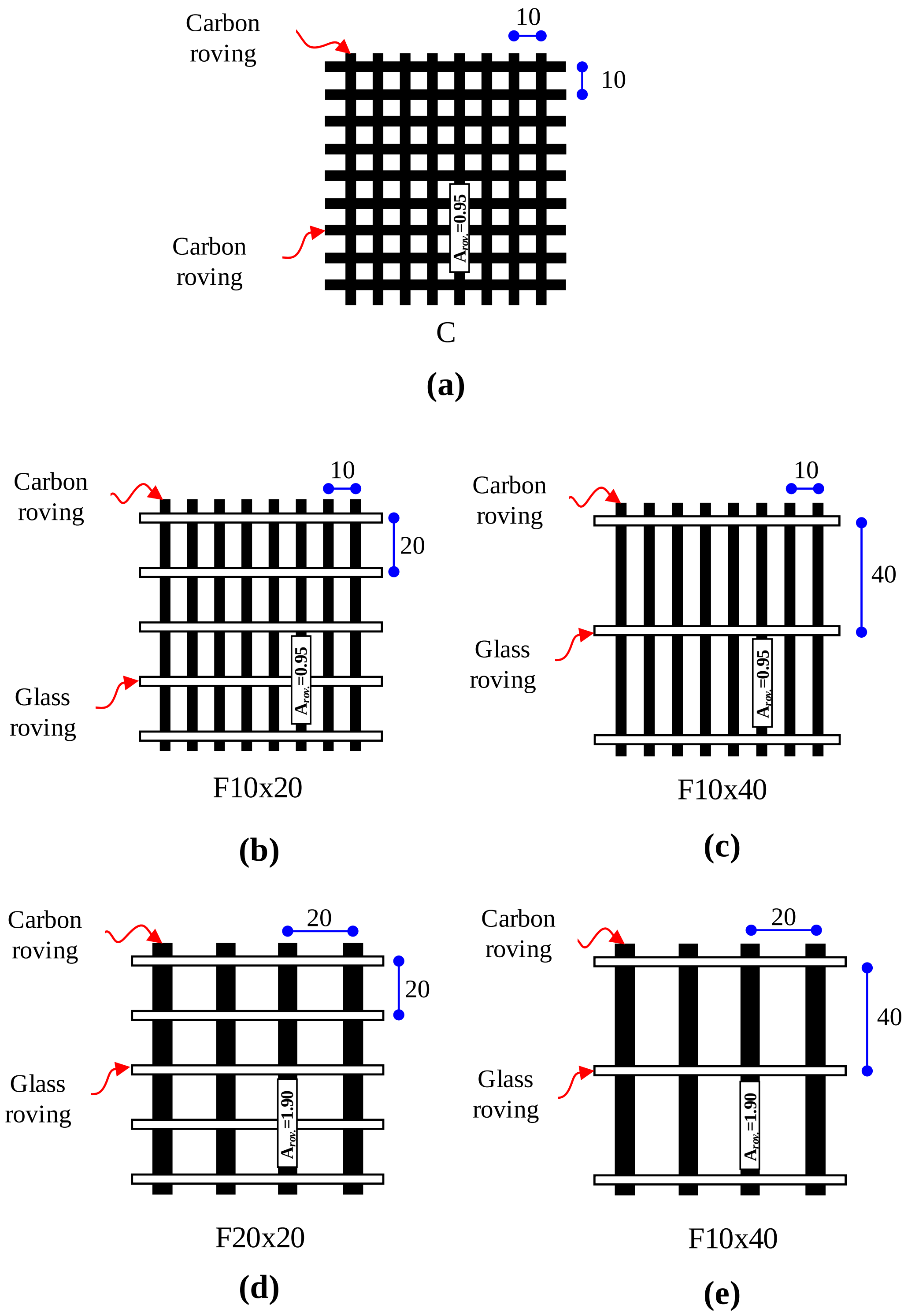

Figure 6.12. Schematic drawing of the carbon fibres textile and the four types of hybrid textiles.

Table 6.6. Strengthening configuration and materials properties of test specimens.

Specimen	No. of layers	ρ_f (%)	$E_{f,TRM}$ (GPa)	Concrete Strength (MPa)		Mortar Strength (MPa)	
				Compre-ssive	Tensile splitting	Compre-ssive	Flexur-al
CON	-	-	-	21.7	2.32	-	-
M1_C*	1	0.0475	166.8	19.9	2.16	39.2	9.8
M3_C*	3	0.1425	166.8	19.9	2.16	39.2	9.8
F10x20_1	1	0.0475	165.6	21.7	2.32	35.6	8.1
F10x20_3	3	0.1425	165.6	21.7	2.32	35.6	8.1
F10x40_1	1	0.0475	169.1	21.7	2.32	35.6	8.1
F10x40_3	3	0.1425	169.1	21.7	2.32	35.6	8.1
F20x20_1	1	0.0475	161.1	20.8	2.24	37.3	8.7
F20x20_3	3	0.1425	161.1	20.8	2.24	37.3	8.7
F20x40_1	1	0.0475	159.3	20.8	2.24	37.3	8.7
F20x40_3	3	0.1425	159.3	20.8	2.24	37.3	8.7

*presented in Section 6.1.

Textile geometry	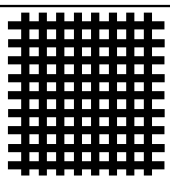	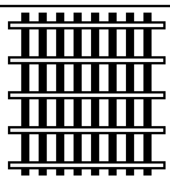	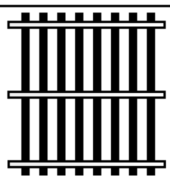	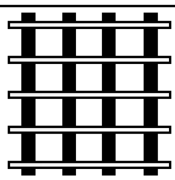	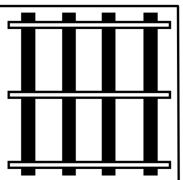
Specimen name	M1_C M3_C	F10x20_1 F10X20_3	F10x40_1 F10X40_3	F20x20_1 F20X20_3	F20x20_1 F20X40_3

Figure 6.13. Description of the tested beams.

The compressive and splitting tensile strength of the concrete and the compressive and flexural strength of the mortar were determined on the day of testing and the results are presented in Table 6.6. The tensile properties of the steel bars used for flexural and shear reinforcement were the same of that reported in Section 6.1.1.2.

The strengthening procedure has also already been described in Section 6.1.1.3 and also documented here in Figure 6.14a-d.

Figure 6.14. Strengthening procedure: (a) Concrete surface preparation; (b) application of first layer of mortar, (c) application and impregnation of textile with mortar; and (d) application of final layer of mortar.

Finally, the beams were tested as simply supported and were subjected to four-point bending (see Figure 6.4).

6.2.2 Experimental results

The response of all tested beams is presented in Figure 6.15 in form of load-deflection curves, whereas key results are reported in Table 6.7. As in the case of the load-deflection curves of the beams described in Section 6.1.2.1. The curves of tested beams were also characterised by three distinct stages up to the maximum load. These stages were (see also Figure 6.5): un-cracked stage, cracked stage, and post-yielding stage. After reaching the ultimate load, the load was dropped to the level of the un-retrofitted (CON) beam indicating that the effect of strengthening had totally been lost.

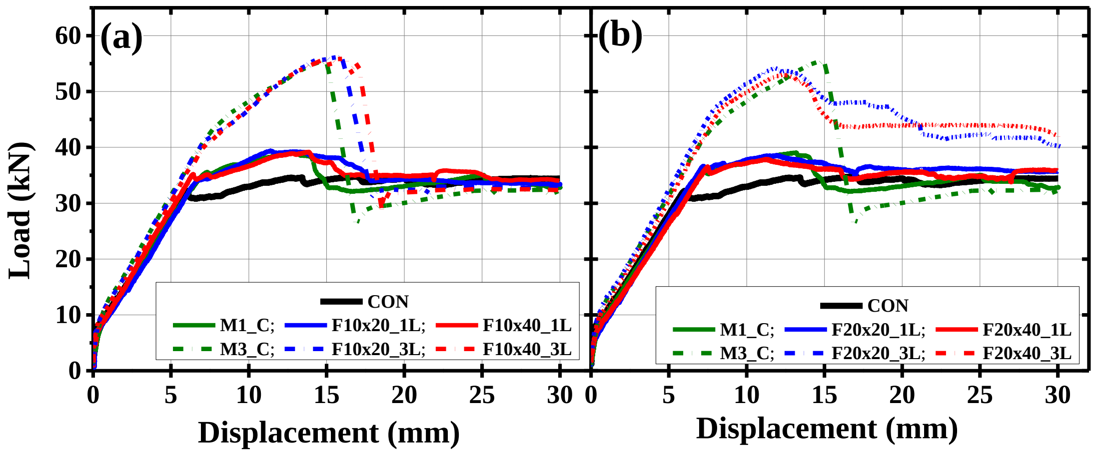

Figure 6.15. Load versus mid-span deflection curves of tested beams for; (a) beams strengthened with F10x20 and F10x40 textile materials; and (b) beams strengthened with F20x20 and F20x40 textile materials.

Table 6.7. Summary of test results.

Specimens name	Load (kN)			Deflection (mm)			(7) Capac-ity increase (%)	(8) Failure mode [a]
	(1) Crack (P_{cr})	(2) Yield (P_y)	(3) Ultimate (P_u)	(4) Crack (δ_{cr})	(5) Yield (δ_y)	(6) Ultima-te (δ_u)		
CON	8.0	31.7	34.6	0.3	6.01	13.4	-	CC
M1_C	10.0	35.6	39.0	1.0	7.3	13.2	12.7	S
M3_C	12.8	43.0	55.3	1.0	7.6	14.7	59.8	D
F10x20_1	7.6	34.0	39.4	0.4	6.6	13.6	13.9	S
F10x20_3	12.0	41.4	56.2	0.9	7.2	15.8	62.4	D
F10x40_1	8.2	34.6	39.2	0.5	6.4	13.9	13.3	S
F10x40_3	10.7	40.0	55.9	0.7	7.0	15.76	61.6	D
F20x20_1	6.1	36.5	38.6	0.4	7.2	11.9	11.6	S
F20x20_3	13.5	47.0	54.2	1.0	8.0	12.0	56.6	DS
F20x40_1	7.0	36.5	37.9	0.4	7.3	11.23	9.5	S
F20x40_3	10.9	47.6	53.0	0.7	8.5	11.8	53.2	DS

[a] CC: Concrete crushing after steel yielding; S: slippage and partial rupture of the fibres through the mortar; D: debonding of TRM from concrete substrate; DS: debonding of TRM from concrete followed by slippage of the fibres through the mortar.

The reference beam (CON) failed as designed in flexure at an ultimate load of 34.8 kN. The failure was due to yielding of the tensile reinforcement concrete followed by concrete crushing at the compression zone. As mentioned in Section 6.1.2.2, specimens M1_C and M3_C attained an ultimate load of 39.0, and 55.3 kN, respectively, yielding an increase in the flexural capacity of 12.7 and 59.8%, respectively due to application of strengthening. Similarly, specimens F10x20_1, F10x20_3, F10x40_1 and F10x40_3 recorded an ultimate load of 39.4, 56.2, 39.2, and 55.9 kN, respectively, resulting in 13.9, 62.4, 13.3, and 61.6%, respectively, increase in the flexural capacity due to application of strengthening compared to the control beam. The failure of specimens F10x20_1, and F10x40_1 was due to slippage of the fibres through the mortar accompanied by partial rupture of the fibres (Figure 6.16a and c). This failure mode was identical to the failure observed in the counterpart specimen M1_C which was strengthened with one layer of dry carbon fibres textile (see Figure 6.7g). The failure of specimens F10x20_3 and F10x40_3 on the other hand was due to debonding of the TRM from concrete substrate accompanied by peeling off part of the concrete cover (Figure 6.16b and d). This type of failure mode was also identical to the failure of specimen M3_C which was strengthened with three layers of dry carbon fibres textile (see Figure 6.7i).

Finally, the peak load recorded for specimens F20x20_1, F20x20_3, F20x40_1 and F20x40_3 was 38.6, 54.2, 37.9, and 53.0 kN, respectively, which yields (compared to the control beam) 11.6, 56.6, 9.5, and 53.2%, increase in the flexural capacity, respectively. The failure of specimens F20x20_1 and F20x40_1 was attributed to slippage and partial rupture of the fibres through the mortar (Figure 6.16e and g) which was identical to the failure mode observed in specimens M1_C, F10x20_1 and F10x40_1. Whereas the failure mode of specimens F20x20_3 and F20x40_3 was combination of debonding followed by slippage of the rovings within the mortar (Figure 6.16f and h). It is noted that this failure mode was different from their counterpart specimens strengthened with three layers (i.e. specimens M3_C, F10x20_3 and F10x40_3).

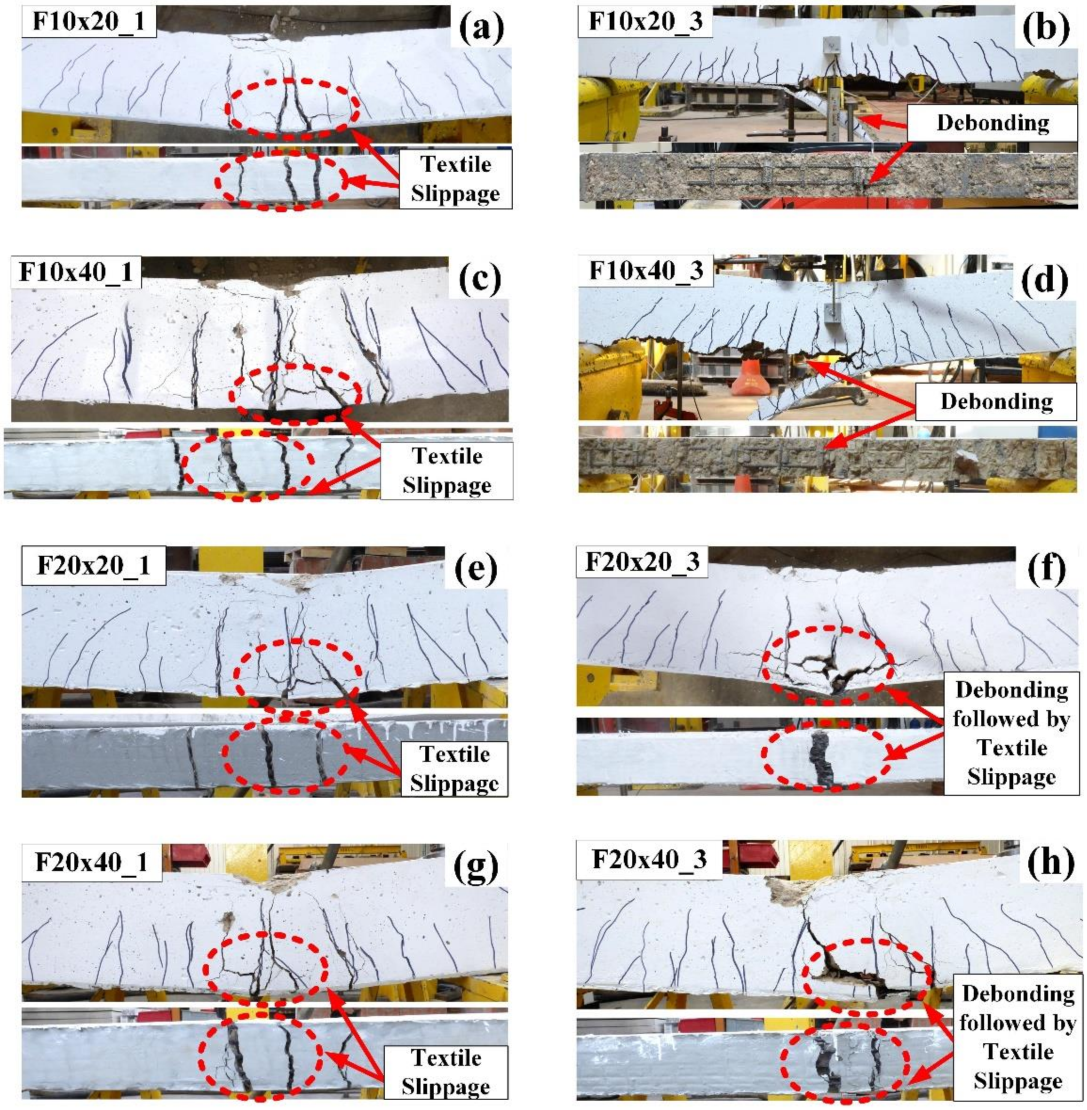

Figure 6.16. Failure mode of specimens strengthened with the hybrid textiles.

6.2.3 Discussion

All strengthened specimens responded as designed and failed by the loss of strengthening after yielding of the internal steel reinforcement. Based on the various parameters investigated in this experimental programme, an examination of the results (Table 6.7) in terms of flexural capacity increase and failure modes, revealed the following information.

6.2.3.1 Influence of number of layers

The influence of number of layers on the flexural capacity increase of beams strengthened with the dry carbon fibres textile (C) and the four-hybrid textiles (F10x20, F10x40, F20x20, and F20x40) is depicted in Figure 6.17a. Tripling the number of layers resulted in dramatical improvement (non-proportional increase to the number of layers) in the effectiveness of TRM in enhancing the flexural capacity.

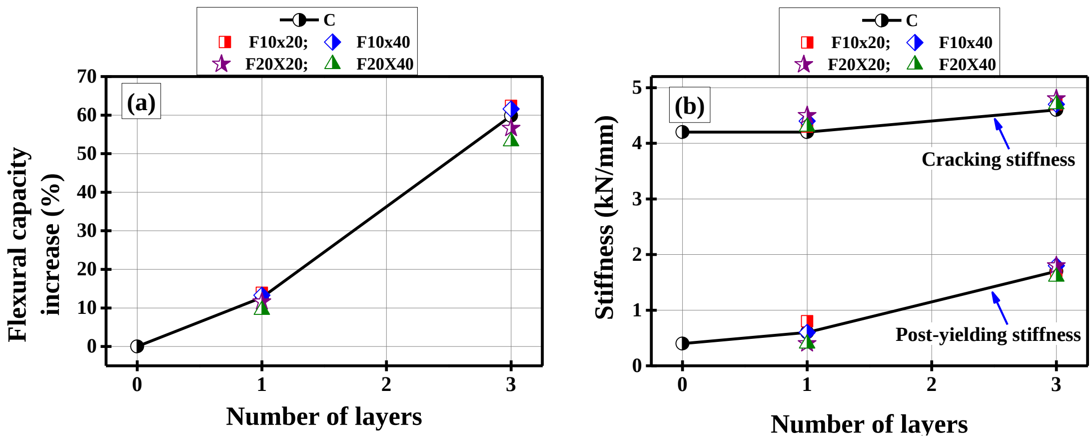

Figure 6.17. Effect of number of layers on: (a) the flexural capacity increase; and (b) the cracking stiffness, and post-yielding stiffness.

The cracking and post-yielding stiffness were also influenced by the number of layers. As shown in Figure 6.17b, increasing the number of layers from 1 to 3 resulted in slight enhancement in the cracking stiffness but considerable improvement in the post-yielding stiffness (see also Table 6.8).

The failure mode was also sensitive to the number of layers; for one TRM layer strengthened specimens, the failure was due a local damage as a result of slippage the fibres through the mortar. With three layers, the local damage was completely as in the case of specimens M3_C, F10x20_3, and F10x40_3 (see Figure 6.16b and d) or partially as in the case of specimens F20x20_3, and F20x40_3 (Figure 6.16f and h) prevented, and the failure was shifted to the concrete substrate. Improving the mechanical interlocking due to the overlapping the textile layers is believed to be the reason of such behaviour.

Table 6.8. Comparison of stiffness at pre-cracking, cracking and post-yielding stage.

Specimens	**Pre-cracking stiffness (kN/mm)**	**Cracking stiffness (kN/mm)**	**Post-yielding stiffness (kN/mm)**
CON	26.7	4.2	0.4
M1_C	10.2	4.1	0.6
M3_C	12.8	4.6	1.7
F10x20_1	19.0	4.3	0.8
F10x20_3	12.9	4.7	1.7
F10x40_1	16.4	4.5	0.6
F10x40_3	15.1	4.7	1.8
F20x20_1	15.3	4.5	0.4
F20x20_3	13.5	4.8	1.8
F20x40_1	17.5	4.3	0.4
F20x40_3	15.6	4.7	1.6

6.2.3.2 Influence of textile geometry

This paragraph discusses the influence of textile geometry on the flexural capacity enhancement, cracking and post-yielding stiffness, and also, the failure mode. The term "textile geometry" includes: (a) the area of a single roving in the direction of loading, and (b) the materials and spacing between rovings in the transversal direction. As described in Section 3.3, the dry carbon textile and the four types of the hybrid textiles had the same quantity of carbon fibres in the direction of loading. The only difference is the area of rovings (A_{rov}_ Figure 6.12); in specific, the area of a single carbon roving of the hybrid textiles F20x20 and F20x40 is equal to A_{rov}= 1.90 mm^2 which is double than the area of a single roving of the dry carbon textile (C), F10x20, and F10x40 (A_{rov}= 0.95 mm^2). The materials and spacing between rovings in the transversal direction were also different; in particular, the dry carbon fibres textile (C) had carbon fibres rovings with 10 mm spacing, whereas, the hybrid textiles F10x20, and F10x40 had glass fibres rovings of 20, and 40 mm spacing in the transversal, respectively. Similarly, the hybrid textiles F20x20, and F20x40 had also glass fibres rovings of spacing equal to 20 and 40 mm in the transversal direction, respectively.

The influence of the area of a single roving (A_{rov}) in the direction of loading on the flexural capacity increase is presented in Figure 6.18. Doubling the area of the rovings in the loading direction, resulted in slight reduction in the TRM effectiveness in enhancing the flexural capacity of both 1 and 3 TRM strengthened specimens. This is attributed to the degree of impregnation of a single roving into mortar; with smaller area of rovings, the degree of impregnation is better achieved resulted in improving the bond characteristics between the mortar and the textile reinforcement, consequently the flexural capacity of strengthened beams was also enhanced.

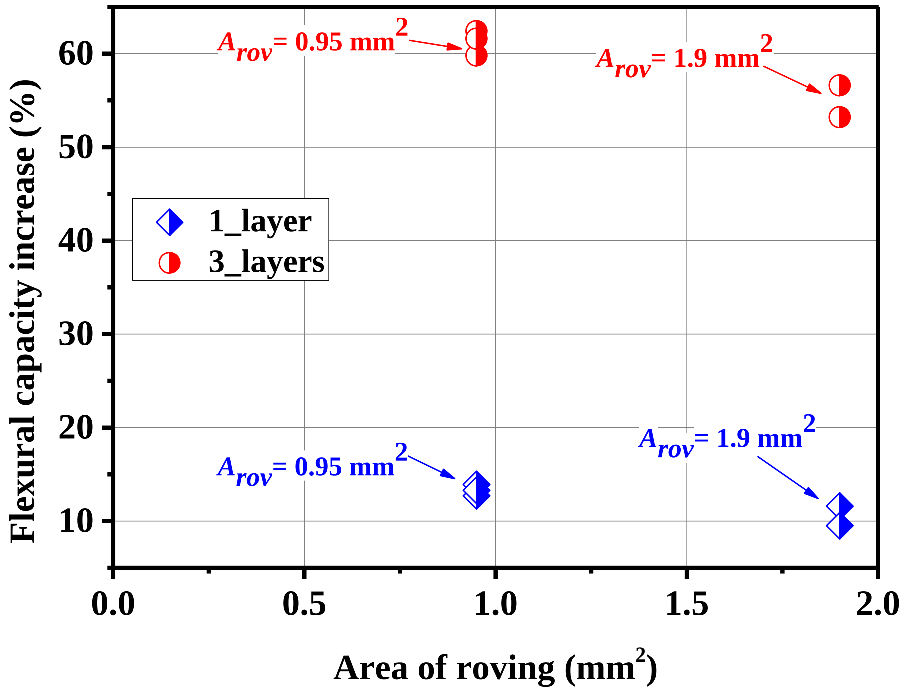

Figure 6.18. Effect of area of rovings in the direction of loading on the flexural capacity increase.

The failure mode of 1 TRM layer strengthened beams was not affected from the area of rovings in the loading direction and was always slippage of the fibres through the mortar with partial rupture of the fibres. However, when the number of TRM layers increased from 1 to 3, doubling the area of rovings led to change in the failure mode. In specific, specimens M3_C, F10x20_3 and F10x40_3 (A_{rov}=0.95 mm^2), failed due to fully debonding of TRM from concrete substrate with a part of concrete cover being attached (Figure 6.16b and d), whereas the failure mode of specimens F20x20_3 and F20x40_3 (A_{rov}=1.90 mm^2), was combination of debonding followed by slippage of fibres through the mortar (Figure 6.16f and h). This change in the failure mode could also be attributed to the degree of impregnation of a single fibre into mortar; a good impregnation of fibres into mortar is difficult to achieve with bigger area of rovings, consequently, the bond characteristics between fibres and mortar would be not enough to ensure fully debonding of TRM from concrete substrate.

The effect of textile material and spacing between rovings in the transversal direction on the flexural capacity increase is presented Figure 6.19a and b. A comparison of the results reveals that the textiles material (carbon or glass) and spacing (10, 20 or 40 mm) between transversal rovings had very limited effect on the flexural capacity enhancement for both one and three carbon fibre layers of A_{rov}= 0.95 and 1.90 mm^2 in the direction of loading.

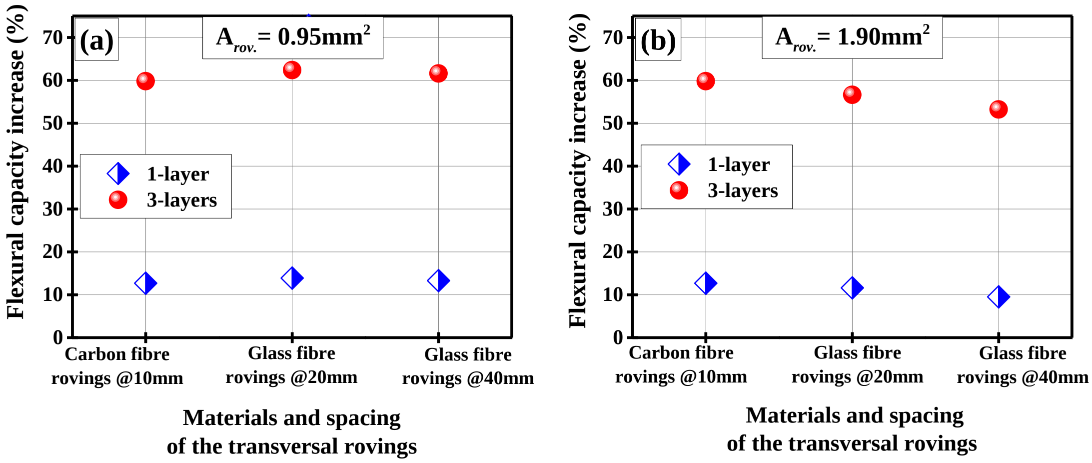

Figure 6.19. Effect of material and spacing between rovings in the transversal direction of the textile on the flexural capacity increase for textile having area of rovings in the loading direction of: (a) A_{rov}= 0.95 mm^2 and (b) A_{rov}= 1.90 mm^2.

According to these findings, it seems that main function of the transversal rovings is to maintain the stability of the overall geometry of the textile. This conclusion leads to a significant reduction of the overall cost of textile reinforcement due to the considerable savings in the material of fibres in the transversal direction.

6.2.4 Summary

This section investigates the influence of textile geometry on the performance of TRM in flexural strengthening of RC beams. Parameters examined were: (a) the number of layers (1 and 3); (b) the geometry of textile reinforcement namely: the area of rovings in the direction of loading, and the material and spacing between rovings in the transversal direction. The main findings of this section can be summarized as below:

- Increasing the number of layers from 1 to 3, dramatically enhanced the flexural capacity and also altered the failure mode.
- Doubling the area of a single roving in the direction of loading resulted in limited but adverse effect on the flexural capacity enhancement.
- The materials and spacing between rovings in the transversal direction had no effect on both the flexural capacity increase and the failure mode providing that the same amount of carbon fibres in the loading direction is used. This would significantly reduce the overall cost of the textile reinforcement due to the considerable saving of fibres' materials in the transversal direction of the textile reinforcement.

According to the above findings, and to produce an effective textile geometry combining acceptable flexural performance and low cost, the following suggestions could be beneficial: (a) the area and spacing between rovings in the loading direction would be as smaller as possible. This creates a denser mesh pattern which would improve the bond characteristics between the textile and mortar. In any case, the size of perforations between the rovings should be sufficient to ensure that cement mortars protruded through them; and (b) low-cost fibre materials can be used in the transversal direction with a spacing between rovings large as possible but ensuring the stability of the overall textile geometry.

Chapter 7

TRM VERSUS FRP IN FLEXURAL STRENGTHENING OF RC BEAMS: BEHAVIOUR AT HIGH TEMPERATURE

ABSTRACT

This chapter presents the flexural behaviour of RC beams strengthened with TRM and FRP composites and compares both at ambient and for the first time at high temperatures. The investigated parameters were: (a) the strengthening material, namely TRM versus FRP, (b) the number of strengthening layers, (c) the textile surface condition (dry and coated), (d) the textile material (carbon, basalt or glass fibres) and (e) the end-anchorage of the flexural reinforcement. The results showed that TRM exhibited excellent performance as strengthening material in increasing the flexural capacity at high temperature; in fact, TRM maintained an average effectiveness of 55%, compared to its effectiveness at ambient temperature, contrary to FRP which totally lost its effectiveness when subjected to high temperature. In specific, from the high temperature test it was found that by increasing the number of layers, the TRM effectiveness was considerably enhanced and the failure mode was altered; coating enhanced the TRM effectiveness; and the end-anchorage at high temperature improved significantly the FRP and marginally the TRM effectiveness. Finally, the formula proposed by the fib Model Code (2010) was used to predict the mean debonding stress in the TRM reinforcement, and using the experimental results obtained in this study, a reduction factor to account for the effect of high temperature on the flexural strengthening with TRM was proposed.

** The content of this work has been submitted as a journal paper: "TRM versus FRP in Flexural Strengthening of RC Beams: Behaviour at High Temperatures", Construction and Building Materials.*

7.1 Experimental Programme

7.1.1 Test specimen, Investigated parameters, Materials and strengthening procedure

The main objective of this study was to compare the effectiveness of TRM versus FRP in enhancing the flexural capacity of RC beams at high temperature. A total of 23 half-scale rectangular section RC beams were constructed, strengthened and tested under 4-point bending load as follows: eleven beams were tested at high temperature (150 ^{0}C), whereas the remaining twelve beams were tested at ambient temperature and presented in Section 6.1. The geometry, internal reinforcement of the test beams is identical to that beams presented in Section 6.1.1.1 (see Figure 6.1a and b). The parameters investigated in this study were: (a) the strengthening system (TRM versus FRP), (b) the number of strengthening layers (one, three, and seven), (c) the material of the textiles fibres (carbon, glass and basalt), (d) the textile surface condition (coated versus dry) of carbon-fibre textiles, and (e) the end-anchorage of the main FRP/TRM reinforcement using U-shaped jacketing made of FRP/TRM. Three different textiles were used as external reinforcement, namely the carbon-fibre textile (dry_C and coated_CCo), the coated basalt fibre-textile (BCo), and the dry glass-fibre textile (G). Details of the textiles are illustrated Figure 3.1. As mentioned in Section 6.1.1.1, seven layers of basalt or glass -fibre textile have approximately the same axial stiffness of the one layer of dry carbon textile.

Table 7.1 supported by Figure 7.1a, provide description of the tested specimens and strengthening configurations. The strengthened specimens were named following the notation BN_F_T, where B denotes the type of bonding agent (M for cement mortar and R for epoxy resin); N the number of TRM or FRP layers; F the type of textile fibres material (C for dry carbon fibres, CCo for coated carbon fibres, BCo for basalt fibres and G for glass fibres); and T denotes the temperature at which the specimens were exposed (20 ^{0}C or 150 ^{0}C). For the specimens that received U-jackets at their ends (Figure 7.1b), an additional suffix (EA-End anchorage) is added to the notation. For example, ‘M3_C_20’ refers to a beam strengthened with 3 layers of dry carbon TRM and tested at 20 ^{0}C, whereas 'R3_C_EA_150’ refers to a beam strengthened with 3 layers of carbon FRP, anchored at its ends using two layers of U-shaped jacket, and tested at temperature of 150 ^{0}C.

Table 7.1. Strengthening configuration and materials properties of test specimens.

Specimen	**t_f (mm)**	**No. of layers**	**Temperature (^{0}C)**	**Concrete Strength (MPa)**		**Mortar Strength (MPa)**	
				Compressive strength	**Tensile splitting strength**	**Compressive strength**	**Flexural strength**
CON	-	-	20	19.9	2.1		
TRM-retrofitted							
M1_C_20	0.095	1	20	19.9	2.1	39.2	9.8
M1_C_150	0.095	1	150	20.7	1.9	16.2	2.3
M1_CCo_20	0.095	1	20	19.9	2.1	39.2	9.8
M1_CCo-150	0.095	1	150	20.7	1.9	16.2	2.3
M3_C_20	0.095	3	20	19.9	2.1	39.2	9.8
M3_C_150	0.095	3	150	20.7	1.9	16.2	2.3
M7_BCo_20	0.0371	7	20	19.9	2.1	39.2	9.8
M7_BCo_150	0.0371	7	150	20.7	1.9	16.2	2.3
M7_G_20	0.044	7	20	19.9	2.1	39.2	9.8
M7_G_150	0.044	7	150	20.7	1.9	16.2	2.3
M3_C_EA_20[1]	0.095	3	20	21.7	2.4	39.2	9.8
M3_C_EA_150	0.095	3	150	20.7	1.9	16.2	2.3
FRP-retrofitted							
R1_C_20	0.095	1	20	21.7	2.4	-	-
R1_C_150	0.095	1	150	20.1	2.2	-	-
R3_C_20	0.095	3	20	21.7	2.4	-	-
R3_C_150	0.095	3	150	20.1	2.2	-	-
R7_BCo_20	0.0371	7	20	21.7	2.4	-	-
R7_BCo_150	0.0371	7	150	20.1	2.2	-	-
R7_G_20	0.044	7	20	21.7	2.4	-	-
R7_G_150	0.044	7	150	20.1	2.2	-	-
R3_C_EA_20	0.095	3	20	21.7	2.4	-	-
R3_C_EA_150	0.095	3	150	20.1	2.2	-	-

The beams were cast in different groups using the same concrete mix-design. The compressive and splitting tensile strength of the concrete were determined on the day of testing and the results are presented in Table 7.1. The binding material used for TRM strengthened beams was the cement mortar described in Section 3.1. The compressive and flexural strength (at 20 and 150 ^{0}C) of the mortar are given in Table 7.1.

Textile material	**TRM**		**FRP**		**Strengthening configuration**
	Temperature		**Temperature**		
	20 ^{0}C	**150 ^{0}C**	**20 ^{0}C**	**150 ^{0}C**	
Carbon Fibres	M1_C_20 M1_CCo_20 M3_C_20	M1_C_150 M1_CCo_150 M3_C_150	R1_C_20 R3_C_20	R1_C_150 R3_C_150	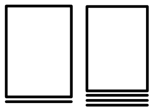
Coated basalt Fibres	M7_BCo_20	M7_BCo_150	R7_BCo_20	R7_BCo_150	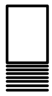
Glass Fibres	M7_G_20	M7_G_150	R7_G_20	R7_G_150	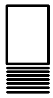
Carbon Fibres+ End anchorage	M3_C_EA_20	M3_C_EA_150	R3_C_EA_20	R3_C_EA_150	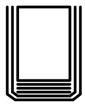

(a)

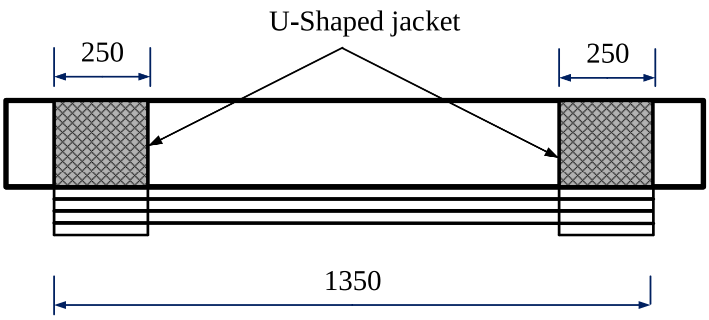

(b)

Figure 7.1. (a) Group of specimens; and (b) details of end anchorage system (dimensions in mm).

The tensile properties of the steel bars used for flexural and shear reinforcement were the same of that reported in Section 6.1.1.2. For those beams retrofitted with FRP, the epoxy resin described in Section 3.2 was used as a binding material. The strengthening material (TRM or FRP) was bonded to the beams' soffit over a length of 1350 mm. The strengthening procedure for both strengthening systems had the characteristics of a typical wet lay-up application as described Section 6.1.1.3 (see Figure 6.3a-h).

7.1.2 Experimental setup

7.1.2.1 Development of the heating system

Figure 7.2a shows the heating system designed and manufactured to provide heating along the critical flexural span of the beams. The heating system comprised five 1000 W ceramic heaters of 60 mm width, 245 mm length and 30 mm thickness. The maximum surface temperature for each single heater is about 700 ^{0}C. The heaters were fixed to steel boxes which also facilitated the wiring of the heaters to the power supply (Figure 7.2a). Those steel boxes where then mounted to a steel frame (Figure 7.2b) with a length of 1350 mm, namely equal to length of the strengthened area of the beams. The steel frame was designed to be portable for allowing fast removal of the heating system from underneath the beams in case of emergency. At the same time the steel frame legs height was adjustable for controlling the distance between the heaters and beam's soffit. Moreover, to protect the heaters from falling parts of concrete and TRM or FRP in case of abrupt failures, a protection steel cage was fixed at the top the steel frame, as illustrated in Figure 7.2a.

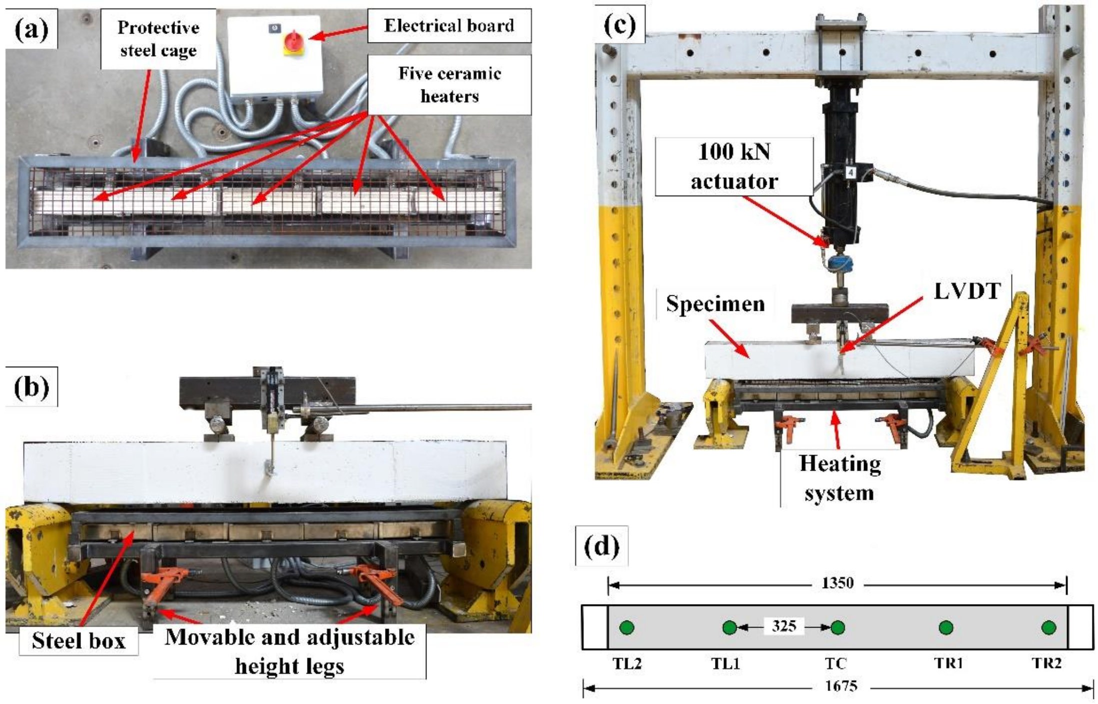

Figure 7.2. Test setup: (a) heating system; (b) front view; (c) overall test setup; and (d) distribution of thermocouples along the strengthened area.

7.1.2.2 Testing protocol and instrumentations

All beams were simply supported and subjected to four-point bending. The flexural span was 1500 mm, and the selected configuration resulted in a 340 mm-long constant moment zone and a 580 mm-long shear span (see Figure 6.1). The load was applied using a 100 kN-capacity servo-hydraulic actuator which was fixed on a stiff reaction frame. A picture of the test setup is shown in Figure 7.2c. The beams were loaded monotonically up to failure at a displacement rate of 1 mm/min. Two LVDTs were fixed at the mid-span of the beam (one on each side) to measure independently the mid-span deflection.

For the beams tested at high temperature, five type K thermocouples were mounted to the concrete surface prior the application of the strengthening materials in order to monitor the temperature at concrete-adhesive interface. As shown in Figure 7.2d, the thermocouples were distributed along the critical strengthened flexural span to ensure that the targeted temperature (i.e. 150 ^{0}C) is uniformly reached along that span. The test procedure at high temperature included the following steps: the heating system was placed underneath the specimen; the height of the legs was adjusted in order to achieve a distance of 100 mm (to allow for beam's deflection) between the heaters and the beam's soffit. The specimen was heated up to the predefined temperature (i.e. 150 ^{0}C), and then loaded monotonically up to failure, while the temperature at the concrete-adhesive interface was approximately kept constant at 150 ^{0}C. The data of the tests was recorded using a fully-computerized data acquisition system.

7.1.2.3 Temperature profile

Figure 7.3a and b shows typical time-temperature curves obtained from the five thermocouples (affixed at the concrete- adhesive interface) for specimens R3_C_150 and M3_C_150, respectively. It can be observed that: (a) the heating rate was approximately identical between the two specimens, (b) the temperature measured along the critical flexural span was consistent indicating the effectiveness of the heating system, and (c) the maximum variation of temperature from the targeted one during all tests was approximately 7 ^{0}C. (see Figure 7.3a, b). Note that the consistency in the heating procedure for all tested specimens is important to reduce errors, obtain reliable and comparable results, and hence increase the level of confidence in the obtained results.

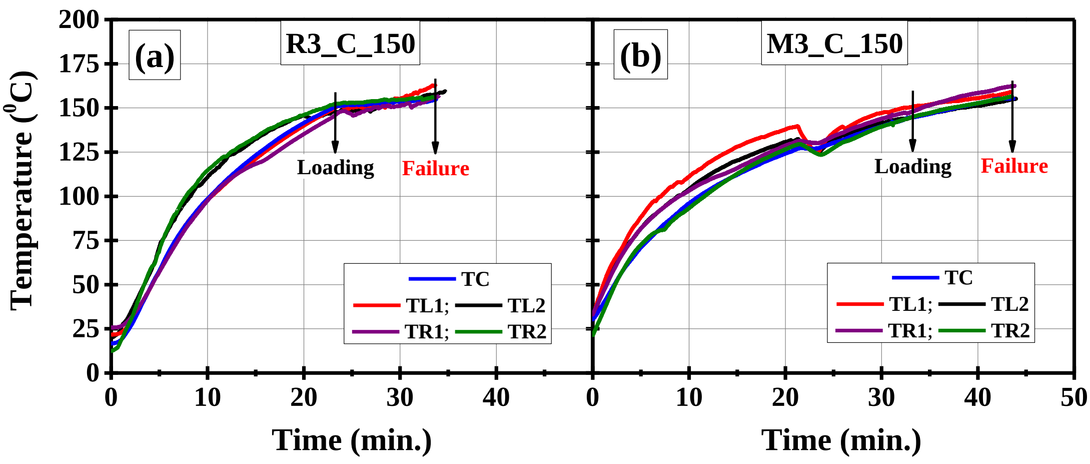

Figure 7.3. Temperature-time curves: (a) FRP-strengthened beam (R3_C_150), and (b) TRM-retrofitted beam (M3_C_150).

7.2 Experimental Results

Table 7.2 summarizes the main results of all tested beams both at ambient temperature and 150 ^{0}C. The results of ambient temperature tests (also presented in Table 6.2) include: (1) The ultimate recorded load (P_u). (2) The flexural capacity increases due to application of the strengthening. (3) The observed failure mode. Whereas, the results of the high temperature tests comprise: (1) The cracking load (P_{cr}). (2) The yield load (P_y) (which is defined as the load corresponding to the steel yielding). (3) The ultimate recorded load (P_u). (4) The displacement corresponding to cracking load (δ_{cr}). (5) The displacement corresponding to the yielding load (δ_y) (average mid-span deflection from two LVDTs corresponding to P_y). (6) The displacement at ultimate load (δ_u) (average of mid-span deflection from two LVDTs at the ultimate load (P_u). (7) The flexural capacity increase due to strengthening. (8) The observed failure mode. The last column in Table 7.2 reports the reduction of the contribution of FRP/TRM reinforcement (as a percentage) to the total flexural capacity due to the effect of high temperature, expressed by the ratio, $(f_{c,\,A.T} - f_{c,\,H.T}) / f_{c,\,A.T}$.

Table 7.2. Summary of test results of beams tested at ambient temperature and at 150 ^{0}C.

Specimen	Ambient temperature (20 ^{0}C)			Ambient temperature (150 ^{0}C)								
				Load (kN)			Deflection (mm)					
	(1) Ultimate load (P_u)	(2) Flexural capacity increase ($f_{c,\,A.T}$) (%)	(3) Failure mode [a]	(1) Crack (P_{cr})	(2) Yield (P_y)	(3) Ultimate (P_u)	(4) Crack (δ_{cr})	(5) Yield (δ_y)	(6) Ultimate (δ_u)	(7) Flexural capacity increase $f_{c,\,H.T}$ (%)	(8) Failure mode[a]	($f_{c,\,A.T}$ - $f_{c,\,H.T}$)/ $f_{c,\,A.T}$ (%)
CON	34.6	-	CC	-	-	-	-	-	-	-	-	-
TRM-retrofitted												
M1_C	39.0	12.7	S	6.8	35.2	37.7	0.7	7.1	9.1	9.0	S	29.5
M1_CCo	41.3	19.4	ID	8.0	34.4	38.3	0.6	5.9	8.1	10.7	ID	44.8
M3_C	55.3	59.8	D	7.4	34.7	44.7	0.74	6.1	8.9	29.2	D	51.2
M7_BCo	46.9	35.5	FR	10.8	34.5	41.1	1.15	6.1	13.7	18.8	S	47.2
M7_G	43.2	24.9	FR	7.6	36.8	38.8	0.67	7.2	10.3	12.1	S	51.2
M3_C_EA	57.1	65.0	DS	11.3	41.4	46.2	0.93	7.43	10.5	33.5	DS	48.4
FRP-retrofitted												
R1_C	43.9	26.9	D	8.8	34.4	35.9	0.74	6.5	8.7	3.8	AF	86.0
R3_C	60.4	74.6	D	8.2	35.6	36.7	0.61	6.7	8.2	5.8	AF	92.2
R7_BCo	54.2	56.6	FR	8.0	33.6	36.5	0.8	6.3	11.6	5.5	AF	90.3
R7_G	48.2	39.3	FR	7.5	29.8	35.8	0.4	5.6	19.45	3.5	AF	91.2
R3_C_EA	83.7	141.9	FR	10.0	42.6	57.5	0.53	6.8	25	66.2	AS	53.4

[a] CC: Concrete crushing; S: slippage and partial rupture of the fibres through the mortar; ID: TRM debonding at the textile-mortar interface (inter-laminar shearing); D: TRM debonding from concrete substrate; AF: adhesive failure at the concrete- resin interface; DS: Debonding of TRM from concrete substrate, followed by slippage of the fibres at the region where the longitudinal TRM meets the TRM U-jacket; and AS: adhesive failure at the concrete- resin interface in the non-anchorage zone followed by partial rupture and slippage of the fibres at the region where the longitudinal FRP meets the FRP U-jacket.

7.2.1 Load-displacement curves

The response of all beams tested at ambient and high temperature is presented in Figure 7.4a-c in the form of load- displacement curves.

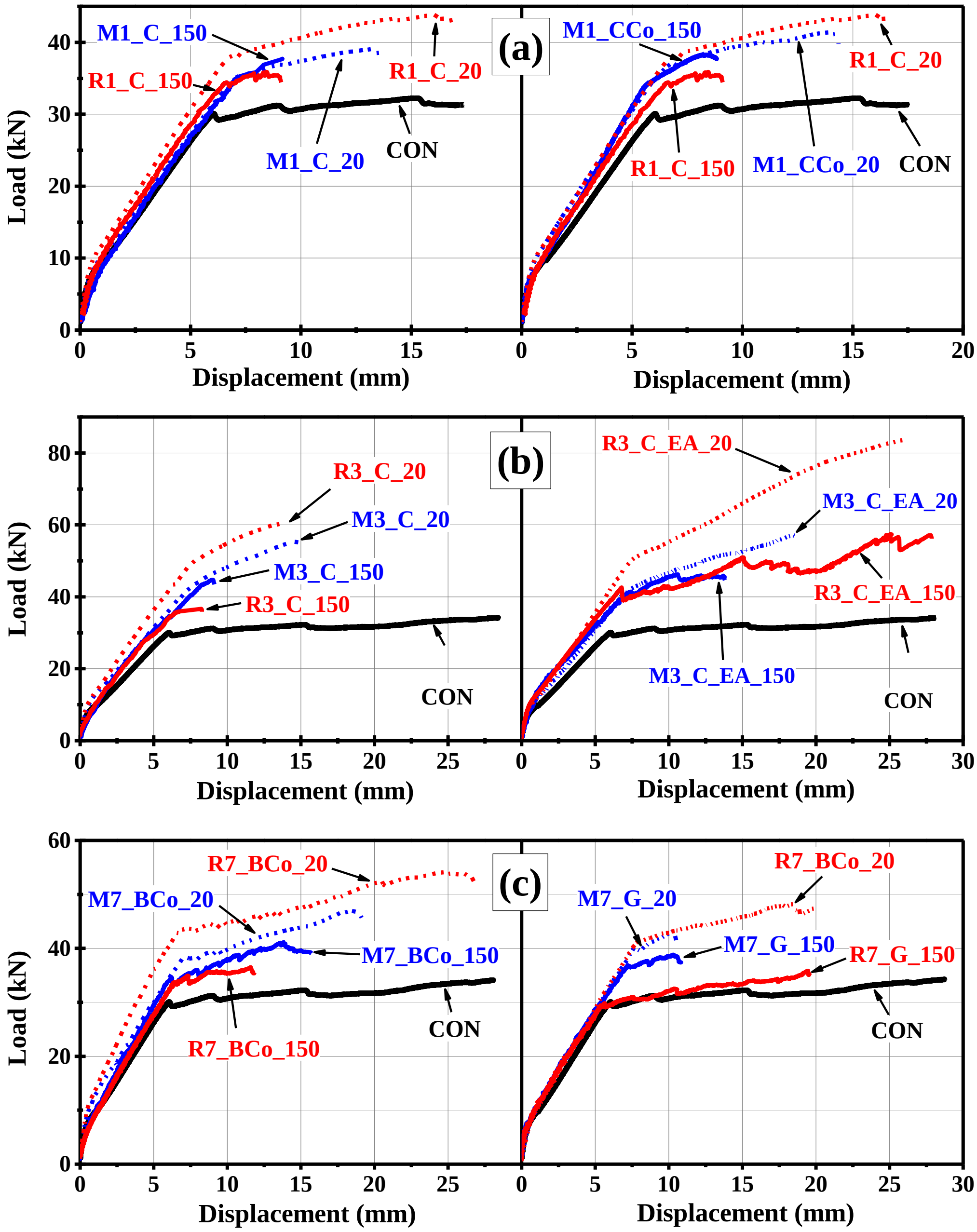

Figure 7.4. Load versus mid-span deflection curves of beams tested at ambient and high temperature and strengthened with: (a) one layer of carbon fibres textile, (b) three layers of carbon fibres textile without and with providing end-anchorage system, and (c) seven layers of basalt or glass fibres textile.

As shown in Figure 7.4a-c, the load- displacement curves are characterized by three distinct stages: (1) Stage I: un-cracked beam; (2) Stage II: initiation of cracking up to steel yielding; and (3) Stage III: post-yielding response up to failure. The observed gain in flexural strength is due to the contribution of TRM/FRP reinforcement, and is completely lost after the peak-load (when this reinforcement is lost), with the load capacity dropped to the un-retrofitted (CON) beam level (the post-peak behaviour of the load-displacement curves was removed for the sake of clarity).

7.2.2 Ultimate load and failure mode

The control specimen (CON) sustained a peak load of 34.6 kN (Table 7.2) and failed in flexure. After yielding of the longitudinal reinforcement, the concrete in the compression zone crushed (Figure 7.5a).

7.2.2.1 FRP strengthened beams

All FRP-strengthened beams tested at ambient temperature failed in flexure at an ultimate load substantially higher than that of the control beam. The peak load recorded for specimens R1_C_20, R3_C_20, R7_BCo_20, R7_G_20, and R3_C_EA_20 was 43.9, 60.4, 54.2, 48.2, and 83.7 kN, respectively, yielding 26.9, 74.6, 56.6, 39.3, and 141.9 % gain in load- carrying capacity, respectively (Table 7.2). Two different failure modes were observed, namely: debonding of FRP from the beam's soffit including part of the concrete cover (Figure 7.5b -specimens R1_C_20 and R3_C_20), and rupture of the fibres at the constant moment region of the beam (Figure 7.5d, f and h – specimens R7_BCo_20, R7_G_20, and R3_C_EA_20, respectively).

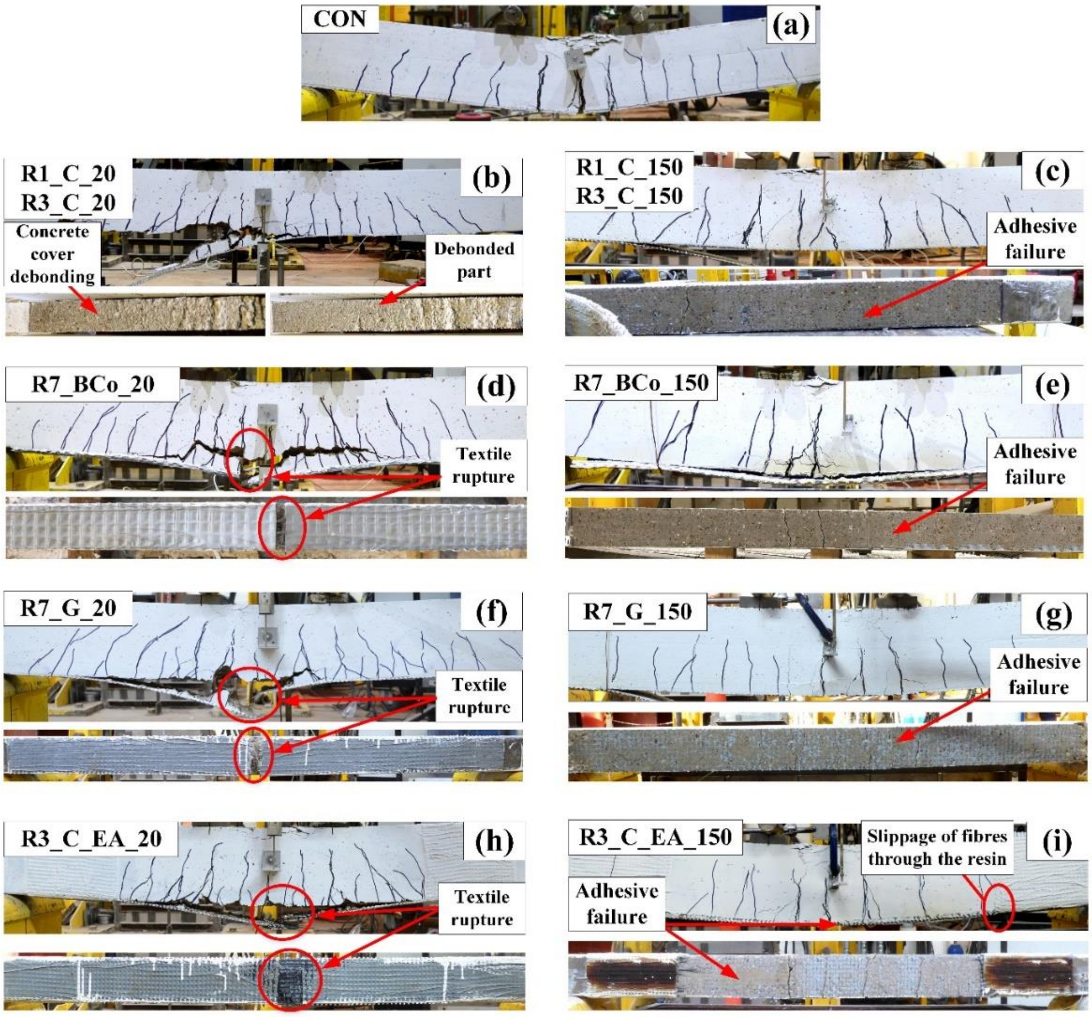

Figure 7.5. Failure modes observed in: (a) Un-retrofitted beam; and FRP strengthened beams with: (b and c) 1 and 3 layers of carbon; (d and e) 7 layers coated basalt, (f and g) 7 layers glass, and (h and i) 3 layers carbon provided with end-anchorage; tested at 20 ^{0}C and 150 ^{0}C, respectively.

All FRP-retrofitted beams tested at 150 ^{0}C failed also in flexure but at ultimate loads significantly lower (except from specimen R3_C_EA_150) than their counterpart specimens tested at 20 ^{0}C. The peak load attained by specimens R1_C_150, R3_C_150, R7_BCo_150, and R7_G_150 was 35.9, 36.7, 36.5, and 35.8 kN (Table 7.2), respectively, resulting in negligible increases in the flexural capacity equal to 3.8, 5.8, 5.5, and 3.5%, respectively. Thus, the effectiveness of FRP reinforcement in increasing the flexural capacity of the beams was decreased (in average) by 90% at 150 ^{0}C in comparison with ambient temperature. In all of these specimens, adhesive failure at the concrete-resin interface was observed (Figure 7.5c, e and g), namely the FRP composite detached from concrete substrate without including any parts of concrete cover. This is attributed to the poor bond behaviour of epoxy resin at temperatures above T_g. Finally, specimen R3_C_EA_150 having an anchorage system provided by U-shaped FRP strip at the ends of the beam attained an ultimate load of 57.5 kN, which yields 53.4% reduction in the effectiveness of the FRP reinforcement compared to its corresponding ambient temperature. Failure of this specimen initiated by adhesive debonding at the concrete-resin interface in the mid-span which propagated to the anchorage zones, and then followed by slippage and partial rupture of the rovings through the resin, which lost its strength at high temperature (Figure 7.5i).

7.2.2.2 TRM strengthened beams

Similar to the FRP strengthened beams, the TRM ones tested at ambient temperature, sustained considerably higher loads than the control beam. The ultimate load-carrying capacity of specimens M1_C_20, M1_CCo_20, M3_C_20, M7_BCo_20, M7_G_20 and M3_C_EA_20 was 39, 41.3, 55.3, 46.9, 43.2, and 57.1 kN, respectively, resulting an increase in the flexural capacity of 12.7, 19.4, 59.8, 35.5, 24.9, and 65.0% in comparison with the control beam. Five different failure modes were observed depending on the investigated parameters. In particular, failure of specimen M1_C_20 was attributed to partial rupture and slippage of the fibres within the mortar (Figure 7.6a), whereas specimen M1_CCo_20 failed due to debonding of TRM at the textile-mortar interface (interlaminar shearing) (Figure 7.6c). Failure of specimen M3_C_20 was identical to R3_C_20, namely due to TRM debonding including part of the concrete cover (Figure 7.6e). Failure due to rupture of textile glass and basalt fibres was respectively observed in both M7_BCo_20 and M7_G_20 specimens (Figure 7.6g and i). Finally, specimen M3_C_EA_20 failed due to TRM debonding from concrete substrate, followed by slippage of the fibres at the region where the longitudinal TRM meets the TRM U-jacket (Figure 7.6k).

The performance of the TRM-strengthened beams tested at 150 ^{0}C was far better compared to their FRP counterparts. In particular, specimens M1_C_150, M1_CCo_150, M3_C_150, M7_BCo_150, M7_G_150 and M3_C_EA_150, reached an ultimate load of 37.7, 38.3, 44.7, 41.1, 38.8, and 46.2 kN, respectively, resulting in 9, 10.7, 29.2, 18.8, 12.1, and 33.5% increase in the flexural capacity. Consequently, the effectiveness of the TRM at 150 ^{0}C was decreased in average by about 45% in comparison with its performance at 20 ^{0}C.

Specimen M1_C_150, failed identically to its counterpart tested at 20 ^{0}C due to partial rupture and slippage of the fibre rovings through the mortar (Figure 7.6b). Specimen M1_CCo_150 failed due to debonding of TRM at the textile-mortar interface (Figure 7.6d) similar to its counterpart specimen tested at ambient temperature. Specimen M3_C_150 failed also identically to its counterpart M3_C_20, namely TRM debonding from the concrete substrate involving parts of concrete cover (Figure 7.6f), indicating the good bond between the concrete substrate and the TRM reinforcement even at high temperature. Specimens M7_BCo_150 and M7_G_150 had different failure modes compared to their counterpart specimens tested at 20 ^{0}C, as they failed due to slippage of textile fibres (although some debonding was observed in specimen M7_G_150) through the mortar (Figure 7.6h and j). The alteration of failure mode is attributed to the reduction of the mortar strength at high temperature (see Table 7.1). Finally, the failure mode of specimen M3_C_EA_150 was also identical to its counterpart M3_C_EA_20 that is debonding of TRM from concrete substrate, followed by slippage of the fibres at the region where the longitudinal TRM meets the TRM U-jacket (Figure 7.6l).

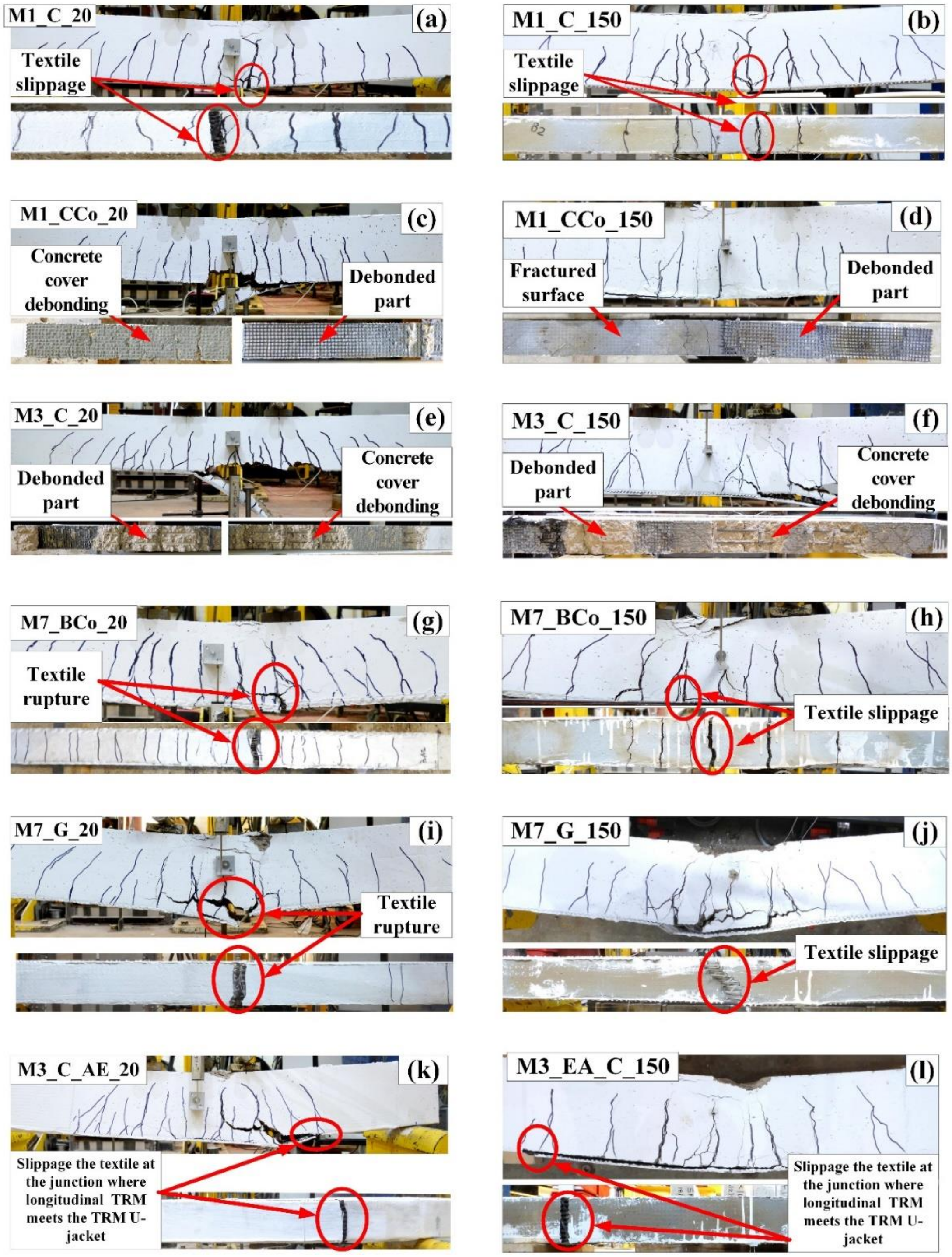

Figure 7.6. Failure modes of TRM strengthened beams with: (a and b) 1 layer dry carbon, (c and d) 1 layer coated carbon, (e and f) 3 layers of carbon, (g and h) 7 layers coated basalt, (I and j) 7 layers of glass, and (k and l) 3 layers carbon provided with end-anchorage; tested at 20 ^{0}C and 150 ^{0}C, respectively.

7.2.3 Bending stiffness

Table 7.3 reported the bending stiffness of the tested beams at high temperature in pre-cracking, cracking and post-yielding stages. As shown in this Table, the application of the FRP or TRM resulted in enhancing of both the cracking and post-yielding stiffness compared to the control beam. The average percentage increase in the cracking stiffness of both strengthening systems was approximately the same (17%). However, the percentage increase of the post-yielding stiffness of TRM strengthened beams was dramatically higher than that of the corresponding FRP-reinforced beams (see Table 7.3).

Table 7.3. Comparison of stiffness at pre-cracking, cracking and post-yielding stage

Specimens	Pre-cracking stiffness (kN/mm)	Cracking stiffness (kN/mm)	Post-yielding stiffness (kN/mm)
CON	9.2	4.0	0.19
TRM-retrofitted			
M1_C	9.7	4.4 (11)*	1.3 (558)*
M1_CO	13.3	5.0 (25)*	1.8 (833)*
M3_C	10.0	5.1 (27)*	3.6 (1780)*
M7_B	9.4	4.8 (20)*	0.9 (357)*
M7_G	11.3	4.5 (12)*	0.6 (240)*
M3_C_EA	12.2	4.6 (16)*	1.6 (723)*
FRP-retrofitted			
R1_C	11.9	4.4 (11)*	0.7 (250)*
R3_C	13.4	4.5 (12)*	0.7 (250)*
R7_B	10.0	4.7 (16)*	0.5 (188)*
R7_G	18.8	4.3 (7)*	0.4 (128)*
R3_C_EA	18.9	5.2 (30)*	0.8 (331)*

*Percentage increase in stiffness with respect to CON included in parentheses

7.3 Discussion

All specimens behaved as designed and failed in flexural, by failure of the EB TRM/FRP reinforcement after yielding of the internal steel reinforcement. In terms of the various parameters investigated in this experimental programme, an examination of the results in terms of flexural capacity, and failure modes, revealed the following information.

7.3.1 Matrix material (TRM versus FRP): performance at high temperature

FRP was more effective than TRM in increasing the flexural capacity of RC beams at ambient temperatures, however at high temperature TRM outperformed FRP (Figure 7.7a-c), maintaining on average of 55 % of its effectiveness at ambient temperature, whereas, FRP maintained only 10% (Figure 7.8). This reduction in effectiveness is clearly related to bigger deterioration in the epoxy resin mechanical properties at high temperatures in comparison with the mortar.

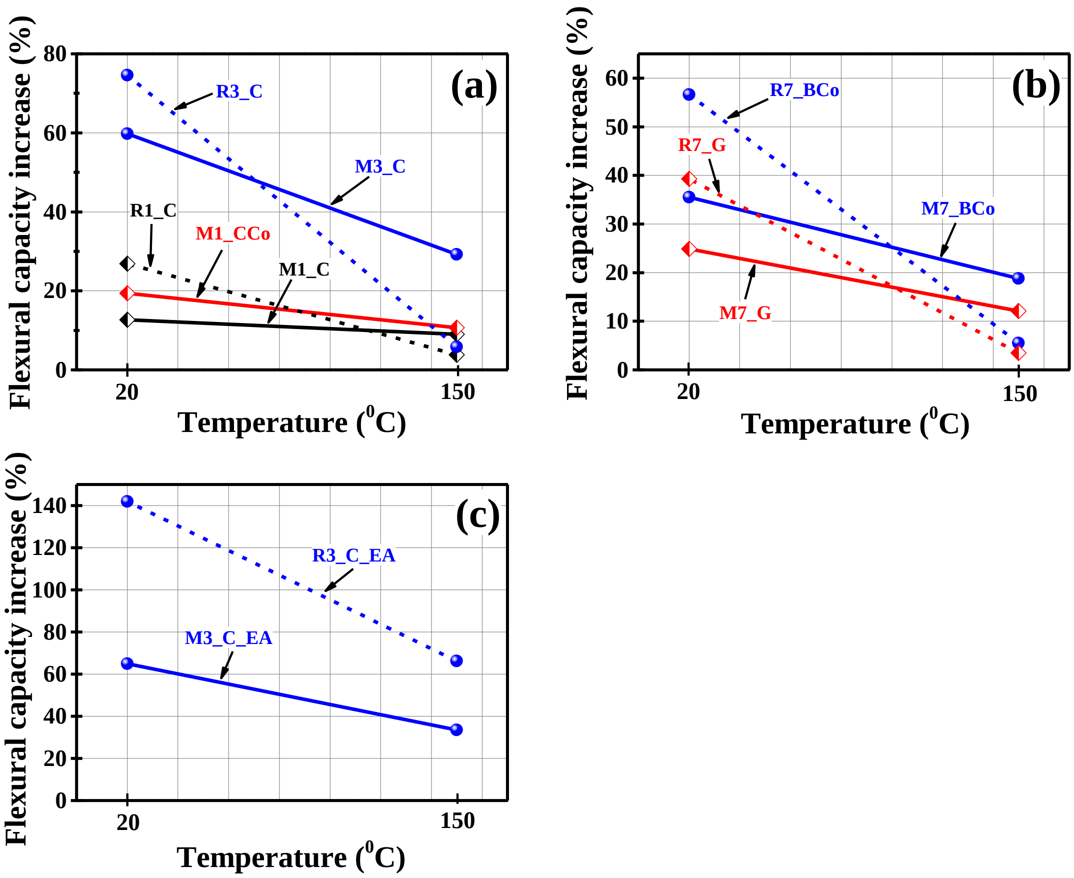

Figure 7.7. Effect of temperature on the flexural capacity enhancement for both TRM and FRP system.

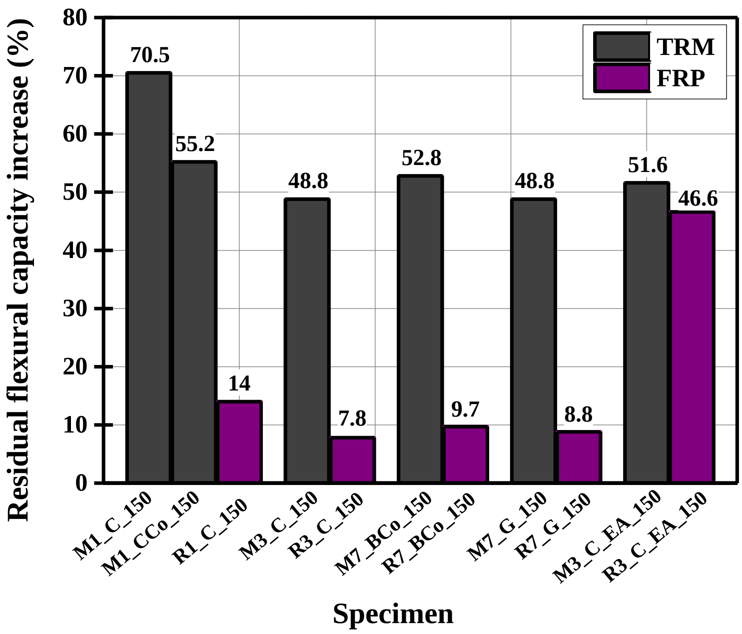

Figure 7.8. Comparison of residual flexural capacity increase of TRM versus FRP strengthened beams at 150 ^{0}C.

In the next sections a comparison between the effectiveness of FRP versus TRM materials at high temperatures in terms of the number of layers, the textile fibres materials, and the end-anchorage system is made. The effect of textile coating on the performance of TRM strengthened specimens in increasing the flexural capacity is also discussed.

7.3.2 Number of strengthening layers

The effect of the number of TRM layers on the beams flexural capacity enhancement at high temperature was investigated only for the case of dry carbon-fibre textiles, and is depicted in Figure 7.9. Increasing the number of layers from 1 to 3 layers, resulted in an almost proportional enhancement in the flexural capacity of 3.25 times. For FRP specimens the corresponding increase was nearly zero as can be seen in Figure 7.7a and Figure 7.9. When the number of TRM layers was increased from one to three, the failure mode altered from local fibre slippage to TRM debonding with concrete cover due to the better mechanical interlock, for both ambient and high temperatures, indicating that the failure mode was not affected from the increase of the temperature. For FRP strengthened specimens however, the increase in the number of layers did not affect the failure mode, which was adhesive failure at the concrete-resin interface (Figure 7.5c), attributed to the deterioration of the epoxy tensile strength above the T_g, as also reported in bond of FRP-to-concrete tests presented in Chapter 5.

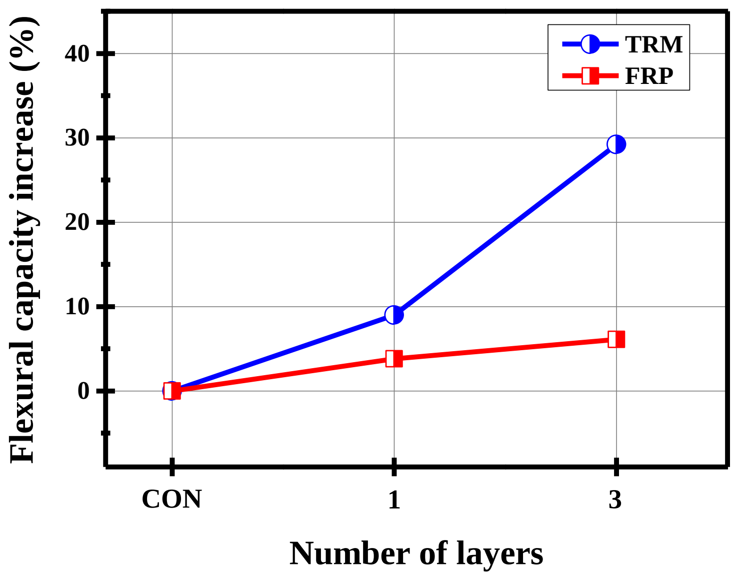

Figure 7.9. Effect of the number of layers on the ultimate flexural capacity at 150 ^{0}C.

7.3.3 Textile fibre coating

Coating was applied to the dry carbon-fibres textile to prevent the premature failure due to slippage of the fibre that was observed with dry carbon fibres textile. As a result of coating, the flexural capacity of specimen M1_CCo_150 was further increased by 19% compared to specimen M1_C_150. In fact, the effectiveness of the coated carbon textile was dropped compared to its effectiveness at ambient temperature (52%), most possibly due to the adverse effect of high temperature on the properties of the epoxy resin that used for coating.

The failure mode was altered from slippage to TRM debonding at the textile-mortar interface (Figure 7.6d) because coating the textile improved the bond between the inner and outer filaments, and hence, prevented slippage. Identical failure mode was also observed at ambient temperature (see Section 6.1.3.1), indicating that the failure mode was not affected by the increase of the temperature.

7.3.4 Textile fibre material

No clear conclusions on the influence of the textile fibre material can be made at high temperatures. The behaviour of the FRP strengthened beams was controlled by the adhesive failure at the concrete-resin interface as described in section 7.3.1. Whereas the flexural capacity increases for TRM strengthened specimens that received reinforcement with the same axial stiffness (M7_BCo versus M1_CCo_150 and M7_G_150 versus M1_C_150), are mainly attributed to the effect of the increased number of layers (see discussion 7.3.2), rather the material properties themselves.

7.3.5 End-anchorage with U-jackets

Providing end-anchorage enhanced significantly the effectiveness of FRP at high temperature (11.4 times compared to the non-anchorage beam). The corresponding enhancement for the TRM-strengthened beams was ten time less (only 1.14) due to the observed failure modes observed (sections 7.2.2.1 and 7.2.2.2, respectively).

7.3.6 TRM versus FRP effectiveness factor

Table 7.4 reports the values of TRM versus FRP effectiveness factor (α_{hT}) at high temperature, which is defined as the ratio of the TRM to FRP in terms of flexural capacity enhancement. This factor was varying between 0.5 and 5.1 depending on the investigated parameter. Increasing the number of layers from one to three (for dry carbon fibres textile), resulted in an increase of the α_{hT} factor from 2.4 to 5.1 (2.12 times) due to the change in failure mode, as discussed in Section 4.2. On the other hand, coating the dry carbon textile in the case of one TRM layer increased the α_{hT} factor from 2.4 to 2.8 due to prevention of slippage of the fibres. The effectiveness factor α_{hT} for both specimens retrofitted with 7 basalt or glass TRM (M7_BCo_150 and M7_G_150) was approximately the same (about 3.4) due to their identical failure mode (slippage of fibres through the mortar). Finally, the low value of 0.5 for specimen M3_C_EA_150 that received end-anchorage, is related to the observed failure mode (see section 3.2.2).

7.4 Effective Stress Reduction Factor for FRP and TRM

The effective stress is defined here as the tensile stress of the composite material in the region of maximum moment at the instant of ultimate load. For all tested beams, the effective stress of the FRP or TRM reinforcement for both ambient (σ_{eff}) and high ($\sigma_{eff, high}$) temperature was calculated following the same procedure described in section 6.1.4 and using the experimental values of the flexural moment of resistance, $M_{u,exp}$ (Table 7.4) and the mechanical properties of the TRM and FRP reinforcement (E_f and f_{fu}) reported in Table 3.2 and Table 3.3, respectively.

The effective stress of FRP or TRM jackets at high temperature, $\sigma_{eff, high}$, is a reduced value of their effective stress, σ_{eff}, at ambient temperature. It is expressed by the following equation:

$$\sigma_{eff,high} = k\ \sigma_{eff} \quad (7.1)$$

The values of the effective stress of TRM and FRP jackets at both ambient and high temperature, σ_{eff} and $\sigma_{eff, high}$, respectively are given in Table 7.4. The calculated stress reduction factor, k varies with the strengthening material (TRM, FRP) and investigated parameter (see Table 7.4). For the FRP strengthened beams, the average values of k was quite low and equal to 0.29, whereas, the corresponding values of k for TRM strengthened beams was far higher and equal to 0.7.

Table 7.4. Effectiveness factor, experimental values of ultimate moment capacity and effective stress in TRM/FRP reinforcement.

Specimen	**TRM versus FRP effectiveness factor, α_{hT}**	**f_{fu} (MPa)**	**$M_{u,exp.}$* kN.m**	***A.T.* σ_{eff}** (MPa)**	***H.T.* $\sigma_{eff,high}$*** (MPa)**	**k^{a}**
CON	-		10.03	-		
TRM-retrofitted						
M1_C_150	2.4	1518	10.93	1368	1301	0.95
M1_CCo_150	2.8	2843	11.11	1825	1404	0.77
M3_C_150	5.1	1518	12.96	1434	834	0.58
M7_BCo_150	3.4	1190	11.92	1019	637	0.63
M7_G_150	3.5	794	11.25	658	411	0.62
M3_C_EA_150	0.5	1518	13.40	1501	934	0.62
FRP-retrofitted						
R1_C_150	n.a.	2936	10.41	2190	576	0.26
R3_C_150	n.a.	2936	10.61	1796	338	0.19
R7_BCo_150	n.a.	1501	10.59	1493	298	0.20
R7_G_150	n.a.	1019	10.38	914	257	0.28
R3_C_EA_150	n.a.	2936	16.68	3110	1577	0.51

* Ultimate moment capacity obtained experimentally.
** Effective stress in TRM/FRP reinforcement calculated based on experimental results at ambient temperature presented in Table 6.5.
*** Effective stress in TRM/FRP reinforcement calculated based on experimental results at high temperature.
a The ratio of effective stress at high temperature ($\sigma_{eff,high}$) to the effective stress at ambient temperature (σ_{eff}).

As reported in Section 6.1.4, Eq. 6.11 which suggested by *Fib Model Code (2010)* can satisfactory predicted the stress of the TRM composite, ($f_{fbm,theor}$), (without safety factors) for those specimens failed due to debonding.

Figure 7.10 shows the relationship between the effective stress at high temperature $\sigma_{eff,\text{high}}$ and the product $\rho_f E_f$; together with the curve corresponding to Eq. 6.11. Where ρ_f is the textile fibres reinforcement ratio ($\rho_f = A_f / bh$), and E_f is the modulus of elasticity of the composite material obtained from coupon tests. It is clear from this Figure that Eq. 6.11 significantly overestimated the effective stress in FRP reinforcement due to the premature adhesive failure. Nevertheless, this was not the case in the TRM reinforcement where it seems that Eq. 6.11 can be used by providing a suitable reduction factor.

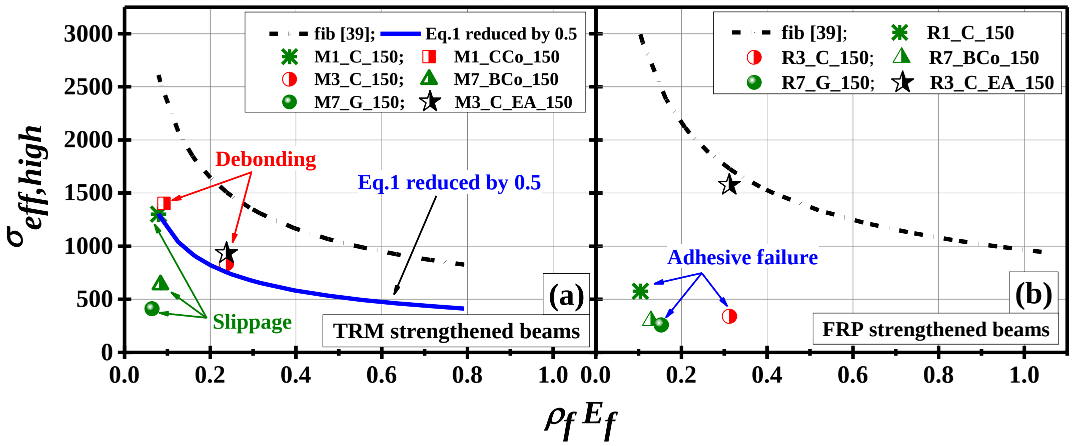

Figure 7.10. Experimentally obtained effective stress versus ρ_f E_f and comparison with the theoretical formula suggested by fib model code (2010) and its modification for 150 ^{0}C for: (a) TRM and (b) FRP strengthened beams.

Hence, for design purposes, FRP is not recommended for flexural strengthening of RC beams when fire or high temperature is a critical issue, unless proper protective (thermal insulation) systems are provided. For TRM strengthened beams on the other hand, and based on the limited experimental results presented in this study in the flexural design of beams strengthened with TRM and exposed to high temperature (up to e 150 ^{0}C), the effective stress for those specimens failed due to debonding can be the minimum value obtained from coupon tests (f_{fu}) and Eq. 6.11, after applying a reduction factor k equal to 0.5. It is worth mentioning that a reduction factor of 0.4 was proposed by Tetta and Bournas (2016) for shear design of beams strengthened with TRM jacketing and exposed to high temperature up to 250 ^{0}C.

7.5 Summary

This chapter compares for the first time the effectiveness of TRM versus FRP in increasing the flexural capacity of RC beams subjected to high temperature. Parameters examined were: the strengthening system (TRM versus FRP), the number of layers, the textile surface condition, the textile fibres materials and (e) the end anchorage system. The results of high temperature tests revealed the following information:

- TRM showed far better effectiveness than FRP in increasing the flexural capacity of RC beams subjected to high temperature. TRM sustained an average of 55% of its ambient temperature effectiveness, contrary to FRP which totally lost its effectiveness.
- Increasing the number of TRM layers (from 1 to 3) enhanced the flexural capacity and altered the failure mode. Whereas, the corresponding effect of the number of FRP layers was negligible due to the premature adhesive failure.
- Coating the dry carbon fibres with epoxy adhesive improved the TRM effectiveness in increasing the flexural capacity (approximately 20% compared to the dry one).
- The effect of textile materials (having approximate same axial stiffness) in the FRP-strengthened beams disappeared due to their identical adhesive failure at the concrete-resin interface.
- Providing end-anchorage to the FRP-retrofitted beam significantly enhanced the flexural capacity increase (compared to the non- anchorage beam). This enhancement was limited in the corresponding TRM-reinforced beam due to the witnessed failure mode.
- Different types of failure modes were observed in the TRM-retrofitted beams including: slippage of the fibres, interlaminar shear and debonding of TRM

including parts of concrete cover. On the other hand, the only observed failure mode in the FRP strengthened specimens (except from specimen R3_C_EA_150) was adhesive failure.

- The *fib model code (2010)* formula, which predicted the experimental TRM debonding effective stress with good accuracy, can be also used in the flexural design of beams strengthened with TRM and exposed to high temperature (up to 150 ^{0}C), after halving the ambient temperature effective stress.

Chapter 8

CONCLUSIONS AND RECOMMENDATIONS FOR FUTURE RESEARCH

8.1 Introduction

There is a growing need for strengthening of existing structures due to their deterioration as a result of aging, degradation induced environmental conditions, inadequate maintenance, and the need to meet the requirements of the current design codes. Recently, a new composite cement-based material, namely textile-reinforced mortar (TRM) has been introduced as an external strengthening. TRM is an attractive retrofitting solution because it combines the outstanding properties of composite materials (e.g. high-strength, light weight, corrosion resistance) with the favourable characteristics offered by mortars and cannot be found in resins (e.g. fire resistance, low cost, and low temperatures, air permeability of the substrate.

It is well known that the effectiveness of any externally bonded strengthening system in increasing the load-carrying capacity of concrete members substantially depends on the bond between that strengthening material and the member's substrate. Due to granularity of cement mortars, the impregnation of a single roving is difficult to achieve, hence, the bond between TRM and concrete has become an issue.

This PhD Thesis provides extensive experimental study on the bond between textile reinforced and concrete substrate and, also evaluates the effectiveness of TRM in flexural strengthening of RC beams. Firstly, the tensile properties of the bare textiles reinforcement and TRM coupons were experimentally determined. Secondly, the bond behaviour between TRM and concrete substrate at ambient and for the first time at high temperature was extensively studied by conducting 148 double-lap shear tests (80 at ambient and 68 at high temperature). The key investigated parameters at ambient temperature were: (a) the bond length (50-450 mm); (b) the number of layers (1 to 4 which is beyond the current limit of two); (c) the concrete surface preparation (grinding versus sandblasting); (d) the concrete compressive strength (15 and 30 MPa); (e) the textile surface condition (dry versus coated); and (f) the anchorage through wrapping with TRM jackets. Whereas, the corresponding parameters examined at high temperature included; (a) the strengthening systems (TRM versus FRP), (b) the temperature at which the specimens were exposed; (c) the number of FRP/TRM layers; and (d) the loading conditions. Furthermore, the effectiveness of TRM in flexural strengthening of RC beams at ambient and for the first time at high temperature was also investigated on 32 half-scale beams. The examined parameters comprised: (a) the strengthening system (TRM versus FRP); (b) the number of layers; (c) the textile surface condition; (d) the textile fibre material; (e) the end-anchorage system of the external reinforcement; and (f) the textile geometry (only at ambient temperature). Finally, a simple formula used for predicting the mean FRP debonding stress was modified for predicting the TRM reinforcement effective stress based on the experiment data available.

8.2 Conclusions

In general, according to the results presented in this Thesis, TRM reinforcement can be considered as a promising strengthening system for retrofitting concrete structures. In the next sections, the conclusions obtained from the experimental work (grouped according to the chapters of this Thesis) are drawn:

8.2.1 Tensile characterisation of textile reinforcement

This part of the Thesis describes the experimental work carried out to determine the tensile properties (the ultimate tensile stress, the ultimate tensile strain and the modulus of elasticity) of: (a) bare textile reinforcement, (b) TRM coupons made of one and two layers and, (c) FRP coupons made of one layer. The main findings of this part are summarised below:

- The tensile properties of the textile reinforcement obtained from testing a bare textile were approximately identical to that measured from TRM composite. Hence, for design purposes, it is suggested that both tests can be used to determine the tensile properties of TRM as a composite material.
- Increase the number of TRM layers from one to two decreased the ultimate tensile strength by 4%, and increased the ultimate tensile strain by 4%. Thus, the tensile properties of TRM composite obtained from testing one TRM layer can be used for design purposes.
  - The influence of textile materials (carbon or glass) and distance between rovings (10, 20 or 40 mm) in the transversal direction (of textiles having the same amount of carbon fibre in the loading direction) on the tensile properties was very limited. This could potentially lead to cost reduction of the textile reinforcement, especially if low-cost fibres are used in the transversal direction.
- The type of binding materials (cement mortar or epoxy resin) significantly affects the tensile properties of the resulted composite materials. FRP composite showed considerably higher tensile properties than that of the corresponding equivalent TRM composite made of the same textile fibres materials.

8.2.2 Bond between TRM and concrete: double-lap shear test at ambient temperature

The main findings of the experimental study conducted to investigate the bond between TRM and concrete substrates are summarized below:

- By increasing either the bond length or the number of layers, the failure load increases in a non-proportional way. However, beyond a certain bond length, the increase in the ultimate load was not significant. This bond length so-called effective bond length which was ranging from 200 mm to 300 mm for number of layers up to four and for the textile fibres materials used in this study.
- For the same bond length, increasing the number of TRM layers resulted in non-proportional increase in the ultimate load. The increase was more pronounced when shifting from one to two layers, whereas for three and four layers it was gradually becoming less significant.
- The number of layers has a significant effect on the failure mode; for one and two TRM layers the failure was slippage of the fibres through the mortar, whereas, for three and four TRM layers the failure was debonding of TRM at the concrete-mortar interface including a thin layer of concrete cover. The type of failure mode is consistent with the typical failure mode observed in FRP-to-concrete bonded strip.
- The influence of concrete surface preparation methods (grinding and formation of a grid of grooves versus sandblasting) was very limited on the bond characteristics in terms of ultimate load and failure mode, suggesting that both methods are suitable.
- The effect of concrete compressive strength on the ultimate load was not significant; a 50% reduction in compressive strength of the concrete resulted in 7.5% average decrease in the ultimate bond, and with the same failure mode.

- Coating the textile with an epoxy adhesive has a twofold effect: (a) change in the failure mode from slippage through the mortar to TRM debonding at textile-mortar interface, and (b) the ultimate load by 75% and 15% (comapred to their counterpart speicmens strengthened wiht dry textile) for specimens retrofitted with one and two layers, respectively.
- The anchorage of TRM strips through wrapping with TRM jackets results in a substantial increase of the bond strength (up to 28% and 45% for 3 and 4 TRM layers, respectively), by preventing the premature debonding from the concrete substrate.

According to the above findings, and to improve the bond condition between TRM and concrete in real applications of TRM, the following recommendations can be considered: (a) preventing the premature slippage of the fibres through the mortar; this can be achieved by providing more than two TRM layers, (b) using coated textiles when it is possible, and (c) anchoring TRM strips through wrapping with TRM jackets wherever it is applicable.

8.2.3 Bond between TRM and concrete: double-lap shear test at high temperatures

The main conclusions of the experimental programme performed to examine the bond performance between TRM and concrete interfaces at high temperatures are summarized below:

- The bond performance of TRM strengthening system with concrete remains excellent at high temperatures, contrary to FRP.
- In steady state tests, the bond strength at the FRP-concrete interface was significantly deteriorated with the increase of the temperature, however, this was

not the case for TRM-retrofitted specimens. The average reduction in the bond strength of FRP-specimens was about 83% when the temperature reached 150 ^{0}C, whereas the corresponding values of bond strength in TRM-concrete interface was about 15% when the temperature attained 400 ^{0}C.

- Two types of failure modes were observed in the FRP specimens tested in steady state condition. At ambient and moderate temperature (50 ^{0}C) cohesive failure was observed; in which parts of concrete cover being removed from concrete substrate, whereas, at elevated temperatures (i.e. 75, 100, and 150 ^{0}C), adhesive failure at the concrete-resin interface was occurred. On the other hand, the only observed failure mode of the TRM specimens subjected to high temperatures up to 500 ^{0}C, was debonding of TRM with parts of concrete cover being peeled off.
- The effect of loading condition on the bond strength of FRP specimens was not significant. The bond strength of the FRP specimens as a function of temperature was nearly identical regardless the loading condition (steady state or transient condition). On the other hand, the bond strength of the corresponding TRM specimens was sensitive to the loading condition. In specific, TRM specimens tested at steady state condition showed higher bond strength compared to the corresponding specimen tested in the transient condition.

Overall, TRM shows a

8.2.4 Flexural strengthening of RC beams with TRM

8.2.4.1 TRM versus FRP in flexural strengthening of RC beams

The main findings of this part of PhD Thesis are summarized as below:

- Generally, TRM system was less effective than FRP in increasing the loading carrying capacity of retrofitted beams. Nevertheless, TRM effectiveness was sensitive to the number of strengthening layers; by increasing the number of layers from 1 to 3, the effectiveness factor (*k*) increased from 0.47 to 0.80.

- Coating the dry carbon fibres textile with epoxy adhesive significantly enhanced the performance of TRM materials. Providing one layer of coated carbon textile instead of dry one resulted in substantial gain in the flexural capacity increased (about 55% enhancement).
- Different textile fibres materials (carbon, coated basalt, and glass) having approximately the same axial stiffness resulted in different flexural capacity increases. In both strengthening systems, seven layers of coated basalt-fibre textile layers measured the highest flexural capacity enhancement, followed by seven layers of dry glass-fibre textile, and finally by one carbon-fibre textile layer. This variance in the performance was related to the effect of number of layers but also to the textile surface condition (dry or coated textiles) in TRM strengthening system.
- Providing end-anchorage system using U-shaped jackets to FRP-retrofitted beams resulted in 90% enhancement in the flexural capacity compared to non-anchorage beam. However, the corresponding enhancement in TRM-retrofitted beam was not significant recording only 9% due to the observed failure mode.
- Two types of failure mode were observed in the FRP-retrofitted beams, namely; debonding including parts of concrete cover for specimens M1_C and M3_C, and fibres rupture for specimens M7_BCo, M7_G and M3_C_EA. In the TRM-retrofitted beams, five different failure modes were noted including: slippage of the fibres (specimen M1_C), debonding at the textile-matrix interface (specimen M1_CCo), debonding with peeling off parts concrete cover (specimen M3_C and M5_C), and rupture of the textile fibres (M7_BCo and M7_G) and debonding of

TRM from the concrete substrate followed by slippage of the fibres at a different region (specimen M3_C_EA). These failure modes were sensitive to the number of TRM layers, the fibres materials (carbon, coated basalt or glass fibres), and the textile surface condition (dry or coated fibres).

- The failure mode observed in the TRM strengthened beams tested in flexural was identical to that failure of TRM strengthened specimens tested under double-lap shear, for the same number of TRM layers and the same textile fibre materials.
- For both strengthening systems (TRM and FRP), the cracking and post-yielding stiffness of strengthened beams was enhanced compared to the unstrengthened beam (up to 72% and 1298%, respectively).
- A formula proposed by *fib model code (2010)* was used to predict the debonding stress in FRP reinforced for those specimens failed due to debonding of FRP from concrete substrate. This formula was also used to predict the debonding stress of TRM reinforcement for those specimens that have same failure mode (i.e. debonding). It was found that this formula is in a good agreement with the effective stress calculated based on the experimental results providing that TRM properties are obtained from coupon tests.

Based on the above conclusions, it is obvious that the number of TRM layers plays important roles in enhancing the TRM effectiveness in increasing the flexural capacity of RC beams. Hence, in real applications of TRM, it is suggested to use more than two TRM layers in order to prevent the premature failure due to slippage of the fibres and consequently enhancing the TRM effectiveness.

8.2.4.2 Influence of textile geometry on the performance of TRM in flexural strengthening of RC beams

This section studied the effect of the textile geometry on the flexural performance of RC beams strengthened with TRM. The main conclusions of this part are summarized below:

- Increasing the number of TRM layers from 1 to 3 resulted in improving the flexural capacity, and altering the failure mode from slippage of the fibres (for 1 layer strengthened beam) to a total or partial debonding of TRM from concrete substrate (for 3 layers retrofitted beams).
- Doubling the area of a single carbon fibres roving in the loading direction reduced slightly the textile effectiveness in enhancing the flexural capacity.
- The materials and spacing between the rovings in the transversal direction had no effect on the textile effectiveness in enhancing the flexural capacity. This conclusion leads to a considerable reduction of the overall cost of the textile reinforcement achieved by saving the materials in the transversal direction of the textile reinforcement.

According to the above findings, and to produce an effective textile reinforcement in terms of cost and flexural performance, the following suggestions are made: (a) smaller area and spacing between rovings in the direction of loading could enhance the flexural performance of the textile reinforcement. This is due to creating a denser mesh pattern that improves the bond condition between the rovings and the mortar; and (b) low-cost fibre materials can be used in the transversal direction with a spacing between rovings as large as possible but ensure the stability of the overall textile geometry.

8.2.5 TRM versus FRP in flexural strengthening of RC beams: behaviour at high temperature

The main findings of the experimental work carried out on RC beams strengthened with TRM and FRP composites subjected to high temperatures are summarized below:

- TRM showed far better effectiveness than FRP in increasing the flexural capacity of RC beams subjected to high temperature. TRM maintained an average of 55% of its ambient temperature effectiveness, contrary to FRP which totally lost its effectiveness.
- Increasing the number of TRM layers (from 1 to 3) enhanced the flexural capacity and altered the failure mode. Whereas, the corresponding effect of the number of FRP layers was negligible due to the premature adhesive failure.
- Coating the dry carbon fibres with epoxy adhesive improved the TRM effectiveness in increasing the flexural capacity (approximately 20% compared to the dry one).
- The effect of textile materials (having approximate same axial stiffness) in the FRP-strengthened beams disappeared due to their identical adhesive failure at the resin-reinforcement interface.
- Providing end-anchorage to the FRP-retrofitted beam significantly enhanced the flexural capacity increase (compared to the non- anchorage beam). This enhancement was limited in the corresponding TRM-reinforced beam due to the witnessed failure mode.
- Different types of failure modes were observed in the TRM-retrofitted beams including: slippage of the fibres, interlaminar shear and debonding of TRM including parts of concrete cover. On the other hand, the only observed failure mode in the FRP strengthened specimens (except from specimen R3_C_EA_150) was adhesive failure.

- The *fib model code (2010)* formula, which predicted the experimental TRM debonding effective stress with good accuracy, can be also used in the flexural design of beams strengthened with TRM and exposed to high temperature (up to e 150 ^{0}C), after halving the ambient temperature effective stress.

8.3 Recommendations for Future Research

TRM is a promising alternative strengthening materials to FRP, even with experimental evidence presented in this PhD Thesis, further experimental studies are required in order to consolidate the obtained results. In this context, further research could be directed towards the following fields:

1. Investigating the bond of TRM made of different types of textiles and concrete, and deriving analytical expressions for calculating the effective bond length and the effective stress in the TRM composites.
2. Durability issues are important, and research on the durability of TRM is scarce; therefore, it is important to assess the bond performance between TRM and concrete substrate at to extreme environmental conditions such as cycles of freezing and thawing.
3. To generalize the results obtained from the flexural tests, further experimental studies are required on full-scale beams in order to confirm the reliability of existing design models for FRP and/or to develop new reliable ones.
4. Further research could be directed towards examining the fatigue behaviour of RC beams strengthened with TRM and subjected to cyclic loading.
5. More studies are required on the flexural behaviour RC beams strengthened with TRM and subjected to high temperature (above 150 ^{0}C), to transient load histories

and to real fires. Testing full-scale beams is also needed for increasing the level of confidence of the obtained results.

6. Finally, developing a fire-resistant cement mortars (such as using a refractory cement) is important as the cement mortar plays a crucial role in increasing the effectiveness of TRM as an external strengthening.

REFERENCES

ACI Commitee. Guide for the Design and Construction of Externally Bonded FRP Systems for Strengthening Concrete Structures *(*440.2 R-08); 2008.

ACI Committee 440. Guide Test Methods for Fiber-Reinforced Polymers (FRPs) for Reinforcing or Strengthening Concrete Structures (ACI 440.3R-04). American Concrete Institute, Farmington Hills, USA, 2004, P40.

Aljewifi, H., Fiorio, B. & Gallias, J.-L. Pull-out behaviour of a glass multi-filaments yarn embedded in a cementitious matrix. EURO-C 2010–Computational Modelling of Concrete Structures, 2010.

Awani, O., El Refai, A. & El-Maaddawy, T. 2015. Bond characteristics of carbon fabric-reinforced cementitious matrix in double shear tests. *Construction and Building Materials*, 101**,** 39-49.

Babaeidarabad, S., Caso, F. D. & Nanni, A. 2013. Out-of-plane behavior of URM walls strengthened with fabric-reinforced cementitious matrix composite. *Journal of Composites for Construction*, 18**,** 1-11.

Babaeidarabad, S., Loreto, G. & Nanni, A. 2014. Flexural strengthening of RC beams with an externally bonded fabric-reinforced cementitious matrix. *Journal of Composites for Construction*, 18**,** 04014009.

Banholzer, B. 2004. *Bond behaviour of a multi-filament yarn embedded in a cementitious matrix.* Bibliothek der RWTH Aachen.

Banholzer, B., Brockmann, T. & Brameshuber, W. 2006. Material and bonding characteristics for dimensioning and modelling of textile reinforced concrete (TRC) elements. *Materials and structures,* 39**,** 749-763.

Bentur, A., Peled, A. & Yankelevsky, D. 1997. Enhanced Bonding of Low Modulus Polymer Fibers-Cement Matrix by Means of Crimped Geometry. *Cement and Concrete Research,* 27**,** 1099-1111.

Bisby, L., Stratford, T., Hart, C. & Farren, S. 2013. Fire Performance of Well-Anchored TRM, FRCM, and FRP Flexural Strengthening Systems. *Advanced Composites in Construction*.

Bournas, D. & Triantafillou, T. 2010. Bar buckling in RC columns confined with composite materials. *Journal of Composites for Construction,* 15 (3)**,** 393-403.

Bournas, D. & Triantafillou, T. 2011. Bond strength of lap-spliced bars in concrete confined with composite jackets. *Journal of Composites for Construction,* 15 (2)**,** 156-167.

Bournas, D. 2016. *Strengthening of existing structures: Selected case studies. In: Triantafillou TC, editor,* Textile fibre composites in civil engineering (Ch. 17), Elsevier, Woodhead Publishing Limited.

Bournas, D. A. & Triantafillou, T. C. 2013. Biaxial bending of reinforced concrete columns strengthened with externally applied reinforcement in combination with confinement. *ACI Structural Journal,* 110 (2)**,** 193-203.

Bournas, D. A., Lontou, P. V., Papanicolaou, C. G. & Triantafillou, T. C. 2007. Textile-reinforced mortar versus fiber-reinforced polymer confinement in reinforced concrete columns. *ACI Structural Journal,* 104 (6)**,** 740-748.

Bournas, D. A., Triantafillou, T. C., Zygouris, K. & Stavropoulos, F. 2009. Textile-reinforced mortar versus FRP jacketing in seismic retrofitting of RC columns with continuous or lap-spliced deformed bars. *Journal of Composites for Construction,* 13**,** 360-371.

Brameshuber, W. 2006a. *Report 36: Textile Reinforced Concrete-State-of-the-Art Report of RILEM TC 201-TRC*, RILEM publications.

Brameshuber, W. 2006b. State-of-the-art report of RILEM technical committee 201 TRC: textile reinforced concrete (RILEM Report 36). *Bagneux: RILEM Publications SARL*.

BS EN 1015-11: Methods of Test for Mortar for Masonry–Part 11. Determination of flexural and compressive strength of hardened mortar. London: British Standard Institution; 1999.

BS EN 12390-3: Testing hardened concrete–Part 3: Compressive strength of test specimens. London: British Standard Institution; 2009.

BS EN 12390-6: Testing hardened concrete- Tensile splitting strength of test specimens. London: British Standard Institution; 2009.

BS EN 1992-1-1. Eurocode 2: Design of Concrete Structures: Part 1-1: General Rules and Rules for Buildings, British Standards Institution: 2004.

Carloni, C., Bournas, D. A., Carozzi, F. G., D'antino, T., Fava, G., Focacci, F., Giacomin, G., Mantegazza, G., Pellegrino, C. & Perinelli, C. 2016. Fiber reinforced composites with cementitious (inorganic) matrix. *Design Procedures for the Use of Composites in Strengthening of Reinforced Concrete Structures.* Springer.

Chowdhury, E. U., Bisby, L. A., Green, M. F. & Kodur, V. K. 2007. Investigation of insulated FRP-wrapped reinforced concrete columns in fire. *Fire Safety Journal,* 42**,** 452-460.

Colombo, I., Colombo, M., Magri, A., Zani, G. & Di Prisco, M. 2011. Textile Reinforced Mortar at High Temperatures. *Applied Mechanics and Materials,* 82**,** 202-207.

D'ambrisi, A. & Focacci, F. 2011. Flexural strengthening of RC beams with cement-based composites. *Journal of Composites for Construction,* 15**,** 707-720.

D'ambrisi, A., Feo, L. & Focacci, F. 2012. Bond-slip relations for PBO-FRCM materials externally bonded to concrete. *Composites Part B: Engineering,* 43**,** 2938-2949.

D'ambrisi, A., Feo, L. & Focacci, F. 2013. Experimental analysis on bond between PBO-FRCM strengthening materials and concrete. *Composites Part B: Engineering,* 44**,** 524-532.

D'antino, T., Carloni, C., Sneed, L. & Pellegrino, C. 2014. Matrix–fiber bond behavior in PBO FRCM composites: A fracture mechanics approach. *Engineering Fracture Mechanics,* 117**,** 94-111.

D'antino, T., Sneed, L. H., Carloni, C. & Pellegrino, C. 2015. Influence of the substrate characteristics on the bond behavior of PBO FRCM-concrete joints. *Construction and Building Materials,* 101**,** 838-850.

D'antino, T., Pellegrino, C., Carloni, C., Sneed, L. H. & Giacomin, G. Experimental analysis of the bond behavior of glass, carbon, and steel FRCM composites. Key Engineering Materials, 2014. Trans Tech Publ, 371-378.

D'antino, T., Pellegrino, C., Carloni, C., Sneed, L. H. & Giacomin, G. Experimental analysis of the bond behavior of glass, carbon, and steel FRCM composites. Key Engineering Materials, 2015. Trans Tech Publ, 371-378.

De Andrade Silva, F., Butler, M., Hempel, S., Toledo Filho, R. D. & Mechtcherine, V. 2014. Effects of elevated temperatures on the interface properties of carbon textile-reinforced concrete. *Cement and Concrete Composites,* 48**,** 26-34.

Ebead, U., Shrestha, K. C., Afzal, M. S., El Refai, A. & Nanni, A. 2016. Effectiveness of fabric-reinforced cementitious matrix in strengthening reinforced concrete beams. *Journal of Composites for Construction***,** 1-14.

Elsanadedy, H. M., Almusallam, T. H., Alsayed, S. H. & Al-Salloum, Y. A. 2013. Flexural strengthening of RC beams using textile reinforced mortar–Experimental and numerical study. *Composite Structures,* 97**,** 40-55.

Fib Model Code (2010). Model code for concrete structures. Bulletin 14, Lausanne; Switzerland.

Firmo, J. P., Correia, J. R. & Bisby, L. A. 2015b. Fire behaviour of FRP-strengthened reinforced concrete structural elements: A state-of-the-art review. *Composites Part B: Engineering,* 80**,** 198-216.

Firmo, J., Correia, J., Pitta, D., Tiago, C. & Arruda, M. 2015a. Experimental characterization of the bond between externally bonded reinforcement (EBR) CFRP strips and concrete at elevated temperatures. *Cement and Concrete Composites,* 60**,** 44-54.

Harajli, M., Elkhatib, H. & San-Jose, J. T. 2010. Static and cyclic out-of-plane response of masonry walls strengthened using textile-mortar system. *Journal of materials in civil engineering,* 22**,** 1171-1180.

Hartig, J., Häußler-Combe, U. & Schicktanz, K. 2008. Influence of bond properties on the tensile behaviour of Textile Reinforced Concrete. *Cement and Concrete Composites,* 30**,** 898-906.

Hegger, J., Bruckermann, O., Chudoba, R., Di Prisco, M., Felicetti, R. & Plizzari, G. 134. A smeared bond-slip relation for multi-filament yarns embedded in fine concrete. 6th International RILEM Symposium on Fibre Reinforced Concretes, 2004. RILEM Publications SARL, 1453-1462.

Hegger, J., Will, N., Bruckermann, O. & Voss, S. 2006. Load–bearing behaviour and simulation of textile reinforced concrete. *Materials and structures,* 39**,** 765-776.

Jesse, F., Weiland, S. & Curbach, M. 2008. Flexural strengthening of RC structures with textile-reinforced concrete. *Special Publication,* 250**,** 49-58.

Kodur, V. K., Bisby, L. A. & Green, M. F. 2006. Experimental evaluation of the fire behaviour of insulated fibre-reinforced-polymer-strengthened reinforced concrete columns. *Fire safety journal,* 41**,** 547-557.

Koutas, L. N. & Bournas, D. A. 2016. Flexural strengthening of two-way RC slabs with textile-reinforced mortar: experimental investigation and design equations. *Journal of Composites for Construction,* 21 (1)**,** 1-11.

Koutas, L., Bousias, S. & Triantafillou, T. 2014. Seismic strengthening of masonry-infilled RC frames with TRM: experimental study. *Journal of Composites for Construction,* 19 (2)**,** 1-12.

Loreto, G., Leardini, L., Arboleda, D. & Nanni, A. 2013. Performance of RC slab-type elements strengthened with fabric-reinforced cementitious-matrix composites. *Journal of Composites for Construction,* 18 (3)**,** 1-9.

Ombres, L. & Verre, S. 2015. Structural behaviour of fabric reinforced cementitious matrix (FRCM) strengthened concrete columns under eccentric loading. *Composites Part B: Engineering,* 75**,** 235-249.

Ombres, L. 2011. Flexural analysis of reinforced concrete beams strengthened with a cement based high strength composite material. *Composite Structures,* 94**,** 143-155.

Ombres, L. 2012. Debonding analysis of reinforced concrete beams strengthened with fibre reinforced cementitious mortar. *Engineering Fracture Mechanics,* 81**,** 94-109.

Ombres, L. 2015a. Analysis of the bond between Fabric Reinforced Cementitious Mortar (FRCM) strengthening systems and concrete. *Composites Part B: Engineering,* 69**,** 418-426.

Ombres, L. Confinement effectiveness in eccentrically loaded masonry columns strengthened by Fiber Reinforced Cementitious Matrix (FRCM) jackets. Key Engineering Materials, 2015b. Trans Tech Publ, 551-558.

Orlowsky, J. & Raupach, M. 2008. Durability model for AR-glass fibres in textile reinforced concrete. *Materials and Structures,* 41**,** 1225-1233.

Ortlepp, R., Hampel, U. and Curbach, M., 2006. A new approach for evaluating bond capacity of TRC strengthening. *Cement and concrete composites*, 28(7), pp.589-597.

Ortlepp, R., Lorenz, A. & Curbach, M. 2010. Column strengthening with TRC: Influences of the column geometry onto the confinement effect. *Advances in Materials Science and Engineering,* 2009.

Ortlepp, R., Ortlepp, S., Curbach, M., Di Prisco, M., Felicetti, R. & Plizzari, G. 137. Stress transfer in the bond joint of subsequently applied textile reinforced concrete strengthening. 6th International RILEM Symposium on Fibre Reinforced Concretes, 2004. RILEM Publications SARL, 1483-1494.

Papanicolaou, C. G., Triantafillou, T. C., Karlos, K. & Papathanasiou, M. 2007. Textile-reinforced mortar (TRM) versus FRP as strengthening material of URM walls: in-plane cyclic loading. *Materials and structures,* 40**,** 1081-1097.

Papanicolaou, C. G., Triantafillou, T. C., Papathanasiou, M. & Karlos, K. 2008. Textile reinforced mortar (TRM) versus FRP as strengthening material of URM walls: out-of-plane cyclic loading. *Materials and Structures,* 41**,** 143-157.

Papanicolaou, C., Triantafillou, T. & Lekka, M. 2011. Externally bonded grids as strengthening and seismic retrofitting materials of masonry panels. *Construction and Building Materials,* 25**,** 504-514.

Papanicolaou, C., Triantafillou, T., Papantoniou, I. & Balioukos, C. 2009. Strengthening of two-way reinforced concrete slabs with Textile Reinforced Mortars (TRM).

Peled, A. & Bentur, A. 1998. Reinforcement of cementitious matrices by warp knitted fabrics. *Materials and structures,* 31**,** 543-550.

Peled, A. & Bentur, A. 2000. Geometrical characteristics and efficiency of textile fabrics for reinforcing cement composites. *Cement and concrete research,* 30**,** 781-790.

Peled, A. 2007. Confinement of damaged and nondamaged structural concrete with FRP and TRC sleeves. *Journal of Composites for Construction,* 11**,** 514-522.

Peled, A., Bentur, A. & Yankelevsky, D. 1998. The nature of bonding between monofilament polyethylene yarns and cement matrices. *Cement and Concrete Composites,* 20**,** 319-327.

Peled, A., Bentur, A. & Yankelevsky, D. 1999. Flexural performance of cementitious composites reinforced with woven fabrics. *Journal of materials in civil engineering,* 11**,** 325-330.

Peled, A., Yankelevsky, D. & Bentur, A. 1997. Microstructural characteristics of cementitious composites reinforced with woven fabrics. *Advances in cement research,* 9**,** 149-155.

Peled, A., Zaguri, E. & Marom, G. 2008. Bonding characteristics of multifilament polymer yarns and cement matrices. *Composites Part A: Applied Science and Manufacturing,* 39**,** 930-939.

Rambo, D. a. S., De Andrade Silva, F., Toledo Filho, R. D. & Gomes, O. D. F. M. 2015. Effect of elevated temperatures on the mechanical behavior of basalt textile reinforced refractory concrete. *Materials & Design,* 65**,** 24-33.

Raoof, S. M., Koutas, L. N. & Bournas, D. A. 2016. Bond between textile-reinforced mortar (TRM) and concrete substrates: Experimental investigation. *Composites Part B: Engineering,* 98**,** 350-361.

Schladitz, F., Frenzel, M., Ehlig, D. & Curbach, M. 2012. Bending load capacity of reinforced concrete slabs strengthened with textile reinforced concrete. *Engineering structures,* 40**,** 317-326.

Serbescu, A., Guadagnini, M. & Pilakoutas, K. 2013. Standardised double-shear test for determining bond of FRP to concrete and corresponding model development. *Composites Part B: Engineering,* 55**,** 277-297.

Sneed, L. H., D'antino, T. & Carloni, C. 2014. Investigation of Bond Behavior of PBO Fiber-Reinforced Cementitious Matrix Composite-Concrete Interface. *ACI Materials Journal,* 111.

Sneed, L., D'antino, T., Carloni, C. & Pellegrino, C. 2015. A comparison of the bond behavior of PBO-FRCM composites determined by double-lap and single-lap shear tests. *Cement and Concrete Composites,* 64**,** 37-48.

Soranakom, C. & Mobasher, B. 2009. Geometrical and mechanical aspects of fabric bonding and pullout in cement composites. *Materials and structures,* 42**,** 765-777.

Teng, J., Chen, J.-F., Smith, S. T. & Lam, L. 2002. FRP: strengthened RC structures. *Frontiers in Physics***,** 266.

Tetta, Z. C. & Bournas, D. A. 2016. TRM vs FRP jacketing in shear strengthening of concrete members subjected to high temperatures. *Composites Part B: Engineering,* 106**,** 190-205.

Tetta, Z. C., Koutas, L. N. & Bournas, D. A. 2015. Textile-reinforced mortar (TRM) versus fiber-reinforced polymers (FRP) in shear strengthening of concrete beams. *Composites Part B: Engineering,* 77**,** 338-348.

Tran, C. T. M., Stitmannaithum, B. & Ueda, T. 2014. Investigation of the bond behaviour between PBO-FRCM strengthening material and concrete. *Journal of Advanced Concrete Technology,* 12**,** 545-557.

Triantafillou, T. & Papanicolaou, C. G. 2006. Shear strengthening of reinforced concrete members with textile reinforced mortar (TRM) jackets. *Materials and structures,* 39**,** 93-103.

Triantafillou, T. & Papanicolaou, C. G. Textile reinforced mortars (TRM) versus fiber reinforced polymers (FRP) as strengthening materials of concrete structures. Proceedings of the 7th ACI International Symposium on Fibre-Reinforced (FRP) Polymer Reinforcement for Concrete Structures, 2005. American Concrete Institute, 99-118.

Triantafillou, T. 2006. *Strengthening and Seismic Retrofitting od Concrete and Masonry Structures with Composites,* Greece, University of Patras.

Triantafillou, T. 2011. Innovative textile-based composites for strengthening and seismic retrofitting of concrete and masonry structures. *Advances in FRP Composites in Civil Engineering.* Springer.

Triantafillou, T., Papanicolaou, C. G., Zissimopoulos, P. & Laourdekis, T. 2006. Concrete confinement with textile-reinforced mortar jackets. *ACI structural journal,* 103**,** 28.

Xu, S., Krüger, M., Reinhardt, H.-W. & Ozbolt, J. 2004. Bond characteristics of carbon, alkali resistant glass, and aramid textiles in mortar. *Journal of materials in civil engineering,* 16**,** 356-364.

Yao, J., Teng, J. & Chen, J. 2005. Experimental study on FRP-to-concrete bonded joints. *Composites Part B: Engineering,* 36**,** 99-113.

Yin, S., Xu, S. & Lv, H. 2013. Flexural behavior of reinforced concrete beams with TRC tension zone cover. *Journal of Materials in Civil Engineering,* 26**,** 320-330.

Zastrau, B., Lepenies, I. & Richter, M. 2008. On the multi scale modeling of textile reinforced concrete. *Technische Mechanik,* 28**,** 53-63.

APPENDIX A – Design of beams

A.1 Flexural and Shear design of the Control Beam

The aim of this part of experimental work was to evaluate the contribution of TRM composite in increasing the flexural capacity of RC beams. Therefore, the control (unstrengthened) beam was intentionally designed to be under reinforced simulating a flexural-deficient beam. The procedure for designing of the beam was as follows:

1. Calculating the ultimate moment capacity of the control beam and proposing steel reinforcement.
2. Designing the control beam for shear so as to ensure that the failure of the strengthened beams would always be in flexure.
3. Proposing the maximum area of strengthening materials (i.e. the number of FRP/TRM layers), and calculating the ultimate moment capacity of the strengthened beams.
4. Performing calculations to ensure that a minimum required anchorage length (L_a_ see Figure A.1) is provided.

To calculate the ultimate moment capacity of the control beam, the following measurements were assumed:

- The beam cross-section is rectangular with dimensions of 100mm width, 200 mm high, and flexural span of 1.5 m (Figure A.1).
- The concrete cover is equal to 15 mm.

- The concrete compressive strength, $f_{ck} = 18\,MPa$ in order to simulate a real situation of deteriorated concrete compressive strength as a result of aging, or degradation induced environmental conditions.
- The average yield stress in the steel rebar is equal to 560 MPa (obtained experimentally_ see Table A.1 and Figure A.2).

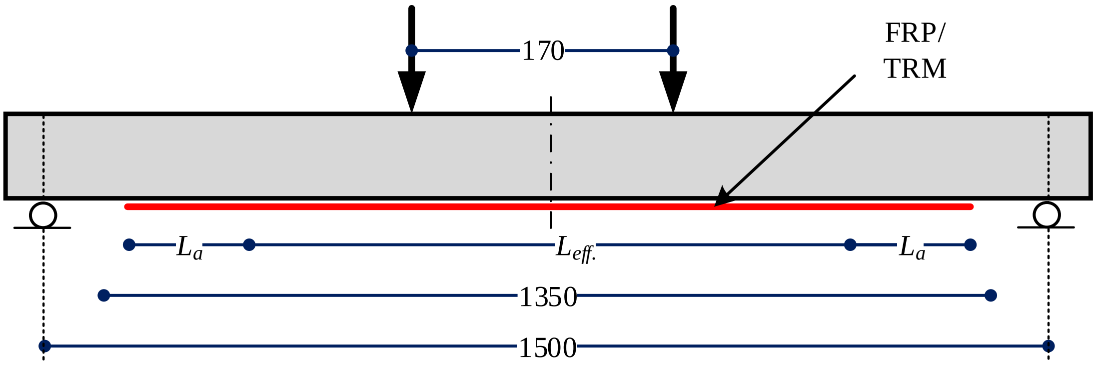

Figure A.1. Geometry of the strengthened beam.

Table A.1. Summary of results of the tensile tests of steel reinforcement.

Bar diameter (mm)	f_y **(MPa)**	ε_y **(%)**	f_u **(MPa)**	ε_u **(%)**
8-mm	569	0.283	631	7.85
12-mm	561	0.490	637	12.8

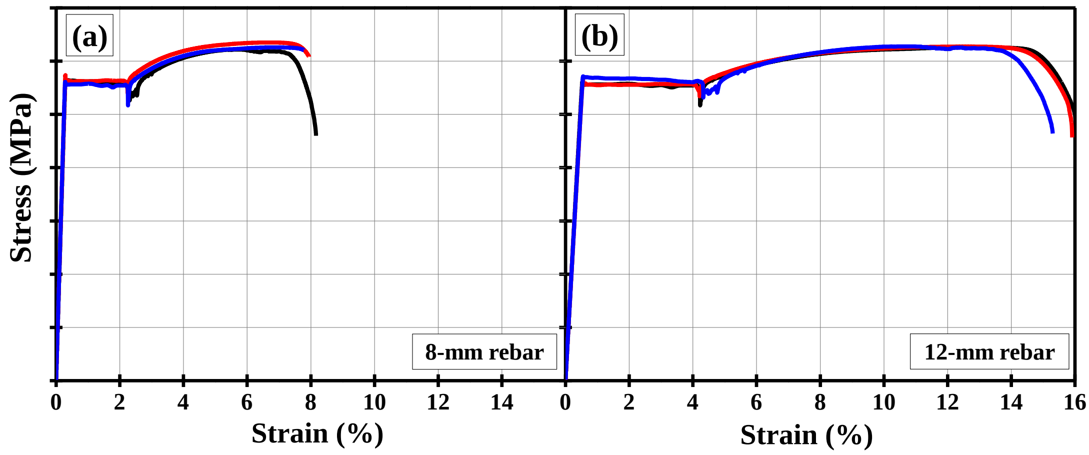

Figure A.2. Stress strain curves of steel bars; (a) 12 mm diameter, and (b) 8-mm diameter.

For design practice, Eurocode2 (2004) suggested a normalized balanced moment (k_{bal}) equal to k_{bal}= 0.206. This value ensures that the failure of the beam is due to steel yielding at the tension zone followed by concrete crushing at the compression zone (under reinforced beam). Hence, the corresponding design balanced moment ($M_{Rd,bal}$) and the lever arm (z) can be directly calculated from Eq. A.1 and Eq. A.2, respectively (Eurocode2, 2004).

$$M_{Rd,bal} = 0.206\, b\, d^2 f_{ck} \quad A.1$$

$$z = \frac{d}{2}\left(1 + \sqrt{1 - 3.53 k_{bal}}\right) \le 0.95d \quad A.2$$

substitute to get,

$$M_{Rd,bal} = 0.206 * 100 * 173^2 * 18 = 11.1\ kN.m$$

and,

$$z = \frac{173}{2}\left(1 + \sqrt{1 - 3.53 * 0.206}\right) = 132\ mm \le 0.95 * 173 = 164.4\ mm$$

now, the required area of steel in tension (without safety factor) can be calculated from Eq. A.3:

$$A_s = \frac{M_{Rd,bal}}{f_y\, Z} \qquad A.3$$

Eq. A.3 gives $A_s = \frac{11.1*10^6}{560*132} = 150\ mm^2$

The minimum area of reinforcement can be calculated from Eq. A.4 (Eurocode2, 2004):

$$A_{s,min} = 0.26\ \frac{f_{ctm}}{f_{yk}} bd, but\ not\ less\ than\ 0.0013bd \qquad A.4$$

with, $f_{ctm} = 0.3(f_{ck})^{\frac{2}{3}} = 2.06\ MPa$

Eq. A.4 gives $A_{s,min} = 24\ mm^2$

Using $2H8$ yields an area of steel reinforcement equal to $101\ mm^2$ which is less than the balanced area ($A_{s,bal} = 150\ mm^2$) and is greater than the minimum required area of steel $A_{s,min} = 24\ mm^2$. This area of steel was select in order to simulate a flexural-deficient beam. According to the selected area of steel reinforcement, the ultimate moment resistant of the control beam (obtained from standard cross section analysis) is equal to $M_u = 9.1\ kN.m$ and the corresponding ultimate load based on the loading configuration shown in Figure A.1 is equal to $36.1\ kN$.

It is worth mentioned that the beam was provided with compression reinforcement comprising $2H12mm$ ($A_{s2} = 226\ mm^2$) in order to prevent the failure of the retrofitted beams due to concrete crushing in the compression zone and ensure that the failure would occur within the strengthening material (i.e. full utilization of the strengthening material).

The beam was designed for shear using a factorized load seven times greater than the predicted ultimate load of the control beam ($36.1\ kN$). The procedure for the shear design was conducted according to Eurocode2 (2004).

The H8 was used as shear links (shear reinforcement), hence the spacing between the shear links can be calculated from Eq. A.5.

$$S = \frac{A_{sw} f_y z \cot\theta}{V_{R,max}} \qquad A.5$$

where $A_{sw} = 2\frac{\pi D^2}{4} = 100\ mm^2$, $V_{R,max} = 7 * 36.1 = 252.7\ kN$, $\alpha_{cw} = 1.0$, $z = 0.9d$, and θ was assumed equal to $22°$ as a conservative estimation.

Eq. A.5 gives $S = \frac{100\times560\times0.9\times173\times\cot 22}{252.7\times10^3} = 85\text{ mm; use S} = 80\text{mm}$

A.2 Calculation of Anchorage Length

The strengthened material was bonded to the beam's soffit over a length of 1350 mm. Simple calculations were made to ensure that this bond length provides a sufficient anchorage length. The anchorage length (L_a_ see Figure A.1) is defined as the length just outside the effectively strengthened area. Providing a sufficient anchorage length ensures that the strengthening materials sustained a maximum stress when the failure due to debonding induced intermediate crack (Teng et al., 2002). In the next sections, the calculations of the anchorage length for both the FRP and TRM strengthened beams is provided.

A.2.1 Anchorage length for FRP strengthened beams

The procedure for calculations of the anchorage length was made according to the procedure described in Triantafillou (2006). It is noted that the calculations of the anchorage length were made for the 3 layers FRP strengthened beam (which was the maximum number of FRP layers used for strengthening).

The required anchorage length is calculated from Eq. A.6:

$$L_a = 0.6\sqrt{\frac{E_f t_f}{\sqrt{f_{ctm} * k_b}}} \qquad A.6$$

and,

$$k_b = \sqrt{\frac{1.5(2-\frac{b_f}{b})}{1+\frac{b_f}{100}}} \geq 1 \qquad A.7$$

where E_f= the modulus of elasticity of fibres (according to manufacturer data sheet), t_f= the nominal thickness of the fibres, f_{ctm}= the mean tensile strength of concrete, b_f= width of fibres and b= beam's width.

Eq. A.7 gives $k_b = \sqrt{\frac{1.5(2-\frac{100}{100})}{1+\frac{100}{100}}} = 0.87 < 1, use\ k_b = 1$

and, Eq. A.6 gives $L_a = 0.6\sqrt{\frac{225*10^3*3*.095}{\sqrt{2.06*1}}} = 127\ mm$

For the case of debonding at intermediate cracking, the effective strain in the fibre (ε_{eff}) is calculated from Eq. A.8 (with no safety factors):

$$\varepsilon_{eff} = \sqrt{\frac{0.6*f_{ctm}*k_b}{E_f t_f}} \qquad A.8$$

Eq. A.8 gives $\varepsilon_{eff} = \sqrt{\frac{0.6*2.06*1}{225*10^3*3*.095}} = 0.0044$

use $\varepsilon_{eff} = 0.005$

Hence, the ultimate moment capacity of the 3 layers strengthened beams is calculated from standard cross section analysis and is equal to $14.3\ kN.m$.

The procedure for calculation the anchorage length was as follows:

1. Calculating the tension force (N_{Ed}) provided by the ultimate moment and the tension force provided by tension steel (N_{Rsd}).
2. Dawning the moment diagram (in terms of forces).
3. Intersecting the line corresponding to the tensile force carried by tension steel with the ultimate tensile force envelope provided by the ultimate moment. The section beyond that intersection point is the actually provided anchorage length (residual anchorage length_ L_{resd}).
4. Checking whether the provided anchorage length is greater than or equal the required anchorage length calculated from Eq. A.6.

To apply the above procedure, the tension force resulted from the ultimate moment $(M_{Ed})$is calculated from Eq. A.9:

$$N_{Ed} = \frac{M_{Ed}}{Z} \qquad A.9$$

where

$Z = 0.95\ d$

hence Eq. A.9 gives $N_{ED} = \frac{14.3}{0.95*173} = 87\ kN,$

and, the tension force calculated from the tension steel (N_{Rsd}) is:

$N_{Rsd} = 560 * 100 = 56\ kN$

The value of x shown in Figure A.3 can be calculated form triangle similarity which resulted in a value of $x = 180\ mm.$

Hence check whether the residual anchorage length (L_{resd}) is equal or greater than the required anchorage length (L_a) calculated form Eq. A.6. The residual length is calculated as follows:

$$L_{resd} = 675 - 170 - x - 0.9d$$

$$L_{resd} = 675 - 170 - 180 - 0.9 * 173 = 169.3\ mm > L_a = 127\ mm, OK$$

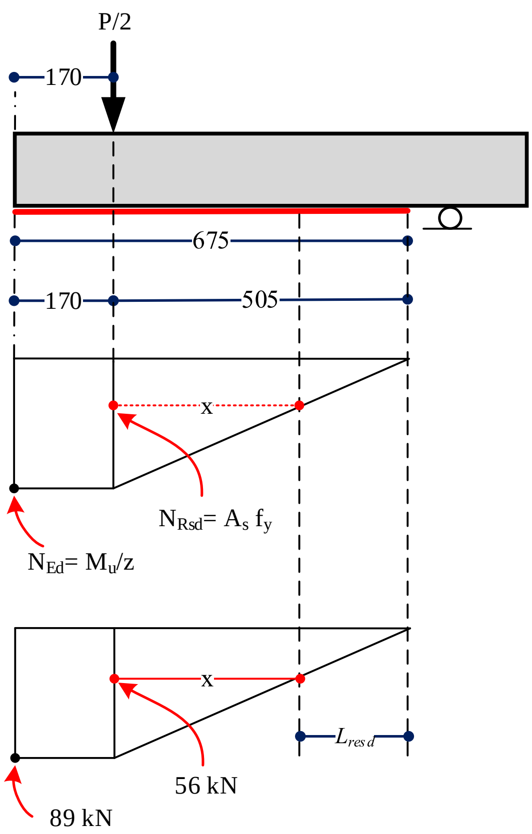

Figure A.3. Calculations of the anchorage length of 3 layer FRP strengthened beam.

A.2.2 Anchorage length for TRM strengthened beams

According the results of the bond tests described in Chapter 4, the effective anchorage length of TRM is 200 mm. Therefore, it was decided to consider this length as an anchorage length of the TRM strengthened beams. The same procedure described for the FRP strengthened beams is also adopted here so as to ensure that an anchorage length of 200 mm is secured. The only difference in the calculations was the determination of the effective strain (ε_{eff}) in the TRM reinforcement which was obtained directly from the bond test of the specimen strengthened with 3 TRM layers and had bond length of 200 mm as follows:

The ultimate load of the 3 layers TRM strengthened specimen was 36 kN (see Table 4.2). The corresponding effective stress is 790 MPa, hence the corresponding effective strain is:

$$\varepsilon_{eff} = \frac{\sigma_{eff}}{E_f} = \frac{790}{225 * 10^3} = 0.0035$$

Form the cross-section analysis, the ultimate moment of the 3 layer TRM strengthened beam is $12.6\ kN.m$.

now the tension force resulted from the ultimate moment and from the tension steel reinforcement is:

$N_{ED} = \frac{12.6}{0.95*173} = 76.7\ kN$, and $N_{Rsd} = 560 * 100 = 56\ kN$, respectively.

from triangle similarity, the value of $x = 136.3\ mm$ (Figure A.4).

hence the residual anchorage length (L_{resd}) is:

$$L_{resd} = 675 - 170 - 136.3 - 0.9 * 173 = 213\ mm > L_a = 200, OK.$$

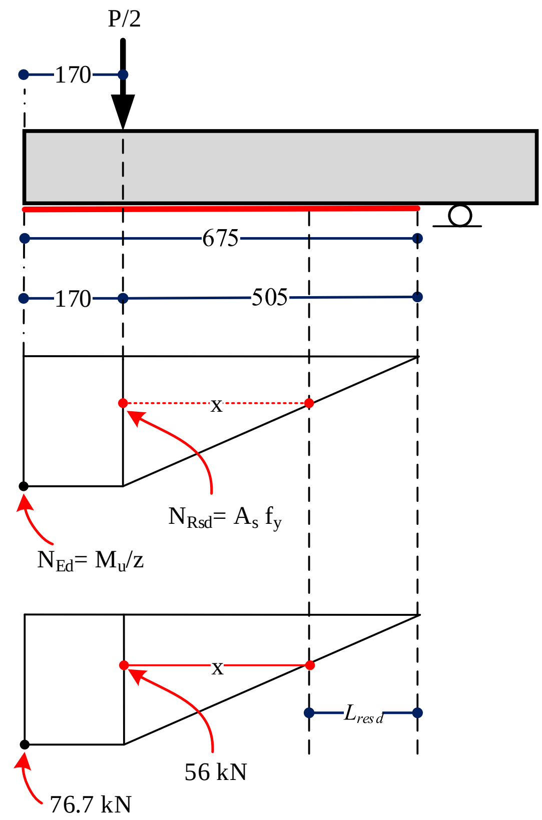

Figure A.4. Calculations of the anchorage length of 3 layer TRM strengthened beam.

Personal Development

Journals Papers

Raoof, S.M., Koutas, L.N. and Bournas, D.A., 2016. “Bond between textile-reinforced mortar (TRM) and concrete substrates: Experimental investigation”. *Composites Part B: Engineering*, *98*, pp.350-361.

Raoof, S.M., Koutas, L.N. and Bournas, D.A., 2017. Textile-reinforced mortar (TRM) versus fibre-reinforced polymers (FRP) in flexural strengthening of RC beams. *Construction and Building Materials*, 151, pp.279-291.

Raoof, S.M. and Bournas, D.A., 2017. “Bond between TRM versus FRP Composites and Concrete at High Temperatures”. *Composites Part B: Engineering*, 127, pp. 150-165.

Raoof, S.M. and Bournas, D.A., 2017. “TRM versus FRP in Flexural Strengthening of RC Beams: Behaviour at High Temperatures”. submitted to *Construction and Building Materials journal*.

Conferences Papers

Raoof, S.M. and Bournas, D.A. 2017. “Effect of High Temperature on the Bond Between TRM and FRP to Concrete Substrates”, *IFireSS 2017 – 2nd International Fire Safety Symposium*, Naples, Italy, June 7-9, 2017.

Raoof, S.M., Koutas, L.N. and Bournas, D.A., 2017. “Effectiveness of TRM versus FRP in flexural strengthening of RC beams”, *ACIC 2017, Advanced Composites in Construction 2017*, Sheffield, UK (Submitted).

Presentations

Raoof, S.M. 2017. "Bond between textile-reinforced mortar (TRM) and concrete substrates: Experimental investigation", the university of *Sheffield, October 2016, Sheffield, UK.*

Raoof, S.M. 2017. "Bond between textile-reinforced mortar (TRM) and concrete substrates: Experimental investigation", *CSEI seminar, May 2017, Nottingham, UK.*